Inaugural dissertation

for

obtaining the doctoral degree

of the

Combined Faculty of Mathematics, Engineering and Natural Sciences

of the

Ruprecht-Karls-University

Heidelberg

Presented by

Philipp Pöschko, M.Sc.

Born in: Heidelberg

Oral examination: 23.10.2024

Plant hormone-based chemical inducers of proximity for live cell and in vivo applications enabling precise control of protein localization

Referees: PD Dr. Richard Wombacher

Prof. Dr. Andres Jäschke

Abstract

Proximity-dependent protein interactions are crucial for many cellular processes, which makes methods to precisely control protein localization highly desirable. Chemical inducers of proximity (CIPs) are a tool that enables such manipulation by bringing specific protein domains together that can be fused to proteins of interest (POIs).

This work focusses on the development of different strategies for precise control of protein localization in live cells and in vivo derived from plant hormone-based CIPs.

To introduce a further control over the chemically induced protein proximity, I developed Mandi-Dopa-C6-Indole, an antagonist for the plant hormone-based CIP mandipropamid (Mandi), that is able to reverse protein proximity previously induced by Mandi in live mammalian cells.

Moreover, I demonstrate that pMandi, a photocaged derivative of Mandi, can be used to induce protein proximity in live mammalian cells and in live medaka embryos upon light irradiation as external stimulus. Although pMandi enables precise temporal control over the induction of protein proximity, spatial control is limited by the high permeability of Mandi.

For the design of a photocaged CIP that enables also precise spatial control over the induction of protein proximity with single-cell resolution, I repurposed the abscisic acid (ABA) agonist opabactin (OP) from plant research as CIP. The carboxylic acid moiety of OP renders the molecule less cell permeable and enables intracellular trapping. When the carboxylic acid moiety is protected as acetoxymethyl (AM) ester, the addition of this compound induces protein proximity in live mammalian cells and in live medaka embryos at low working concentrations comparable to Mandi. The photocaged derivative of OP, pOP, allows inducing protein proximity upon irradiation with light in single live mammalian cells and enables the manipulation of individual cells in the same sample.

To extend the CIP system based on Mandi from dimerization to trimerization, I split one of the interacting proteins into two fragments and demonstrated that the fragments can reconstitute and recruit the second interacting protein in the presence of the CIP in live mammalian cells when spatial proximity of the split fragments is given. I further successfully applied this split system to construct a logic gate in combination with the CIP rapamycin.

Kurzzusammenfassung

Proteininteraktionen die auf Annäherung beruhen sind für viele zelluläre Prozesse substanziell. Dies macht Methoden mit denen die Proteinlokalisation präzise gesteuert werden kann sehr attraktiv. Chemische Induktoren für Proteinnähe (CIPs) sind ein Werkzeug, das eine solche Manipulation ermöglicht, indem sie spezifische Proteindomänen zusammenbringen, die mit den zu untersuchenden Proteinen verknüpft werden können.

Diese Arbeit behandelt die Entwicklung von verschiedenen Strategien zur präzisen Kontrolle der Proteinlokalisation in lebenden Zellen und in vivo abgeleitet von Pflanzenhormon-basierten CIPs.

Um eine weitere Kontrolle über die chemisch induzierte Proteinnähe zu erlangen, habe ich Mandi-Dopa-C6-Indole entwickelt, einen Antagonisten für den Pflanzenhormon basierten CIP Mandipropamid (Mandi), der die zuvor durch Mandi induzierte Proteinnähe in lebenden Säugetierzellen umkehren kann.

Zudem zeige ich, dass pMandi, ein photogeschütztes Derivat von Mandi, dazu benutzt werden kann um in lebenden Säugetierzellen und lebenden Medakaembryonen Proteinnähe durch Lichtbestrahlung als externen Stimulus zu induzieren. Obwohl pMandi eine präzise zeitliche Kontrolle über die Induktion von Proteinnähe ermöglicht, ist die räumliche Kontrolle durch die hohe Permeabilität von Mandi begrenzt.

Für die Entwicklung eines photogeschützten CIPs, der auch eine präzise räumliche Kontrolle über die Induktion der Proteinnähe mit Einzelzellauflösung ermöglicht, habe ich den Abscisinsäure(ABA)-Agonisten Opabactin (OP) als CIP umgenutzt. Die Carbonsäure-Funktionalität von OP macht das Molekül weniger zellpermeabel und ermöglicht es intrazellulär zu fangen. Wenn die Carbonsäure-Funktionalität als Acetoxymethyl(AM)-Ester geschützt ist, induziert die Zugabe dieser Verbindung in lebenden Säugetierzellen und lebenden Medakaembryonen Proteinnähe bei vergleichbaren Konzentrationen zu Mandi. Das photogeschützte Derivat von OP, pOP, erlaubt es Proteinnähe in einzelnen lebenden Säugetierzellen bei Bestrahlung mit Licht zu induzieren und macht die Manipulation einzelner Zellen in derselben Probe möglich.

Um das auf Mandi basierende CIP-System von Dimerisierung zu Trimerisierung zu erweitern, habe ich eines der interagierenden Proteine in zwei Fragment ausgespalten und gezeigt, dass die Fragmente in Gegenwart des CIPs in lebenden Säugetierzellen rekonstituieren und das zweite interagierende Protein rekrutieren können, wenn eine räumliche Nähe der Fragmente gegeben ist. Darüber hinaus habe dieses System erfolgreich zur Konstruktion eines Logikgatters in Kombination mit dem CIP Rapamycin verwendet.

Acknowledgements

First, I would like to thank my supervisor Richard Wombacher for giving me the opportunity to do my doctoral thesis in his research group, his trust and support. I am grateful that I have been able to learn so many new thinks during the last few years.

Moreover, I would like to express my gratitude to Kai Johnsson for hosting Richard Wombacher and his group in the Department of Chemical Biology at the Max Planck Institute for Medical Research (Heidelberg). I thank for providing excellent laboratory facilities and equipment, scientific input and discussions as well as any kind of financial support.

I would also like to thank Andres Jäschke for being my second examiner and the other examiners for taking the time to be part of my examination committee and for reviewing this work.

A special thank goes to Caroline Berrou, whom I supervised during her master's thesis, for synthesis of opabactin and related compounds and carrying out preliminary experiments.

Additionally, I would like to thank Joachim Wittbrodt for collaborating on the medaka experiments and Kaisa Pakari for conducting the medaka experiments with me very smoothly.

I further want to acknowledge Miroslav Tarnawski and his team at the protein expression and characterization core facility protein expression for expressing proteins for me, as well as Sebastian Fabritz and his team at the mass spectrometry core facility for measuring my samples.

Also, I am grateful to Birgit Koch, senior scientist and lab manager in the Department of Chemical Biology for providing support regarding microscopy and cell culture and Julien Hiblot, senior scientist in the Department of Chemical Biology for support regarding biochemistry.

I would also like to thank the technicians in the Department of Chemical Biology (Carmen Grosskurth, Jana Kress, Bettina Réssy and Dominik Schmidt and Andrea Bergner) for technical assistance and providing reagents.

Furthermore, I want to acknowledge the staff at the Max Planck Institute for Medical Research (Heidelberg) working on providing good working conditions for scientists, especially Gwenaëlle Matthies for help with administrative issues.

Last but not least I would like to thank all people from the Department of Chemical Biology at the Max Planck Institute for Medical Research (Heidelberg) for the nice working atmosphere and socializing also beside work. Especially, I would like to thank Kristina Bayer, my colleague in the group of Richard Wombacher, for the nice time we had in the lab, the office and on conferences and my office colleagues Laurin Schulze-Forster and Bastian Bühler.

Finally, I would like to thank my family and my partner for their support in all circumstances and their love.

This work was conducted at the Max Planck Institute for Medical Research (Heidelberg) in the Department of Chemical Biology from July 2021 until August 2024.

Table of contents

1 Introduction

1.1 General principles of chemically induced (protein) proximity

Many cellular mechanisms are regulated by protein-protein interactions (PPIs) that rely on spatial proximity. To manipulate and investigate these processes so called chemical inducers of proximity (CIPs) have been developed and are widely used. CIPs are small organic molecules that induce protein proximity between two specific protein domains upon non-covalent interactions. These protein domains can be expressed as fusion proteins with proteins of interest (POIs) that can consequently be brought into proximity in the presence of the CIP (Figure 1). CIPs are also called dimerizers or chemical inducers of dimerization (CIDs). This class of proximity inducing molecules has been used in the context of artificially controlling protein localization and transport, inducing signaling and protein degradation, regulating gene expression and reconstituting split proteins.[1,2]

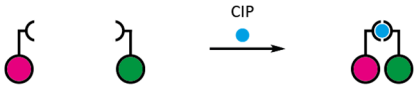

Figure 1: Schematic representation of inducing (protein) proximity with a CIP. The proteins of interest (POIs) are marked in red and green, the CIP in blue and the protein domains that interact with the CIP are displayed as semicircles.

CIPs can be distinguished by their mechanism of inducing protein proximity (Figure 2). Molecular glues are bivalent or heterobifunctional molecules that have binding moieties for both interacting proteins. Because of this mode of action, at increased concentration of the CIP less complex formation is observed since the binding sites on both proteins are occupied by the CIP and these individual protein-CIP complexes cannot interact anymore (Hook effect). Immunosuppressant-based CIPs (see Section 1.2) like rapamycin and its analogs as well as proteolysis targeting chimeras (PROTACs) and the plant-hormone based CIP auxin (see Section 1.3.2) are part of this group. CIPs that act via the molecular ratchet mechanism in contrast only bind to one interacting protein, called receiver protein. Only upon this binding event a conformational change is induced in the protein and a binding site for the second interacting protein, called receiver protein, is formed. With this mechanism no Hook effect is observed making this type of CIP more user friendly. The plant hormone-based CIPs gibberellic acid (GA_3), abscisic acid (ABA) and mandipropamid (Mandi) are part of this group (see Sections 1.3.1, 1.3.3 and 1.3.4).[3]

Further requirements for ideal CIPs are bioorthogonality[4] and low toxicity, both often conferred by plant hormone-based CIP systems, as well as good cell permeability and a fast and efficient induction of protein proximity.[1]

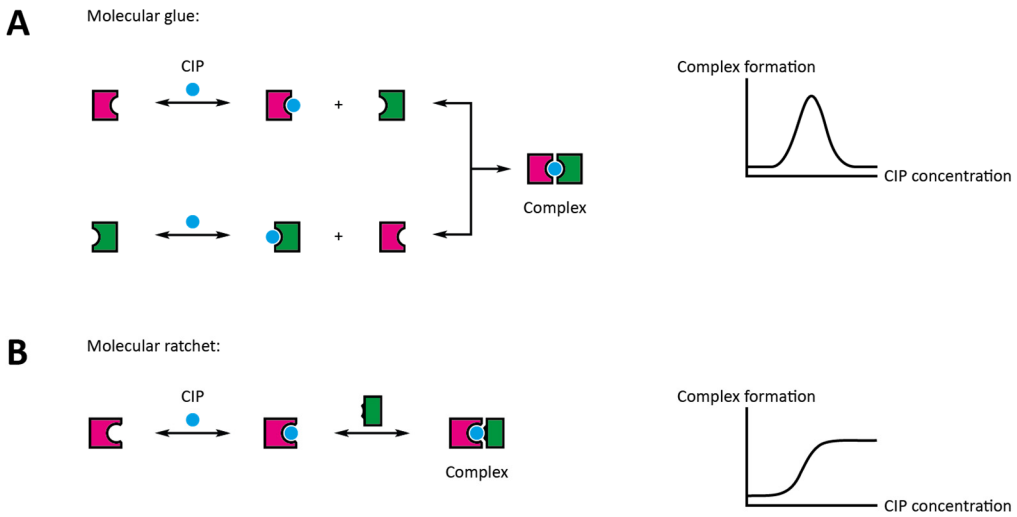

Figure 2: Schematic representation of the mechanism of different types of CIPs. The interacting protein domains are displayed in red and green, the CIP in blue. (A) Molecular glue: The ligand (CIP) binds to both proteins, at high concentration less complex formation is observed because of the Hook effect. (B) Molecular ratchet: The ligand (CIP), binds only to one receptor protein and in a next step the second receiver protein is recruited, no Hook effect is observed. Figure adapted from literature[5].

To achieve further control over the induction of protein proximity, photocaged CIPs can be used that release the active CIP upon light irradiation (photoactivation) (Figure 3). Light is an attractive tool to probe processes in a non-invasive way and enables precise spatiotemporal control. Photocaged CIPs can reach the targeted area while being inactive and directly release the active CIP there upon irradiation, which makes the induction of protein proximity independent of permeability and improves the rate of the manipulation process.[6]

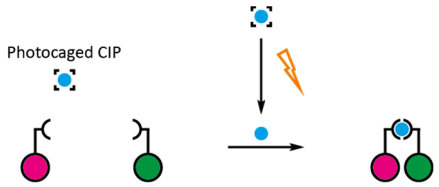

Figure 3: Schematic representation of inducing (protein) proximity with a photocaged CIP. The photocage is cleaved upon irradiation and the active CIP is released. The proteins of interest (POIs) are marked in red and green, the CIP in blue and the protein domains that interact with the CIP are displayed as semicircles.

1.2 Immunosuppressant-based CIP systems

The first systems to chemically induce protein proximity were based on immunosuppressants. Based on the discovery that specific small molecule immunosuppressants act by inducing protein proximity, these systems were used to artificially induce protein proximity.[7]

1.2.1 FK506, rapamycin and analogs

In 1991, it was discovered that the molecule FK506 (Tacrolismus) (Figure 4), isolated form the bacterium *streptomyces tsukubaensis*, binds the proteins FKBP12 (FK506 binding protein) and calcineurin. This interaction leads to the inhibition of transcription factors responsible for T cell activation.[8] Based on this system two covalently linked FK506 molecules (FK1012) (Figure 4) were used to bring FKBP12 proteins in proximity. The system was used to oligomerize cell surface receptors expressed as fusion proteins with FKBP12 and thereby specifically activate signal transmission as well as specific target genes in live mammalian cells (1993).[9]

Another immunosuppressant that acts by inducing protein proximity is rapamycin, that was isolated from the bacterium *streptomyces hygroscopicus*. Rapamycin (Figure 4) binds the proteins FRAP (FKBP-rapamycin associated protein, also called: mTOR (mammalian target of rapamycin)) and FKBP12 and inhibits cell-cycle progression in specific cell types (1994).[10] In 1995, it was found that only a small part of FRAP is responsible for FKBP12-rapamycin binding, the FKBP12-rapamycin-binding (FRB) domain.[11] Also, a crystal structure of the ternary FKBP12-rapamycin-FRB complex was obtained, revealing that the two proteins are associated by the binding of rapamycin to hydrophobic pockets on both proteins (1996).[12] In 1996, this system was used to induce proximity of FKBP12 (12.0 kDa) and FRB (11.4 kDa) upon treatment with rapamycin to control gene expression, the first use of rapamycin as CIP in another context than immunosuppressants.[13]

Also, synthetic ligands for FKBP12 have been developed that are structurally less complex. In 1993, synthetic ligands for FKBP12 based on FK506 and rapamycin were developed and the FKBP12-ligand complexes were investigated by X-ray crystallography.[14] Based on this work, the molecule AP1510 (Figure 4) was designed as a dimer of two covalently linked synthetic ligands for FKBP12 (1997).[15] Different linker lengths were screened achieving a molecule with low nanomolar affinity to dimerize two FKBP12 proteins. AP1510 is more potent then FK1012 and characterized by less structural complexity and a lower molecular weight since it only consists of two binding domains to FKBP12 that are linked together.[15]

If immunosuppressants are used as CIPs to induce protein proximity in live mammalian cells, the problem arises that in addition to the desired interaction, also interactions with the endogenous proteins occur and native cell signaling is disturbed. To solve this issue and to achieve bioorthogonality

both, the corresponding proteins as well as the ligands were modified. Analogs of rapamycin were called rapalogs.[7]

In 1997, a first study on nontoxic ligands for FKBP12 and FRB was conducted. Various rapamycin derivatives were screened in an inducible gene expression assay against FKBP12 and a FRB library identifying a rapalog that binds native FKBP12 and a triple mutant of FRB (K2095P, T2098L, and W2101F) with selectivity over native FRB but with reduced affinity compared to rapamycin.[16] Later it was shown, that the nontoxic rapalog AP21967 (Figure 4) binds to FKBP12 and a single mutant of FRB (T2098L) and not to native FRB (2006).[17] In 2010 the use of AP21967 as CIP was demonstrated.[18] The FRB mutations have only a very little effect on rapamycin binding and the affinity of rapamycin to both FRB mutants is about one order of magnitude higher than the affinity of the rapalogs.[16,17]

Also, FKBP12 was optimized to bind nontoxic rapalogs. By introducing a F36V mutation a binding pocket was created at the FKBP-ligand interface, then different ligands were tested against this mutation. This led to the identification of a ligand that showed sub-nanomolar affinity to the mutated protein and an about three orders of magnitude lower affinity to wildtype FKBP12. The homodimer of this compound, AP1903, was used to bring two FKBP12 (F36V) proteins into proximity (Figure 4). Cells expressing the chimeric protein can be modified without interference with endogenous FKBP12 (1998).[19] The rapalog AP20187 (Figure 4) is structurally similar to AP1903 but has a different linker between the two protein binding domains.[20]

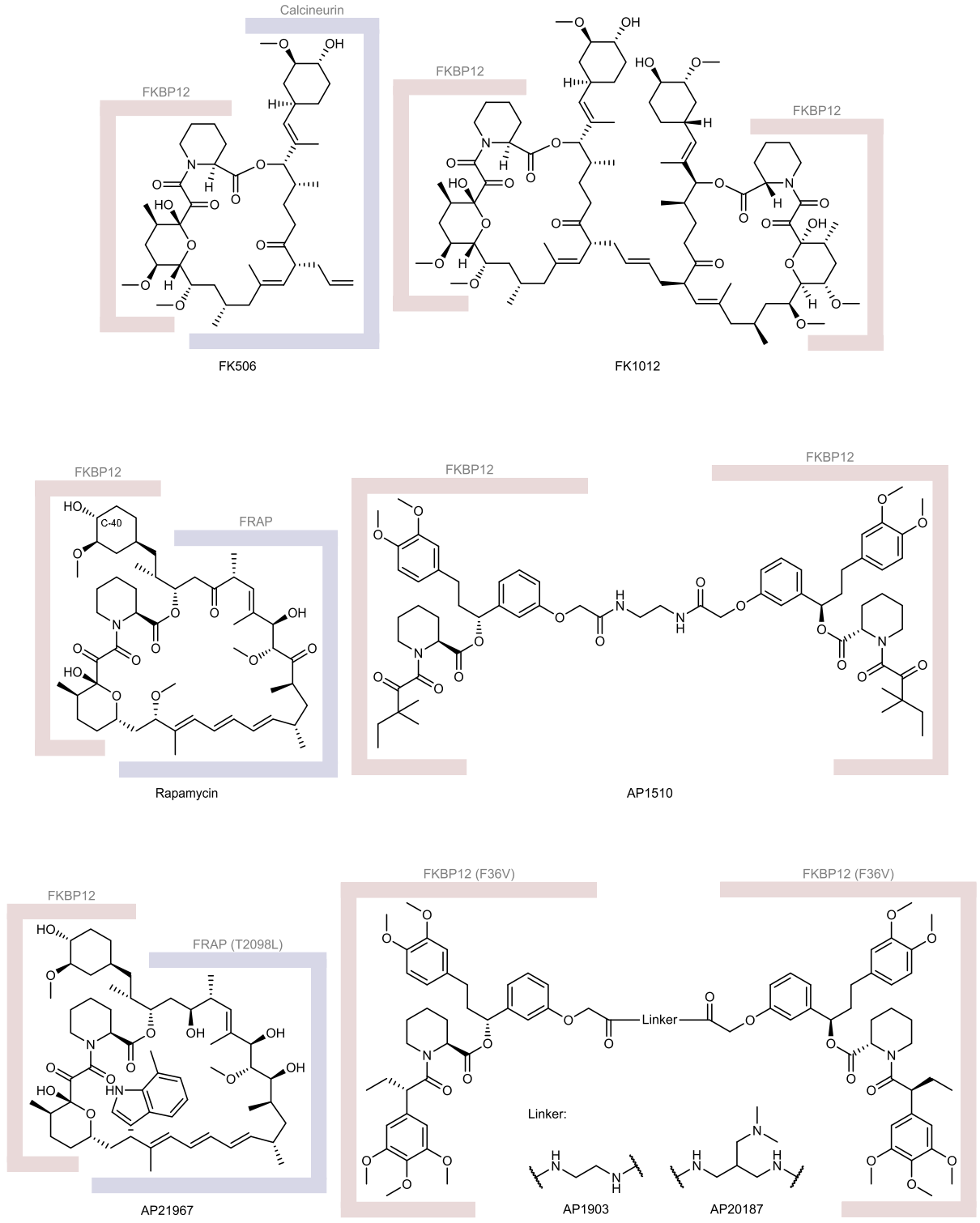

Figure 4: Chemical structures of FK506, FK1012, rapamycin, AP21967 as well as of AP1903 and AP20187. Binding proteins are depicted schematically in light red and light blue.

Application in CAR T cell therapy

Rapalogs have also been applied in the medical research to implement a safety switch in CAR T cell therapy. CAR T cell therapy is an approved treatment of leukaemia. In this therapy, T cells are isolated from the patient's blood and genetically modified to produce a chimeric antigen receptor (CAR) against surface exposed proteins of the cancer cells. Then, CAR T cells are able to recognize and bind to the

cancer cells. Upon binding, CAR T cells are activated and convert into cytotoxic T cells that destroy the cancer cells. Prior reinjection of the CAR T cells, the patient is treated with chemotherapeutics to reduce the level of endogenous immune cells. The CAR T cells proliferate inside the patient and provide a long-lasting protection against the cancer. CAR receptors consist of extracellular binding domain (an antibody fragment that binds a surface antigen of the cancer cell), a transmembrane domain (to anchor the CAR in the cell membrane of the T cell) and a signaling domain (that upon binding of the CAR to a cancer cell activates the T cell).[21]

However, problems of CAR T cell therapy are a lack of external control after injection of the CAR T cells into the patient as well as the absence of a dose-response relationship. An often observed side effect is an overreaction, also known as cytokine release syndrome, which can lead to death of the patient.[21] To finetune the activity of CAR T cells, the development of on- and off-switches is off high interest. In this context, CIPs that can be externally administered provide a potential solution.

In 2011, the rapalog AP20187 was investigated as off-switch for CAR T cell therapy. FKBP12 (F36V) was fused to the inducible caspase 9 that upon treatment with the CIP and induction of dimerization became activated and induced cell death. This mechanism was introduced into CAR T cells and it was shown, that in patients treated with these CAR T cells rapid cell death of cells expressing this construct is induced upon exposure to AP20187.[22]

Already in 1993 it was reported, that the rapalog FK1012 can be used to activate membrane receptors through induction of oligomerization.[9] Based in this strategy an on-switch CAR was developed and used in CAR T cells in 2015.[23] The CAR was split into two parts, one consisting of the extracellular binding domain, the transmembrane domain and FKBP12 and the other one consisting of the transmembrane domain linked to intracellular FRB (T2098L) and a signaling domain. Upon treatment with the rapalog AP21967 the split CAR is reconstituted to a functional receptor that is able to activate CAR T cells. The applicability of this system was shown with on-switch CAR T cells injected into mice.[23]

Photoactivation

Photoactivatable derivatives of immunosuppressant-based CIPs have been developed[24–27] but face the challenge that due to the large molecular size and thus a large interaction surface with the relevant proteins, sufficiently suppressing the activity by attaching a photolabile protecting group is difficult because of insufficient steric hindrance.

In a first approach, this issue was circumvented by chemically linking rapamycin to biotin via a photocleavable linker. This compound was incubated with the biotin binding protein avidin resulting in a complex that is unable to cross the plasma membrane. Upon irradiation, rapamycin was released from the complex, which was able to enter the cells and induce light triggered protein proximity (2011).[27]

In the same year a rapamycin derivative linked to a photolabile nitrobenzyl group via a carbonate at the hydroxyl moiety at the C-40 position (Figure 4) of rapamycin was developed (pRap). It was hypothesized that this hydroxyl moiety forms an essential hydrogen bond to a glutamine residue (Q53) of FKBP12. However, pRap induced protein proximity of wildtype FKBP12 and FRB also without light irradiation to a similar extend than with light irradiation. Based on this observation the authors tested iFKBP[28], a FKBP12 variant that was claimed to have increased mobility in the loop region between K52 and E54. When live mammalian cells expressing iFKBP and FRB were treated with pRap, protein proximity was only induced upon irradiation and not in the absence of light, proofing successful photoactivation.[24]

In 2015, a rapamycin dimer consisting of two rapamycin units linked by a photocleavable linker at their C-40 positions was developed (dRap). This molecule binds to two FRB proteins in the absence of light and was shown to induce protein proximity between FKBP12 and FRB in live mammalian cells upon irradiation.[26]

An optimized version of photoactivatable rapamycin (aRap) was presented in 2021. A very bulky photolabile nitrobenzyl-based group was linked to the hydroxyl moiety at the C-40 position of rapamycin. With this photocaged derivative no association of wildtype FKBP12 and FRB in the presence of aRap and without irradiation was observed, only upon irradiation protein proximity was induced. It was shown, that this system can be used for light-trigger temporal control over the reconstitution of split proteins, protein stability and protein localization in live mammalian cells. The application of aRap was also demonstrated in live zebrafish (*danio rerio*) embryos. However, in vivo this molecule can only be used to investigate mTOR signaling and not as bioorthogonal CIP, because rapamycin also targets of the endogenous protein FRAP and FKPB12.[25]

1.2.2 Induction of protein trimerization with rapamycin

In 2020, it was demonstrated that small molecule non-covalent binding CIPs cannot only be used to induce protein dimerization but also trimerization. Based on the CIP rapamycin and the target proteins FRB (T2098L) and FKBP12 a trimerization system was developed based on splitting one of the interacting proteins into two fragments. Starting from a crystal structure of the ternary FRB-rapamycin-FKBP12 complex, split pairs of FRB (T2098L) or FKBP were generated with split sites in different solvent exposed loops. These split pairs were screened for their ability to induce trimerization with their respective full-length partner FKBP or FRB (T2098L) in the presence of rapamycin, identifying a split FRB variant as best hit to induce rapamycin-dependent proximity of both FRB (T2098L) split fragments and FKBP12. It was shown, that this system can be applied to combine the formation of bi-organellar junction sites with recruitment of a cytosolic protein as well as to induce a tri-organellar junction formation in live mammalian cells. However, this trimerization system suffers from the non-

orthogonality of rapamycin in mammalian cells and the rapamycin-triggered association of the split fragments in the absence of their protein partner.[29]

1.3 Plant hormone-based CIP systems

Besides immunosuppressants, also plant hormones have been investigated to chemically induce protein proximity in a non-covalent manner. CIP systems based on plant hormones have the advantage that they are bioorthogonal, since usually neither the plant hormones themselves nor the corresponding proteins are present in mammalian cells and have a function there. Moreover, plant hormones are smaller in size than immunosuppressants making them easier to access synthetically via standard organic chemistry and also facilitating the inactivation of the molecule by attaching photolabile protecting groups.

Systems based on the following CIPs (Figure 5) have been develop and applied as described below.

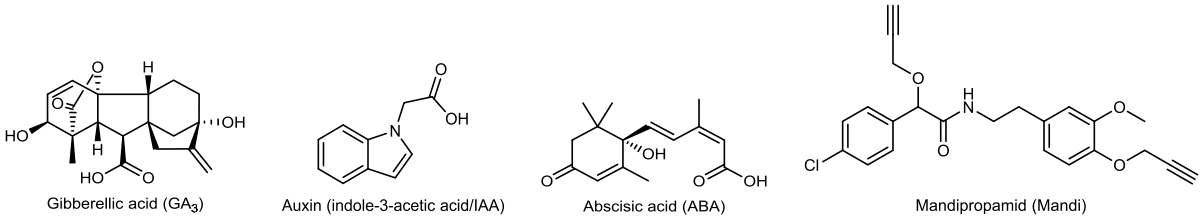

Figure 5: Chemical structures of gibberellic acid (GA_3), auxin (indole-3-acetic-acid/IAA), abscisic acid (ABA) and mandipropamid (Mandi).

1.3.1 Gibberellic acid (GA_3)

Gibberellic acid (GA_3) (Figure 5) is a plant hormone from the group of gibberellins (tetracyclic diterpene acids) that play a role in many developmental processes in plants.[30] GA_3 binds to the receptor protein GID1 (gibberellin insensitive dwarf 1) and induces a conformational change resulting in the recruiting of the receiver protein GAI (gibberellin insensitive), that is part of the family of transcriptional regulator DELLA proteins.[31] Upon this recruiting event the DELLA proteins are enabled to recruit the ubiquitin ligase complex SCF (consisting of Skp1, Cullin, an F-box protein and RBX1) leading to the ubiquitination and degradation of the DELLA proteins.[30]

In 2012, this system was first used to induce protein proximity in live mammalian cells.[32] The polar carboxylic acid moiety of GA_3 was caged as acetoxymethyl (AM) ester so that the molecule can cross the plasma membrane. Intracellularly, the AM group is cleaved via endogenic esterases and unprotected GA_3 is released. AM-protection of carboxylic acid moieties is a common strategy to improve the cell permeability of small organic molecules by reducing their polarity.[33] The GAI protein was truncated to reduce its size and exclude protein binding sites that are relevant for protein degradation. Upon expression of GID1 (38.6 kDa) and truncated GAI (13.0 kDa) (both from *arabidopsis thaliana*) in mammalian cells, protein proximity could be induced upon addition of AM-protected GA_3. A CIP system was obtained that is orthogonal to the CIP system based on rapamycin and it was shown that both CIPs can be combined to construct logic gates.[32]

GA_3 was also used as on-switch in CAR T cells. Upon treatment with the CIP a split CAR T receptor was reconstituted and the CAR T cells were activated (2015).[23]

The CIP GA_3 is also compatible with a use in mice as demonstrated in a study with cancer cells expressing GID and GAI fusion proteins that were injected into mice.[34]

Photoactivation

The carboxylic acid moiety of GA_3 is crucial for the interaction with the receptor protein GID1[35], thus attaching a photolabile protecting group at this position via an ester bond enables photoactivation. Upon irradiation and cleavage of the photolabile protecting group the active compound is released and protein proximity is induced. In 2015, the application of different nitrobenzyl-caged GA_3 derivatives for photoactivation was demonstrated in live mammalian cells (2015).[36,37]

Since GA_3 has limited cell permeability because of its carboxylic acid moiety the molecule is trapped inside the cell upon uncaging after irradiation. This enabled to induce protein proximity in individual cells spatiotemporally separated upon successive irradiation of different cells in the same cell culture dish.[36,37]

1.3.2 Auxin (IAA)

Auxin, also called IAA (indole-3-acetic acid) (Figure 5), is a plant hormone controlling growth and development via a protein degradation system. In plants, it induces protein proximity between the F-box protein transport inhibitor response 1 (TIR1) and Aux/IAA transcriptional coregulator proteins, called AIDs (auxin-inducible degrons).[38] The TIR1 protein is part of the ubiquitin ligase complex SCF (consisting of Skp1, Cullin, an F-box protein and RBX1), therefore auxin-induced recruiting of AIDs leads to their ubiquitination and degradation by the proteasome and regulates related transcription in plants.[39]

In 2009, it was shown that not only in plant cells but also in live mammalian cells artificially expressing TIR1 (from *oryza sativa* which is more thermostable than TIR1 from *arabidopsis thaliana*) and AID (from *arabidopsis thaliana*) a target protein fusion fused to AID can be degraded upon treatment with auxin.[40] To make the system usable to induce protein proximity not only in the context of targeted protein degradation TIR1 was modified to lose its binding affinity to Skp1 in order to inhibit the formation of the SCF complex.[41] Moreover, the AID protein was reduced in size to minimize perturbance of the fused protein of interest (POI).[41] The resulting CIP system with TRI1* (64.1 kDa) and AIDΔ34 (10.2 kDa) as interacting domains is orthogonal to other plant hormone-based systems, shows dose-dependency and reversibility (2018).[41] Auxin is also compatible with a use in live zebrafish embryos.[42]

Photoactivation

Auxin was further photocaged at its carboxylic acid moiety and the resulting derivatives were used for photoactivation. For experiments in plants, auxin was photocaged via an ester bond with different nitrobenzyl groups and as amide with the 4-methoxy-7-nitroindolinyl-group. All compounds could be used for photoactivation, but the amide-caged derivative exhibited the lowest background activity justified in the highest stability in the absence of irradiation (2009/2015).[43,44] A nitrobenzyl-caged auxin derivative was also applied in live mammalian cells in the context of targeted protein degradation and it was shown that spatiotemporal control is possible. Upon irradiation of only a specific region of interest (ROI) on a cell culture dish only there protein degradation was induced (2018).[45]

1.3.3 Abscisic acid (ABA)

The plant hormone abscisic acid (ABA) (Figure 5) regulates plant development as well as responses of plants to stress. Because it plays a role in the water consumption and drought tolerance of plants it is of particular interest in plant research. In periods of water deficiency for instance, plants produce elevated levels of ABA which leads to closure of the guard cell aperture in the epidermis and less water transpiration (and also higher leaf temperature).[46]

Upon binding of (+)-(*S*)-abscisic acid to the binding pocket of receptor proteins of the PYL/PYR/PCAR family a conformational change is induced in the binding protein. This change creates a binding surface on top of the binding pocket for receiver proteins of the protein phosphatase 2C (PP2C) family (e.g. ABI1 (ABA insensitive 1) or HAB1 (hypersensitive to ABA 1)), which are inhibited upon binding and further signal transduction events are regulated.[47,48,49] It was shown that the binding of the PP2C protein significantly boosts the apparent ligand binding affinity. ITC (isothermal titration calorimetry) experiments revealed that the affinity of the ligand to both interacting proteins is 50-fold to 100-fold higher than the affinity of the ABA receptor alone to its ligand in the absence of a PP2C receiver protein.[50,51]

In 2011, ABA was first used as CIP in live mammalian cells. Based on the crystal structure[47] of the protein PYL1 (pyrabactin resistance like 1) in complex with ABA and the protein ABI1, the protein sequences were reduced to the relevant binding sites. Moreover, a D143A mutation was introduced to ABI1 to suppress phosphatase activity. The resulting proteins PYL (20.4 kDa) and ABI (32.6 kDa) (both from *arabidopsis thaliana*) were used to induce protein proximity in live mammalian cells with ABA and orthogonality to rapamycin and the proteins FKBP12 and FRB was demonstrated. No signs of toxicity were observed.[52]

ABA has been used as CIP in live mammalian cells for several application[53] as well as in cancer cells expressing the ABA-based CIP system that were injected in mice[34].

It was also shown that by using the more cell permeable AM ester of ABA the working concentration could be lowered and the translocation time to induce protein proximity in live mammalian cells upon addition of the CIP decreased (2021).[54]

Photoactivation

By attaching photolabile protecting groups to the carboxylic acid moiety of ABA the molecule is inactivated. In 2015, nitroveratryl- and coumarin-caged ABA derivatives were used to induce protein proximity in live mammalian cells upon irradiation.[55] However, upon irradiation half of the released ABA is converted into the inactive cis-isomer.[55] It is known, that the double bond close to the carboxylic acid moiety of ABA is prone to isomerization upon light exposure. In fact, photoinduced isomerization of the biologically active cis-isomer to the nearly inactive trans-isomer may also be a control mechanism in plants.[56]

ABA agonists

Since ABA is of high interest in plant research, effort have been made to identify and develop agonists that allow to influence ABA related signaling in plants. These molecules were aimed to be characterized by higher potency, no light sensitivity and less structurally complexity making them easier to synthesize compared to ABA. The structure-activity relationship was investigated for several ABA analogues.[57]

First ABA agonists were based on the core structure of abscisic acid, extending the cyclohexenol motif of abscisic acid by an aromatic phenyl system yielding tetralone abscisic acid (Figure 6) (2006).[58]

In 2009, it was shown that the synthetic growth inhibitor pyrabactin (Figure 6) binds to the ABA binding pocket of PYR1 (pyrabactin resistance 1), induces HAB1 recruiting, its inhibition and further ABA signaling. Pyrabactin also activates other ABA receptor proteins in the presence of HAB1 but with a lower sensitivity. The structure of pyrabactin was not based on abscisic acid and consists of two aromatic systems linked via a sulphonamide.[49]

In a screen of a large library of compounds to activate five different ABA receptors in the presence of HAB1 a yeast two-hybrid assay was used as readout identifying the sulfonamide quinabactin as ABA agonist (2013). It is characterized by a 3-fold higher potency to inhibit HAB1 upon binding to PYR1 compared to ABA and a 6-fold higher potency compared to pyrabactin. Moreover, the activation of other ABA receptor proteins in the presence of HAB1 was improved compared to pyrabactin.[59]

In 2017, the ABA agonist cyanabactin was developed, which is more selective towards PYR1 in the presence of HAB1 than quinabactin. The sulfonamide cyanabactin inhibits HAB1 upon binding to PYR1 equally well as quinabactin, but inhibits HAB1 in the presence of other ABA receptor proteins and with reduced potency.[60]

To further design an ABA agonist with a higher affinity to a large variety of ABA receptor proteins a virtual screen with available ligands was conducted (2019).[51] The hits could be clustered into

sulfonamides like pyrabactin, cyanabactin and quinabactin, substituted aminopropanediols and amino acid amides. Since the class of the amides showed the highest activity across all tested ABA receptor proteins, the most active amide was further chemically optimized based on the structural motifs of existing ABA agonists as well as on crystal structure-based anticipations. This led to the compound opabactin (OP) (Figure 6) that has a 7-fold higher affinity to PYR1 and HAB1 than ABA. The binding affinity was determined by ITC to K_d = 28 nM compared to K_d = 201 nM for ABA and K_d = 103 nM for quinabactin.[51]

None of the ABA agonist was up to now investigated regarding an application as CIP besides probing ABA signaling in plants.

ABA antagonists

To have the ability to not only activate but also negatively regulate ABA signaling in plants, ABA antagonists have been developed. These molecules have in common that they bind to the ABA binding pocket of ABA receptor proteins but block the interaction with the receiver proteins of the PP2C family. The formation of a ternary complex is prevented and the signaling cascade interrupted.

Most ABA antagonists are ABA derivatives covalently linked to an alkyl chain. Based on crystal structure models this chain points outside the binding pocket towards the receiver protein. Different chains were investigated that differ in length, rigidity, terminal moiety and chemical reconstitution, also different positions to attach the extension to ABA were tested (2014-2021).[61]

Moreover, ABA antagonists were developed to specifically block the interaction to a conserved tryptophan residue on the receiver proteins. In 2018, the ABA antagonist PANMe (Figure 6) was published that mimics the indole moiety of tryptophan with a phenyl ring.[62] This compound was also applied in live mammalian cells (under the name revABA) to reverse protein proximity that was previously induced with ABA (2021).[54]

The most potent ABA antagonist was reported in 2021, called antabactin (ANT) (Figure 6). For increased binding affinity to ABA receptor proteins, it is based on the ABA agonist opabactin (OP). This binding motif is covalently linked to fluoroquinoline group that blocks the interaction to the conserved tryptophan residue on the receiver proteins. Moreover, the fluoroquinoline group increases the affinity by occupying the tryptophan binding cleft on the receptor protein.[63]

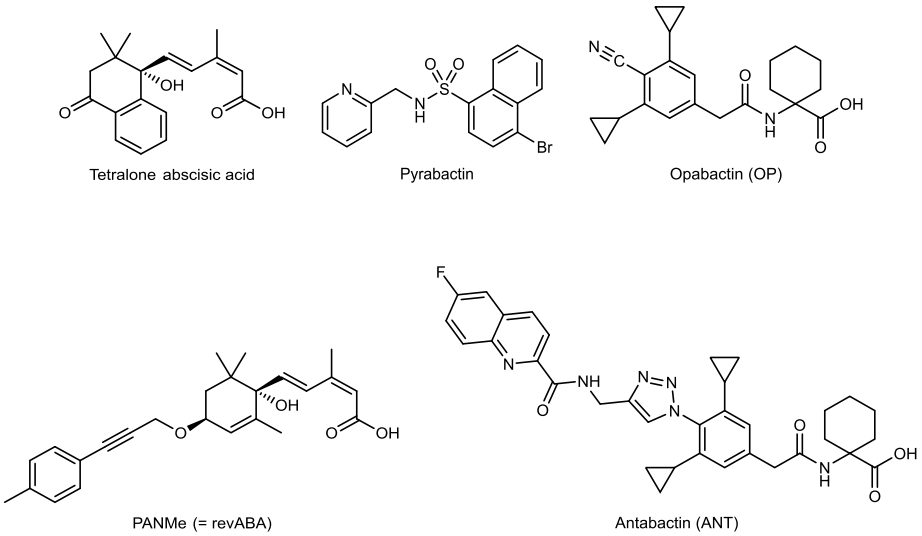

Figure 6: Chemical structures of the ABA agonists tetralone abscisic acid, pyrabactin and opabactin (OP) as well as the ABA antagonists PANMe (= revABA) and antabactin (ANT).

Another class of ABA derivatives are ABA-biotin conjugates. Similar to ABA antagonists these molecules only bind to ABA receptor proteins but can additionally be recruited via the biotin group to a biotin binding protein (e.g. streptavidin). Hence, they were used to identify ABA binding proteins (2013-2019).[64]

Protein engineering on ABA responsive proteins

In 2015, it was first shown that the native ABA receptor protein can be modified to respond to other molecules than ABA. As described in Section 1.3.4 below all single mutants of the 25 residues in the ABA binding pocket of PYR1 were screened against 15 different agrochemicals. Each mutant was tested individually and after several rounds of mutagenesis including the combination of positive mutations and DNA shuffling the modified ABA receptor PYR^{Mandi} was obtained that responds to Mandi with nanomolar sensitivity in the presence of the receiver protein HAB1.[65]

Biosensors for organophosphates and cannabinoids based on the ABA receptors were published in 2022. This time, a larger library of PYR1 mutants with double mutants of the amino acids in the ABA binding pocket was used as starting point. To facilitate selection of positive clones a yeast two-hybrid growth selection was performed. Then, DNA shuffling was performed with positive clones and PYR1 variants were obtained that respond to specific neurotoxic organophosphates and specific cannabinoids with nanomolar sensitivity in the presence of the receiver protein HAB1.[66]

Moreover, a cannabinoid responding PYR variant was immobilized on magnetic nanorods and applied for detecting cannabinoids in vitro (2023).[67]

In the above described approaches only the ABA receptor protein PYR1 was reengineered, the receiver protein HAB1 was not mutated and is recruited from all obtained PYR1 variants.[65,66]

In 2023, an orthogonal PYR1/HAB1 pair was developed including also the engineering of the receiver protein HAB1. First, libraries of PYR1 and HAB1 with single amino acid mutations at their binding interface were screened against their native partners to identify non-binders in the presence of ABA. These non-binding variant of PYR1 and HAB1 were co-transformed and after a growth-based yeast two-hybrid selection in the presence of ABA a binding pair with an additional salt bridge at binding interface of PYR1 and HAB1 was identified. However, this orthogonal binding pair showed reduced affinity towards its ligand. In a next step, the orthogonalizing mutations were introduced onto the PYR^{Mandi}/HAB1 pair and to improve the sensitivity further mutagenesis of the binding interface combined with positive and negative selections yeast two-hybrid selections was conducted. This led to the identification of a $PYR1^{Mandi}$*/HAB1* pair that is orthogonal to native PYR1 and HAB1 (PYR1 does not recruit HAB1* in the presence of ABA, $PYR1^{Mandi}$* does nor recruit HAB1 in the presence of Mandi) and showed nanomolar responsiveness to Mandi. The same strategy was also demonstrated for an orthogonal PYR1/HAB1 pair responding to the organophosphate azinphos-ethyl. The developed orthogonal PYR1*/HAB1* pairs can be used for the sensing of different analytes in same system, as orthogonal CIP systems, for logic gating and as an orthogonal CIP system or biosensor in plants without interfering ABA signaling. Moreover, the authors claim that their strategy is the starting point to build CIP systems around user defined ligands.[68]

1.3.4 Mandipropamid (Mandi)

In a study on transgenic plants the modified ABA receptor protein PYR^{Mandi} was developed that binds mandipropamid (Mandi) (Figure 5) instead of ABA but has the same downstream functions: The binary PYR^{Mandi}-Mandi complex recruits PP2C proteins and initiates ABA signaling in plants (2015).[65] Since compounds that activate ABA receptors were not yet approved for use in agriculture, the authors wanted to engineer an ABA receptor that responds to an already existing agrochemical. First, the ABA responsiveness of PYR1 (from *arabidopsis thaliana*) was eliminated by introducing a K59R mutation, then a single amino acid mutant library of the 25 amino acids in the binding pocket for ABA was created and screened against 15 different agrochemicals using a yeast two-hybrid assay. Positive mutations were combined and after several rounds of mutagenesis (e.g. DNA shuffling) the sextuple mutant PYR^{Mandi} = PYR1 (Y58H, K59R, V81I, F108A, S122G, F159L) with nanomolar sensitivity to Mandi in the presence of a receiver protein was obtained. Upon binding to PYR^{Mandi} Mandi inhibits both receiver proteins, HAB1 and ABI1 equally well.[65]

Mandi is an approved agrochemical (trade name: Revus)[69] and acts as fungicide against the pathogen (*phytophthora infestans*) that causes late blight on potato and tomato plants. It also shows good efficacy as a fungicide against the downy mildew pathogen (*plasmopara viticola*) on grape vine.[69] The fungicidal effect of Mandi is not related to binding to plant hormone receptors.

A crystal structure of PYR^{Mandi} in complex with Mandi and a receiver protein could not be obtained, but of the quadruple mutant PYR^{Mandi*} that already selectively binds Mandi but with lower affinity in complex with Mandi and HAB1.[65] The ternary PYL1-ABA-ABI1 complex and the ternary PYR^{Mandi*}-Mandi-HAB1 complex are structurally very similar (Figure 7).

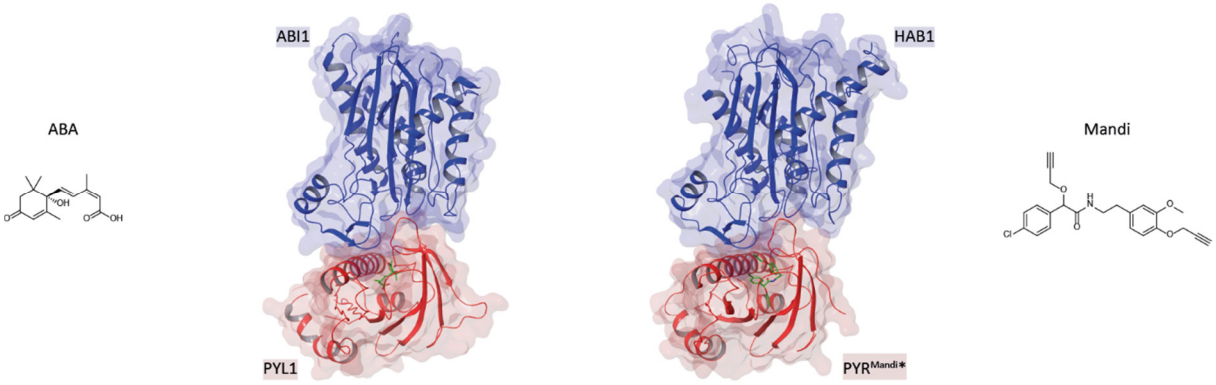

Figure 7: Crystal structures of the PYL1-ABA-ABI1 complex (pdb: 3JRQ) and the PYR^{Mandi*}-Mandi-HAB1 complex (pdb: 4WVO) with chemical structures of the respective ligands ABA and Mandi.

In 2021, it was demonstrated that Mandi in combination with its receptor protein PYR^{Mandi} cannot only be used to control the ABA responses in plants, but also to induce protein proximity between PYR^{Mandi} (21.5 kDa) and ABI (32.6 kDa) fusion proteins in live mammalian cells as well as in zebrafish embryos.[54] In comparison with the plant hormone-based CIPs GA_3 and ABA as well as the immunosuppressant-based CIP rapamycin, Mandi achieves faster translocation times and requires lower working concentrations in live mammalian cells. The CIP Mandi is further characterized by a small molecular size and the absence of charged functional groups resulting in good cell permeability and possesses low toxicity and a high affinity to PYR^{Mandi} and ABI. Mandi is semi-orthogonal to the CIP ABA since both compounds bind to different receptor proteins, PYR^{Mandi} or PYL, but recruit the same receiver protein, ABI, derived from the PP2C family. This property was used for targeted shuttling of an ABI fusion protein to different subcellular location where the respective receptor proteins were located.[54]
Mandi is easily accessible via chemical synthesis[70], so that potential derivatives can be produced with only few synthetic steps.

2 Objective

The investigation and regulation of cellular processes requires tools to manipulate these processes with high specificity. To achieve this, chemical inducers of proximity (CIPs) are an attractive and versatile tool to precisely manipulate protein-protein interaction and study complex biological processes in live cells and in vivo.[2]

Especially the plant hormone-based CIP systems based on GA_3, ABA and Mandi that rely on the molecular rachet mechanism, are non-toxic and bioorthogonal in live mammalian cells are attractive for use in vivo (see Section 1.3).[32,52,54] With regards on translocation times and working concentrations the CIP Mandi is superior (see Sections 1.3.1, 1.3.3 and 1.3.4).[54]

One aim of this work was to introduce a further control over the induction of protein proximity by chemical modification of this CIP.

In this respect, antagonists for the CIP Mandi were to be developed. Antagonists for Mandi are not yet reported and offer the possibility of reversing protein proximity that was previously induced by Mandi and downregulating or switching off the targeted manipulation.

To control protein proximity with an external stimulus, a photocaged derivative of Mandi should be established that puts the induction of protein proximity under the control of light irradiation and can be applied in live mammalian cells and in vivo. Moreover, a tool that allows photoactivation with single-cell resolution was to be developed. This is particularly attractive for applications that require to induce processes in single cells in the same sample. Photoactivatable derivatives of ABA and GA_3 have been reported previously but require high working concentrations and thus cannot easily be applied in vivo (see Sections 1.3.1 and 1.3.3).[36,37,55]

Another aim was to investigate and modify the protein domains that respond to treatment with Mandi. The CIP system based on Mandi was to be extended from protein dimerization to trimerization by splitting one of the interacting protein domains. A system to chemically induce protein trimerization already exists based on the immunosuppressant-based CIP rapamycin[29], but suffers from its non-orthogonality in live mammalian cells. A plant hormone-based inducible trimerization system would overcome this issue.

Additionally, it should be investigated whether the protein domains interacting with the CIP Mandi can be reduced in size to minimize the perturbance of the proteins of interest (POIs) fused to the interacting protein domains responding to Mandi.

3 Results and discussion

3.1 Mandi as CIP

Mandi was described as CIP in 2021. Its applicability to induce protein proximity of the proteins PYR^{Mandi} and ABI at nanomolar working concentration in live mammalian cells was demonstrated, however an accurate determination of the dissociation constant (K_d) of the ternary complex formation was not performed.[54]

Now, to compare the CIP system based on Mandi to other CIP systems and as reference for the characterization of Mandi derivatives designed in this work, I performed ITC experiments with recombinantly expressed proteins (Figure 8).

ITC does not only provide information about the binding affinity (dissociation constant (K_d)), but also about the thermodynamic properties (changes of enthalpy (ΔH), entropy (ΔS) and Gibbs free energy (ΔG)) of the complex formation. As ITC is an in vitro method that does not require any modification or labeling of neither the protein nor the ligand, the interactions can be read out without any interference.

The K_d for the binding of Mandi to the proteins PYR^{Mandi} and ABI was determined to be high double-digit nanomolar (K_d = 90 ± 7 nM). Compared to literature data on the affinity of ABA to its interacting proteins PYR1 and HAB1 by ITC (K_d = 201 ± 14 nM)[51], Mandi is around 2-fold more potent. This is in good alignment with the reported lower working concentration of Mandi as CIP in live mammalian cells compared to ABA.[54] As expected for a complex formation, the entropy decreases and the process is driven by enthalpy (Table 1). The affinity of Mandi to the receptor protein PYR^{Mandi} alone is around 75-fold lower (K_d = 6700 ± 500 nM) than in the presence of ABI. This characteristic is known for ABA receptors[50,51] (see Section 1.3.1) and also applies to the CIP system based on Mandi that is derived from an ABA receptor.

If only the binding affinity is considered, Mandi is less potent compared to the CIP rapamycin, that binds the proteins FRB and FKBP12 with sub-nanomolar affinity (K_d = 0.1 nM)[71,72]. However, the binding characteristics are different: FKBP12 alone binds rapamycin with a similar affinity (K_d = 0.2 nM) than in the presence of FRB which is different form the binding behavior of PYR^{Mandi}. The FKBP12-rapamycin complex has a nanomolar affinity (K_d = 12 nM) to FRB. The other interacting protein FRB alone binds rapamycin with a micromolar affinity (K_d = 26 µM).[71,72]

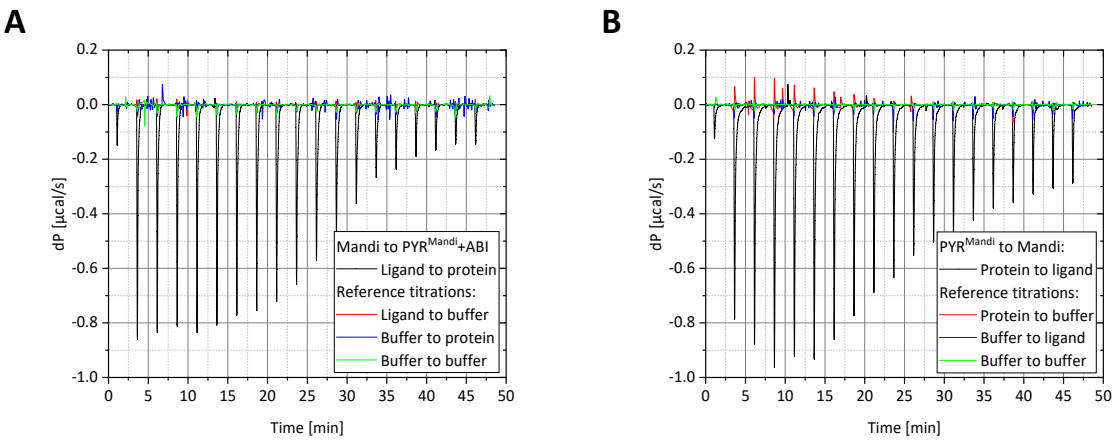

Figure 8: Characterization of the binding of Mandi to PYR^{Mandi} and ABI as well as only to PYR^{Mandi} in vitro. ITC titration of 100 µM Mandi to 20 µM PYR^{Mandi} and ABI (A) as well as of 500 µM PYR^{Mandi} to 50 µM Mandi (B) with reference titrations.

Table 1: Thermodynamic characterization of the binding of Mandi to PYR^{Mandi} and ABI as well as only to PYR^{Mandi} via ITC. Values represent the mean and the standard deviation the mean of the indicated number of replicates.

Ligand	Protein(s)	K_d [nM]	ΔH [kcal/mol]	-TΔS [kcal/mol]	ΔG [kcal/mol]	Number of replicates
Mandi	PYR^{Mandi}+ABI	90 ± 7	-32.2 ± 1.0	22.3 ± 1.0	-9.94 ± 0.05	4
Mandi	PYR^{Mandi}	6700 ± 500	-17.1 ± 1.1	9.8 ± 1.0	-7.30 ± 0.05	3

To investigate and evaluate the Mandi derivatives designed in this work regarding their function to induce or reverse protein proximity in live mammalian cells, I established a colocalization assay.

The receptor protein PYR^{Mandi} was expressed as fusion protein with the red fluorescent protein mCherry and TOMM20, a localization sequence to the outer mitochondrial membrane with the C-terminal attached proteins pointing inside the cytosol. The receiver protein ABI was expressed as fusion protein with the green fluorescent protein eGFP without any localization sequence, resulting in cytosolic expression. The induction of protein proximity between PYR^{Mandi} and ABI, e.g. upon treatment with Mandi, leads to colocalization of mCherry and eGFP fluorescence at the outer mitochondrial membrane (Figure 9). This can be easily read out via fluorescence microscopy.

Live cell experiments were conducted with U2OS cells, a human derived cell line that is adherent, easy to handle and therefore well suited for fluorescence microscopy experiments. Protein constructs were overexpressed under the control of the CMV promotor.[73] Stable cell lines expressing the protein constructs (see Section 5.6.3) were generated und used for all experiments to evaluate the synthesized compounds. This allows more reproducible experiments and a more balanced protein expression compared to transient transfection.

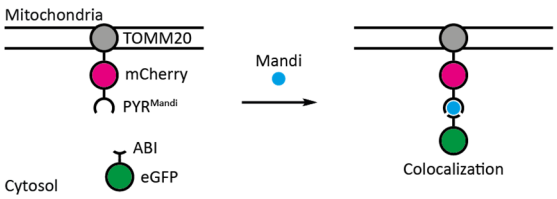

Figure 9: Schematic representation of the used colocalization assay for the induction of protein proximity with Mandi as CIP.

The colocalization assay was validated by a titration of Mandi onto live mammalian cells expressing TOMM20-mCherry-PYR^{Mandi} and eGFP-ABI (Figure 10).

At a concentration of 500 pM Mandi, no induction of protein proximity was observed after 30 min, the cytosolic ABI-GFP fusion construct is not recruited to the outer mitochondrial membrane where the receptor protein PYR^{Mandi} is located. In contrast, addition of 5 nM Mandi resulted in weak recruiting of the cytosolic ABI-GFP protein to the outer mitochondrial membrane after 30 min. At concentrations ≥ 50 nM Mandi, fluorescence colocalization indicating the induction of protein proximity is achieved in less than 5 min. Mandi can thus be used at concentration ≥ 50 nM for rapid induction of protein proximity. In the absence of Mandi, the proteins PYR^{Mandi} and ABI do not associate (Figure 84, Section 7.2).

This results are in good agreement with previous reported literature data on working concentration and translocation time of Mandi as CIP in live mammalian cells.[54]

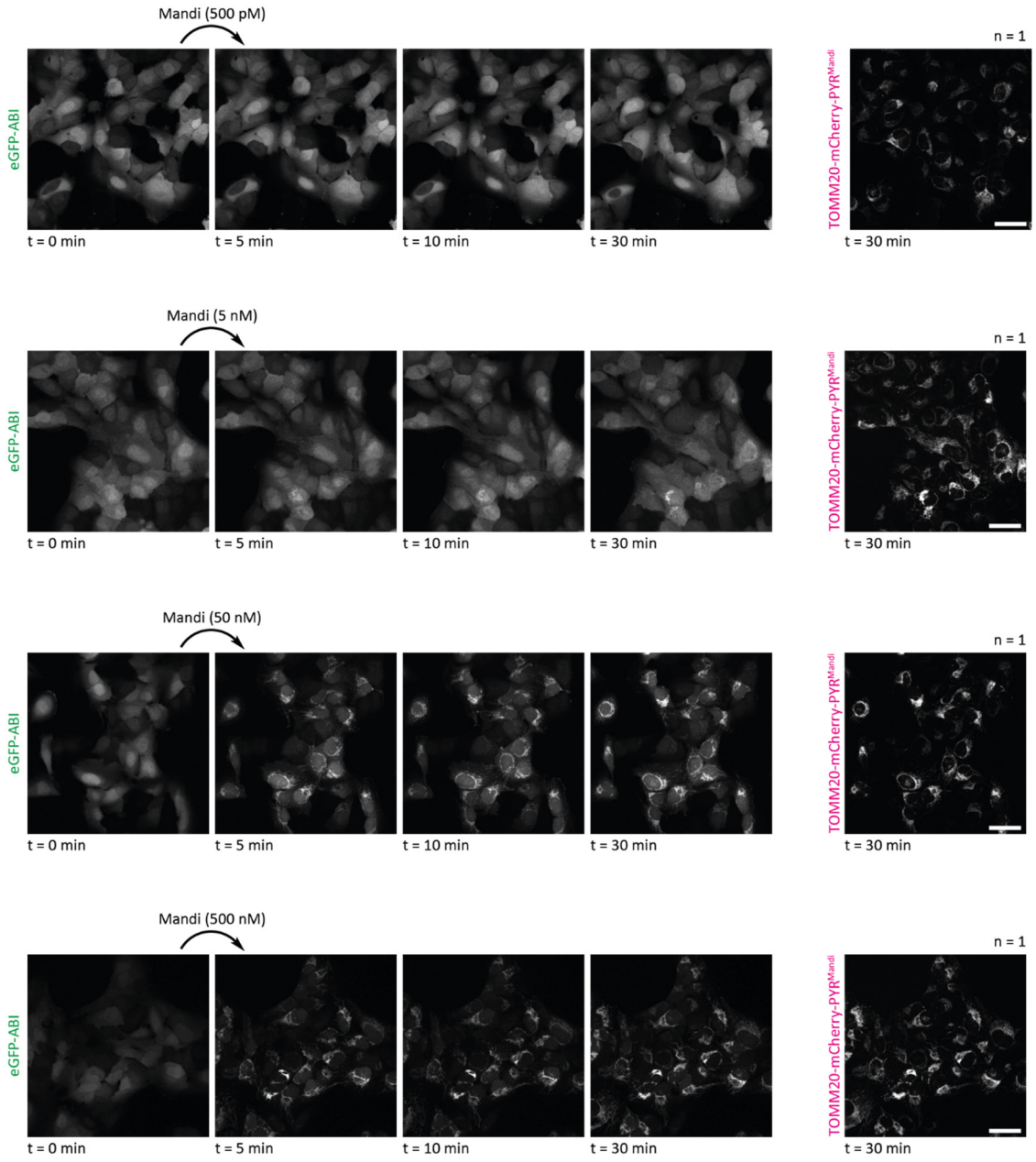

Figure 10: Titration of Mandi on live cells expressing TOMM20-mCherry-PYR^{Mandi} and eGFP-ABI. Confocal microscopy images of U2OS FlpIN cells stably expressing TOMM20-mCherry-PYR^{Mandi} and eGFP-ABI before and at different timepoints post addition of different concentrations of Mandi. Indicated number n of replicates. Scale bars at 40 µm.

It was previously shown that Mandi can be applied as CIP in live zebrafish embryos.[54] In this work, I used live medaka embryos (*oryzias latipes*) as in vivo model (in collaboration with Kaisa Pakari who performed the microinjections).

Similar to experiments in live mammalian cells a colocalization assay with fluorescent proteins as readout was used. As subcellular localization I chose the plasma membrane, the receptor proteins PYR^{Mandi} was expressed as fusion protein with mCherry and Lyn, a localization sequence to the plasma membrane with the C-terminal attached proteins pointing inside the cytosol. The receiver protein ABI was expressed as fusion protein with eGFP without any localization sequence, resulting in cytosolic expression. At the one-cell stage, medaka embryos were microinjected with mRNA (generated via in

vitro transcription) encoding both protein constructs in equal molar amounts. Experiments to induce protein proximity were performed 2 days post fertilization (dpf).[74] At this timepoint, the amount of expressed protein is still high enough to achieve sufficient signal intensity in fluorescence microscopy while at the same time the embryo is as far in its development as possible. Since the mRNA is not stable over time in the medaka embryos and also the expressed proteins are diluted and degraded during the embryonic development, experiments can only be performed in short timeframe after microinjection. However, microinjection of mRNA is an easy and fast method to artificial express proteins in medaka embryos and further results in protein expression in all cells of the embryo. Medaka embryos were dechorionated and mounted in agarose gel. The tail of the medaka embryos was imaged with a confocal florescence microscope. By imaging one plane of the tail, cells in different tissue depths are visualized as well as different cell types. A solution of the CIP in embryo rearing medium (ERM) was added on top of the agarose embedded embryo (see Section 5.8).

For the validation of the in vivo colocalization assay, I treated agarose embedded medaka embryo with different concentrations of Mandi (Figure 11). Recruiting of the cytosolic fusion protein to the plasma membrane was observed at a concentration as low as 500 nM Mandi within 2 h, indicating that protein proximity can be induced at sub-micromolar concentrations in all depths of the tissue. At 5 µM Mandi, protein proximity was induced slightly faster after 90 min. A concentration of 50 nM Mandi was not sufficient to induce protein proximity within 180 min (Figure 88, Section 7.2).

Compared to experiments in live zebrafish embryos presented in literature, the working concentration is the same, but in live zebrafish embryos protein proximity was induced significantly faster, 10-20 min after addition of 500 nM Mandi.[54] This may be because a different amount of agarose gel was used to mount the embryo and hence the time Mandi needs to diffuse to the agarose gel differs or because the permeability inside a medaka embryo is different from the permeability inside a zebrafish embryo. Nevertheless, the experiments showed that Mandi can be used as CIP in live medaka embryos at sub-micromolar concentration.

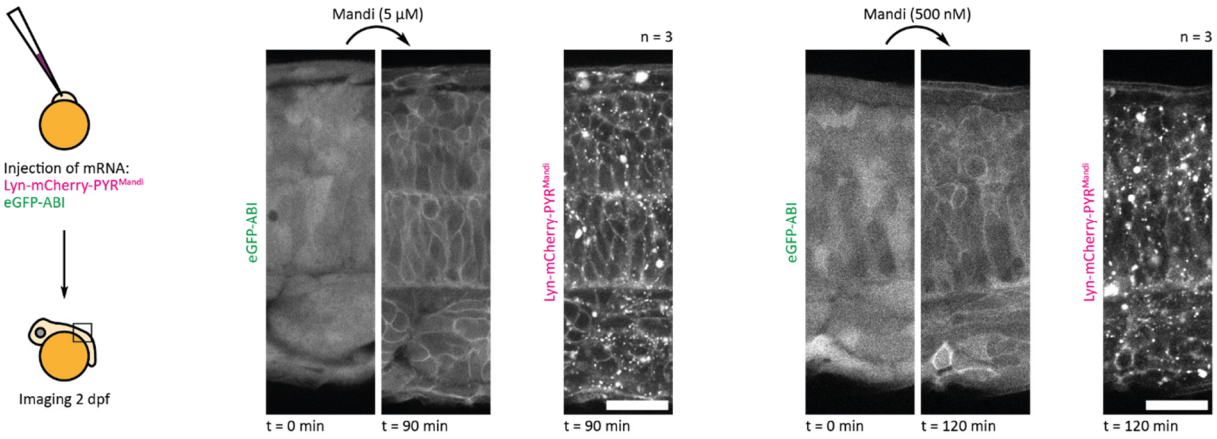

Figure 11: Application of Mandi as CIP in live medaka embryos. Medaka embryos were microinjected with mRNA in the one-cell stage and experiments were performed 2 dpf with agarose embedded embryos. Addition of Mandi induces protein translocation to the plasma membrane in eGFP-ABI and Lyn-mCherry-PYR^{Mandi} mRNA injected embryos. Confocal microscopy images of the medaka embryo tail before and 90 min/120 min post addition of 5 µM/500 nM Mandi. Indicated number n of replicates. Scale bars at 20 µm. Microinjection was performed by Kaisa Pakari.

To introduce a further control over the induction of protein proximity the CIP Mandi is modified chemically. The molecule Mandi can be divided in a mandelic acid part and a dopamine part since it can be synthesized via a peptide coupling from a mandelic acid derivative and a dopamine derivative. In this work chemical modifications on the 4’ position of the mandelic acid part, the 4’ position of the dopamine part as well as modifications on the amide nitrogen were investigated (Figure 12).

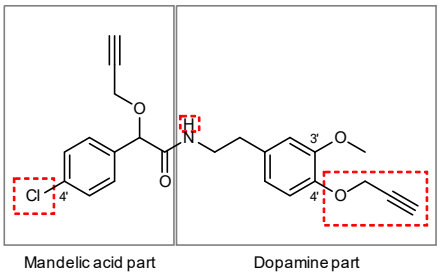

Figure 12: Chemical structure of Mandi. Positions that were modified in this work are marked in red.

3.2 Development of antagonists for Mandi

3.2.1 Methodology to design and investigate antagonists for Mandi

To reverse protein proximity previously induced by Mandi and thus to be able to downregulate or to switch off the targeted manipulation, I developed antagonists for Mandi. Currently no antagonist for CIP Mandi are not reported in literature.

In principle, protein proximity induced by Mandi can also be reversed by washing out the CIP (Figure 13). However, not all experimental setups are easily compatible with washing steps, for example only loosely attached cells or application in higher organisms. An antagonist is an easy and convenient way to confer reversibility.

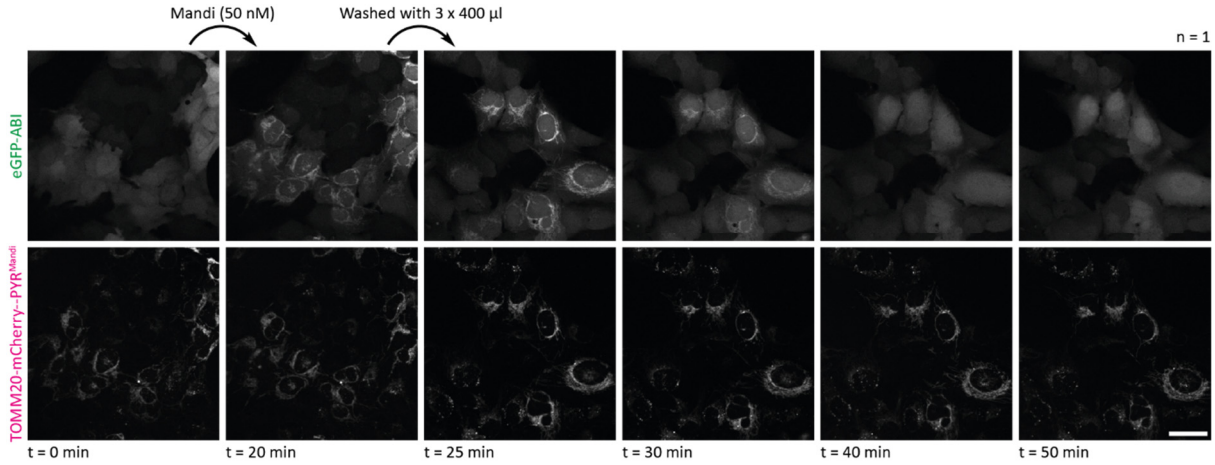

Figure 13: Protein proximity induced by Mandi can be reversed by washing in live mammalian cells. Confocal microscopy images of U2OS FlpIN cells stably expressing TOMM20-mCherry-PYR^{Mandi} and eGFP-ABI before and 20 min post addition of Mandi. Then, cells were washed with 3 x 400 µl medium and further images were taken thereafter. Indicated number n of replicates. Scale bar at 40 µm.

The design of antagonists for Mandi was based on already existing ABA antagonists.[62,63] ABA antagonists have in common that they bind to the ABA receptor protein but block the interaction to the receiver protein (see Section 1.3.3). Mandi has two positions that point outside of the binding pocket towards the receiver protein, the 4' position of the mandelic acid part and the 4' position of the dopamine part (Figure 14). These positions are therefore attractive for attaching moieties that block the interaction to the receiver protein without negatively influencing the binding to the receptor protein PYR^{Mandi}. The residue of the receiver protein in close contact with the binding pocket of the receptor protein are W385 and V393 in HAB1 corresponding to W300 and V308 in ABI1, the full-length version of ABI (ABI = ABI1, amino acids 126-423, D143A). ABA antagonist have been developed that specifically block the interaction to the indole residue of the tryptophan by introducing a linker with a terminal aromatic moieties to their receptor protein binding motif (PANMe[62] and ANT[63]). This approach also increased the binding affinity of the antagonist towards the receptor protein by occupying the binding cleft for the indole moiety on the receptor protein (see Section 1.3.3).

For the development of antagonist for Mandi, in a first step, I attached alkyl chains of different length to the 4’ position of the mandelic acid part and the 4’ position of the dopamine part of Mandi to investigate which length is needed to block the interaction to the receiver protein and to examine which of the two positions is more suitable for the design of antagonists. In a next step, I investigated the attachment of moieties consisting of a linker of different lengths and different terminal aromatic moieties with the aim to specifically block the interaction to the tryptophan of the receiver protein that is close to the Mandi binding pocket and to increase the binding affinity of the antagonists.

Further, I studied the scaffold for the design of Mandi antagonists for fluorescent labeling of the protein PYR^{Mandi} by attaching a fluorophore to Mandi via linker of different lengths. Fluorescent labeling of PYR^{Mandi} could be used to visualize PYR^{Mandi} via fluorescence microscopy, also when it is not expressed as fused to a fluorescent protein. This allows the verification of correct protein localization in experiments where a fusion to a fluorescent protein influences or disturbs the interaction that is to be studied with Mandi as CIP.

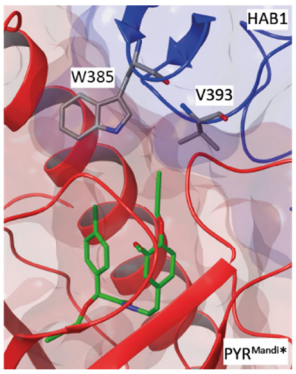

Figure 14: Crystal structure of the binding pocket in the PYR^{Mandi}*-Mandi-HAB1 complex (pdb: 4WVO). Amino acids of HAB1 close to Mandi visualized in gray. W385 and V393 in HAB1 correspond to W300 and V308 in ABI1.

For the screening of the synthesized Mandi antagonist candidates I used two assays in live mammalian cells. First, I investigated whether the antagonist candidates are unable to induce protein proximity of PYR^{Mandi} and ABI at a high concentration of 50 µM (Figure 15). All compounds that induced protein proximity identifying them as Mandi agonists instead of antagonist were excluded from further experiments.

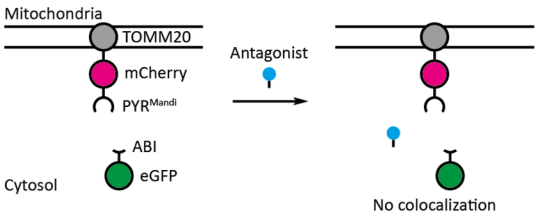

Figure 15: Schematic representation of the used protein constructs and the colocalization assay for screening of antagonist candidates. Antagonists do not induce protein proximity upon addition.

With antagonist candidates that were successful in the first assay, I conducted the following competition assay. First, protein proximity was induced upon treatment with Mandi, then the antagonist candidate was added in excess (1000-fold) and I investigated if the previously induced protein proximity was reversed (Figure 16). Mandi antagonist candidates that successfully reversed protein proximity were tested with a lower excess to Mandi.

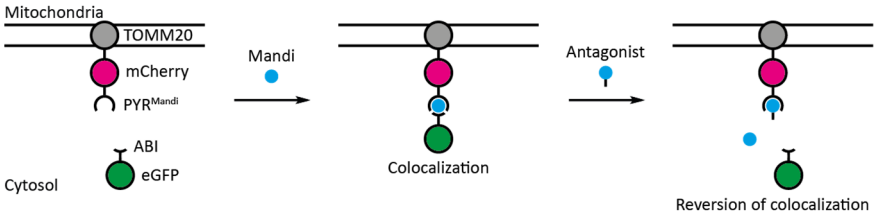

Figure 16: Schematic representation of the used protein constructs and the colocalization assay used for functional validation of antagonist. Upon treatment with Mandi protein proximity is induced that is reversed upon addition of an antagonist.

I kept the initial concentration of Mandi as low as possible (50 nM) to allow huge excess of antagonist (50 µM with 1000-fold excess) and avoid solubility issues of the antagonists at high concentrations. To induce protein proximity 100 nM Mandi were added, that are diluted to 50 nM upon addition of the antagonist candidates. In a negative control experiments, I demonstrated that the dilution of Mandi has no visible effect on protein localization (Figure 17).

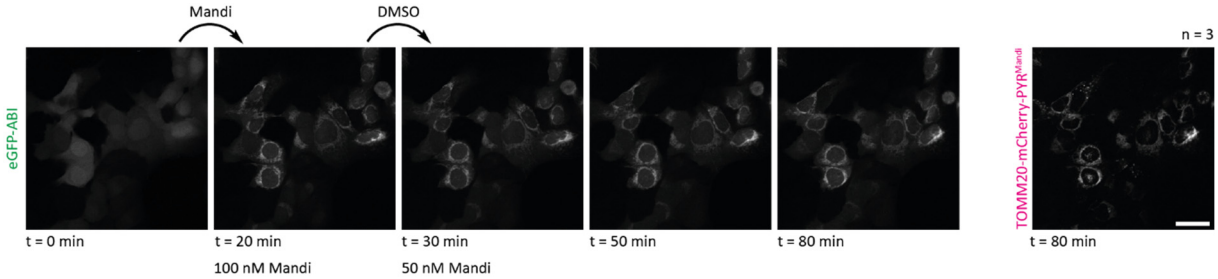

Figure 17: Negative control experiment for the competition assay with Mandi and Mandi antagonists. Confocal microscopy images of U2OS FlpIN cells stably expressing TOMM20-mCherry-PYR^{Mandi} and eGFP-ABI before and 20 min post addition of 100 nM Mandi. Then, DMSO was added and further images were taken thereafter. Indicated number n of replicates. Scale bar at 40 µm.

Further, I investigated the antagonists for Mandi identified in the live cell assays regarding their binding to the receptor protein PYR^{Mandi} in vitro via ITC.

3.2.2 Synthesis and investigation of antagonists for Mandi

Mandi-Dopa-Cn

Mandi antagonist candidates with a linear alkyl extension at the 4’ position of the dopamine part (Mandi-Dopa-Cn) were synthesized via a convergent synthesis from a dopamine building block (**10**-**16**) and a mandelic acid building block (**1**) (Figure 18). For the synthesis of the dopamine building block

(**10**-**16**), the amine moiety of 3-methoxytyramine hydrochloride was protected as formamide (**2**) according to literature[75], then alkyl chains of different length (two to eight carbon atoms, C2-8) were attached to the aromatic hydroxyl group via a nucleophilic substitution (yielding compounds **3**-**9**) and the amine was deprotected again with acid (yielding compounds **10**-**16**). The mandelic acid building block (**1**) was synthesized according to literature[76] from 2-bromo-2-(4-chlorophenyl)acetic acid in a base catalyzed reaction with propargyl alcohol. Then, amide coupling of the two building blocks (**1** and **10**-**16**) yielded Mandi-Dopa-C2-8.

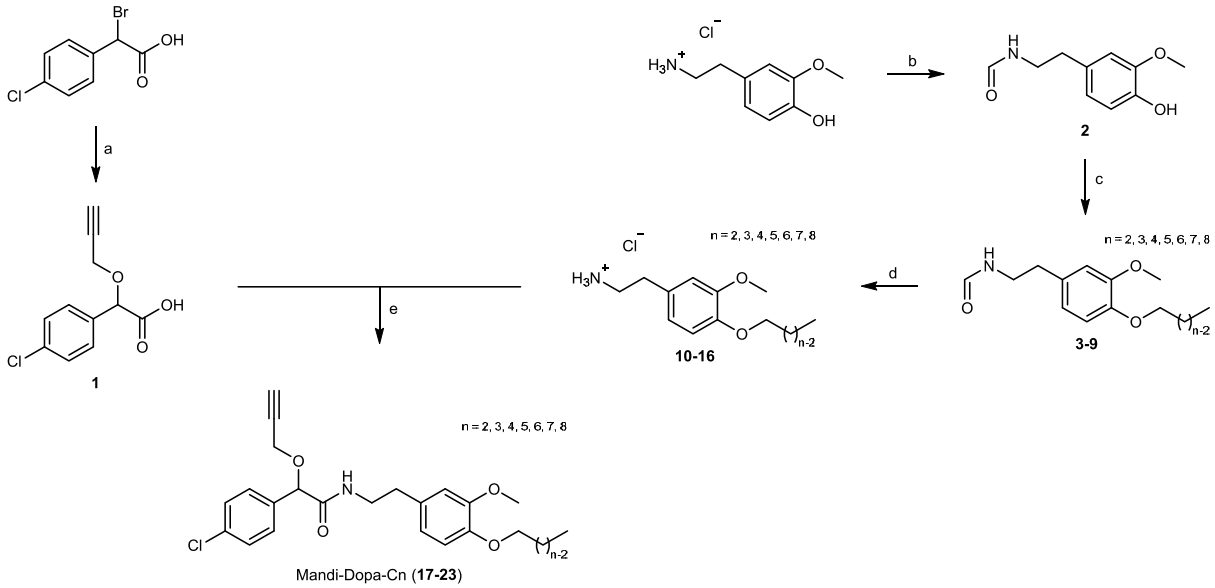

Figure 18: Synthesis of Mandi-Dopa-Cn. a: propargyl alcohol, KOH, rt, 2 h; b: Ac_2O, formic acid, 70 °C, 2 h; c: alkyl bromide, NaOMe, 3 – 4 h, 65 °C or alkyl bromide, K_2CO_3, KI, rt, 22 h; d: HCl, rt, 45 – 92 h; e: HATU, HOBt, DIPEA, rt, 20 – 21 h.

Next, the synthesized Mandi-Dopa-Cn antagonist candidates were tested for their ability to induce protein proximity of PYR^{Mandi} and ABI in live mammalian cells (Figure 19). Mandi-Dopa-Cn compounds with an alkyl extension of two to six carbon atoms induced protein proximity and are Mandi agonists. Only Mandi-Dopa-C7 and Mandi-Dopa-C8 did not induce protein proximity and were further tested in the competition assay (Figure 20). While Mandi-Dopa-C7 only led to partial reversion of the protein proximity previously induced with Mandi after 1 at a 1000-fold excess, treatment with Mandi-Dopa-C8 completely reversed protein proximity within 1 h at a 1000-fold excess. Mandi antagonists were successfully designed by attaching linear alkyl chains to the 4’ position of the dopamine part of Mandi. At a 100-fold excess of Mandi-Dopa-C8, no substantial reversion of protein proximity was observed within 1 h.

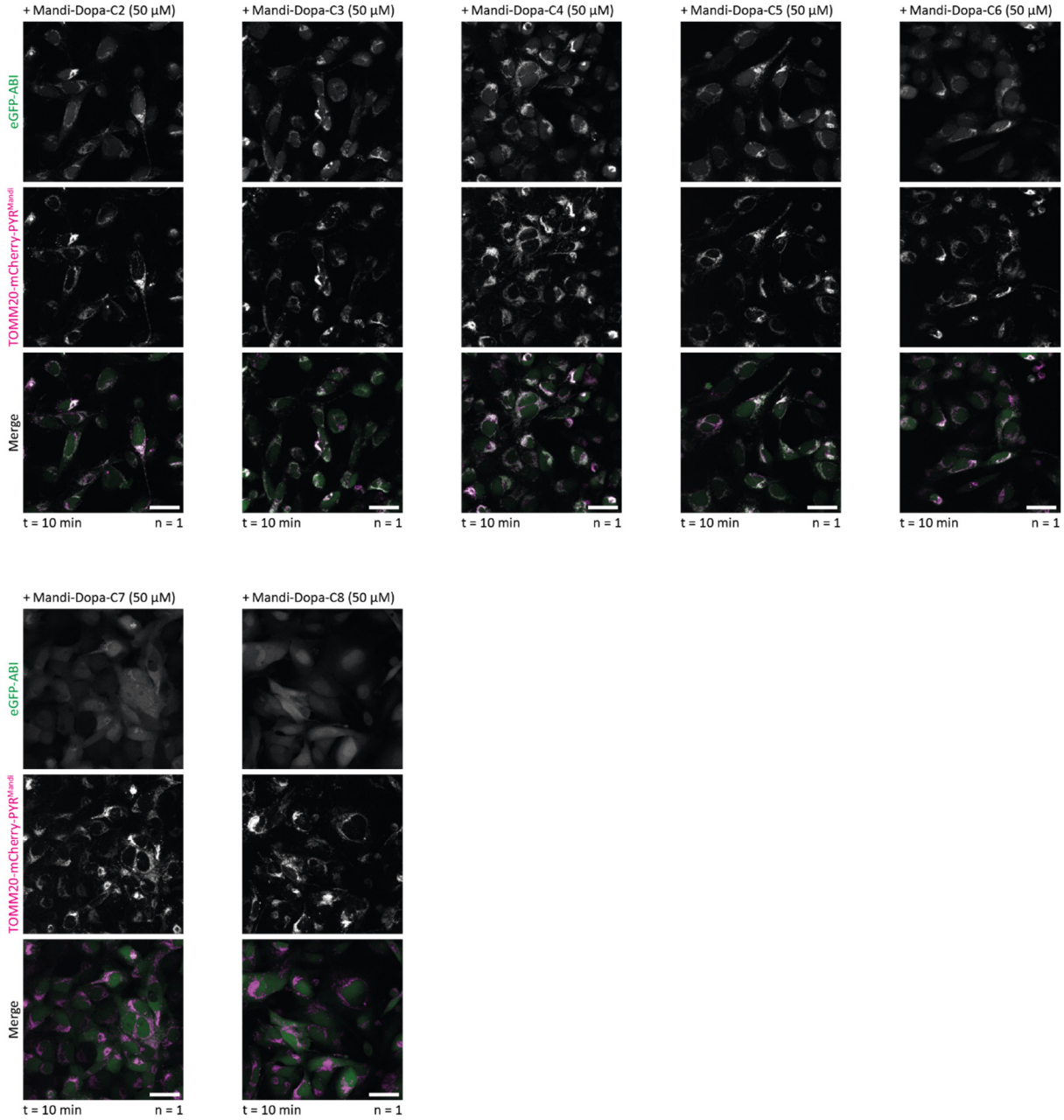

Figure 19: Screen for antagonists with the Mandi-Dopa-Cn scaffold. Confocal microscopy images of U2OS FlpIN cells stably expressing TOMM20-mCherry-PYR^{Mandi} and eGFP-ABI before and 10 min post addition of 50 µM Mandi-Dopa-Cn. Indicated number n of replicates. Scale bars at 40 µm.

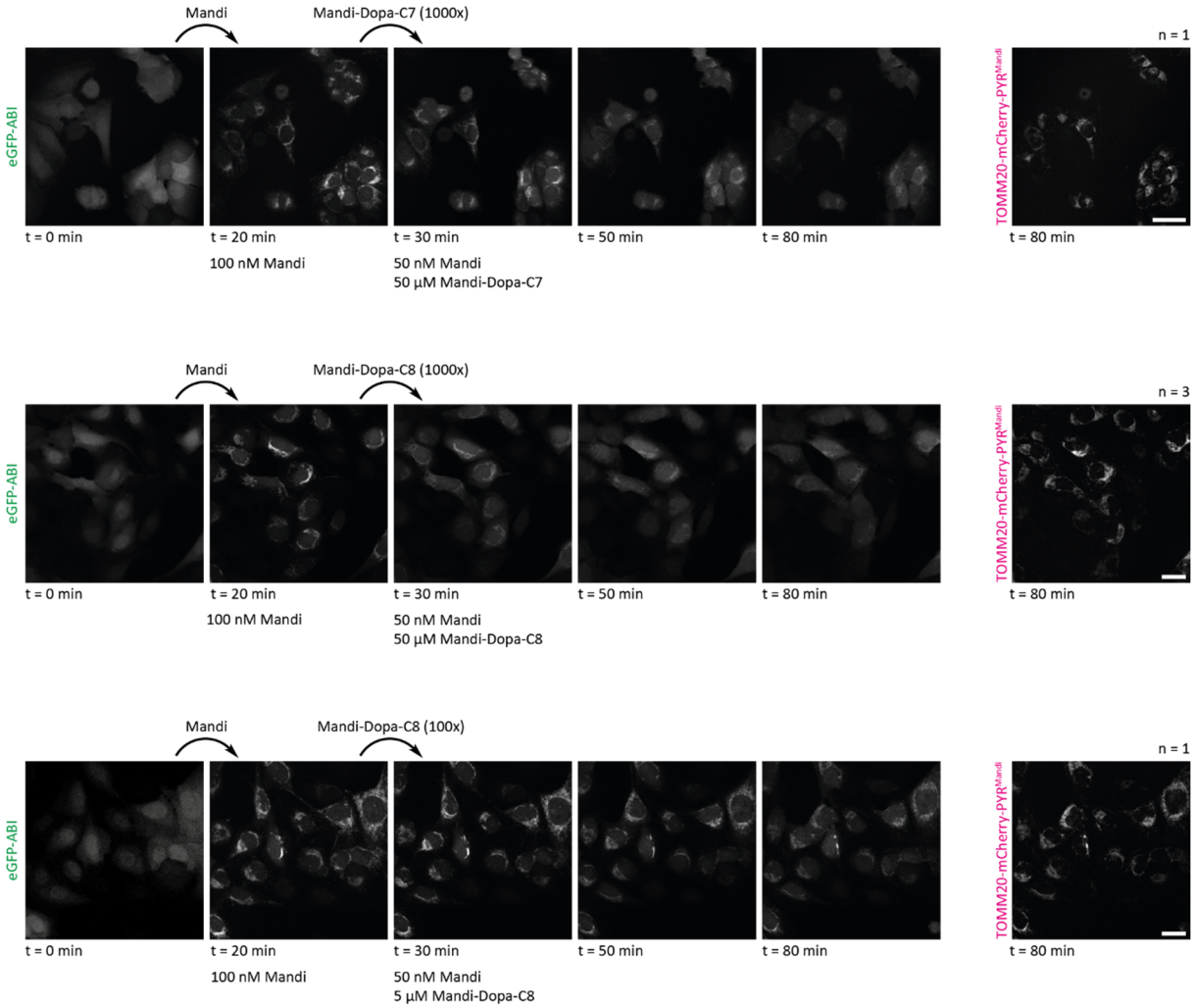

Figure 20: Competition assay with Mandi and Mandi-Dopa-Cn. Confocal microscopy images of U2OS FlpIN cells stably expressing TOMM20-mCherry-PYR^{Mandi} and eGFP-ABI before and 20 min post addition of 100 nM Mandi. Then, different concentrations of Mandi-Dopa-Cn were added and further images were taken thereafter. Indicated number n of replicates. Scale bars at 40 µm.

Mandi-MS-Cn

Mandi antagonist candidates with a linear alkyl extension at the 4' position of the mandelic acid part (Mandi-MS-Cn) were accessed via two different synthetic strategies. The first synthetic strategy involves less steps for the synthesis of only one compound but since the alkyl extensions moieties were attached already in the second synthetic step in total more synthetic steps are required when synthesizing multiple derivatives. In the second strategy the derivatization was carried out in the last synthetic step.

In the first strategy (Figure 21), amide coupling of a dopamine building block (**32**) and different mandelic acid building blocks (**29**-**30**) yielded the final compounds Mandi-MS-C2-3. The dopamine building block (**32**) was synthesized from 3-methoxytyramine hydrochloride according to literature[70,75]. The amine moiety was protected as formamide (**2**) and the aromatic hydroxyl group was reacted with propargyl bromide in a nucleophilic substitution yielding compound **31**. Then the amine was deprotected again with acid to obtain compound **32**. For the synthesis of the mandelic acid

building block (**29**-**30**), the carboxylic acid moiety of 4-hydroxymandelic acid was protected as methyl ester (**24**) and alkyl chains of different length (two to three carbon atoms, C2-3) were attached to the aromatic hydroxyl group via a nucleophilic substitution yielding the compounds **25**-**26**. Then, the aliphatic hydroxyl group was deprotonated and reacted with propargyl bromide to get the compounds **27**-**28**. In a next step the carboxylic acid moiety was deprotected with sodium hydroxide resulting in the formation of the compounds **29**-**30**.

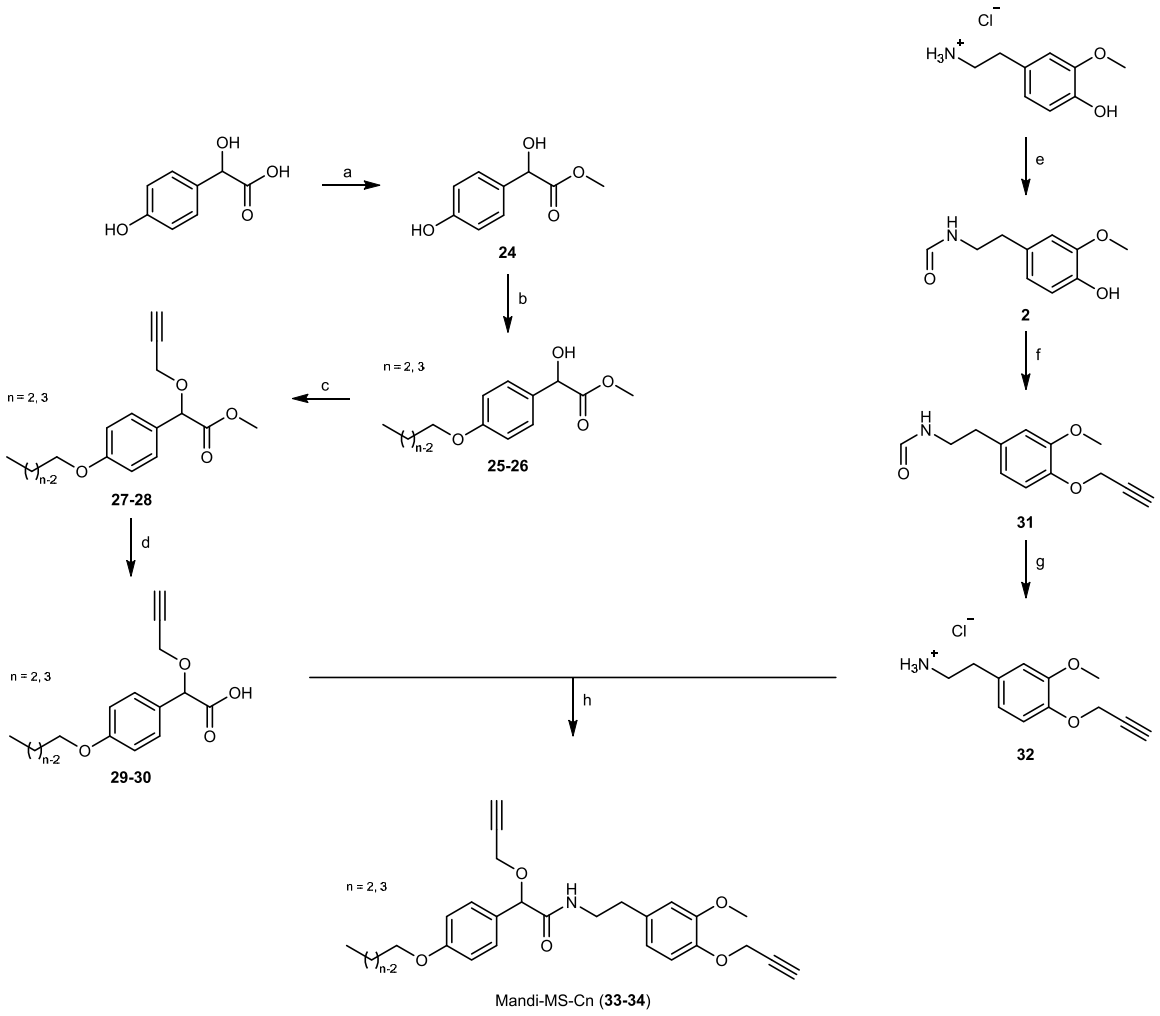

Figure 21: Synthesis of Mandi-MS-Cn, strategy 1. a: MeOH, H_2SO_4, rt, 21 h; b: alkyl bromide, K_2CO_3, KI, rt, 67 h; c: propargyl bromide, NaH, 0 °C -> rt, 2 h; d: NaOH, rt, 16 h; e: Ac_2O, formic acid, 70 °C, 2 h; f: propargyl bromide, NaOMe, 4 h, 65 °C; g: HCl, rt, 91 h; h: HATU, HOBt, DIPEA, rt, 71 h.

In the second strategy (Figure 22), the mandelic acid building block (**37**) was synthesized analogously to strategy 1 but with an allyl protecting group at the aromatic hydroxyl group instead of the alkyl extension. Then, the mandelic acid building block (**37**) was and coupled to the same dopamine building block (**32**) as in strategy 1 via an amide coupling yielding Mandi-MS-Allyl. Thereafter, the allyl protecting group was removed (Mandi-MS-OH) and alkyl chains of different length (four to eight carbon atoms, C4-8) were attached to the aromatic hydroxyl group via a nucleophilic substitution to form Mandi-MS-C4-8.

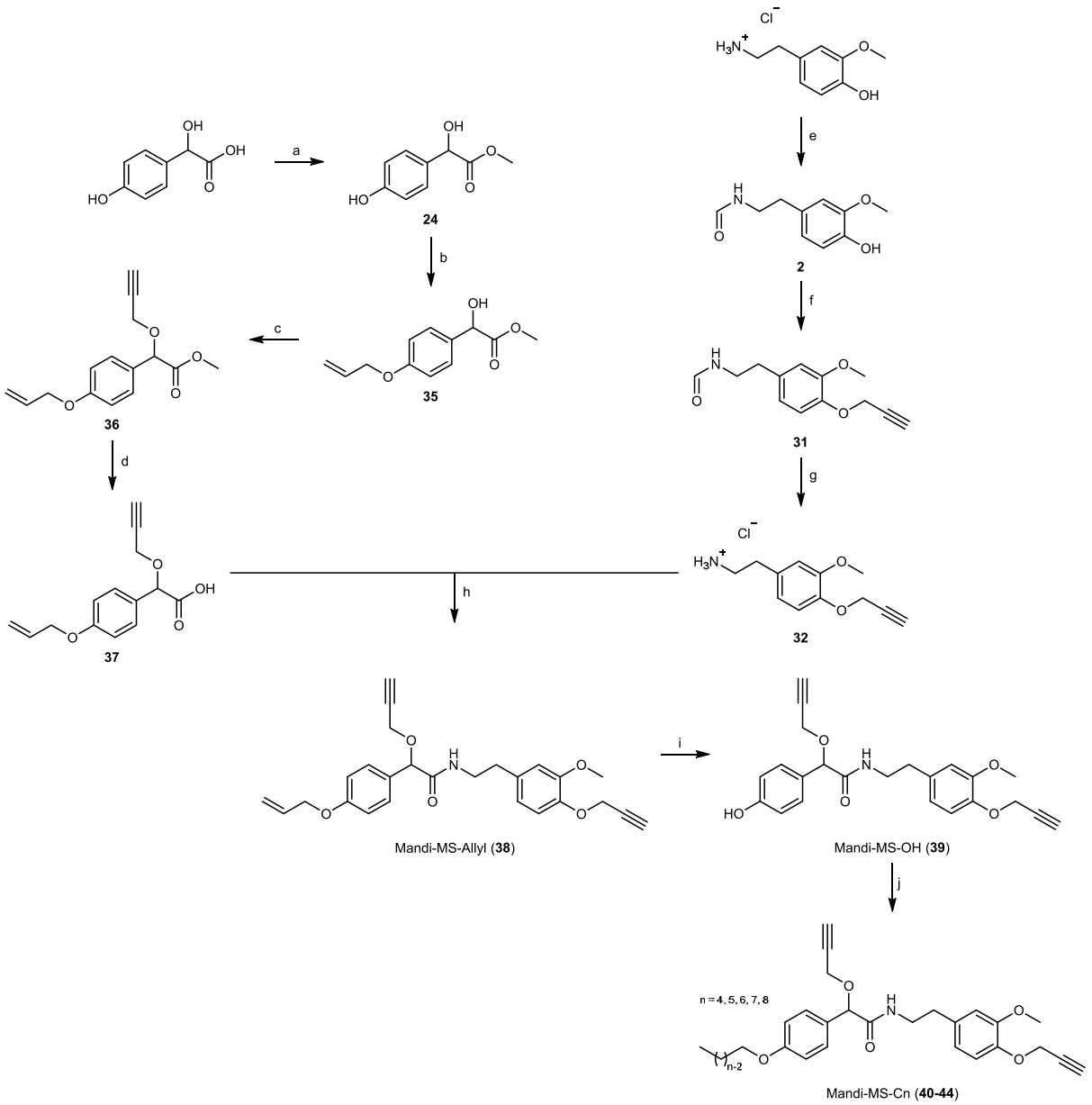

Figure 22: Synthesis of Mandi-MS-Cn, strategy 2. a: MeOH, H_2SO_4, rt, 21 h; b: allyl bromide, K_2CO_3, KI, rt, 70 h; c: 3-bromoprop-1-yne, NaH, 0 °C -> rt, 3 h; d: NaOH, rt, 3 h; e: Ac_2O, formic acid, 70 °C, 2 h; f: 3-bromoprop-1-yne, NaOMe, 4 h, 65 °C; g: HCl, rt, 91 h; h: HATU, HOBt, DIPEA, rt, 19 h; i: $Pd(PPh_3)_4$, K_2CO_3, rt, 2 h; j: alkyl bromide, K_2CO_3, KI, rt, 17 – 72 h.

The synthesized Mandi-MS-Cn antagonist candidates were tested for their ability to induce protein proximity of PYR^{Mandi} and ABI (Figure 23). Similar to the Mandi-Dopa-Cn antagonist candidates the derivatives with an alkyl extension of two to six carbon atoms induced protein proximity and are Mandi agonists. Only compounds with a longer alkyl extension of seven or eight carbon atoms (Mandi-MS-C7 and Mandi-MS-C8) did not induce protein proximity and were investigated in the competition assay (Figure 24).

However, both Mandi-MS-C7 and Mandi-MS-C8 were not able to reverse protein proximity previously induced with Mandi within 1 h when the antagonist candidates were applied at a 1000-fold excess.

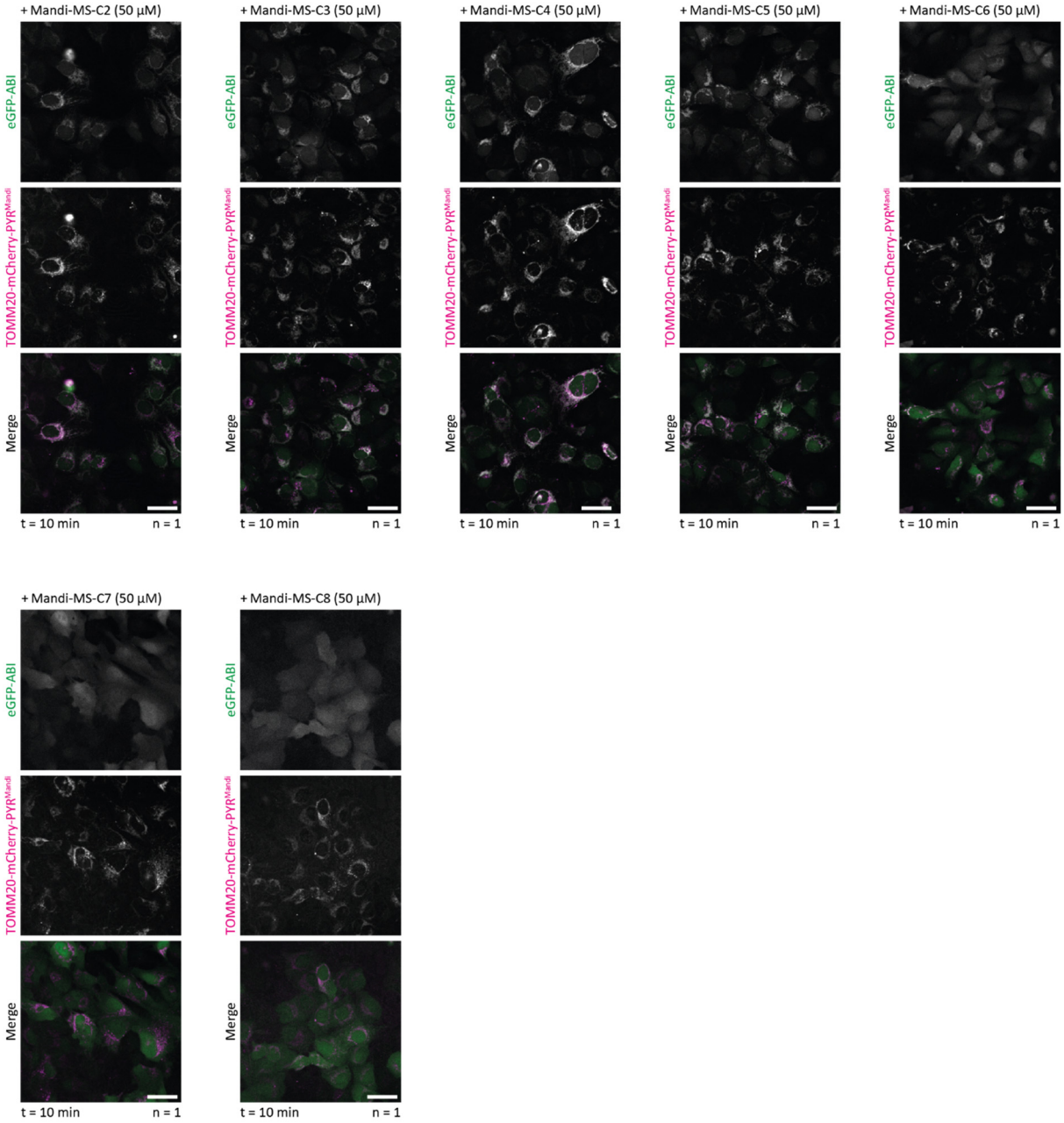

Figure 23: Screen for antagonists with the Mandi-MS-Cn scaffold. Confocal microscopy images of U2OS FlpIN cells stably expressing TOMM20-mCherry-PYR^{Mandi} and eGFP-ABI before and 10 min post addition of 50 µM Mandi-MS-Cn. Indicated number n of replicates. Scale bars at 40 µm.

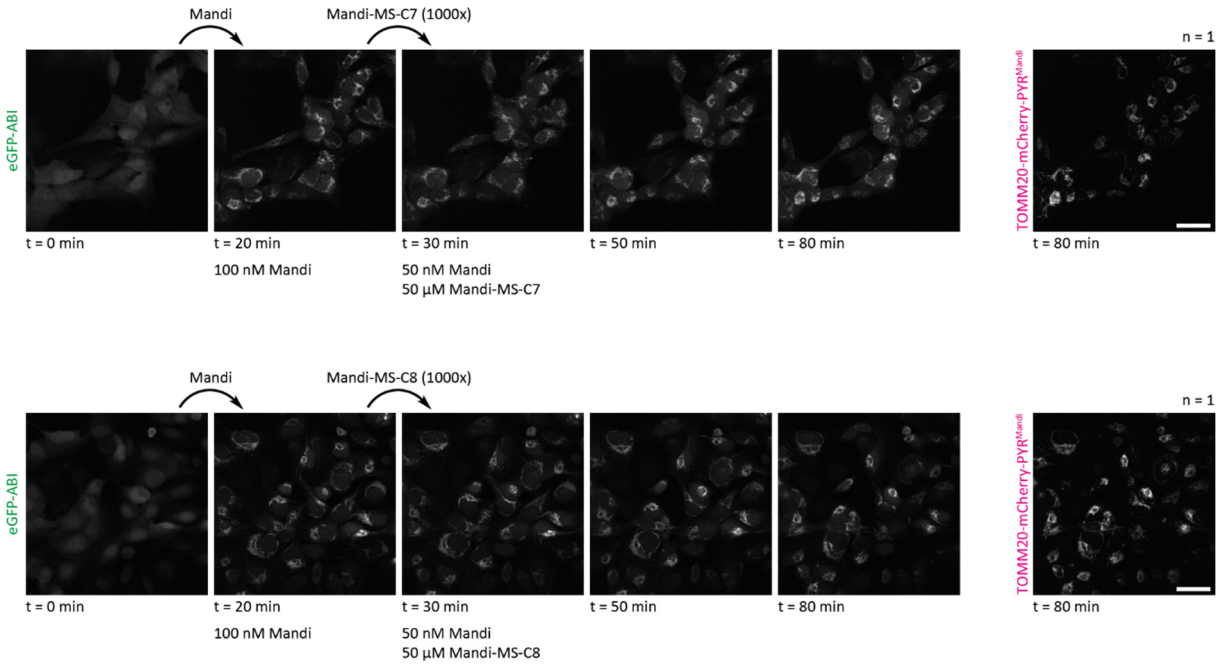

Figure 24: Competition assay with Mandi and Mandi-MS-Cn. Confocal microscopy images of U2OS FlpIN cells stably expressing TOMM20-mCherry-PYR^{Mandi} and eGFP-ABI before and 20 min post addition of 100 nM Mandi. Then, 50 µM Mandi-MS-Cn were added and further images were taken thereafter. Indicated number n of replicates. Scale bars at 40 µm.

Comparing the results of the live cell assays with Mandi derivatives with linear alkyl moieties, Mandi-Dopa-Cn to Mandi-MS-Cn, I concluded that the modification on the 4' position of the dopamine part is more suitable for the design of antagonists for Mandi. Only antagonist candidates with an alkyl extension on the dopamine part were able to reverse protein proximity previously induced by Mandi. Presumably, antagonist candidates with an alkyl extension on the mandelic acid part do not bind PYR^{Mandi} with a sufficiently high affinity while at the same time blocking the interaction to the receiver protein ABI. On the 4' position of the dopamine part, alkyl chains of seven or eight carbon atoms are necessary to block the interaction to the receiver protein ABI, Mandi-Dopa-C8 reversed protein proximity previously induced by Mandi at a 1000-fold excess. In summary, it is possible to design antagonists for Mandi by attaching moieties to the 4' position of the dopamine part.

Mandi-Dopa-Cn-Indole/FQ

To design antagonists for Mandi that require a lower excess to Mandi, extensions with different terminal aromatic moieties were attached to the 4' position of the dopamine part. I hypothesized that these aromatic moieties mimic the interaction of the indole residue of a specific tryptophan on the receiver protein ABI with the receptor protein PYR^{Mandi} (described at the beginning of this Section, Figure 14). Similar modification haven been introduced to ABA antagonists to increase their potency (see at the beginning of this Section and in Section 1.3.3).

In this work, I investigated an indole moiety, the same aromatic moiety that is present in tryptophan, as well as a fluoroquinoline moiety used in the most potent ABA antagonist ANT[63] and screened different linker lengths.

Antagonist candidates with an indole moiety were synthesized from Mandi-Dopa-OH (a Mandi derivative with a free hydroxyl group at the 4' position of the dopamine part), and an indole derivative (**49**-**51**) attached to alkyl linkers of different lengths (**49**-**51**). Mandi-Dopa-OH was synthesized from 3-methoxytyramine hydrochloride and 2-(4-chlorophenyl)-2-(prop-2-yn-1-yloxy)acetic acid (**1**) (generated as described above) via an amide coupling. For the synthesis of the indole building block (**49**-**51**), 2-(1*H*-Indol-3-yl)acetic acid was reacted with amino alkanols with different alkyl chain lengths (four, six or eight carbon atoms, C4,6,8) in an amide coupling yielding the compounds **46**-**48**. Then, the terminal hydroxyl group was converted to a good bromine leaving group in an apple reaction and the resulting the indole derivatives (**49**-**51**) were coupled to Mandi-Dopa-OH via a nucleophilic substitution yielding Mandi-Dopa-C4,6,8-Indole.

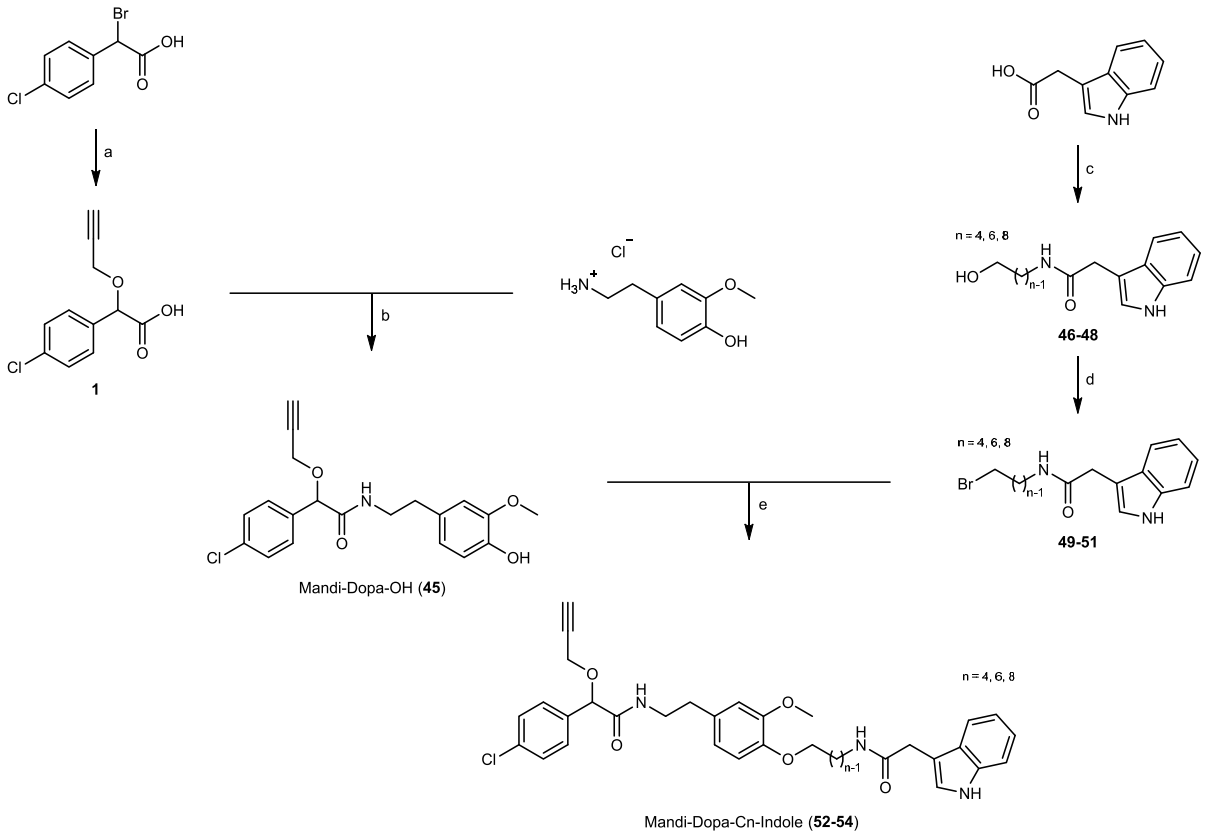

Figure 25: Synthesis of Mandi-Dopa-Cn-Indole. a: propargyl alcohol, KOH, rt, 2 h; b: HATU, DIPEA, rt, 68 h; c: amino alkanol, HATU, DIPEA, rt, 18 h; d: CBr_4, PPh_3, rt, 17 – 24 h; e: K_2CO_3, KI, rt, 21 – 22 h.

For the synthesis of antagonist candidates with a fluoroquinoline moiety, again Mandi-Dopa-OH was used as precursor. Boc-protected amine alkyl bromides with different alkyl chain lengths (six or eight

carbon atoms, C6,8) were linked to Mandi-Dopa-OH in a nucleophilic substitution reaction yielding Mandi-Dopa-Cn-Boc and the terminal amine was deprotected with acid yielding Mandi-Dopa-Cn-Amine. In a next step, 6-fluoroquinoline-2-carboxylic acid was attached via an amide coupling to obtain Mandi-Dopa-C6,8-FQ.

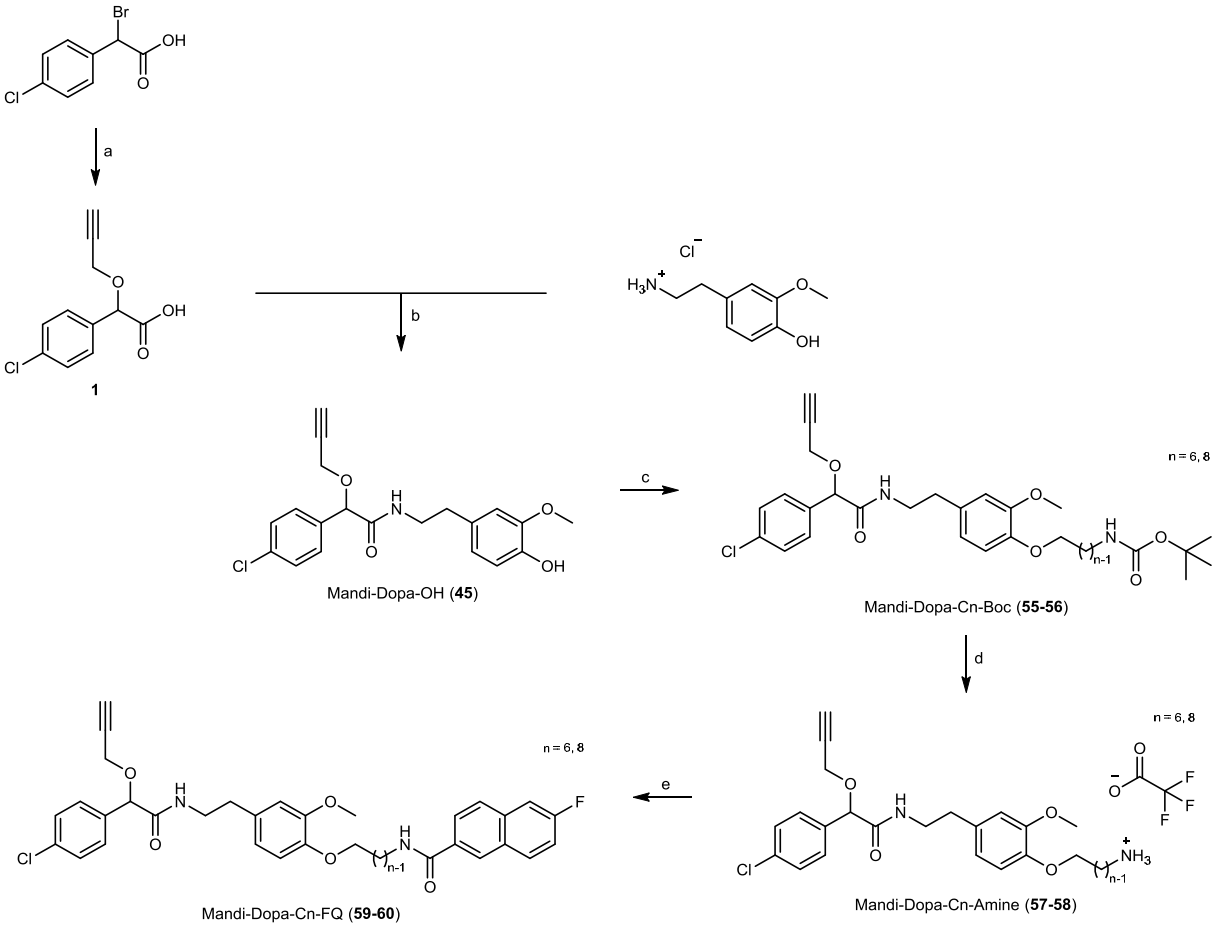

Figure 26: Synthesis of Mandi-Dopa-Cn-FQ. a: propargyl alcohol, KOH, rt, 2 h; b: HATU, DIPEA, rt, 68 h; c: Boc-amine alkyl bromide, K_2CO_3, KI, rt, 19 – 96 h; d: TFA, rt, 2 h; e: 6-fluoroquinoline-2-carboxylic acid, HATU, DIPEA, rt, 22 – 23 h.

The synthesized antagonist candidates Mandi-Dopa-Cn-Indole and Mandi-Dopa-Cn-FQ were tested for their ability to induce protein proximity of PYR^{Mandi} and ABI in live mammalian cells (Figure 27). Only the compound with the shortest linker, Mandi-Dopa-C4-Indole, induced protein proximity. The compounds that did not induce protein proximity were further tested regarding the ability to reverse protein proximity previously induced with Mandi in the competition assay (Figure 28, Figure 29 and Figure 30). Upon addition of Mandi-Dopa-C6-Indole in a 1000-fold excess, protein proximity was already reversed after 30 min. At a 100-fold excess protein proximity was reversed within 1 h to a large extend, at a 10-fold excess to some extent. Treatment with Mandi-Dopa-C8-Indole in a 1000-fold excess also resulted in in rapid reversion of the previously induced protein proximity within 30 min. At a 100-fold excess protein proximity was reversed partially, whereas at a 10-fold excess no effect was

observed. Both antagonist candidates with a fluoroquinoline moiety, only achieved very little reversion of the previously induced protein proximity within 1 h at a 1000-fold and a 100-fold excess.

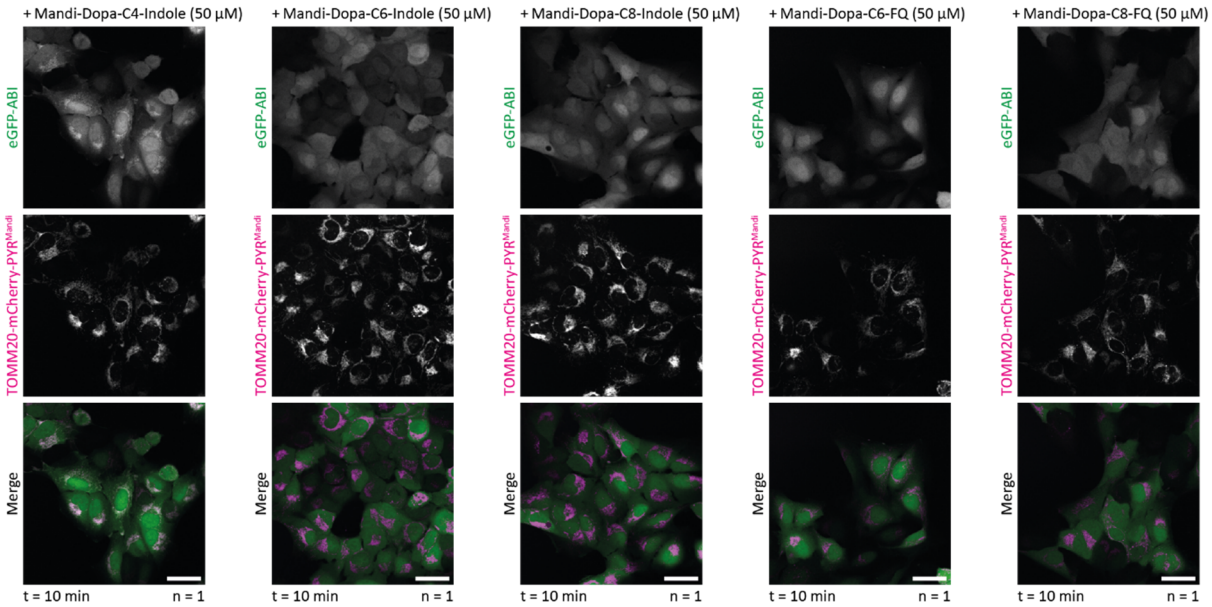

Figure 27: Screen for antagonists with the Mandi-Dopa-Cn-Indole/FQ scaffold. Confocal microscopy images of U2OS FlpIN cells stably expressing TOMM20-mCherry-PYR^{Mandi} and eGFP-ABI before and 10 min post addition of 50 µM Mandi-Dopa-Cn-Indole/FQ. Indicated number n of replicates. Scale bars at 40 µm.

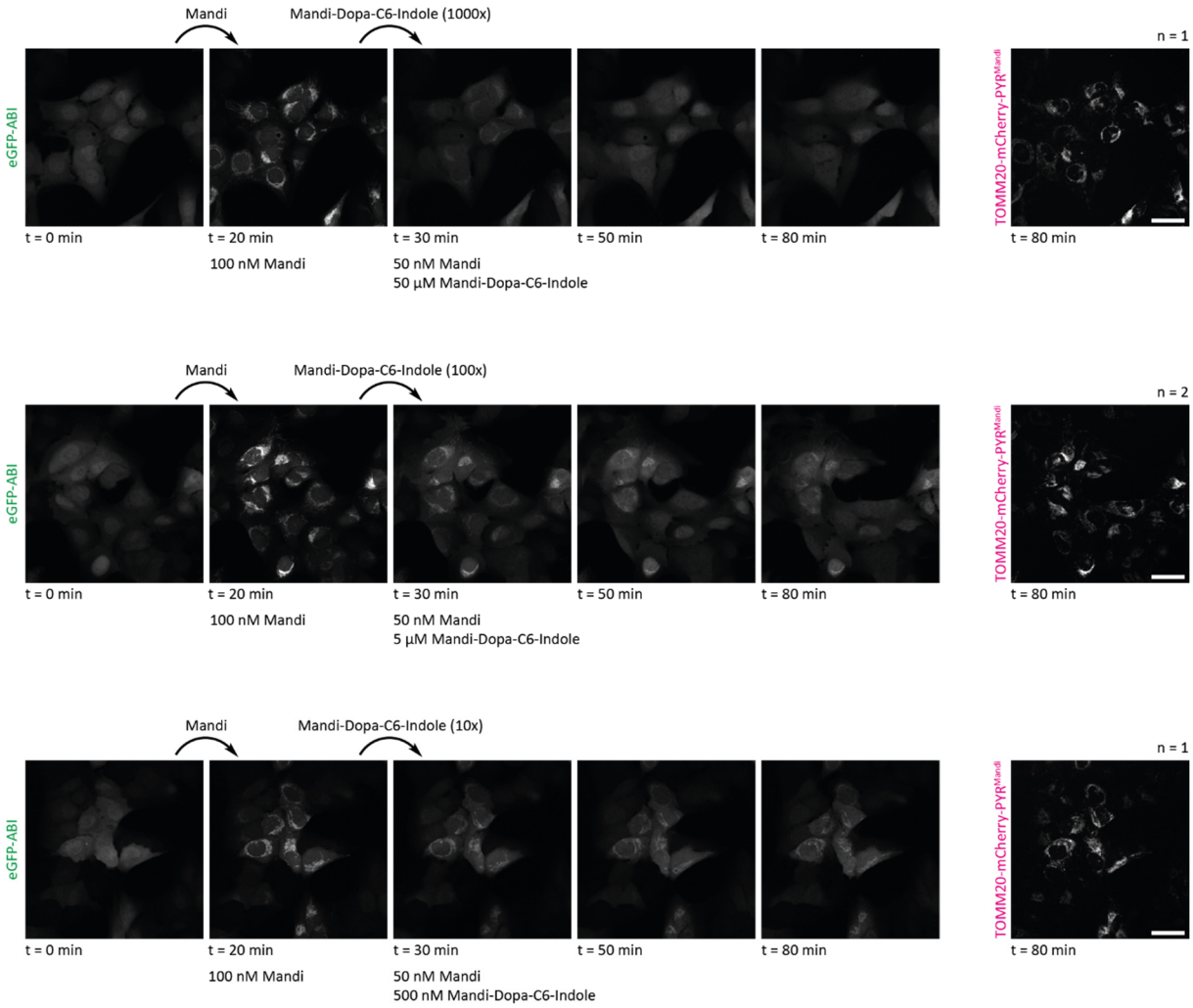

Figure 28: Competition assay with Mandi and Mandi-Dopa-C6-Indole. Confocal microscopy images of U2OS FlpIN cells stably expressing TOMM20-mCherry-PYR^{Mandi} and eGFP-ABI before and 20 min post addition of 100 nM Mandi. Then, different concentrations of Mandi-Dopa-C6-Indole were added and further images were taken thereafter. Indicated number n of replicates. Scale bars at 40 µm.

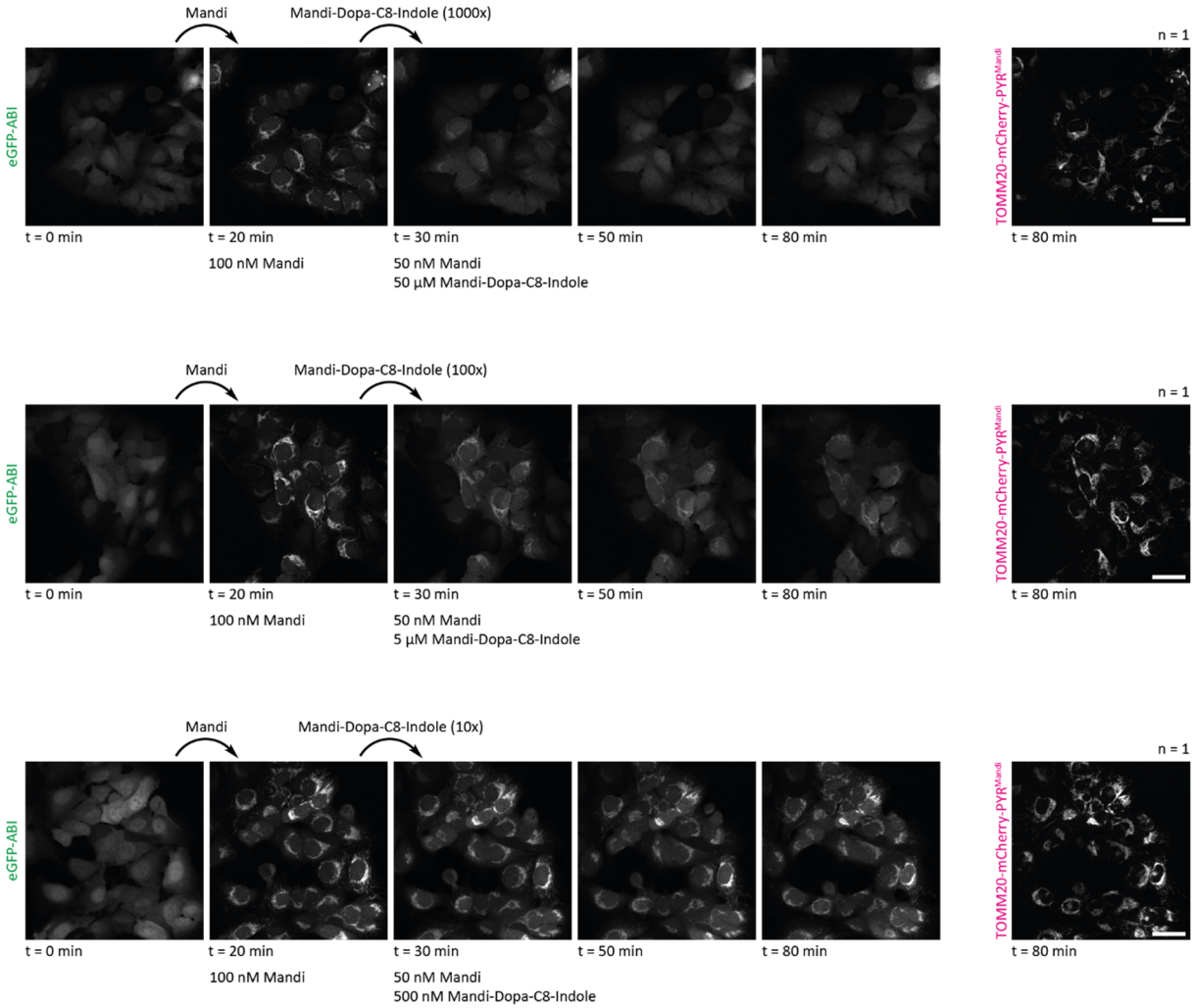

Figure 29: Competition assay with Mandi and Mandi-Dopa-C8-Indole. Confocal microscopy images of U2OS FlpIN cells stably expressing TOMM20-mCherry-PYR^{Mandi} and eGFP-ABI before and 20 min post addition of 100 nM Mandi. Then, different concentrations of Mandi-Dopa-C8-Indole were added and further images were taken thereafter. Indicated number n of replicates. Scale bars at 40 µm.

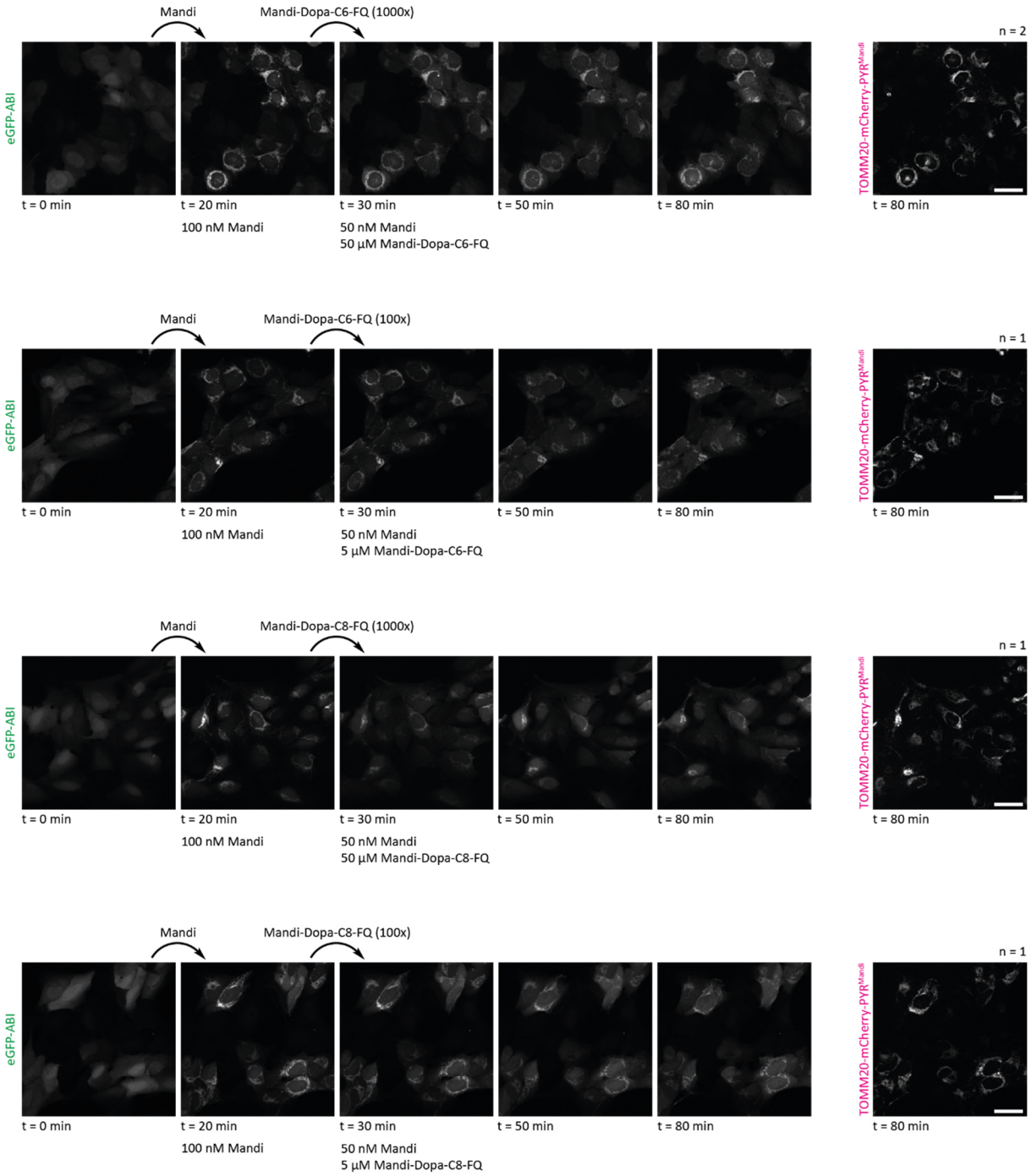

Figure 30: Competition assay with Mandi and Mandi-Dopa-Cn-FQ. Confocal microscopy images of U2OS FlpIN cells stably expressing TOMM20-mCherry-PYR^{Mandi} and eGFP-ABI before and 20 min post addition of 100 nM Mandi. Then, different concentrations of Mandi-Dopa-Cn-FQ were added and further images were taken thereafter. Indicated number n of replicates. Scale bars at 40 µm.

In summary, I identified Mandi-Dopa-C6-Indole as the most potent Mandi antagonist in the live cell competition assay. It can be used to reverse protein proximity previously induced with Mandi at a 100-fold excess. Generally, antagonist candidates with an indole moiety were more potent than antagonists with a fluoroquinoline moiety. Using a 100-fold excess requires the use of 5 µM antagonist in combination with 50 nM Mandi. These concentrations are compatible with a use in live cells. In vivo however, the concentration of Mandi needs to be higher (500 nM in fish embryos, see Section 3.1) and

applying a 100-fold excess there may not be possible due to solubility issues and toxicity at high concentrations of the antagonist.

In the live cell competition assay, Mandi antagonists with an indole moiety were also more potent than Mandi antagonists with a linear alkyl extension. The question, whether the indole moiety of the Mandi antagonists occupies the respective binding cleft on the receptor protein PYR^{Mandi} that is also responsible for the binding of the respective tryptophan residue of ABI was not addressed in this work. This can only be deduced as hypothesis from the experiments performed in this work. A crystal structure of PYR^{Mandi} in complex with Mandi-Dopa-C6-Indole or Mandi-Dopa-C8-Indole would answer this question and could be a starting point for the design of more potent Mandi antagonists with a higher affinity to PYR^{Mandi}.

In vitro characterization of Mandi antagonists

Mandi antagonist candidates that were able to reverse protein proximity previously induced with Mandi were further characterized regarding their binding to PYR^{Mandi} via ITC (Table 2). All compounds showed low micromolar affinity to the receptor protein PYR^{Mandi}. The compound with the highest binding affinity is Mandi-Dopa-C6-Indole, which was also identified as most potent antagonist in the live cell assays. Its binding affinity to PYR^{Mandi} is 4-fold higher than the binding affinity of Mandi to PYR^{Mandi}, suggesting that the indole moiety increases the binding affinity potentially by occupying the the respective binding cleft on PYR^{Mandi}. However, in the colocalization assay, binding of Mandi-Dopa-C6-Indole to PYR^{Mandi} competes with the binding of Mandi to both, PYR^{Mandi} and ABI, which occurs with a 20-fold higher affinity (see Section 3.1 and Table 1). Hence, to have equal amounts of PYR^{Mandi} in complex with Mandi-Dopa-C6-Indole and of Mandi in complex with PYR^{Mandi} and ABI a 20-fold higher concentration of Mandi-Dopa-C6-Indole compared to Mandi is needed. This is also in good agreement with the results from the competition experiments in live mammalian cells where protein proximity could be reversed by applying a 100-fold excess of the antagonist Mandi-Dopa-C6-Indole.

The ranking of the other Mandi antagonist according to their affinity does not match the ranking according to their potency in the live cell competition assay. Mandi-Dopa-C8-Indole was more potent than Mandi-Dopa-C7-Alkyl and Mandi-Dopa-C8-Alkyl but has a slightly lower binding affinity in vitro. Moreover, Mandi-Dopa-C6-FQ showed a higher binding affinity to PYR^{Mandi} than Mandi-Dopa-C8-Indole but was, together with higher Mandi-Dopa-C8-FQ, the least potent antagonist in the live cell competition assay. These results demonstrate, that the potency in live cells does not only depend on the binding affinity of the antagonist to PYR^{Mandi} but also on other properties like cell permeability and target specificity.

Table 2: Thermodynamic characterization of the binding of Mandi antagonists to PYR^{Mandi} via ITC. Values represent the mean and the standard deviation the mean of the indicated number of replicates.

Ligand	Protein	K_d [µM]	ΔH [kcal/mol]	-TΔS [kcal/mol]	ΔG [kcal/mol]	Number of replicates
Mandi-Dopa-C7-Alkyl	PYR^{Mandi}	2.7 ± 0.5	-16.2 ± 2.4	8.4 ± 2.2	-7.88 ± 0.13	3
Mandi-Dopa-C8-Alkyl	PYR^{Mandi}	2.49 ± 0.04	-18.6 ± 0.5	10.7 ± 0.5	-7.900 ± 0.010	3
Mandi-Dopa-C6-Indole	PYR^{Mandi}	1.58 ± 0.16	-29.1 ± 1.5	20.9 ± 1.4	-8.19 ± 0.06	5
Mandi-Dopa-C8-Indole	PYR^{Mandi}	4.3 ± 0.6	-25.2 ± 1.1	17.7 ± 1.1	-7.56 ± 0.07	3
Mandi-Dopa-C6-FQ	PYR^{Mandi}	3.1 ± 0.4	-18.0 ± 0.6	10.2 ± 0.6	-7.77 ± 0.08	3
Mandi-Dopa-C8-FQ	PYR^{Mandi}	8.1 ± 0.5	-13.3 ± 1.4	6.1 ± 1.4	-7.18 ± 0.04	3
Mandi	PYR^{Mandi}	6.7 ± 0.5	-17.1 ± 1.1	9.8 ± 1.0	-7.30 ± 0.05	3

Summary

To conclude, Mandi-Dopa-C6-Indole binds to PYR^{Mandi} with a higher affinity than Mandi, blocks the interaction with ABI and can be used to reverse protein proximity previously induced by Mandi.

In a final experiment, I demonstrated that it is possible to induce, reverse and re-induced protein proximity again with Mandi as agonist and Mandi-Dopa-C6-Indole as antagonist. Live mammalian cells were first treated with Mandi, resulting in the induction of protein proximity between PYR^{Mandi} and ABI. Then, the Mandi antagonist Mandi-Dopa-C6-Indole was added with a 100-fold excess which led to reversion of the protein proximity. In a last step, Mandi was added again at a higher concentration than previously and protein proximity was re-induced again.

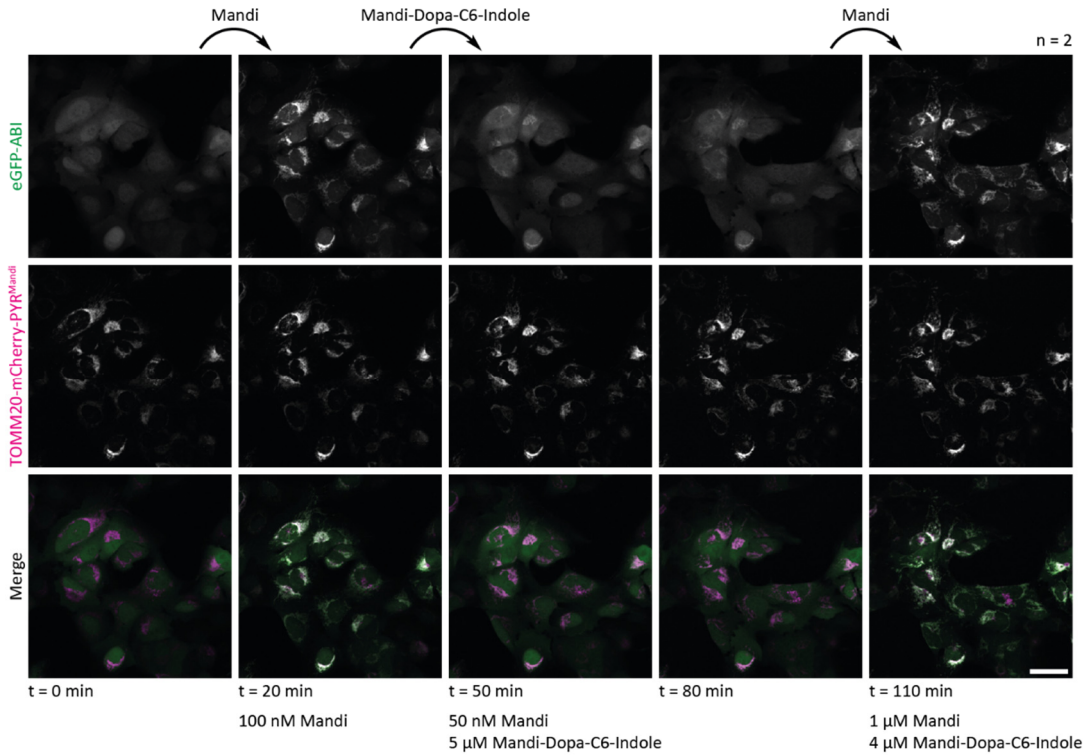

Figure 31: Induction, reversion and re-induction of protein proximity with Mandi and Mandi-Dopa-C6-Indole in live mammalian cells. Confocal microscopy images of U2OS FlpIN cells stably expressing TOMM20-mCherry-PYR^{Mandi} and eGFP-ABI before and 20 min post addition of 100 nM Mandi. Then, 5 µM Mandi-Dopa-C6-Indole was added and images were taken successively. After 80 min, 1 µM Mandi was added and further images were taken thereafter. Indicated number n of replicates. Scale bar at 40 µm.

3.2.3 Fluorescent labeling of PYR^{Mandi}

Having successfully shown in the development of Mandi antagonists that moieties can be attached to the 4' position of the dopamine part of Mandi without decreasing the binding affinity to the receptor protein PYR^{Mandi}, I investigated whether this scaffold can also be used for fluorescent labeling of PYR^{Mandi}. Fluorescent labeling of PYR^{Mandi} could be used to visualize PYR^{Mandi} via fluorescence microscopy, also when it is not expressed as fused to a fluorescent protein. This allows the verification of correct protein localization in experiments where a fusion to a fluorescent protein influences or disturbs the interaction that is to be studied with Mandi as CIP.

I chose the rhodamine-type fluorophore CPY and hypothesized that its aromatic phenyl ring that is not part of the xanthene core of the fluorophore would occupy the binding cleft for the tryptophan W300 residue of ABI. Further, this interaction may stabilize the fluorescent zwitterionic form of CPY resulting in a fluorescence turn-on, since the equilibrium is shifted away from the non-fluorescent spirolactone form towards the open and fluorescent zwitterionic form.

I synthesized the derivates of Mandi covalently linked to CPY (Mandi-Dopa-Cn-CPY) similar to Mandi-Dopa-Cn-FQ (see Section 3.2.2). In the last step, instead of the fluoroquinoline group, CPY-6-COOH was attached via an amide coupling. Mandi-Dopa-Cn-CPY was prepared with four different linker lengths of two, four, six and eight carbon atoms (C2,4,6,8).

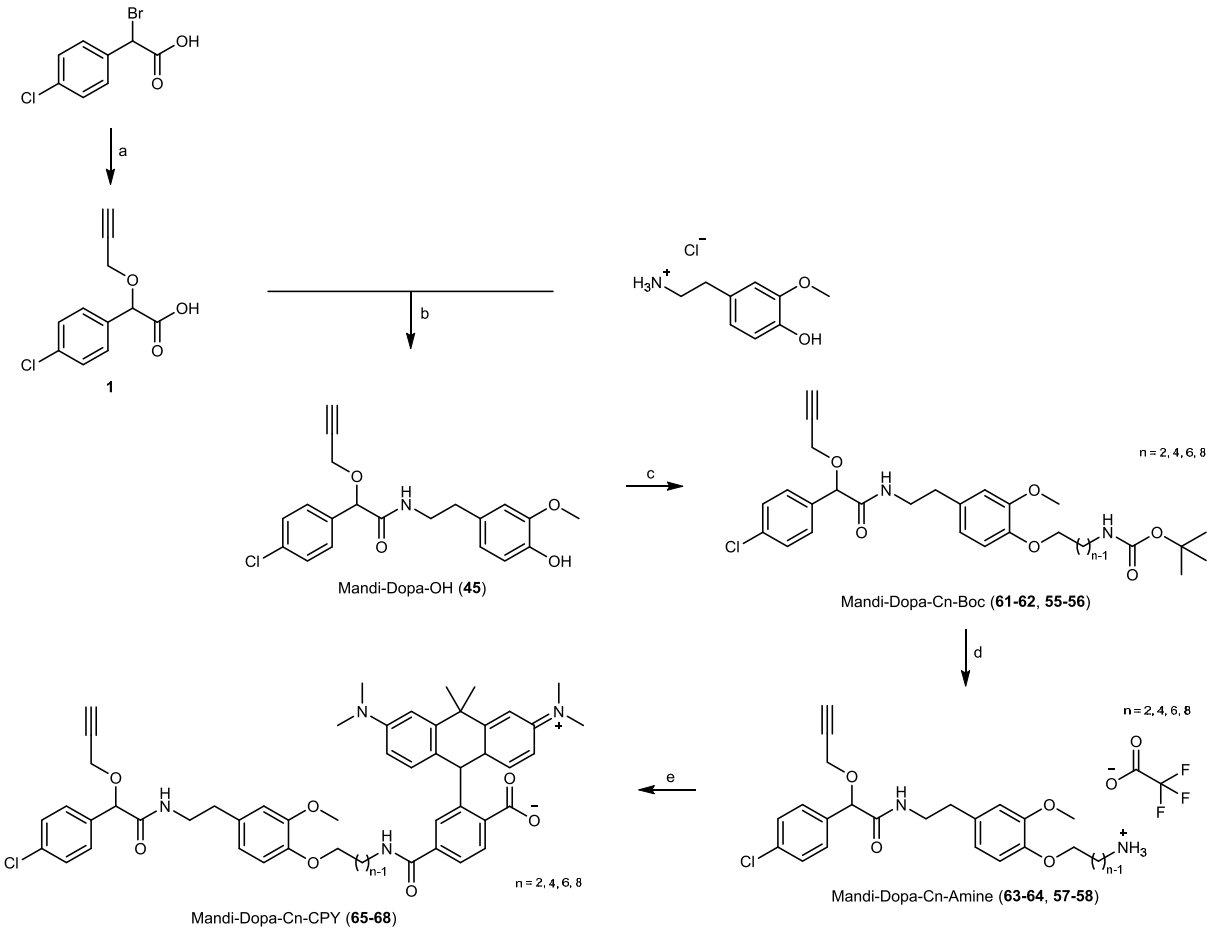

Figure 32: Synthesis of Mandi-Dopa-CPY. a: propargyl alcohol, KOH, rt, 2 h; b: HATU, DIPEA, rt, 68 h; c: Boc-amine alkyl bromide, K_2CO_3, KI, rt, 18 – 40 h; d: TFA, rt, 2 – 3 h; e: CPY-6-COOH, HATU, DIPEA, rt, 19 – 94 h.

Next, I investigated the synthesized compounds via ITC regarding their binding to PYR^{Mandi} (Table 3). Among the tested derivatives, Mandi-Dopa-C6-CPY showed the highest binding affinity towards the receptor protein PYR^{Mandi}. Its low micromolar affinity is in a similar range compared to the Mandi antagonists and only slightly lower than the affinity of the Mandi antagonist with the highest affinity, Mandi-Dopa-C6-Indole (K_d = 1.58 ± 0.16 µM) (see Section 3.2.2). Compounds with a shorter linker length (Mandi-Dopa-C2-CPY and Mandi-Dopa-C4-CPY) are less affine to bind to PYR^{Mandi}, for the derivative with the longest linker (Mandi-Dopa-C8-CPY) no binding could be observed in the ITC experiments.

Table 3: Thermodynamic characterization of the binding of Mandi-fluorophore conjugates to PYR^{Mandi} via ITC. Values represent the mean and the standard deviation the mean of the indicated number of replicates.

Ligand	Protein	K_d [µM]	ΔH [kcal/mol]	-TΔS [kcal/mol]	ΔG [kcal/mol]	Number of replicates
Mandi-Dopa-C2-CPY	PYR^{Mandi}	42 ± 15	-10 ± 3	4 ± 3	-6.24 ± 0.21	3
Mandi-Dopa-C4-CPY	PYR^{Mandi}	10.1 ± 2.8	-17.4 ± 2.4	10.3 ± 2.5	-7.11 ± 0.19	4
Mandi-Dopa-C6-CPY	PYR^{Mandi}	2.18 ± 0.28	-24.1 ± 1.8	16.1 ± 1.7	-8.00 ± 0.07	4
Mandi-Dopa-C8-CPY	PYR^{Mandi}	No binding	No binding	No binding	No binding	3
Mandi	PYR^{Mandi}	6.7 ± 0.5	-17.1 ± 1.1	9.8 ± 1.0	-7.30 ± 0.05	3

After having demonstrated that Mandi-Dopa-C6-CPY binds to the receptor protein PYR^{Mandi} in vitro, I examined whether this compound can be used to fluorescently stain PYR^{Mandi} in live mammalian cells. The other Mandi derivatives linked to CPY were not investigated because of their low binding affinity and because I hypothesized that other properties like cell permeability and target specificity that influence the potency in live mammalian cells are similar for all Mandi derivatives with a CPY moiety.
Addition of Mandi-Dopa-C6-CPY to cells expressing TOMM20-eGFP-PYR^{Mandi} in coculture with wildtype cells resulted in staining of the mitochondria in all cells independently of the expression of the receptor protein PYR^{Mandi} (Figure 33). Since the binding of Mandi-Dopa-C6-CPY to PYR^{Mandi} was demonstrated in vitro and the compound obviously enters the cells, presumably the receptor protein PYR^{Mandi} is stained but the nonspecific stain of the mitochondria with Mandi-Dopa-C6-CPY is dominant.
It is known that rhodamine dyes stain the mitochondria noncovalently.[77] To demonstrate this, I treated cells expressing TOMM20-eGFP-PYR^{Mandi} in coculture with wildtype cells with Halo-CPY, a CPY derivative that lacks the Mandi moiety and is used to covalently stain the self-labeling Halo protein[78]. This also resulted in staining of the mitochondria (Figure 33). The affinity of Mandi-Dopa-C6-CPY to PYR^{Mandi} is obviously too low to stand out over the nonspecific background staining. Hence, Mandi-Dopa-C6-CPY is not suitable for fluorescent labeling of PYR^{Mandi}. The nonspecific staining alone cannot be removed by washing, because also the interaction between Mandi-Dopa-C6-CPY and PYR^{Mandi} is noncovalent and would be reversed.

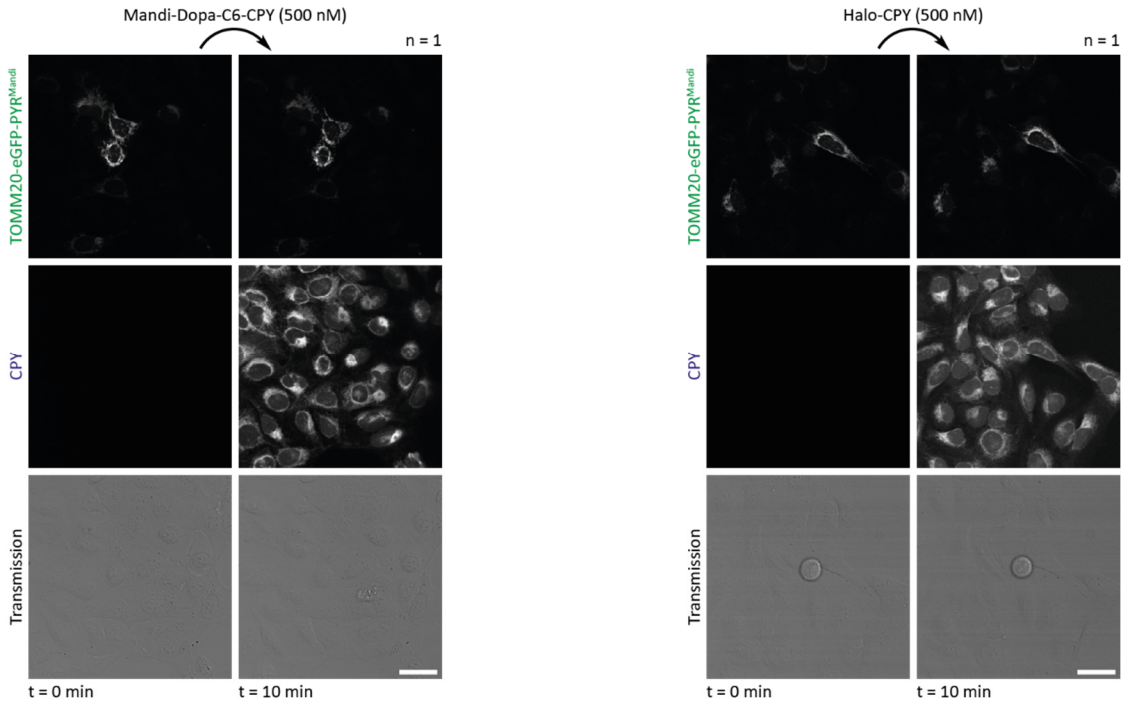

Figure 33: Staining of live mammalian cells with Mandi-Dopa-C6-CPY in comparison to Halo-CPY. Both compounds stain the mitochondria non-specifically. Confocal microscopy images of U2OS FlpIN cells stably expressing TOMM20-eGFP-PYR^{Mandi} in coculture with wildtype U2OS FlpIN TREx cells before and 10 min post addition of 500 nM Mandi-Dopa-C6-CPY or Halo-CPY. Indicated number n of replicates. Scale bars at 40 µm.

For the specific staining of PYR^{Mandi}, Mandi derivatives with a higher binding affinity are necessary. Similar to the potential optimization of the Mandi antagonists (see Section 3.2.2) a crystal structure of PYR^{Mandi} in complex with Mandi-Dopa-C6-CPY would be a starting point for the design of more potent Mandi fluorophore conjugates. Moreover, other fluorophores than rhodamine dyes could be investigated that are less prone to unspecific staining.

3.3 Photoactivation using photocaged Mandi derivatives

3.3.1 pMandi

To initiate protein proximity upon irradiation with light, I designed a photocaged derivative of Mandi, pMandi, with a photolabile nitroveratryl protecting group at the nitrogen atom of the central amide bond already in my master's thesis[79]. The compound releases the active CIP Mandi upon irradiation without any scar originating from the attachment of the photocage and puts the induction of protein proximity under external temporal control by light irradiation. I chose the nitroveratryl group because it is stable under normal lab lighting and can be cleaved with UV or blue light facilitating the handling compared to photoactivation at longer wavelengths. Moreover, photoactivation at this wavelength does not interfere with the excitation of most commonly used fluorescent proteins in fluorescence microscopy.

I synthesized pMandi (**71**) from a mandelic acid building block (**69**) and dopamine building block (**70**) already linked to the photocage (**70**) in a convergent synthesis during my master's thesis[79] (Figure 34). The mandelic acid building block (**69**) was synthesized from 2-bromo-2-(4-chlorophenyl)acetic acid. The propargyloxy group was introduced upon reaction with propargyl alcohol in presence of strong base according to literature[76] yielding compound **1** and the carboxylic acid moiety was converted to an acyl chloride (**69**). The dopamine building block (**70**) was prepared from 3-methoxytyramine hydrochloride. According to literature[70,75] and as described in Section 3.2.2, the amine moiety was protected as formamide (**2**), the aromatic hydroxyl group was reacted with propargyl bromide in a nucleophilic substitution yielding compound **31** and the amine was deprotected again with acid to obtain compound **32**. Subsequently, the nitroveratryl group was attached via a reductive amination to avoid reaction to a tertiary amine and to form compound **70**. Both building blocks (**69** and **70**) were coupled in a base catalyzed reaction to yield pMandi.

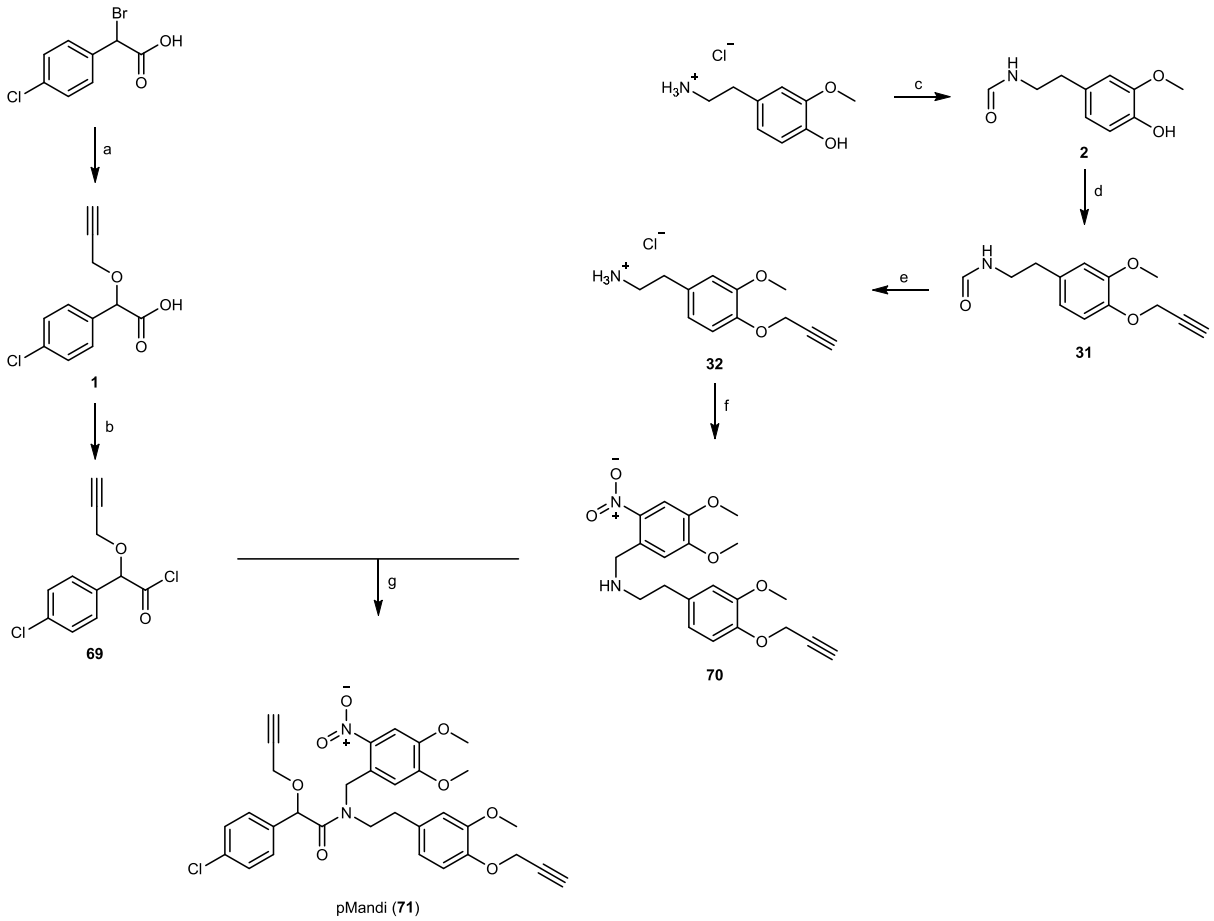

Figure 34: Synthesis of pMandi. a: propargyl alcohol, KOH, rt, 2 h; b: oxalyl chloride, DMF (cat.), 0 °C -> rt, 2 h; c: Ac_2O, formic acid, 70 °C, 2 h; d: propargyl bromide, NaOMe, 65 °C, 4 h; e: HCl, rt, 91 h; f: 1. 4,5-dimethoxy-2-nitrobenzaldehyd, $NaBH(OAc)_3$, rt -> 50 °C, 14 h; g: DIPEA, 0 °C -> rt, 21 h. This synthesis was conducted during my master's thesis[79].

First, the decay of pMandi and the release of the active molecule Mandi from pMandi upon light irradiation was investigated. In vitro irradiation experiments showed that pMandi can be converted to Mandi upon irradiation with light of the wavelengths 365 nm (Figure 35 B) and 405 nm (Figure 36 B). Absorption spectra were recorded after different irradiation times revealing an isosbestic point at approximately 300 nm that indicates a unimolecular decay. Additionally, samples of pMandi before irradiation and after irradiation, when no further change in the absorption spectra was monitored, as well as a sample of Mandi were analyzed by HPLC. The chromatograms demonstrate that Mandi is released from pMandi upon irradiation without undesired side products and any chemical modification that would lead to a retention time different to Mandi (Figure 35 A and Figure 36 A).

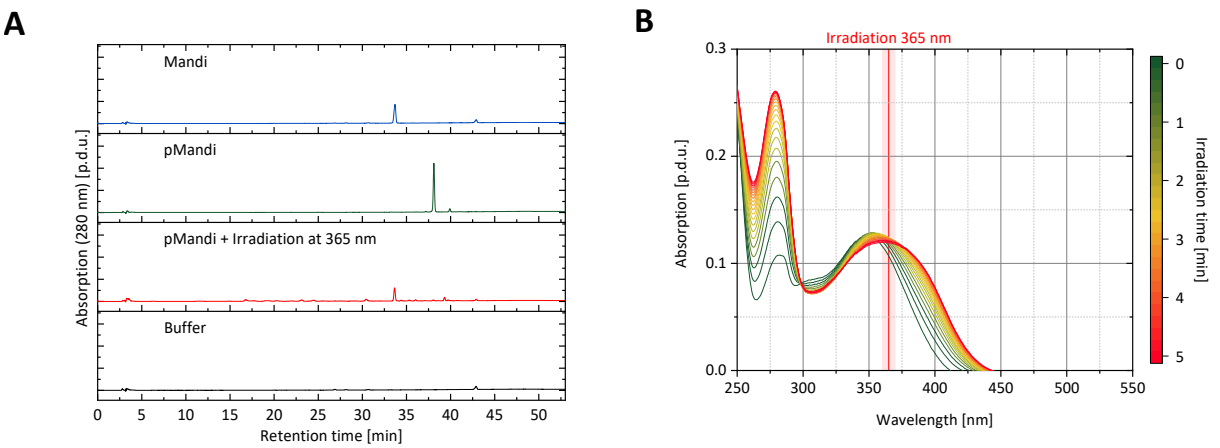

Figure 35: In vitro irradiation of pMandi at 365 nm: pMandi decays to Mandi. (A) HPLC traces at 280 nm of Mandi, pMandi and buffer without irradiation and of pMandi after irradiation (100 mA, 20 min). (B) Absorption spectra of a solution of pMandi after different irradiation times (100 mA). This experiment was conducted during my master's thesis[79].

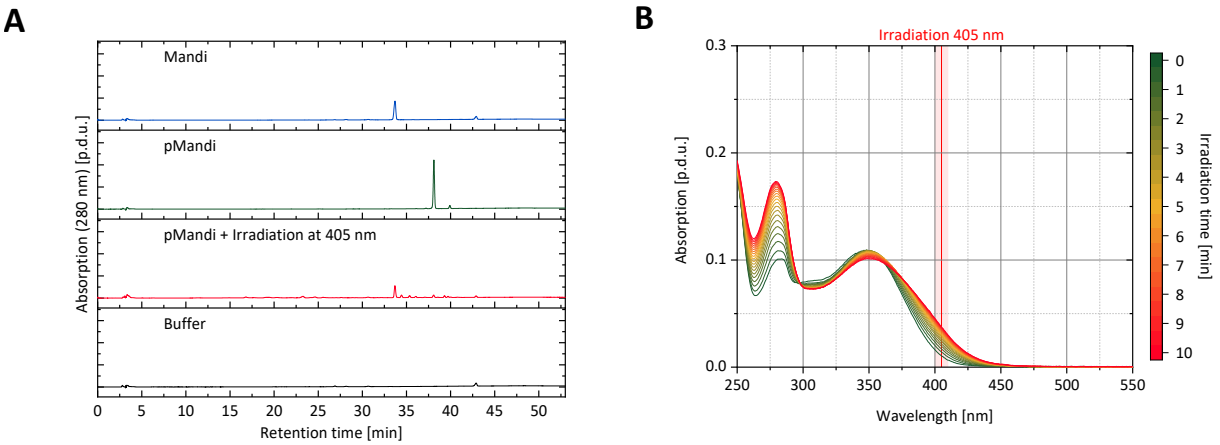

Figure 36: In vitro irradiation of pMandi at 405 nm: pMandi decays to Mandi. (A) HPLC traces at 280 nm of Mandi, pMandi and buffer without irradiation and of pMandi after irradiation (100 mA, 40 min). (B) Absorption spectra of a solution of pMandi after different irradiation times (100 mA).

After having shown that Mandi is released from pMandi upon irradiation, I demonstrated that the photocaged derivative pMandi does not bind to the proteins PYR^{Mandi} and ABI which is a prerequisite for photoactivation. Titration of pMandi to a mixture of both proteins (PYR^{Mandi} and ABI) did not reveal any binding in an ITC experiment (Figure 37).

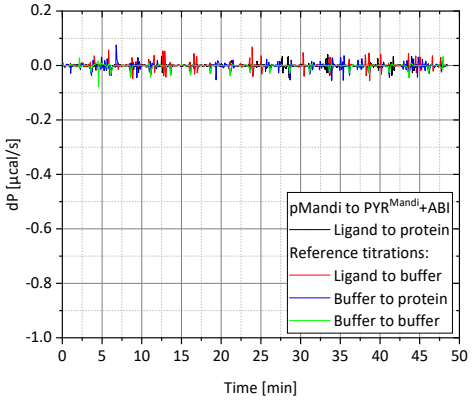

Figure 37: Titration of pMandi to PYR^{Mandi} and ABI monitored by ITC. Representative data of 3 titrations of 100 µM pMandi to 20 µM PYR^{Mandi} and ABI with reference titrations.

Also, in live mammalian cells pMandi did not induce protein proximity of PYR^{Mandi} and ABI without irradiation at a concentration of 500 nM, even after long incubation times (Figure 38). Only when the concentration of pMandi was increased to the micromolar range (5 µM or 50 µM), I observed an induction of protein proximity without irradiation (Figure 86, Section 7.2). However, since these concentrations are more than 100-fold higher than the lowest working concentration of Mandi (50 nM, see Section 3.1) I concluded, that they would also be higher than the working concentration of pMandi and that using 500 nM pMandi in live mammalian cells would allow photoactivation without any apparent basal activity.

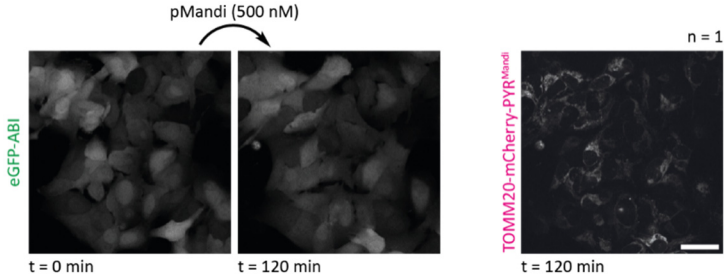

Figure 38: In live mammalian cells pMandi does not induce protein proximity without irradiation. Confocal microscopy images of U2OS FlpIN cells stably expressing TOMM20-mCherry-PYR^{Mandi} and eGFP-ABI before and 120 min post addition of 500 nM pMandi. Indicated number n of replicates. Scale bar at 40 µm.

To demonstrate that pMandi (500 nM) can be converted to the active CIP Mandi upon irradiation and subsequently induce protein proximity in live mammalian cells (Figure 39), I performed strong irradiation (405 nm) off cells treated with pMandi (500 nM) on a widefield microscope (Figure 40). Compared to a confocal microscope, a widefield microscope does not enable precisely confined irradiation. The irradiation resulted in an immediate (≤ 1 min) induction of protein proximity, which persisted over time. Irradiation in the absence of pMandi had no influence on protein localization (Figure 40).

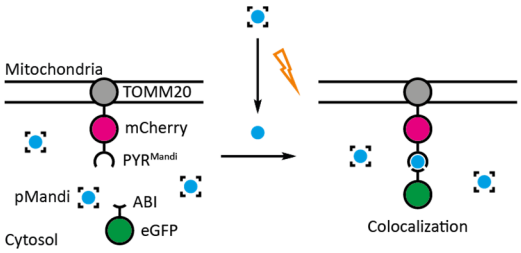

Figure 39: Schematic representation of the used protein construct and the colocalization assay for the investigation of pMandi. Upon irradiation pMandi is converted into the active molecule Mandi and protein proximity is induced.

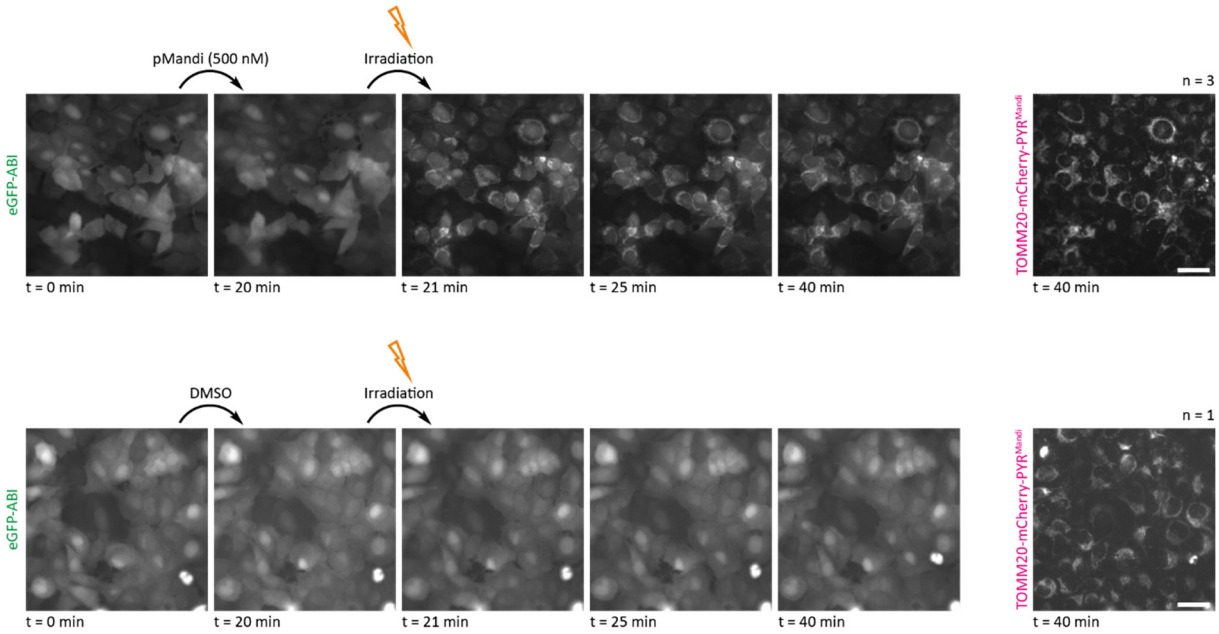

Figure 40: Irradiation (405 nm) of live mammalian cells treated with pMandi with a high light dose on a widefield microscope induces protein proximity without reversion over time. In the DMSO control irradiation has no effect on protein localization. Widefield microscopy images of U2OS FlpIN cells stably expressing TOMM20-mCherry-PYR^{Mandi} and eGFP-ABI before and 20 min post addition of 500 nM pMandi or DMSO. Then, irradiation (30 s, 405 nm) was performed and further images were taken thereafter. Indicated number n of replicates. Scale bars at 40 µm.

Protein proximity of PYR^{Mandi} and ABI could also be induced in cells treated with pMandi (500 nM) upon short irradiation (405 nm) of a defined field of view on a confocal microscope (Figure 41 C). Remarkably, the induced protein proximity reversed with time. I assumed that this is due to diffusion of the active CIP Mandi outside of the irradiated area, dilution its concentration in the field of view (Figure 41 A). The defined field of view was irradiated again, resulting in re-induction of protein proximity that reversed again with time. Upon a third irradiation this process could be repeated again (Figure 41 B). Since each irradiation only converts a fraction of the pMandi into the active CIP Mandi, several cycles of reversible induction of protein proximity are possible. This could be demonstrated for in total three cycles of irradiation with an interval of 20 min between the single irradiations.

To conclude, pMandi can be used at a concentration of 500 nM to induce protein proximity of PYR^{Mandi} and ABI upon irradiation (405 nm) in live mammalian cells. Upon strong and non-precisely confined irradiation and converting a larger fraction or whole pMandi into the active CIP Mandi the induced

protein proximity persists over time. Upon local and short irradiation, only a fraction of pMandi is converted into the active CIP Mandi allowing the induction of protein proximity in a reversible manner. However, because of the high permeability and rapid diffusion of the active CIP Mandi no precise spatial control over the induction of protein proximity is possible.

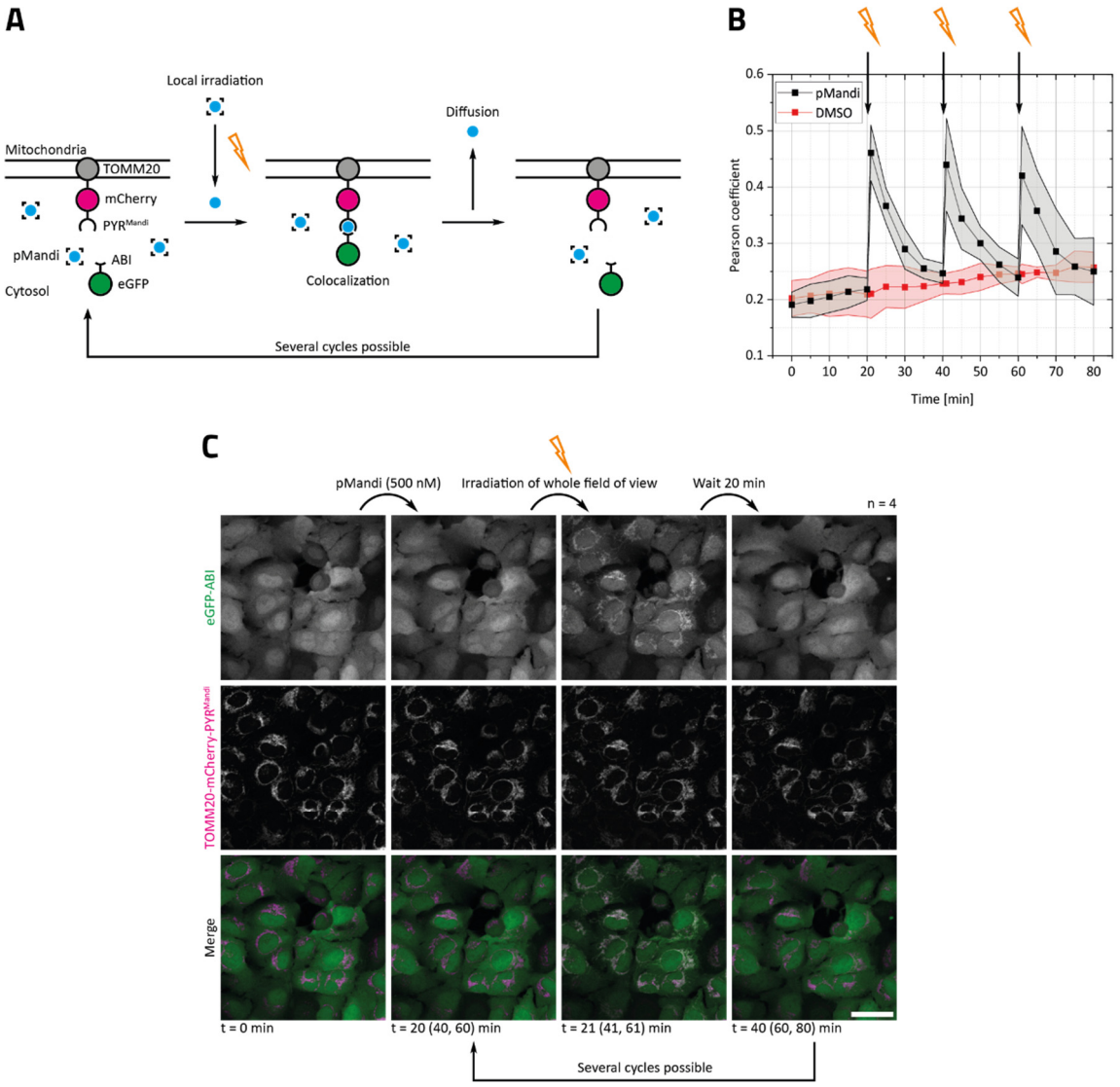

Figure 41: Application of pMandi for reversible induction of protein proximity in live cells upon irradiation. Local irradiation (405 nm) leads to local release of the active molecule Mandi and induction of protein proximity. Due to its high permeability the active molecule Mandi diffuses out of the irradiated area and the colocalization is reversed. Several cycles are possible. (A) Schematic representation of the colocalization assay with pMandi. (B) The Pearson coefficient of the eGFP and mCherry channels was calculated from confocal microscopy images of U2OS FlpIN cells stably expressing TOMM20-mCherry-PYR^{Mandi} and eGFP-ABI in an experiment with 3 successive irradiations (405 nm). The whole field of view was irradiated at 20 min, 40 min and 60 min. Cells were treated with either 500 nM pMandi or DMSO at 0 min. Mean and standard deviation of the mean for each 4 replicates per condition. (C) Confocal microscopy images of U2OS FlpIN cells stably expressing TOMM20-mCherry-PYR^{Mandi} and eGFP-ABI before and 20 min post addition of 500 nM Mandi. Then, the whole field of view was irradiated (405 nm) at 20 min and images were taken thereafter. Several cycles are possible. Indicated number n of replicates. Scale bar at 40 µm.

Having successfully shown that pMandi can be applied in live mammalian cells to induce protein proximity upon irradiation, I investigated whether pMandi can also be used for photoactivation in vivo.

As in vivo model I used live medaka embryos. The assay and the workflow are described in Section 3.1 (simplified sketch in Figure 42 A). I added pMandi to agarose embedded medaka embryos and waited 2 h that the molecule can diffuse inside the embryo. I used a concentration of 5 µM pMandi, a 10-fold higher concentration than the lowest working concentration of Mandi in medaka embryos (the same Mandi/pMandi concentration difference that was successfully applied in experiments in live mammalian cells). Then, I irradiated a region of interest (ROI) in the medaka tail (405 nm) which led to the induction of protein proximity within minutes (recruiting of the cytosolic eGFP-ABI fusion protein to the cell membrane where PYR^{Mandi} is located). As in live mammalian cells, after local irradiation the induced protein proximity reversed over time (within approximately 50 min) (Figure 42 B).

The fact, that irradiation of only the medaka tail is sufficient to induce protein proximity requires that pMandi is present in this region prior irradiation and indicates that pMandi can diffuse inside the medaka embryo and that the release of the active CIP Mandi happens inside the living organism. The time between irradiation and induction of protein proximity (several minutes vs. instantaneously) as well as of the reversion with time after local irradiation (50 min vs. 20 min) are slower than in mammalian cells. This could be due to the fact live medaka embryo experiments were performed at a lower temperature than live mammalian cell experiments (27° C vs 37 °C) and there are differences of cell type, size and permeability. Control experiments showed that pMandi (5 µM) does not induce protein proximity without irradiation in live medaka embryos (Figure 42 C) and irradiation in the absence of pMandi irradiation (405 nm) does not have an effect on protein localization (only slight bleaching of the fluorescent proteins was observed) (Figure 42 D).

To conclude, pMandi (5 µM) enables to induce protein proximity upon irradiation as external stimulus with precise temporal control in live medaka embryos. The exact timepoint of the induction of protein proximity can be accurately controlled and is, compared to the application of a non-photocaged CIP, not dependent on the diffusion time of an active molecule inside the embryo. The photocaged CIP is applied in an inactive form and can diffuse inside the embryos without an effect on protein localization.

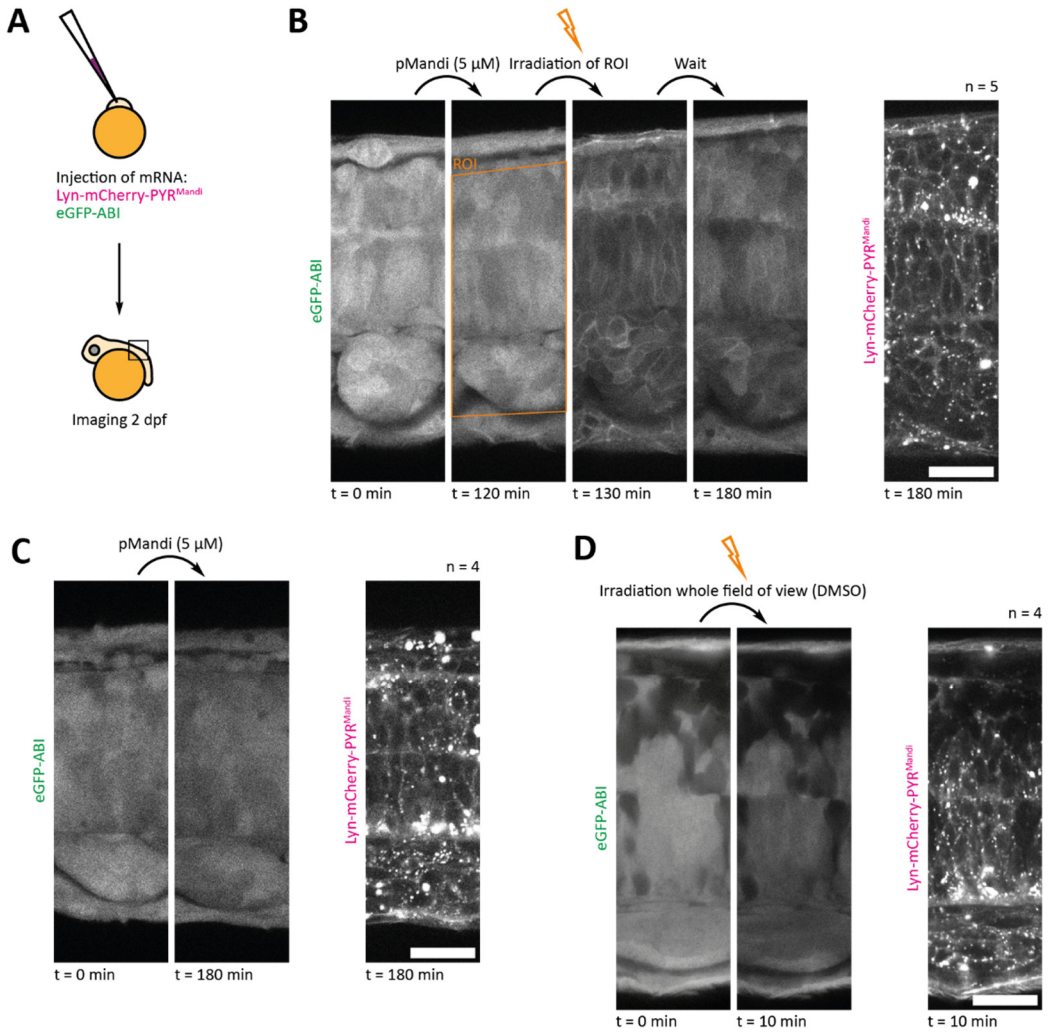

Figure 42: Application of pMandi to induce protein proximity upon irradiation (405 nm) in live medaka embryos. (A) Medaka embryos were microinjected with eGFP-ABI and Lyn-mCherry-PYR^{Mandi} mRNA in the one-cell stage and experiments were performed 2 dpf with agarose embedded embryos. (B) Upon addition of 5 µM pMandi and irradiation (405 nm) protein translocation to the plasma membrane is induced and reverses over time. (C) Without irradiation no protein proximity is induced. (D) Irradiation (405 nm) of medaka embryos not treated with pMandi does not have an effect on protein localization. Confocal microscopy images of the medaka embryo tail before and at different timepoints post addition of 5 µM pMandi or DMSO and post irradiation (405 nm). Indicated number n of replicates. Scale bars at 20 µm. Microinjections was performed by Kaisa Pakari.

3.3.2 Mandi-Dopa-Cn-NV

With the photocaged derivative of Mandi, pMandi, the induction of protein proximity can be precisely controlled in time with light as external stimulus. However, spatial control is limited due to the high membrane permeability of Mandi.

To achieve precise spatial control upon photoactivation, a CIP is required that is cell permeable in its photocaged form, while the active CIP that is released upon irradiation is trapped inside the cell after photoactivation and cannot diffuse out of the cell. With this strategy, spatial control can be increased up to single-cell resolution.

To achieve this, I hypothesized that by introducing a carboxylic acid moiety to the Mandi core structure, an active CIP could be obtained that is cell impermeable because of the increased polarity. Caging this

polar moiety with a photocage should result in the formation of a photocaged CIP that is well cell permeable in its inactive form. A similar strategy has been previously applied to photocaged CIPs based on GA_3[36,37], auxin (mammalian cells[45], plant cells[43]) and ABA[55].

Similar to the design of Mandi antagonists, the carboxylic acid moiety was introduced via the 4' position of the dopamine part with different linker lengths between the Mandi core structure and the carboxylic acid moiety. Modification on the 4' position of the dopamine part does not disturb binding to PYR^{Mandi} and recruiting of ABI when the attached moieties are small in size (see Section 3.2.2). Nevertheless, the linker to the carboxylic acid moiety must not be too short that also the photocaged form can be accommodated in the binding pocket and induce protein proximity.

I prepared the related Mandi derivatives as carboxylic acid derivatives (Mandi-Dopa-Cn-COOH) and nitroveratryl esters (Mandi-Dopa-Cn-NV). Moreover, I derivatized the carboxylic acid derivatives as AM esters (Mandi-Dopa-Cn-AM) that mask the carboxylic acid moiety and are cleaved intracellularly.

The Mandi derivatives were synthesized from Mandi-Dopa-OH, which was synthesized as described in Section 3.2.2. Upon reaction with methyl bromoalkylates and subsequent deprotection of the carboxylic acid moiety Mandi-Dopa-Cn-COOH was formed with attached polar moieties of different lengths (two, four or five carbon atoms, C2,4,5; reaction to attach an extension of three carbon atoms (C3) did not result in product formation). Mandi-Dopa-Cn-COOH was derivatized as AM ester yielding Mandi-Dopa-Cn-AM, and as nitroveratryl ester resulting in the formation of Mandi-Dopa-Cn-NV (Figure 43).

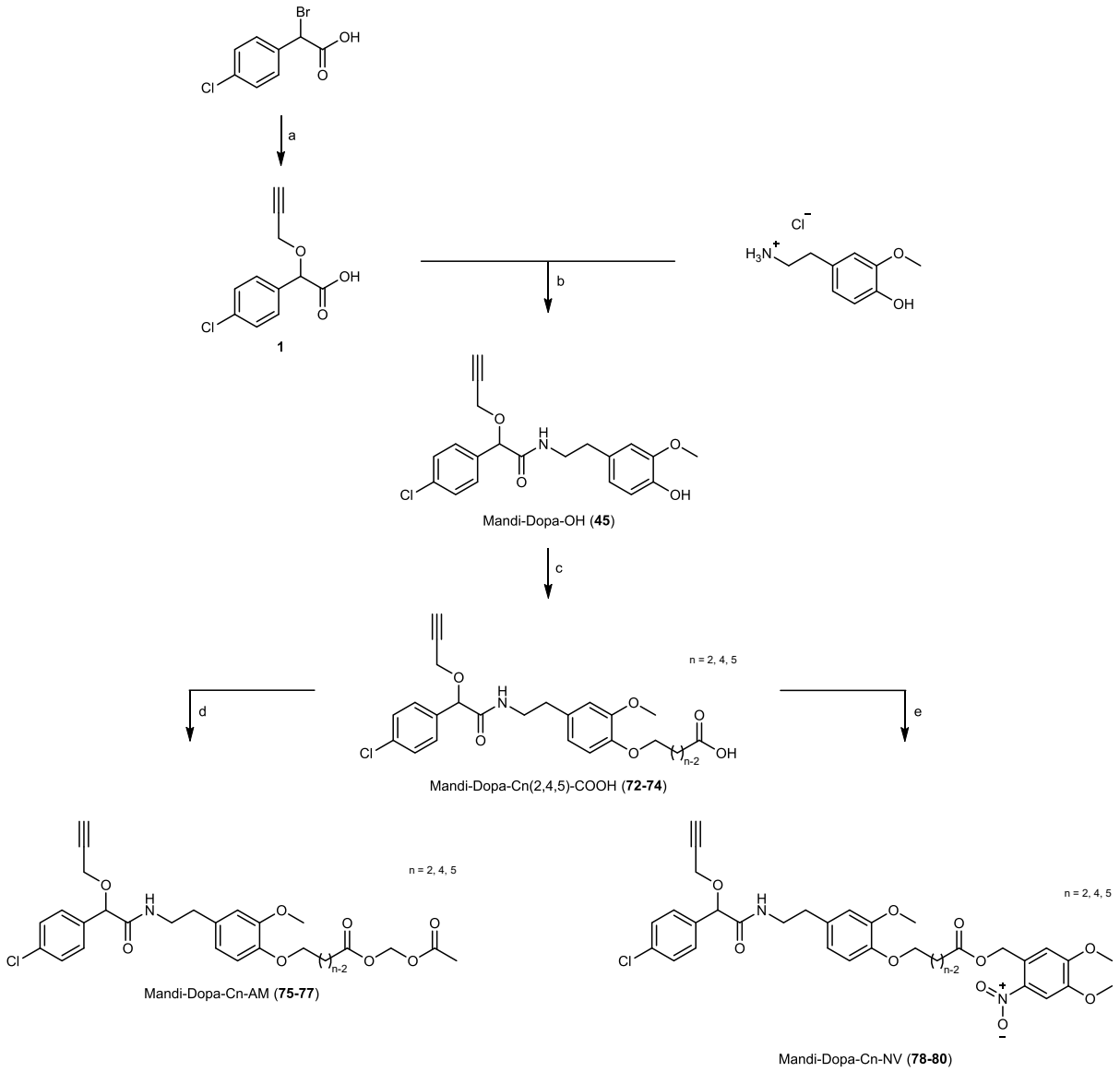

Figure 43: Synthesis of Mandi-Dopa-Cn-COOH/AM/NV. a: propargyl alcohol, KOH, rt, 2 h; b: HATU, DIPEA, rt, 68 h; c: 1. methyl bromoalkylate, NaOMe, 21 – 22 h, 65 °C, 2. NaOH, rt, 4 h; d: bromomethyl acetate, DIPEA, rt, 23 – 39 h; e: 1-(bromomethyl)-4,5-dimethoxy-2-nitrobenzene, DIPEA, rt, 23 – 39 h.

The synthesized Mandi-Dopa-Cn-COOH derivatives were then investigated for their ability to bind to the proteins PYR^{Mandi} and ABI in vitro via ITC (Table 4). The investigated compounds showed binding to the proteins with micromolar affinity. Compared to Mandi the affinity is reduced by at least by 25-fold, obviously the extension with the carboxylic acid moiety disturbs the binding to PYR^{Mandi} and ABI. Especially the compound with the shortest linker to the carboxylic acid moiety (Mandi-Dopa-C2-COOH) showed decreased binding affinity.

Table 4: Thermodynamic characterization of the binding of Mandi-Dopa-Cn-COOH to PYR^{Mandi} and ABI via ITC. Values represent the single experiments and the mean of the replicates for Mandi-Dopa-Cn-COOH and the mean with standard deviation the mean for Mandi.

Ligand	Proteins	K_d [µM]	ΔH [kcal/mol]	-TΔS [kcal/mol]	ΔG [kcal/mol]	Number of replicates
Mandi-Dopa-C2-COOH	PYR^{Mandi}+ABI	44.20	-33.3	1510.0	-6.14	3
		1040.00	-982.0	64000.0	-4.20	
		13.00	-17.3	51.5	-6.89	
	mean	366.00	-344.2	338.5	-5.74	
Mandi-Dopa-C4-COOH	PYR^{Mandi}+ABI	6.35	-58.4	51.1	-7.33	2
		1.87	-33.9	25.8	-8.08	
	mean	4.11	-46.5	38.5	-7.71	
Mandi-Dopa-C5-COOH	PYR^{Mandi}+ABI	3.39	-42.5	34.8	-7.71	2
		1.60	-33.3	25.1	-8.17	
	mean	2.50	-37.9	30.0	-7.94	
Mandi	PYR^{Mandi}+ABI	0.090 ± 0.007	-32.2 ± 1.0	22.3 ± 1.0	-9.94 ± 0.05	4

In parallel, I investigated the synthesized Mandi derivatives in live mammalians cells. In a first experiment, it was examined whether the non-photocaged compounds (Mandi-Dopa-Cn-COOH) can enter the cell and induce protein proximity (Figure 44). At high concentrations (50 µM) all compounds induced protein proximity, especially Mandi-Dopa-C2-COOH had a strong effect. When the concentration was reduced (5 µM) only Mandi-Dopa-C2-COOH induced protein proximity, treatment with Mandi-Dopa-C4-COOH and Mandi-Dopa-C5-COOH had no effect on protein localization. Since it was desired that the active, non-photocaged CIP is not cell permeable and does not induce protein proximity upon addition, derivatives with a C2 linker based on Mandi-Dopa-C2-COOH were excluded from further experiments.

Next, Mandi-Dopa-C4-AM and Mandi-Dopa-C5-AM were added to cells (5 µM) (Figure 45). These molecules should be cell permeable and release the free carboxylic acid derivatives inside the cell that then induce protein proximity. In fact, both compounds induced protein proximity, although Mandi-Dopa-C4-AM induced protein proximity only very weakly visible.

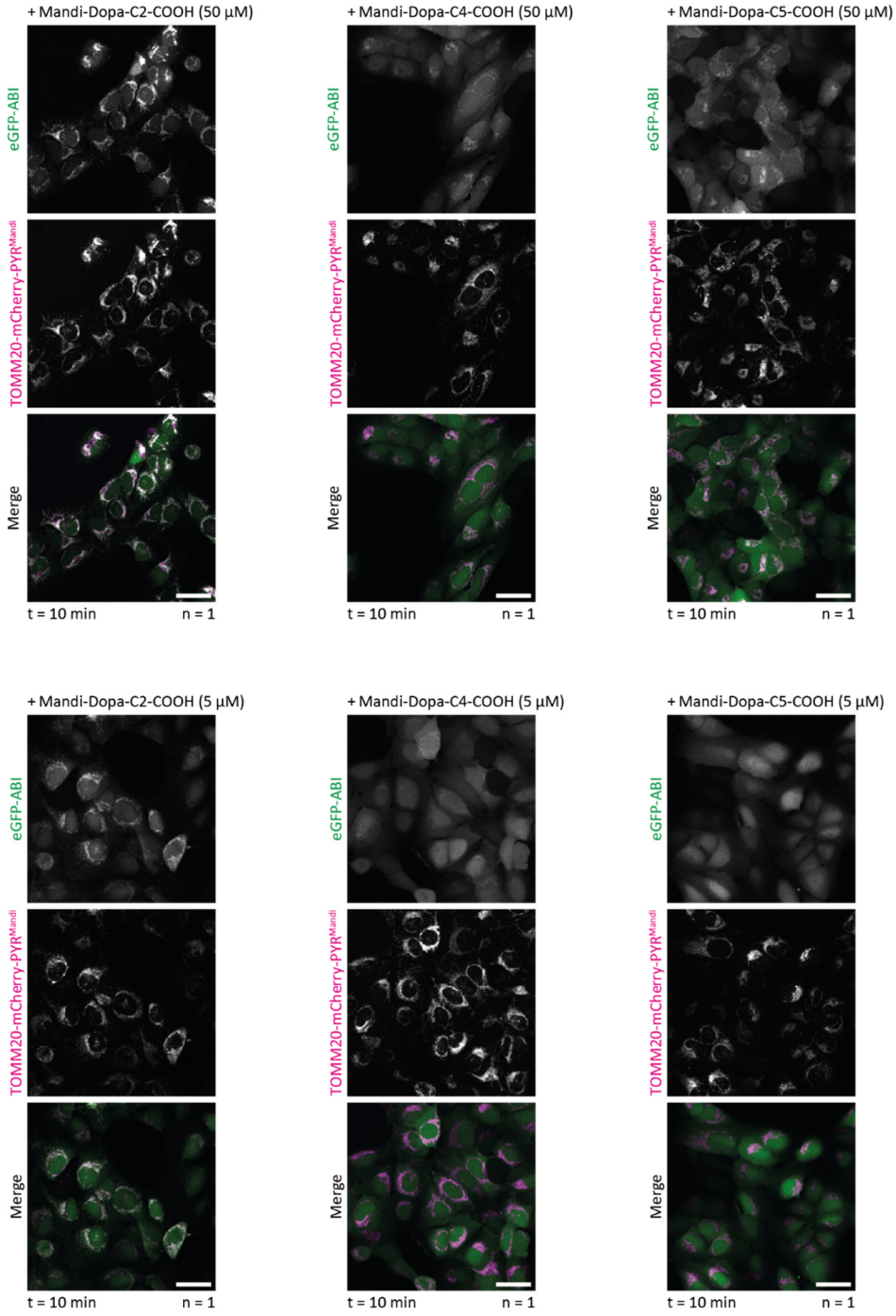

Figure 44: Titration of Mandi-Dopa-Cn-COOH on live cells expressing TOMM20-mCherry-PYR^{Mandi} and eGFP-ABI. Confocal microscopy images of U2OS FlpIN cells stably expressing TOMM20-mCherry-PYR^{Mandi} and eGFP-ABI 10 min post addition of 5 µM or 50 µM of Mandi-Dopa-Cn-COOH. Indicated number n of replicates. Scale bars at 40 µm.

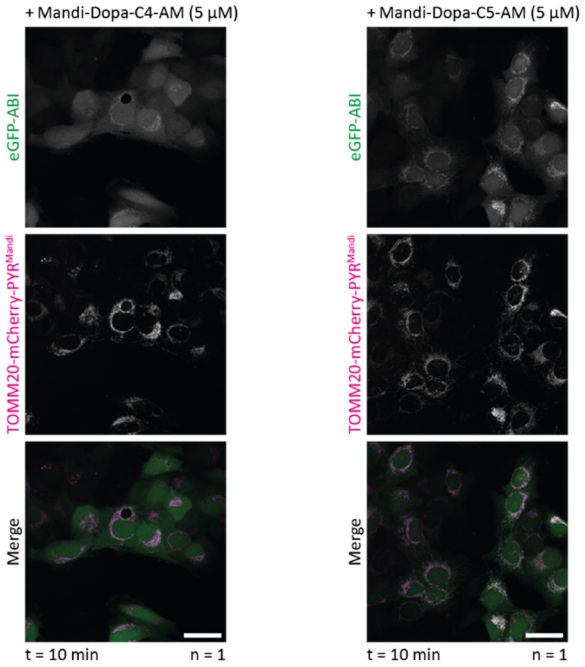

Figure 45: Addition of Mandi-Dopa-C4,5-AM to live cells expressing TOMM20-mCherry-PYR^{Mandi} and eGFP-ABI induces protein proximity. Confocal microscopy images of U2OS FlpIN cells stably expressing TOMM20-mCherry-PYR^{Mandi} and eGFP-ABI 10 min post addition of 5 µM of Mandi-Dopa-C4,5-AM. Indicated number n of replicates. Scale bars at 40 µm.

To investigate whether Mandi-Dopa-C4-NV and Mandi-Dopa-C5-NV can be used for photoactivation, cells were treated with these compounds followed by local irradiation (405 nm) of a defined of field of view (Figure 46). This should result in the induction of protein that persists over time.

Both photocaged compounds did not induce protein proximity without irradiation. Also, upon irradiation of cells treated with Mandi-Dopa-C4-NV no induction of protein proximity was observed. Hence, this compound cannot be applied for photoactivation which may be explained by the low affinity of the deprotected compound Mandi-Dopa-C4-COOH and the observation that protein proximity was induced only very weakly upon addition of the respective AM-protected derivative (Figure 45). In cells treated with Mandi-Dopa-C5-NV protein proximity was induced upon irradiation but reversed with time. This indicates that the released active molecule Mandi-Dopa-C5-COOH is unexpectedly not trapped inside the cell which makes photoactivation with high spatial precision impossible. The carboxylic acid moiety does not prevent the diffusion out of the cell making the molecule inapplicable for the intendent application. Irradiation (405 nm) of cells not treated with any Mandi derivative had no influence on protein localization.

In summary, introducing a carboxylic acid moiety to Mandi and attaching a photolabile protecting group to it does not confer the right properties to allow precise spatial control over the induction of protein proximity up to single-cell resolution.

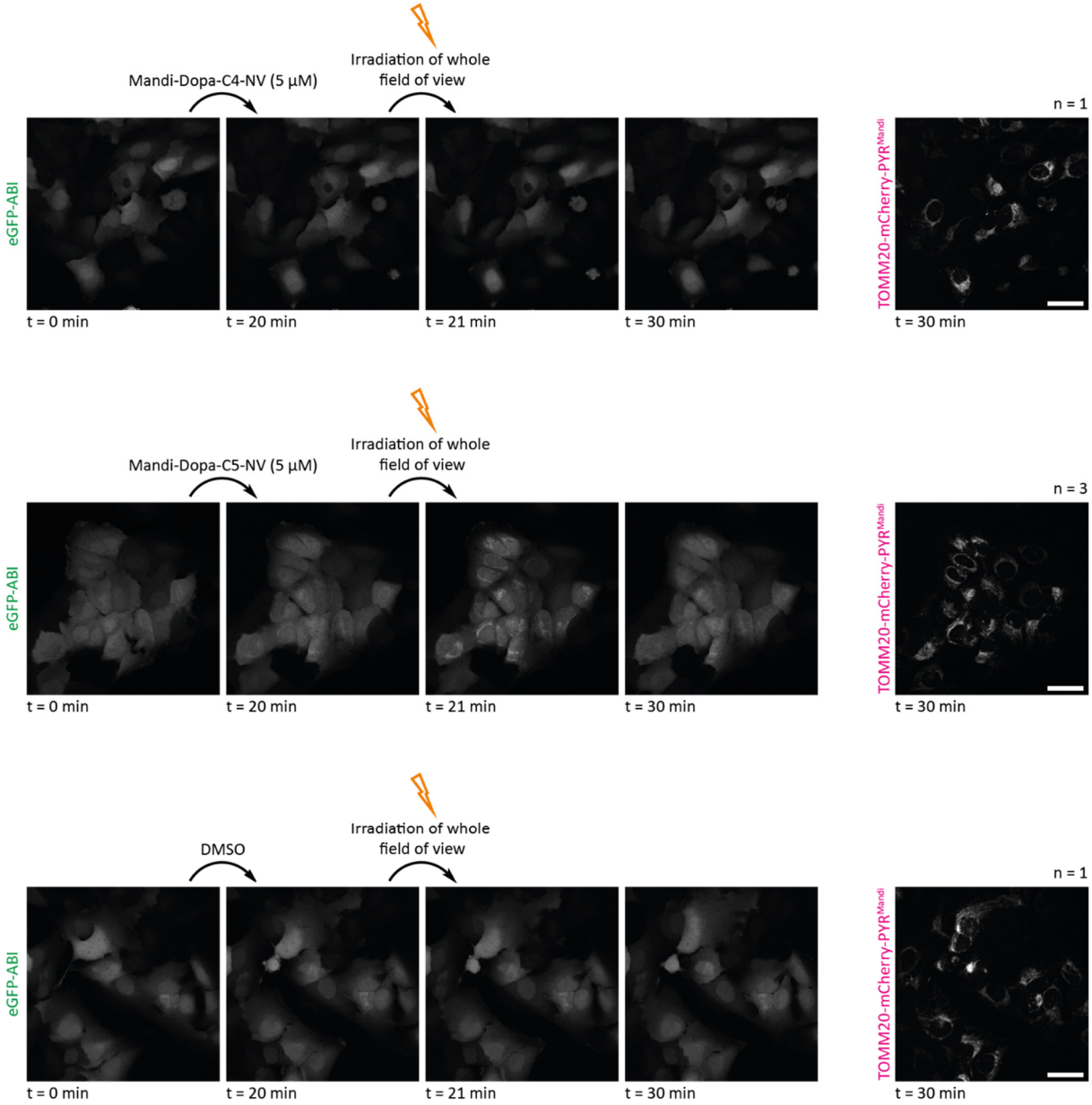

Figure 46: Local irradiation (405 nm) of cells treated with Mandi-Dopa-C4,5-NV and DMSO control. Irradiation (405 nm) does not induce protein proximity that persist over time. Confocal microscopy images of U2OS FlpIN cells stably expressing TOMM20-mCherry-PYR^{Mandi} and eGFP-ABI before and 20 min post addition of 5 µM Mandi-Dopa-C4,5-NV or DMSO. Then the whole field of view was irradiated (405 nm) and further images were taken thereafter. Indicated number n of replicates. Scale bars at 40 µm.

3.4 The ABA agonist OP as novel CIP

Based on the CIP Mandi, precise spatiotemporal control over the induction of protein proximity up to single-cell resolution could not be achieved. Therefore, I identified another candidate to reach this goal, the potent ABA agonist opabactin (OP) developed in plant research to manipulate ABA signaling in plants[51]. This compound already has a carboxylic acid moiety that I hypothesized to convey membrane impermeability and that can be photocaged converting the molecule in a cell permeable form which is the prerequisite for inducing protein proximity upon irradiation in single cells. The carboxylic acid moiety does not have to be artificially introduced to the active molecule making chemical modifications that could potentially lower its affinity obsolete. Further, since OP induces protein proximity of the same proteins as ABA already excising construct for ABA as CIP could be reused for OP as well. OP has a low nanomolar affinity to its target proteins that is 7-fold higher than the affinity of ABA and 3-fold higher than the affinity of Mandi to its interacting proteins (Table 5). Also, the affinity to the receptor protein alone is boosted by this degree. The high affinity of OP would enable low working concentrations making it attractive for the application as CIP in live mammalian cells and particularly in vivo.

Table 5: Thermodynamic characterization of ABA-based CIPs via ITC.

Ligand	Protein(s)	K_d [nM]	ΔH [kcal/mol]	-TΔS [kcal/mol]	ΔG [kcal/mol]	Data source
ABA	PYR1+HAB1	201 ± 14	-10.1 ± 0.3	0.7 ± 0.3	-9.4	Literature[51]
OP	PYR1+HAB1	28 ± 5	-21.9 ± 2.2	11.2 ± 2.3	-10.7	Literature[51]
Mandi	PYR^{Mandi}+ABI	90 ± 7	-32.2 ± 1.0	22.3 ± 1.0	-9.94 ± 0.05	This study
ABA	PYR1	-	-	-	-	No data available
OP	PYR1	1850 ± 260	-5.7 ± 0.1	-2.4 ± 0.2	-3.3	Literature[51]
Mandi	PYR^{Mandi}	6700 ± 500	-17.1 ± 1.1	9.8 ± 1.0	-7.30 ± 0.05	This study

OP was synthesized according to literature[51] and then further derivatized to the nitroveratryl ester yielding pOP (photocaged OP) and the AM ester OP-AM by Caroline Berrou under my supervision (Figure 47). The strategy to protect carboxylic acid moieties as AM esters, that are cleaved intracellularly and release the compound with a free carboxylic acid, was used successfully before for the plant hormone-based CIPs ABA [54] and GA_3[32] to increase cell permeability and reduce the working concentration.

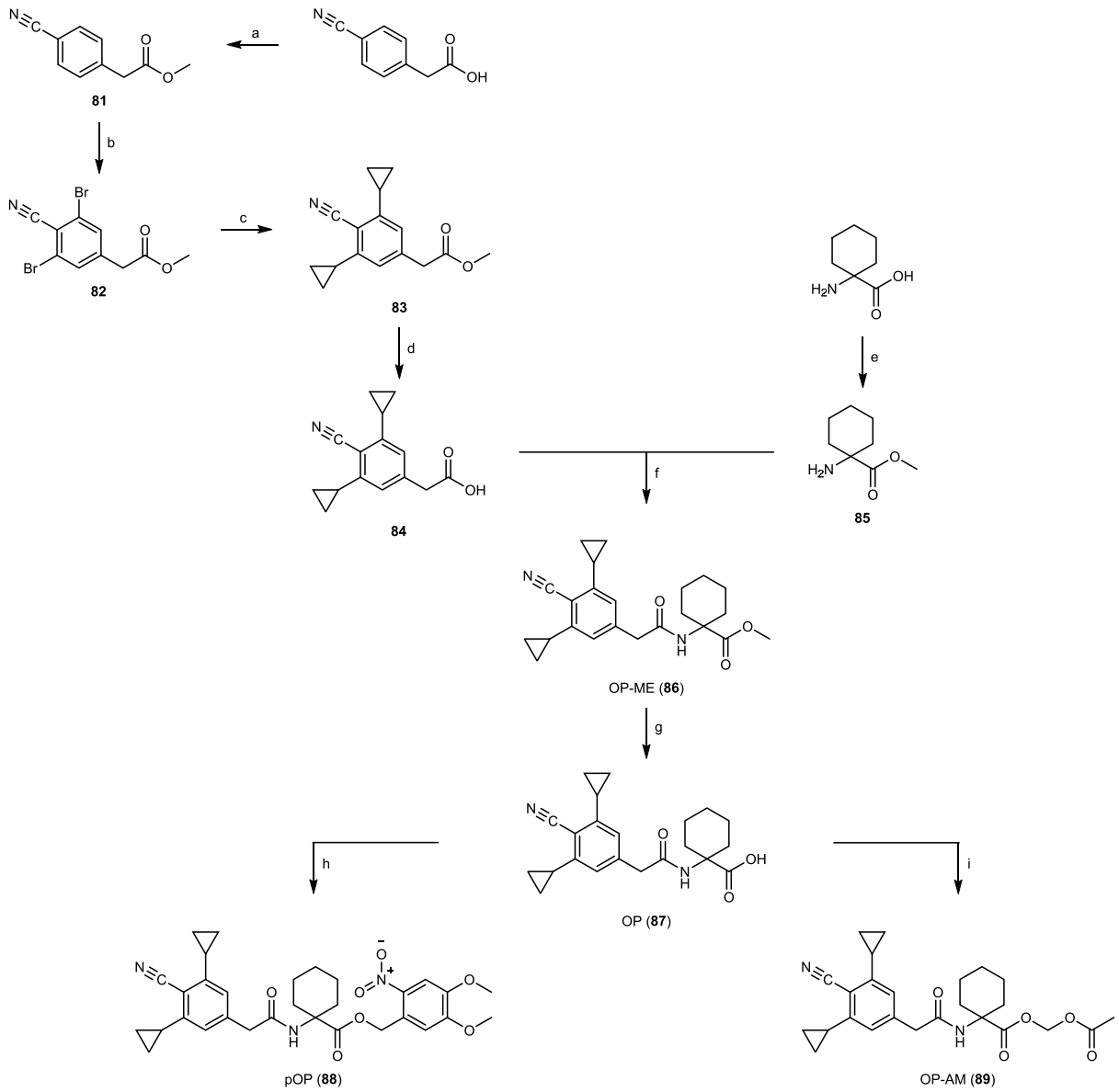

Figure 47: Synthesis of OP, pOP and OP-AM. a: MeOH, H_2SO_4, 0 °C -> rt, 2 h; b: NBS, pTsOH, $Pd(OAc)_2$, 70 °C, 21 h; c: cyclopropylboronic acid, K_3PO_4, $P(Cy)_3$, $Pd(OAc)_2$, 110 °C, 3 h; d: LiOH, rt, 16 h; e: thionyl chloride, 0 °C -> rt, 72 h; f: EDC, DMAP, rt, 16 h; g: LiOH, 50 °C, 4 h; h: 1-(bromomethyl)-4,5-dimethoxy-2-nitrobenzene, DIPEA, rt, 72 bromomethyl acetate, DIPEA, rt, 72 h. This synthesis was conducted by Caroline Berrou under my supervision.

To test OP as CIP in live mammalian cells, I used a colocalization assay similar to the previous investigation of Mandi and Mandi derivatives (see Section 3.1). Only the Mandi receptor protein PYR^{Mandi} was substituted by the ABA receptor protein PYL, while the receiver protein ABI was kept the same, to implement the interacting proteins that were previously reported for ABA as CIP in mammalian cells[52] (Figure 48). The induction of protein proximity can be read out by fluorescence colocalization of eGFP and mCherry at the outer mitochondrial membrane.

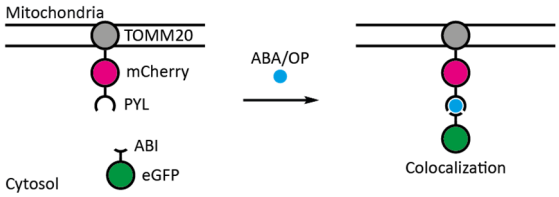

Figure 48: Schematic representation of the used colocalization assay for the induction of protein proximity with ABA/OP as CIP.

First, I performed a titration of OP and OP-AM on live mammalian cells expressing the fusion proteins TOMM20-mCherry-PYL and eGFP-ABI (Figure 49 and Figure 50). OP induced protein proximity at 500 nM within 30 min upon addition and at a concentration of 5 µM in less than 5 min. At 50 nM no induction of protein proximity was observed. Upon addition of OP-AM, protein proximity was induced at 5 nM within 30 min and at a concentration of ≥ 50 nM in less than 5 min. A concentration of 500 pM OP-AM was not sufficient to achieve protein proximity. The AM ester OP-AM can be used at 100-fold lower concentrations than the compound OP, justified in the decreased cell permeability of OP mediated by the free carboxylic acid moiety. In the absence of any CIP, the proteins PYL and ABI does not associate (Figure 85, Section 7.2).

The results demonstrate, that OP can be used as CIP in live mammalian cells and protein proximity can be induced upon addition of low nanomolar concentrations of OP-AM. This is also in good agreement with literature[51] data on the in vitro binding affinity of OP to the respective proteins, that revealed a low nanomolar affinity (Table 5).

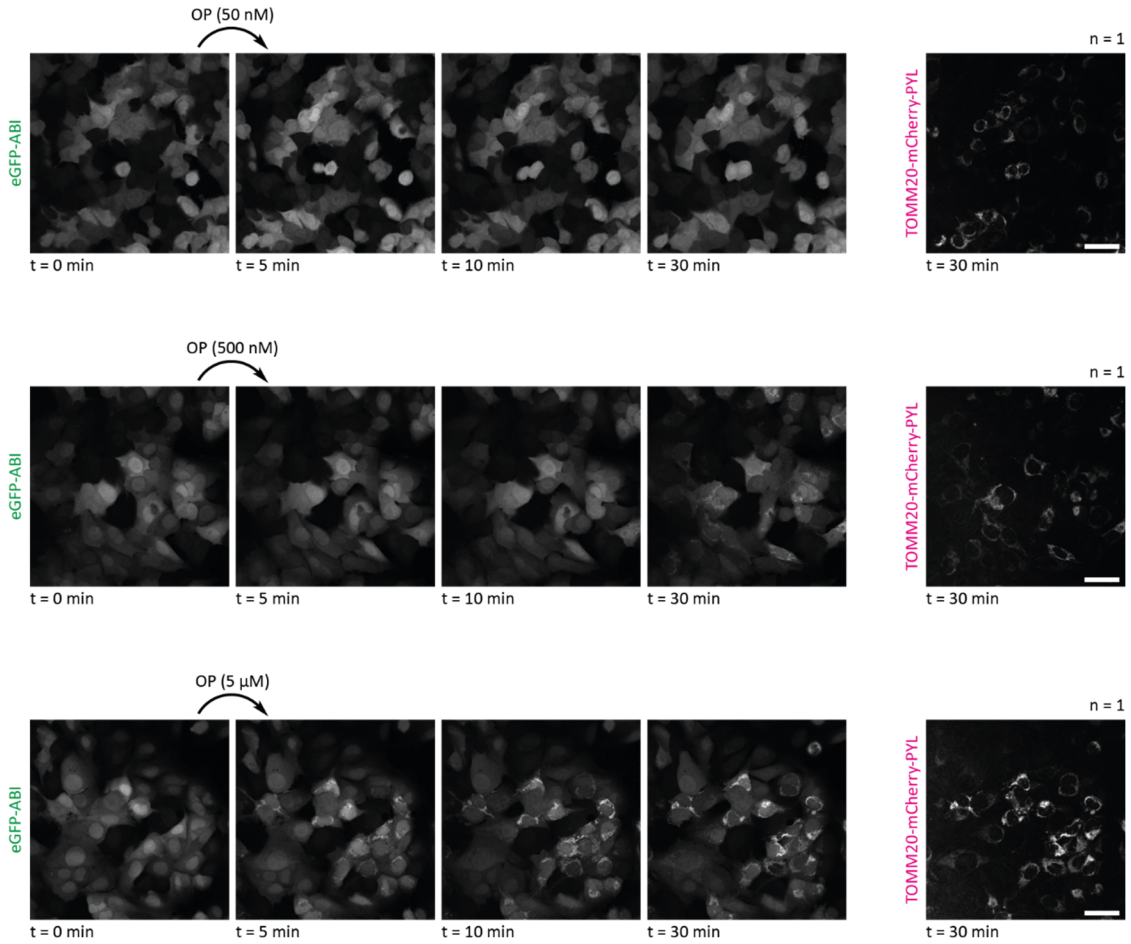

Figure 49: Titration of OP on live cells expressing TOMM20-mCherry-PYL and eGFP-ABI. Confocal microscopy images of U2OS FlpIN cells stably expressing TOMM20-mCherry-PYL and eGFP-ABI before and at different timepoints post addition of different concentrations of OP. Indicated number n of replicates. Scale bars at 40 µm.

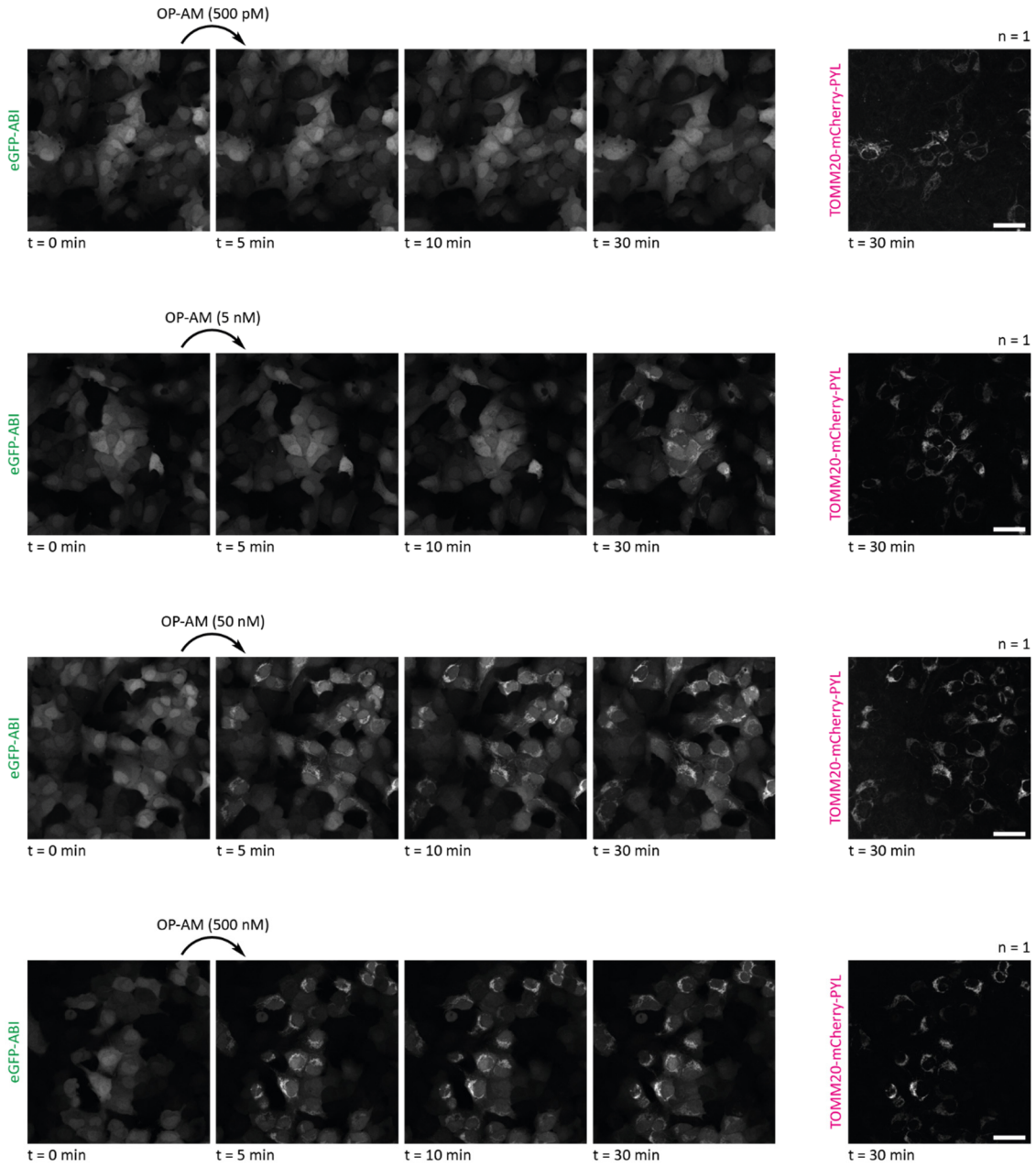

Figure 50: Titration of OP-AM on live cells expressing TOMM20-mCherry-PYL and eGFP-ABI. Confocal microscopy images of U2OS FlpIN cells stably expressing TOMM20-mCherry-PYL and eGFP-ABI before and at different timepoints post addition of different concentrations of OP-AM. Indicated number n of replicates. Scale bars at 40 µm.

Next, I compared OP/OP-AM to the already existing CIP ABA/ABA-AM in the same cellular colocalization assay (Figure 51 and Figure 52). Upon addition of ABA, protein proximity was induced at 5 µM within 10 min and at 50 µM in less than 5 min. Treatment with 500 nM ABA had no influence on protein localization. The AM protected compound ABA-AM induced protein proximity at 500 nM in less than 5 min. At a concentration of 50 nM ABA-AM weak induction of protein proximity was achieved after 10 min, a concentration of 5 nM ABA-AM was not sufficient to induce protein proximity. This results are in good agreement with literature data of ABA/ABA-AM as CIP.[54]

Similar to OP/OP-AM the AM protected derivative of ABA can be used at 100-fold lower concentrations than the compound with the free carboxylic acid moiety. ABA and ABA-AM require the use of 10-fold

higher concentrations than OP and OP-AM respectively. This corresponds well to the difference binding affinities to the proteins reported in literature[51] and determined in vitro (Table 5).

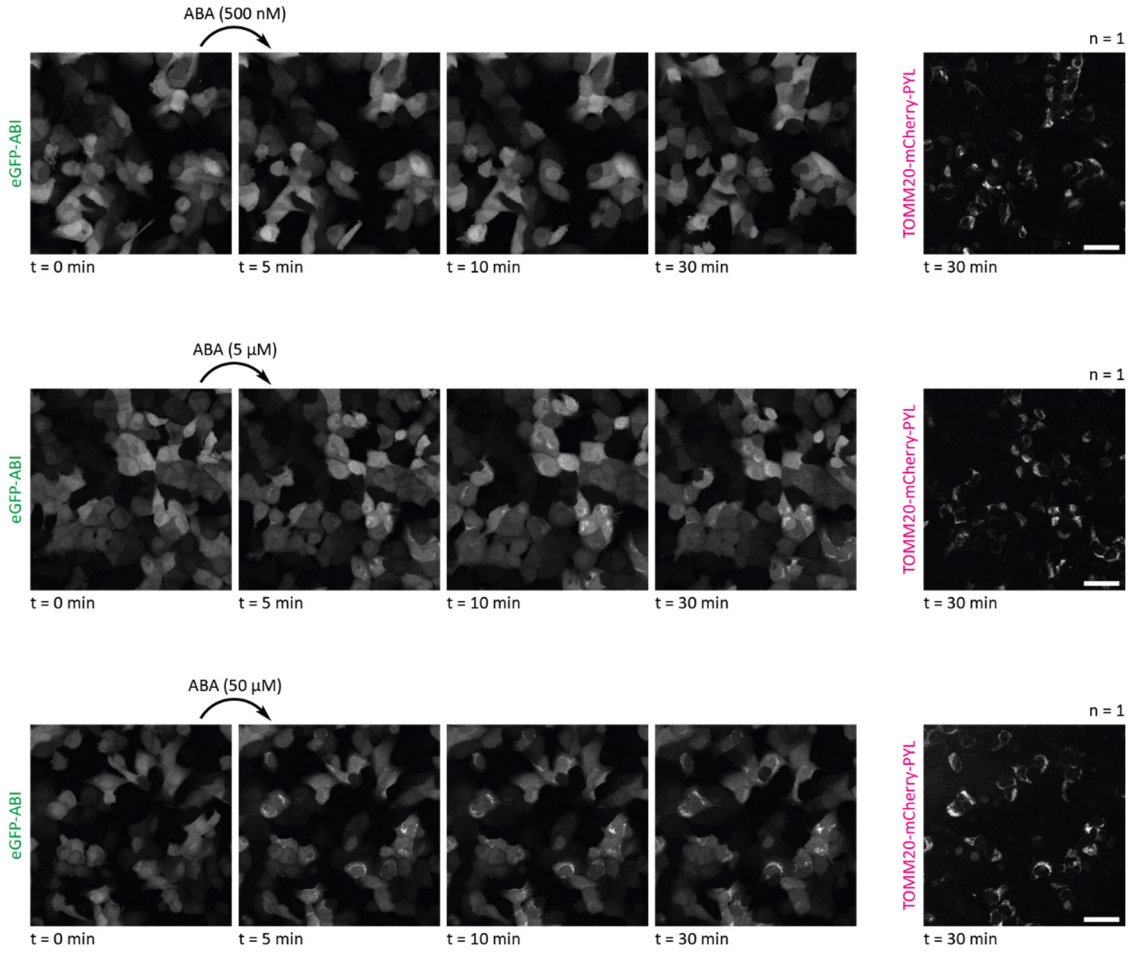

Figure 51: Titration of ABA on live cells expressing TOMM20-mCherry-PYL and eGFP-ABI. Confocal microscopy images of U2OS FlpIN cells stably expressing TOMM20-mCherry-PYL and eGFP-ABI before and at different timepoints post addition of different concentrations of ABA. Indicated number n of replicates. Scale bars at 40 µm.

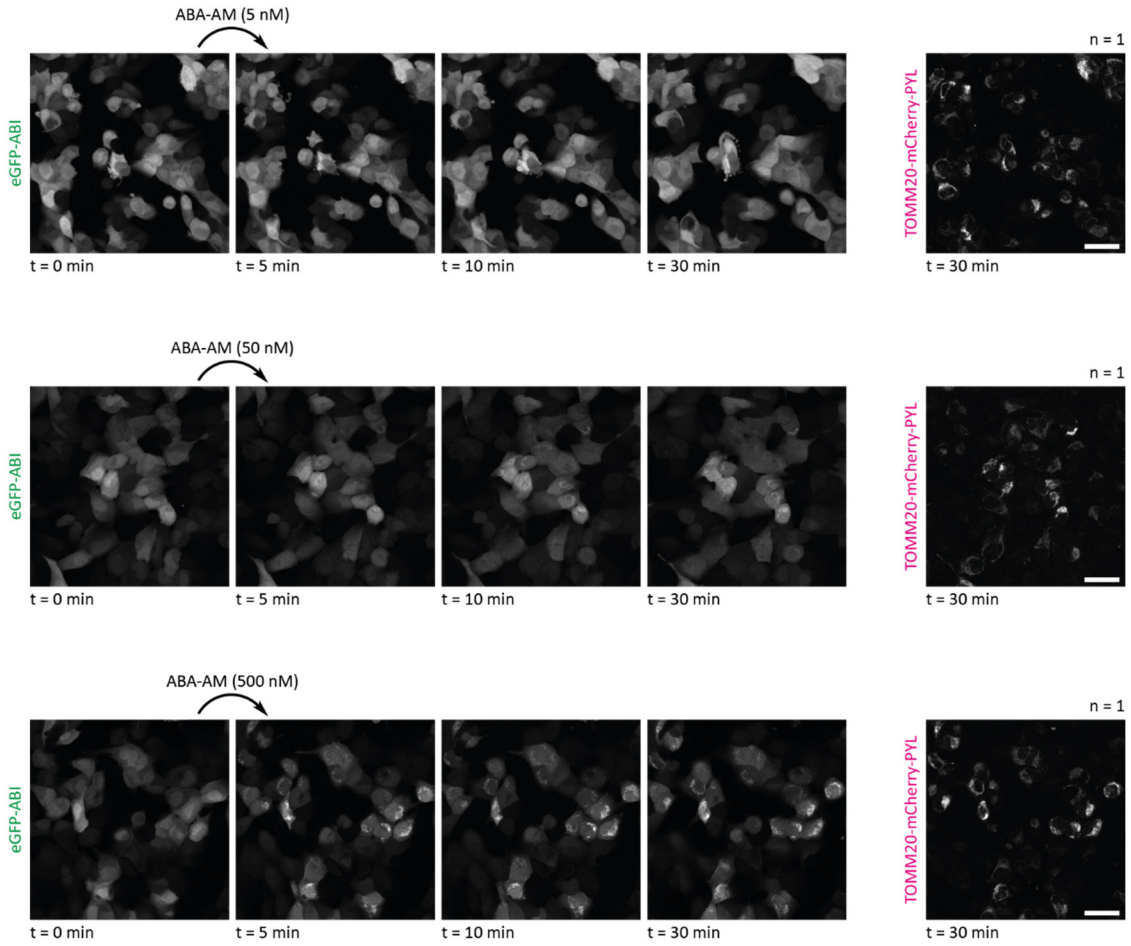

Figure 52: Titration of ABA-AM on live cells expressing TOMM20-mCherry-PYL and eGFP-ABI. Confocal microscopy images of U2OS FlpIN cells stably expressing TOMM20-mCherry-PYL and eGFP-ABI before and at different timepoints post addition of different concentrations of ABA-AM. Indicated number n of replicates. Scale bars at 40 µm.

The receptor protein PYR^{Mandi} was developed to be orthogonal to ABA and thus to not recruit the receiver protein ABI in the presence of ABA.[65] Further, it was previously shown that both CIPs, ABA-AM and Mandi, can be used for shuttling of ABI fusion proteins from the ABA receptor protein PYL (upon treatment with ABA-AM) to the Mandi receptor PYR^{Mandi} (upon treatment with Mandi). This is based on the characteristics that the receptor protein PYR^{Mandi} does not respond to treatment with ABA-AM and that both receptor proteins recruit the same receiver protein.[54]

I therefore assessed, whether the receptor protein PYR^{Mandi} is also orthogonal to OP-AM. Live cells expressing PYR^{Mandi} and ABI were treated with different concentration of OP-AM (Figure 53). Treatment with 50 nM OP-AM did not lead to the induction of protein proximity. Since OP-AM can be applied as CIP with PYL and ABI at this concentration an orthogonal use is possible. However, the orthogonality has its limits at higher concentrations, at 500 nM OP-AM protein proximity of PYR^{Mandi} and ABI was weakly induced, at 5 µM OP-AM strongly induced.

The ABA receptor protein PYL did not respond to treatment with Mandi even at high concentration (50 µM) in live cells expressing PYL and ABI and can consequently be considered as completely orthogonal to Mandi (Figure 54).

To conclude, the use of both CIPs, OP-AM and Mandi, orthogonal to each other is possible with no limits in the concentration of Mandi and low concentrations of OP-AM.

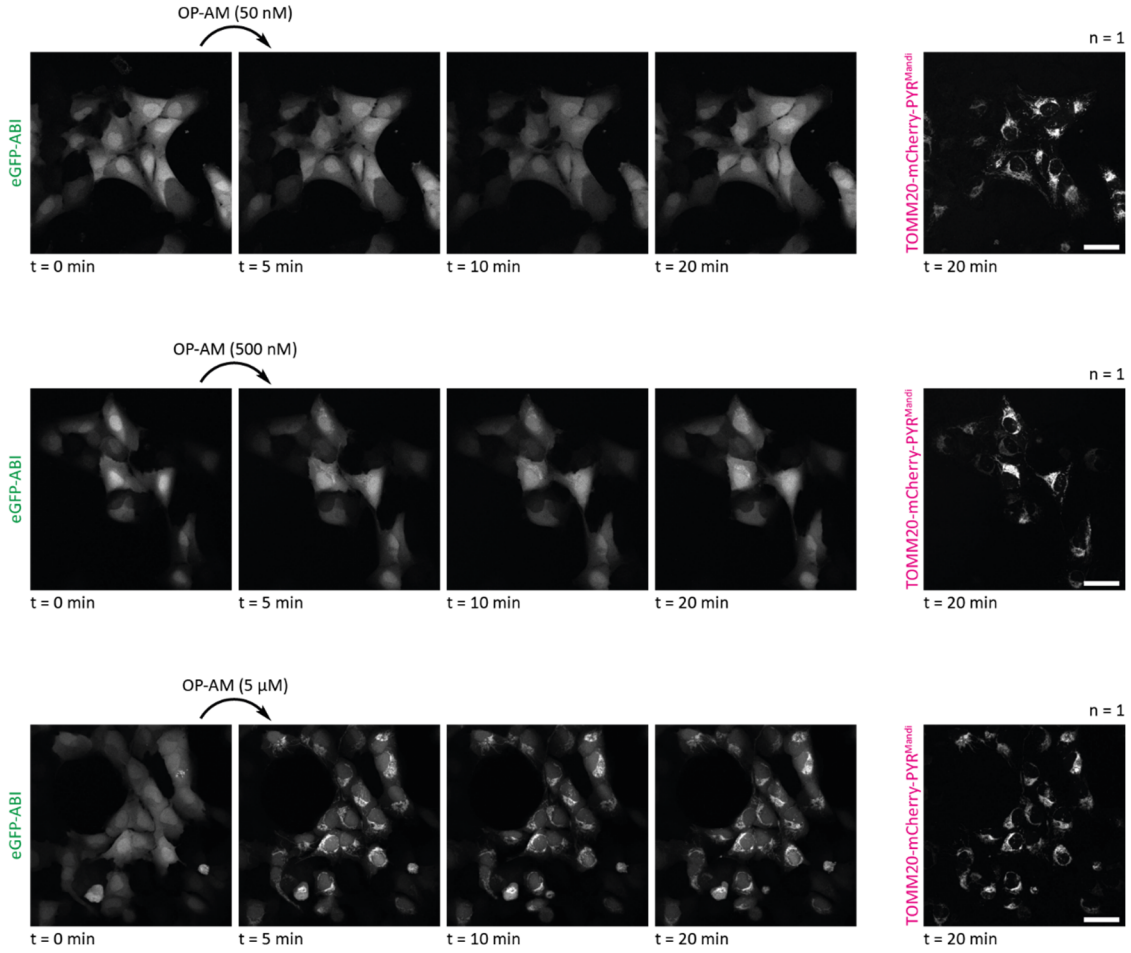

Figure 53: Evaluation of the orthogonality of OP-AM and PYR^{Mandi}. Titration of OP-AM on live cells expressing TOMM20-mCherry-PYR^{Mandi} and eGFP-ABI. Confocal microscopy images of U2OS FlpIN cells stably expressing TOMM20-mCherry-PYR^{Mandi} and eGFP-ABI before and at different timepoints post addition of different concentrations of OP-AM. Indicated number n of replicates. Scale bars at 40 µm.

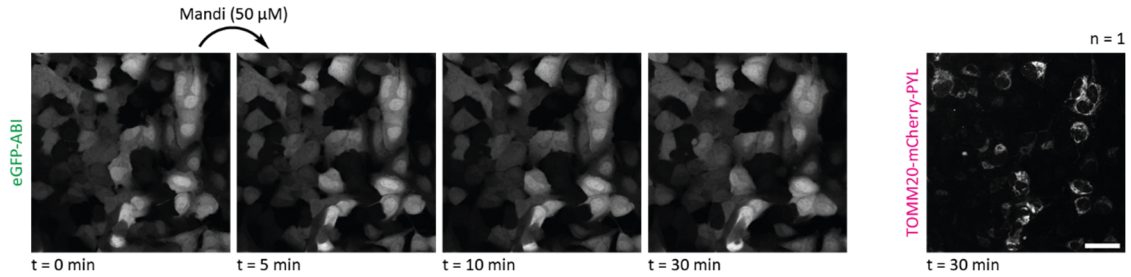

Figure 54: Evaluation of the orthogonality of Mandi and PYL. Titration of Mandi on live cells expressing TOMM20-mCherry-PYL and eGFP-ABI. Confocal microscopy images of U2OS FlpIN cells stably expressing TOMM20-mCherry-PYL and eGFP-ABI before and at different timepoints post addition of different concentrations of Mandi. Indicated number n of replicates. Scale bar at 40 µm.

I further investigated whether OP-AM can be applied as CIP in vivo in live medaka embryos. The same fluorescence colocalization assay as for the evaluation of Mandi and pMandi (see Section 3.1) was used

but with the receptor protein PYL instead of PYR^{Mandi}. Recruiting of the cytosolic eGFP-ABI fusion protein to the cell membrane where the Lyn-mCherry-PYL fusion protein is located indicates the induction of protein proximity. OP-AM was added in solution on top of the agarose embedded embryo (Figure 55).

Upon addition of 500 nM OP-AM, protein proximity was induced within 140 min in all depths of the tissue. OP-AM can be used as CIP in live medaka embryos at sub-micromolar concentrations, similar to Mandi (see Section 3.1). At a concentration as low as 5 µM OP-AM, protein proximity was induced faster, within 90 min upon addition. Addition of 50 nM OP-AM was not sufficient to induce protein proximity within 180 min (Figure 89, Section 7.2).

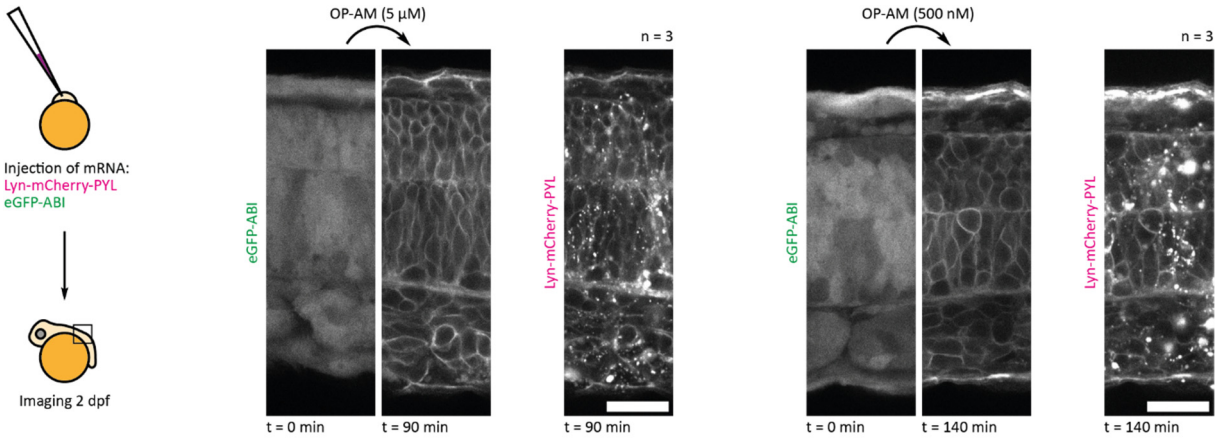

Figure 55: Application of OP-AM as CIP in live medaka embryos. Medaka embryos were microinjected with mRNA in the one-cell stage and experiments were performed 2 dpf. Addition of OP-AM to agarose embedded embryos induces protein translocation to the plasma membrane in eGFP-ABI and Lyn-mCherry-PYL mRNA injected embryos. Confocal microscopy images of the medaka embryo tail before and 90 min/140 min post addition of 5 µM/500 nM OP-AM. Indicated number n of replicates. Scale bars at 20 µm. Microinjection was performed by Kaisa Pakari.

Treatment of live medaka embryos with OP (5 µM) with its free carboxylic acid moiety did not result in the induction of protein proximity (Figure 56). I concluded, that OP cannot penetrate inside the embryo. Possibly, OP can be trapped inside medaka cells after photoactivation.

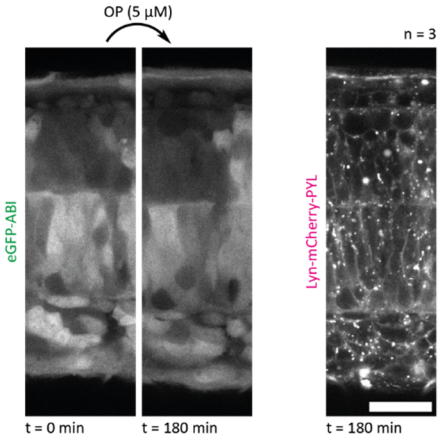

Figure 56: Addition of OP with a free carboxylic acid moiety to live medaka embryos does not induce protein proximity. Medaka embryos were microinjected with mRNA in the one-cell stage and experiments were performed 2 dpf. Addition of OP to agarose embedded embryos does not induce protein translocation to the plasma membrane in eGFP-ABI and Lyn-mCherry-PYL mRNA injected embryos. Confocal microscopy images of the medaka embryo tail before and 180 min post addition of 5 µM OP. Indicated number n of replicates. Scale bar at 20 µm. Microinjections was performed by Kaisa Pakari.

3.5 Photoactivation using photocaged OP

3.5.1 pOP

The photocaged derivative pOP was designed to put the induction protein proximity under the control of light irradiation and enable single-cell resolution.

First, I examined its decay and the release of the active molecule OP upon light irradiation in in vitro irradiation experiments. Solutions of pOP were irradiated with light of the wavelengths 365 nm (Figure 57 B) or 405 nm (Figure 58 B) and absorption spectra were recorded after different irradiation times. An isosbestic point was detected at approximately 320 nm indicating a unimolecular decay. Further, samples of pOP before and after irradiation, when no further change in the absorption spectra was monitored, as well as a sample of OP were analyzed by HPLC. The chromatograms confirmed that OP is released from pOP upon irradiation with light of the wavelengths 365 nm or 405 nm without undesired side products (Figure 57 A and Figure 58 A).

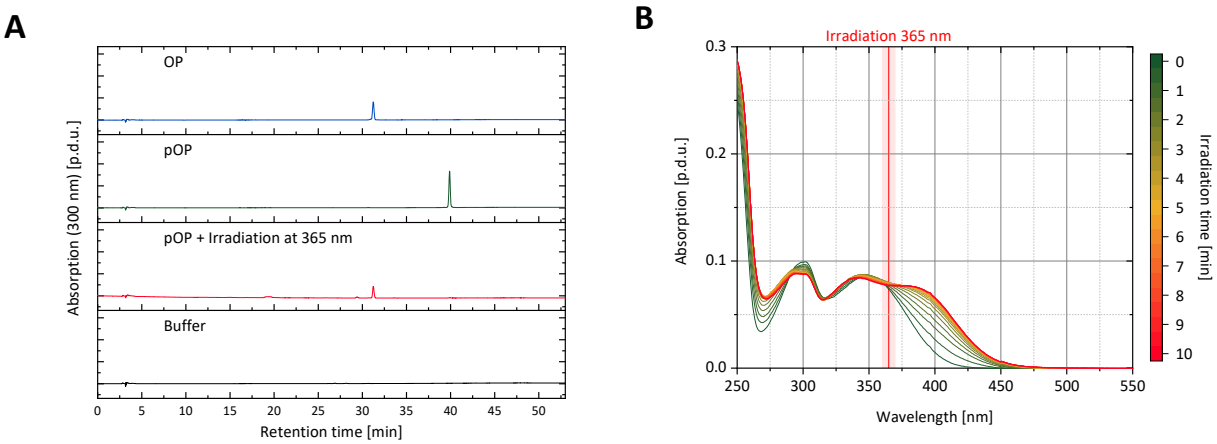

Figure 57: In vitro irradiation of pOP at 365 nm: pOP decays to OP. (A) HPLC traces at 300 nm of OP, pOP and buffer without irradiation and of pOP after irradiation (1000 mA, 10 min). (B) Absorption spectra of a solution of pOP after different irradiation times (1000 mA).

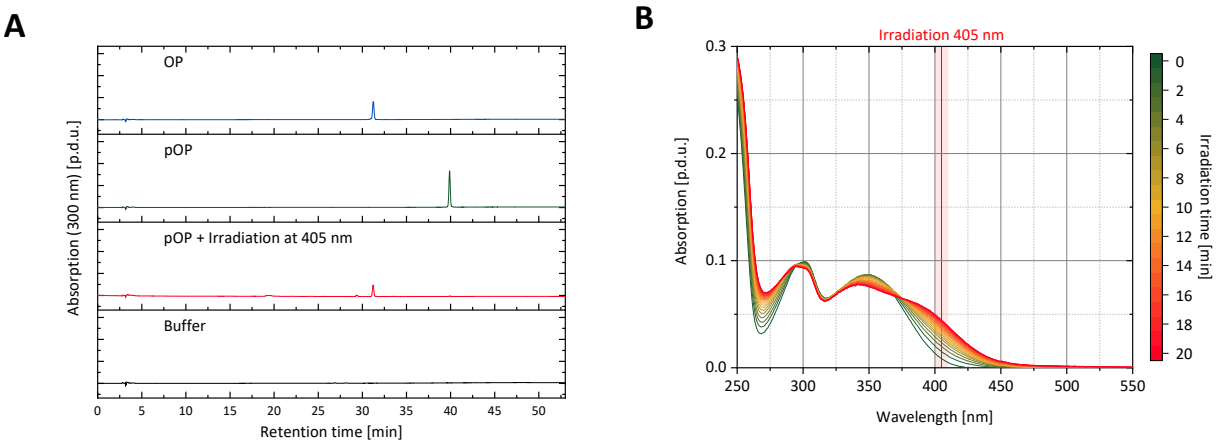

Figure 58: In vitro irradiation of pOP at 405 nm: pOP decays to OP. (A) HPLC traces at 300 nm of OP, pOP and buffer without irradiation and of pOP after irradiation (1000 mA, 40 min). (B) Absorption spectra of a solution of pOP after different irradiation times (1000 mA).

In live mammalian cells, treatment with pOP did not induce protein proximity of ABI and PYL without irradiation after a long incubation time (500 nM, 120 min) (Figure 59). The ester linkage of the photocage to the active molecule is stable in cell culture and there is no apparent basal activity of pOP. Only when the concentration of pOP was raised above micromolar (5 µM or 50 µM), I observed an induction of protein proximity without irradiation (Figure 87, Section 7.2) similar to the experiments with pMandi (see Section 3.3.1). However, I hypothesized using pOP at a working concentration of 500 nM would allow photoactivation without any apparent basal activity, similar to pMandi (see Section 3.3.1).

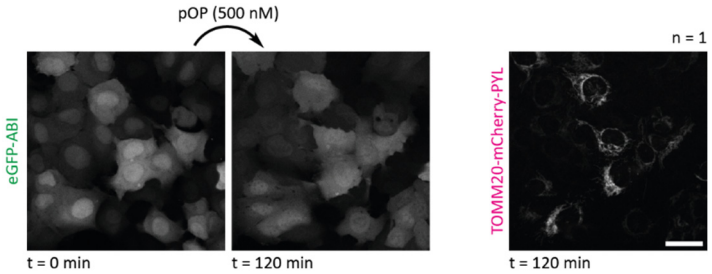

Figure 59: In live mammalian cells pOP does not induce protein proximity without irradiation. Confocal microscopy images of U2OS FlpIN cells stably expressing TOMM20-mCherry-PYL and eGFP-ABI before and 120 min post addition of 500 nM pOP. Indicated number n of replicates. Scale bar at 40 µm.

To investigate, if pOP can be used to induce protein proximity of the proteins PYL and ABI in live mammalian cells (Figure 60) at a concentration of 500 nM and enables precise spatiotemporal control, I irradiated (405 nm) the cells in defined field of view using a confocal microscope (Figure 61). Protein proximity was induced 5 min after irradiation and persisted over time. Since in contrast to pMandi and Mandi-Dopa-C5-NV (see Section 3.4) no reversion of the induced protein proximity was observed over time, I hypothesized that the active molecule OP, released from pOP upon irradiation, is trapped inside the cells and does not diffuse out the cells which allows precise spatial control over the induction of protein proximity. However, the induction of protein proximity did not occur immediately after irradiation (≤ 1 min) as with pMandi, but with a short time delay (5 min) after irradiation. Irradiation in the absence of pOP had no influence on protein localization (Figure 60).

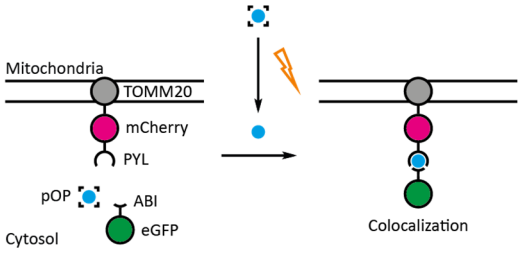

Figure 60: Schematic representation of the used protein construct and the colocalization assay for the investigation of pOP. Upon irradiation pOP is converted into the active molecule OP and protein proximity is induced.

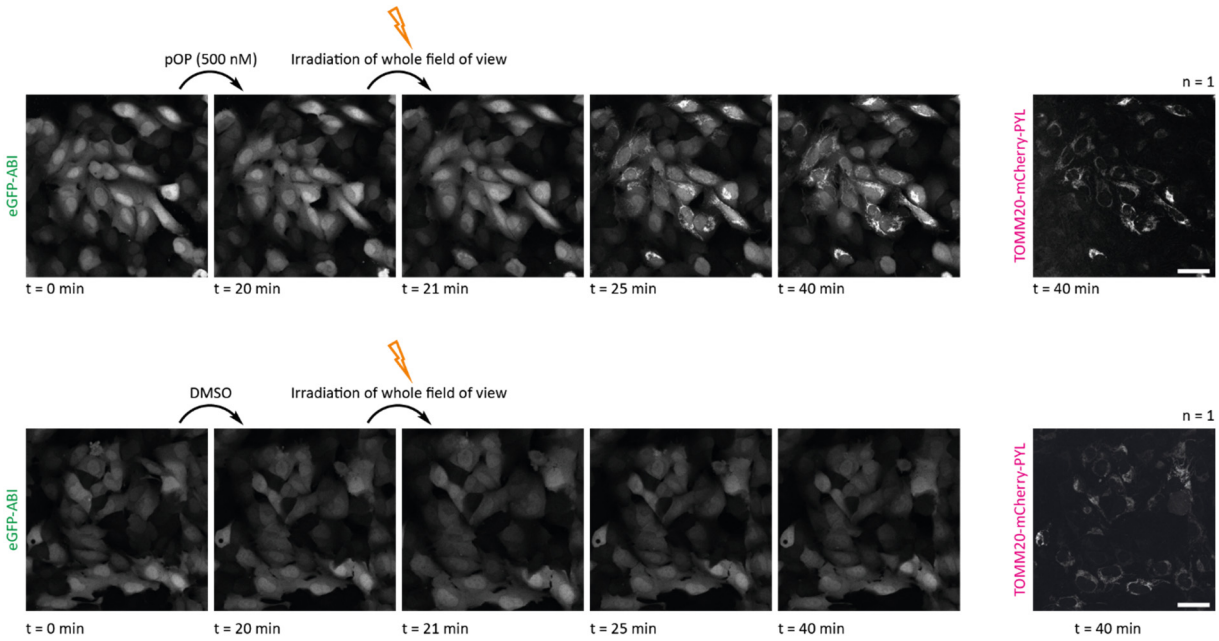

Figure 61: Local irradiation (405 nm) of live cells treated with pOP on a confocal microscope and DMSO control. Treatment with pOP and irradiation (405 nm) leads to induction of protein proximity that persist over time. Confocal fluorescence microscopy images of U2OS FlpIN cells stably expressing TOMM20-mCherry-PYL and eGFP-ABI before and 20 min post addition of 500 nM pOP or DMSO. Then, the whole field of view was irradiated (405 nm) and further images were taken thereafter. Indicated number n of replicates. Scale bars at 40 µm.

In a next step, different single cells treated with pOP in the same field of view were irradiated (405 nm) successively (Figure 62). Upon irradiation of a region of interest (ROI) in the first single cell, protein proximity was induced only in that single cell while protein localization in the other non-irradiated cells remained unaffected. This procedure could be repeated for a second single cell in the same field of view. Finally, to proof that protein proximity can be induced in all displayed cells, the whole field of view was irradiated resulting in the induction of protein proximity in all displayed cells. These results clearly demonstrate that pOP can be used to induce protein proximity in live mammalian cells with precise spatiotemporal control up to single-cell resolution. For at least 40 min after irradiation no effect on cells neighboring the irradiated cell was observed.

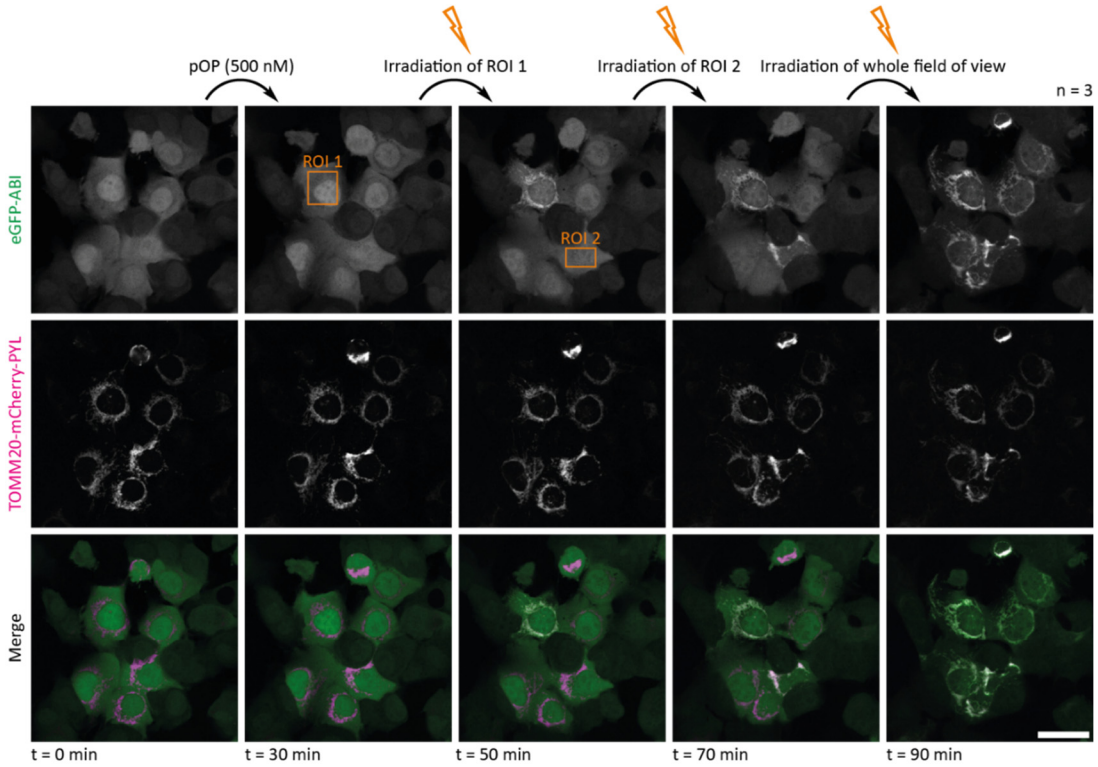

Figure 62: Precise local and temporal control over the induction of protein proximity with pOP. Colocalization is only induced in irradiated (405 nm) cells. Confocal microscopy images of U2OS FlpIN cells stably expressing TOMM20-mCherry-PYL and eGFP-ABI before and at different timepoints post addition of 500 nM pOP and post irradiation (405 nm). Irradiation (405 nm) was performed at 30 min, 50 min and 70 min. Indicated number n of replicates. Scale bar at 40 µm.

Having successfully shown that pOP can be used as photoactivatable CIP in live mammalian cells, I investigated whether photoactivation also works in vivo in live medaka embryos (Figure 63). However, upon addition of pOP (5 µM) to agarose embedded embryos at the same concentration as pMandi (see Section 3.3.1), protein proximity was induced without irradiation. At this concentration of pOP, which is only 10-fold higher than the lowest working concentration of OP-AM in medaka embryos, pOP should not have any background activity. With the same 10-fold OP-AM/pOP concentration difference based on the lowest working concentration of OP-AM, pOP could be successfully applied in experiments with live mammalian cells. I hypothesized, that the photolabile protecting group is cleaved inside the embryo by hydrolysis and not by light irradiation resulting in the release of the active molecule OP. The ester bond, linking the photocage to OP, is obviously not stable in live medaka embryos. pOP is therefore not suitable to induce protein proximity upon irradiation in live medaka embryos.

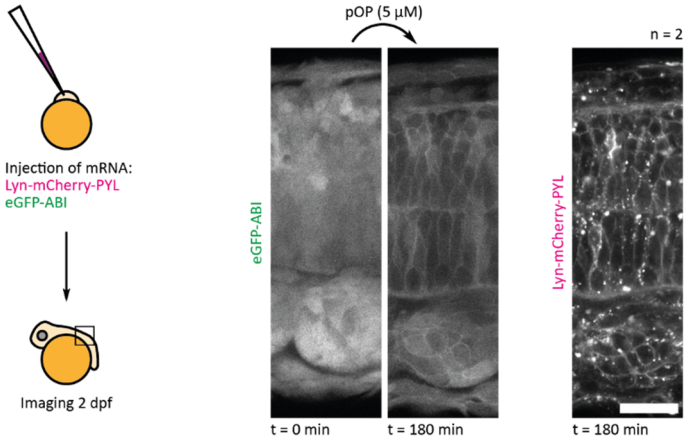

Figure 63: pOP induces protein proximity in live medaka embryos without irradiation. Medaka embryos were microinjected with mRNA in the one-cell stage and experiments were performed 2 dpf. Addition of pOP to agarose embedded embryos induces protein translocation to the plasma membrane in eGFP-ABI and Lyn-mCherry-PYL mRNA injected embryos. Confocal microscopy images of the medaka embryo tail before and 180 min post addition of 5 µM pOP. Indicated number n of replicates. Scale bar at 20 µm. Microinjection was performed by Kaisa Pakari.

3.5.2 Optimization of pOP

To design a photocaged derivative of OP that is stable in vivo, the photocage need to be attached via a linkage that is not prone to hydrolysis like an ester bond. In the design and application of pMandi, I showed that the photolabile protecting group can be attached to the nitrogen atom of an amide bond allowing successful photoactivation in live medaka embryos. This type of linkage is apparently more stable in vivo than a linkage via an ester bond. Since OP also has a central amide bond, I envisioned that it can be photocaged in a similar way to pMandi. To maintain at the same time good cell permeability and enable trapping inside the cells the carboxylic acid moiety needs to be protected as AM ester. For the synthesis of the target molecule pOP-AM, I applied two synthetic strategies (Figure 64). In the first strategy, the photocage should be directly attached to the OP derivative OP-ME. However, nitroveratryl bromide did not react with OP-ME in the presence of the bases sodium hydride, potassium carbonate or sodium methoxide. Also, addition of OP-ME to a mixture of nitroveratryl alcohol, DIAD and triphenylphosphine (Mitsunobu reaction) did not lead to conversion of OP-ME. In a second strategy, the photocage should be coupled to the cyclohexyl part of OP and the product CyHe-NV then be reacted with the dicyclopropylphenyl part of OP (CPP-OH/Cl). The first synthetic step was carried out successfully, but the peptide coupling (HATU, DIPEA) with the dicyclopropylphenyl building block CPP-OH did not lead to any conversion. Likewise, CyHe-NV did not react with the acyl chloride of the dicyclopropylphenyl part CPP-Cl.

The synthesis of pOP-AM via these two strategies was not possible. Potentially because of steric hindrance the amide nitrogen is not accessible for attaching chemical modifications.

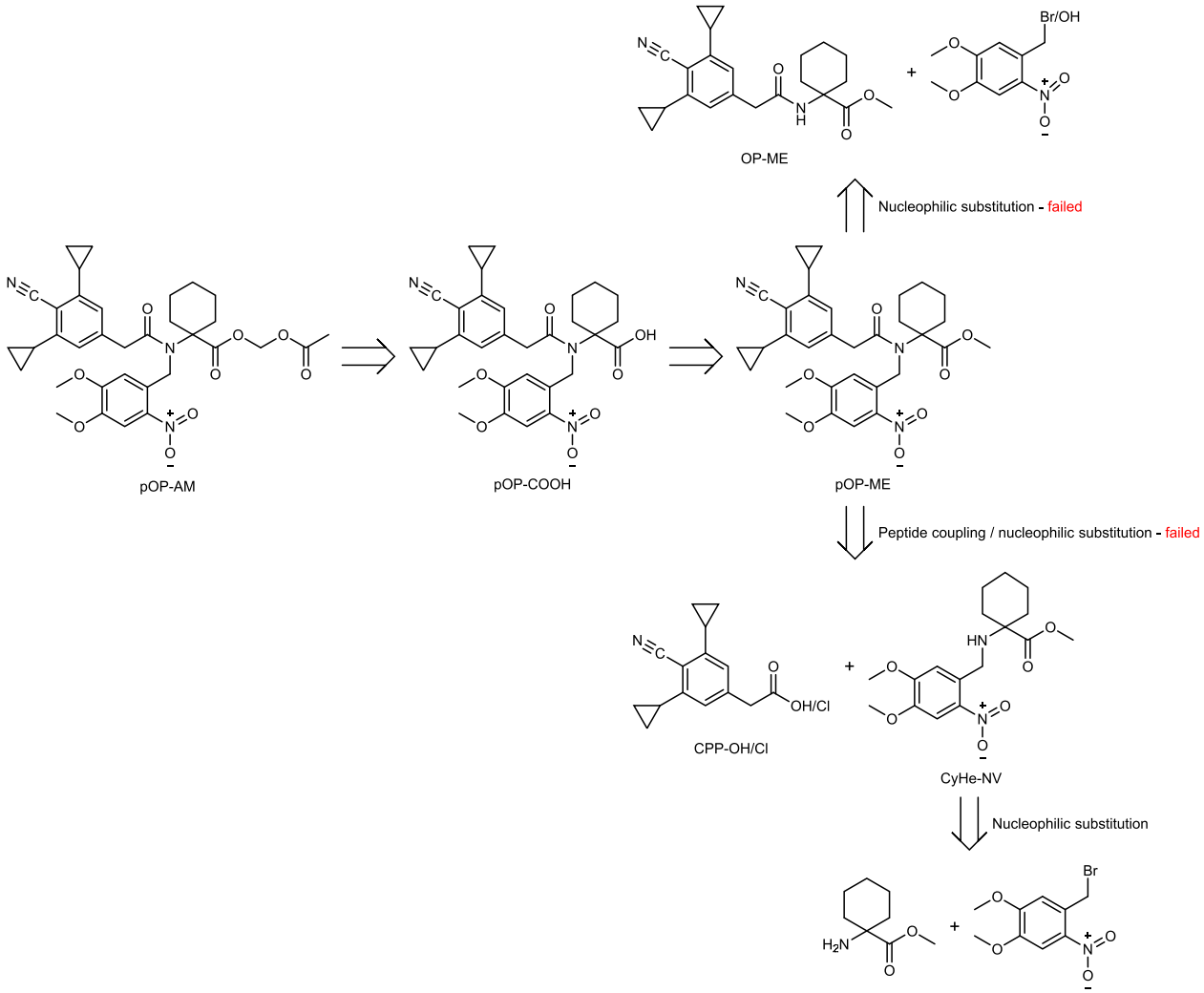

Figure 64: Retrosynthesis of an optimized version of pOP: pOP-AM, a NV- and AM-caged OP derivative.

Outlook

Another strategy to design an OP derivative that is stable in vivo, would be attaching the photocage to the carboxylic acid moiety via a linkage that is more stable against hydrolysis than an ester bond. In a study on photocaged derivatives of auxin, it was reported that an auxin derivative with a photolabile 4-methoxy-7-nitroindolinyl (MNI) protecting group attached to the carboxylic acid moiety via an amide bond is more stable than nitrobenzyl esters in plants in the absence of irradiation.[44] This photocage attached to the carboxylic acid moiety of OP may also lead to a OP derivative (OP-MNI) that is stable in vivo and could potentially be synthesized via a peptide coupling or from the acyl chloride of OP with the indolinyl derivative (Figure 65). Nevertheless, the steric hindrance of the cyclohexyl group of OP may prevent the reaction with MNI that is itself more sterically demanding than nitroveratryl bromide.

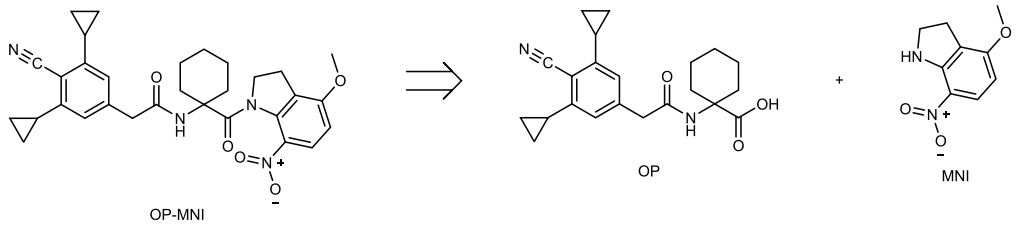

Figure 65: Retrosynthesis of an optimized version of pOP: OP-MNI, a MNI-caged OP derivative.

3.6 Split PYR^{Mandi}

To investigate processes that involve the interaction of three protein or the interaction of two protein at a specific subcellular target, tools are required that allow the induction of proximity of three different interacting protein domains. In 2020, a system to chemically induce protein trimerization based on the CIP rapamycin was developed by splitting the interacting proteins FRB or FKBP12 (see Section 1.22).[29] However, this system has drawbacks, such as the non-orthogonality of rapamycin in mammalian cells and the association of the split fragments in the presence of rapamycin but the absence of the second interacting protein. I envisioned, that these problems could be overcome by engineering a system to induce trimerization based on the proteins PYR^{Mandi} and ABI and the CIP Mandi by splitting PYR^{Mandi} into two fragments. Since PYR^{Mandi} alone binds Mandi with an approximately 75-fold lower affinity than in the presence of ABI, I hypothesized that PYR^{Mandi} split fragments would no associate in the absence of ABI induced by the presence of Mandi. Moreover, in contrast to rapamycin, Mandi is orthogonal in mammalian cells.

To design and identify PYR^{Mandi} split proteins that associate in the presence of Mandi, I adapted a strategy reported in 2022 for the development of split ligand binding proteins that associate in a ligand dependent way.[80] I chose split sites in solvent exposed loops (Figure 66) and inserted the C-terminal split fragment of the firefly luciferase (cLuc) to the C-terminal split fragment of PYR^{Mandi} as well as the N-terminal split fragment of the firefly luciferase (nLuc) to the N-terminal split fragment of PYR^{Mandi} (Figure 67). In this design, ligand-dependent reconstitution of the split PYR^{Mandi} fragments induces the reconstitution of the split luciferase that can be read out via the luciferase activity (generation of bioluminescence in the presence of the luciferase substrate). Split constructs with the largest change in luciferase activity between the presence or the absence of Mandi would identify the most promising split PYR^{Mandi} fragments for the induction of protein trimerization. These fragments should be further investigated in a colocalization assay with live mammalian cells.

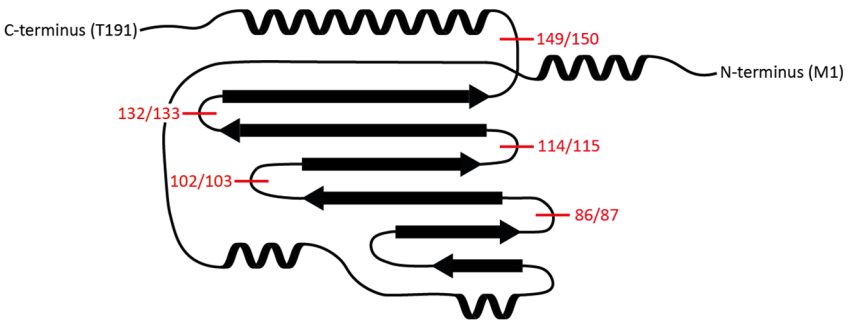

Figure 66: Schematic representation of PYR^{Mandi}. Split sites in solvent exposed loops are marked in red.

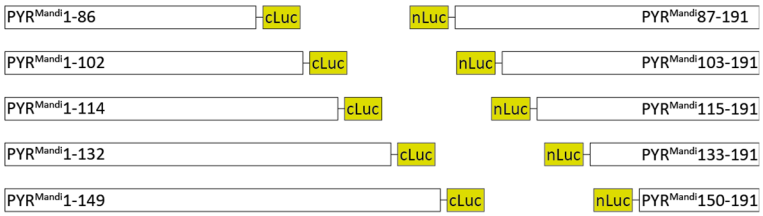

Figure 67: Schematic representation of the split PYR^{Mandi} constructs used for the luciferase assay.

I performed a dual luciferase assay in cell lysate with the split firefly luciferase (split fLuc) fragments attached to the split PYR^{Mandi} fragments and complete renilla luciferase (rLuc) as expression control. First, the assay was conducted only with the split PYR^{Mandi} fragments in the absence of the receiver protein (Figure 68 A). Live mammalian HEK293 cells expressing the respective protein constructs were incubated with Mandi (50 µM) overnight prior lysis. No increased luciferase activity that would indicate complex formation was observed for any split PYR^{Mandi} construct compared to the absence of Mandi (DMSO control). There is no association of the split fragments in the presence of Mandi, but the absence of the second interacting protein. The luciferase activity in the presence of Mandi is slightly lower compared to the DMSO control in all investigated samples including the positive and negative control, indicating that Mandi has a slight inhibitory effect on the luciferase activity. However, this effect is only minor and not large enough to have an impact on the conclusions drawn from the experiment.

The same experiment was conducted with the receiver protein ABI co-expressed with the split PYR^{Mandi} fragments (Figure 68 B). Now, the luciferase assay revealed increased luciferase activity for the construct with the PYR^{Mandi} split site 132/133 in the presence of Mandi compared to the DMSO control. For the other split constructs, no increased complex formation was detected in the presence of Mandi.

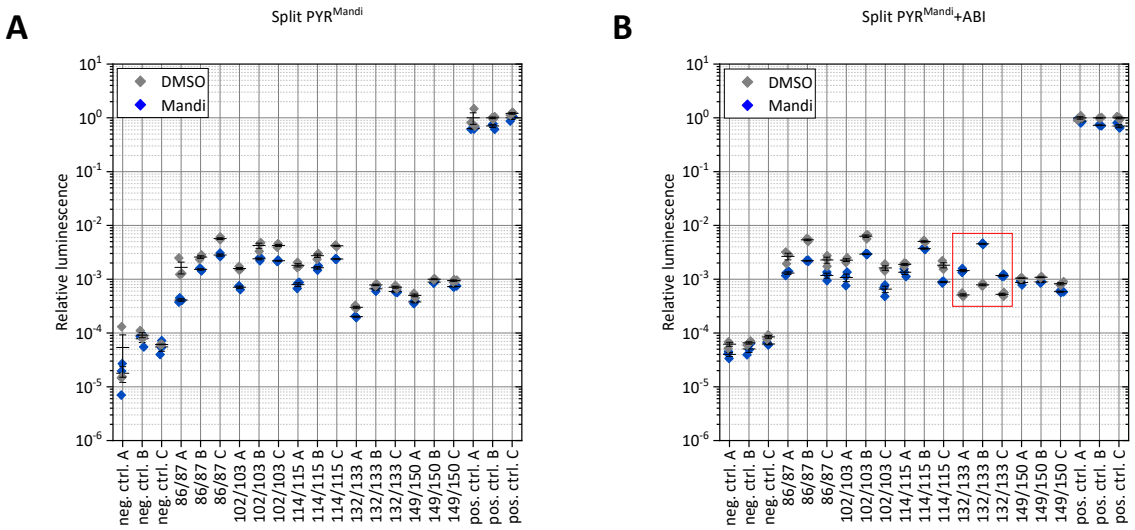

Figure 68: Split luciferase assay in cell lysate without (A) or with (B) co-expression of ABI. Relative luminescence in the presence of Mandi (50 µM) and DMSO control for different split PYR^{Mandi} constructs. A dual luciferase assay with split fLuc was performed. fLuc luminescence was divided by the luminescence of co-expressed complete rLuc and normalized to the luminescence of complete fLuc in the presence of DMSO. Each 3 replicates per conditions (A, B and C) with each 3 measurements represented as single values with mean and standard deviation of the mean. Negative control: rLuc only. Positive control: complete fLuc.

To summarize the results, the relative luminescence in the presence of Mandi was divided by the relative luminescence in DMSO control in the absence of Mandi for all experiments (Figure 69). It becomes apparent, that the split PYR^{Mandi} constructs PYR^{Mandi}1-132 and PYR^{Mandi}133-191 show 4-fold increased complex formation upon treatment with Mandi in the presence of ABI compared to the DMSO control. In the absence of ABI, no increased complex formation in the presence of Mandi compared to the DMSO control was observed. Obviously, the receiver protein is needed to allow reconstitution of the PYR^{Mandi} protein in the presence of Mandi.

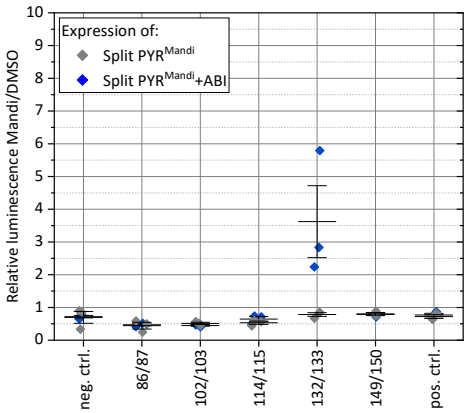

Figure 69: The split PYR^{Mandi} constructs PYR^{Mandi}1-132 and PYR^{Mandi}133-191 show 4-fold increased complex formation upon treatment with Mandi only in the presence of ABI compared to the DMSO control. Relative luminescence in the presence of Mandi (50 µM) divided by the DMSO control for different split PYR^{Mandi} constructs in a split luciferase assay in cell lysate with or without co-expression of ABI. A dual luciferase assay with split fLuc was performed. fLuc luminescence was divided by the luminescence of co-expressed complete rLuc and normalized to the luminescence of complete fLuc in the presence of DMSO. Ratios for each 3 replicates per condition represented as single values with mean and standard deviation of the mean. Negative control: rLuc only. Positive control: complete fLuc.

The identified split fragments PYR^{Mandi}1-132 (15.1 kDa) and PYR^{Mandi}133-191 (6.4 kDa) are of different sizes, but both have contact sites to Mandi (Figure 70).

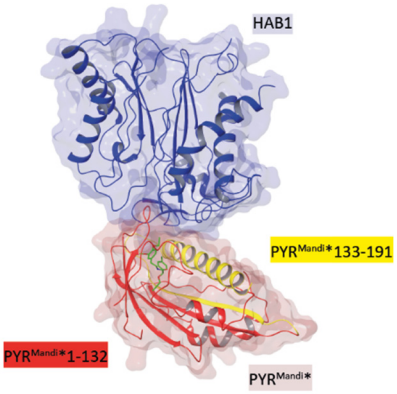

Figure 70: Crystal structure of the PYR^{Mandi}*-Mandi-HAB1 complex (pdb: 4WVO). Split fragments of PYR^{Mandi}* marked in different colors (PYR^{Mandi}*1-132: red, PYR^{Mandi}*133-191: yellow).

After identifying the split fragments PYR^{Mandi}1-132 and PYR^{Mandi}133-191 in the luciferase assay, I further investigated these split proteins in live mammalian cells with a colocalization assay. First, it was tested whether the individual split PYR^{Mandi} fragments alone can recruit the receiver protein ABI (Figure 71 A and B). The split PYR^{Mandi} fragments were each individually expressed in different experiments as fusion protein with the red fluorescent protein mCherry and TOMM20, localizing the fusion proteins to the outer mitochondrial membrane with mCherry and the split PYR^{Mandi} fragment pointing into the cytosol. The receiver protein ABI was co-expressed cytosolically fused to the green fluorescent protein eGFP. Treatment with Mandi at a high concentration (50 µM) did not result in fluorescence colocalization, no protein proximity was induced. The individual split PYR^{Mandi} fragments, PYR^{Mandi}1-132 and PYR^{Mandi}133-191, alone cannot recruit ABI in the presence of Mandi.

Next, both split PYR^{Mandi} fusion proteins were expressed together with eGFP-ABI in live mammalian cells (Figure 71 C). In this experiment, the treatment with Mandi (50 µM) led to the recruiting of the cytosolic protein construct with the receiver protein ABI to the outer mitochondrial membrane where the PYR^{Mandi}1-132 and PYR^{Mandi}133-191 were located. The split PYR^{Mandi} fragments can associate to a functional receptor protein and recruit the receiver protein ABI in the presence of Mandi when expressed at the same subcellular membrane localization in live mammalian cells.

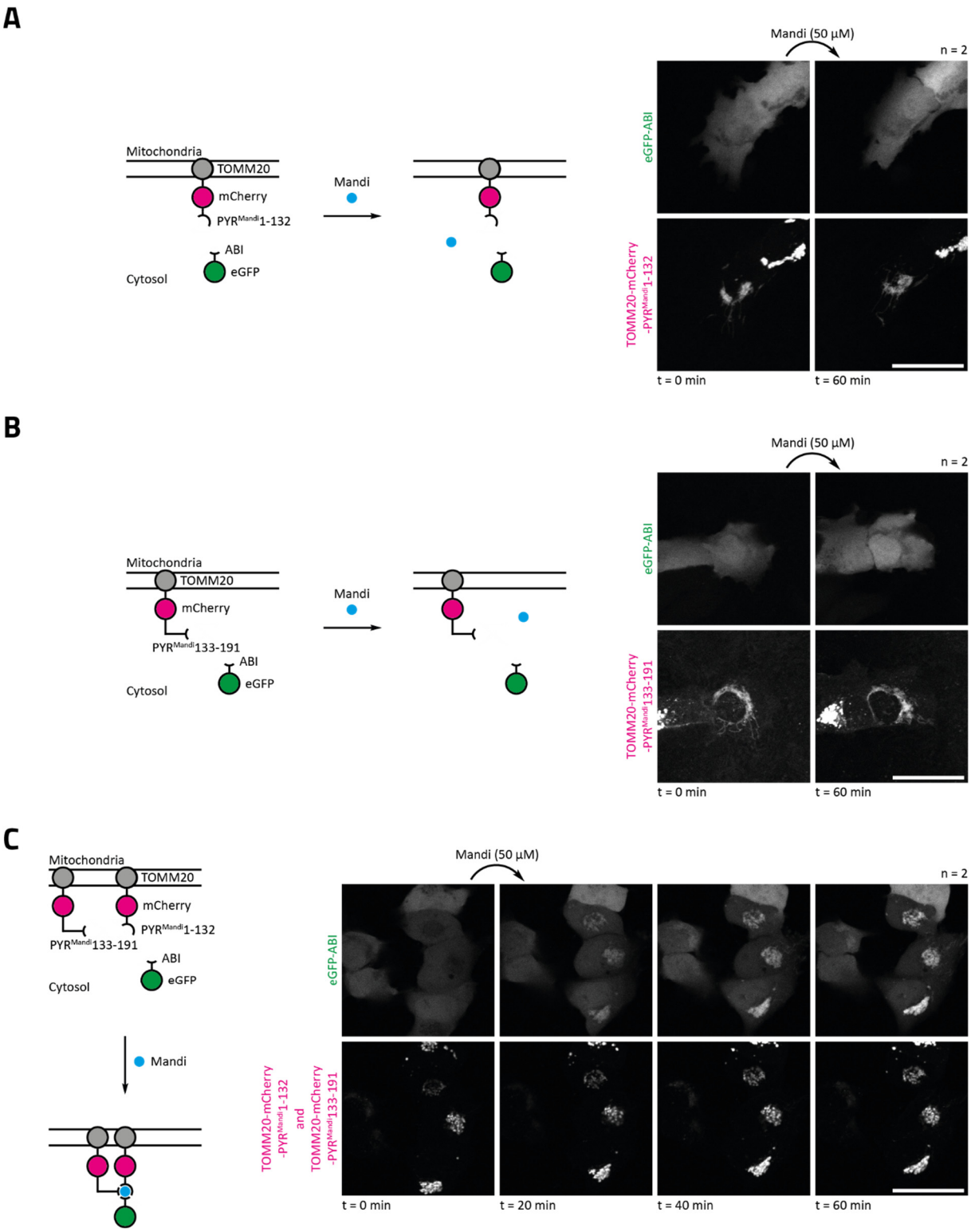

Figure 71: Both, PYR^{Mandi}1-132 and PYR^{Mandi}133-191 alone cannot recruit ABI in the presence of Mandi, but upon co-expression at the same subcellular localization (outer mitochondrial membrane). Schematic representation of the used protein constructs and the colocalization assay as well as confocal microscopy images of U2OS FlpIN TREx cells transiently transfected with TOMM20-mCherry-PYR^{Mandi}1-132 and eGFP-ABI (A), TOMM20-mCherry-PYR^{Mandi}133-191 and eGFP-ABI (B) and TOMM20-mCherry-PYR^{Mandi}1-132, TOMM20-mCherry-PYR^{Mandi}133-191 and eGFP-ABI (C) before and at different timepoints post addition of 50 µM Mandi. Indicated number n of replicates. Scale bars at 40 µm.

Expressing protein constructs at the same subcellular target increases their local concentration and the probability for interactions. In a further colocalization assay in live mammalian cells I investigated,

whether the split PYR^{Mandi} fragments PYR^{Mandi}1-132 and PYR^{Mandi}133-191 can be actively brought into proximity upon addition of Mandi, when they are not expressed at the same subcellular membrane localization.

This characteristic was already demonstrated in the luciferase assay, however a colocalization assay in live mammalian cells provides a more realistic setup to evaluate the induction of trimerization. This is justified in the high sensitivity of the luciferase assay. A luciferase assay already reveals the slightest interaction. Moreover, in general shorter incubation times than overnight as in the luciferase assay are desirable and the expression of one interacting fusion protein at a subcellular localization is of more interest in contrast to the expression of all fusion proteins in the cytosol.

Only one split PYR^{Mandi} fragments was localized to the outer mitochondrial membrane, a fusion protein of PYR^{Mandi}1-132, the self-labeling protein Halo (allowing fluorescent labeling with SiR-Halo) and TOMM20. The other split PYR^{Mandi} fragment PYR^{Mandi}133-191 was fused to mCherry and, as well as eGFP-ABI, expressed in the cytosol. Upon successful induction of protein trimerization, the fluorescence signal of all three construct should colocalize at the outer mitochondrial membrane (Figure 72). This assay also provides information on whether the split PYR^{Mandi} fragments already associate in the absence of Mandi.

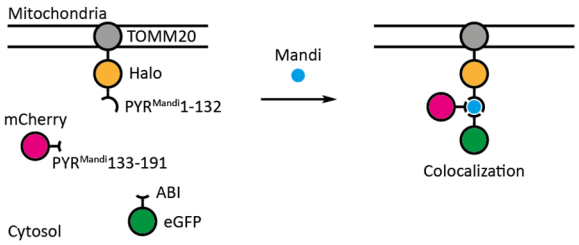

Figure 72: Schematic representation of the used protein constructs and the colocalization assay for the induction of protein trimerization.

When I performed the assay, no association of the split PYR^{Mandi} fragments was observed in the absence of Mandi. But also the presence of Mandi (50 µM) had no effect on protein localization after 2 h, no protein proximity was induced similar to the DMSO control (Figure 73). The difference in the outcome of the colocalization assay compared to the luciferase assay may be explained by the points mentioned above.

To conclude, the split PYR^{Mandi} fragments PYR^{Mandi}1-132 and PYR^{Mandi}133-191 cannot be used in combination with ABI to induce protein trimerization upon treatment with Mandi in live mammalian cells.

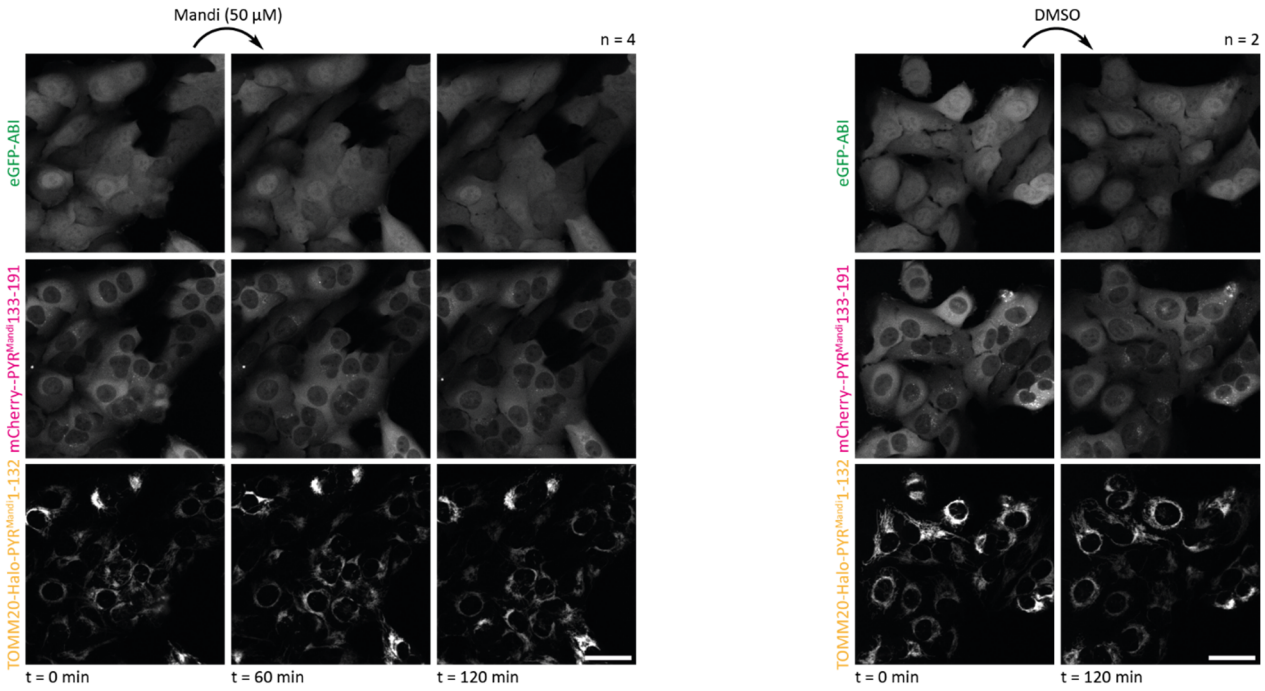

Figure 73: Mandi does not induce trimerization of PYR^{Mandi}1-132, PYR^{Mandi}133-191 and ABI in cellulo. Confocal microscopy images of U2OS FlpIN cells stably expressing TOMM20-Halo-PYR^{Mandi}1-132, mCherry-PYR^{Mandi}133-191 and eGFP-ABI before, 60 min and 120 min post addition of 50 µM Mandi and DMSO control. Halo was stained with SiR-Halo. Indicated number n of replicates. Scale bars at 40 µm.

Since the split PYR^{Mandi} fragments only were able to recruit ABI when they were expressed at the same subcellular membrane localization (outer mitochondrial membrane), I hypothesized that spatial proximity is a prerequisite for their reconstitution to a functional protein. I further investigated this by fusing the split PYR^{Mandi} fragments to the rapamycin responsive proteins FBR and FKBP12 to be able to force them into proximity upon addition of rapamycin (Figure 74). The overall design of the protein constructs was adopted from the previous assay to induce protein trimerization upon addition of Mandi. In the presence of rapamycin and Mandi, protein trimerization would be induced, both fluorescent proteins would be recruited to the outer mitochondrial membrane. In the presence of rapamycin, only mCherry would be recruited to the outer mitochondrial membrane, in the presence of Mandi, protein localization would not change.

Such an inducible design, that only allows recruitment of the ABI fusion protein to the outer mitochondrial membrane only in the presence of both molecules, represents a logic AND gate. However, in contrast to a typical AND gate, one input, the presence of Mandi alone, has no internal influence on the system.

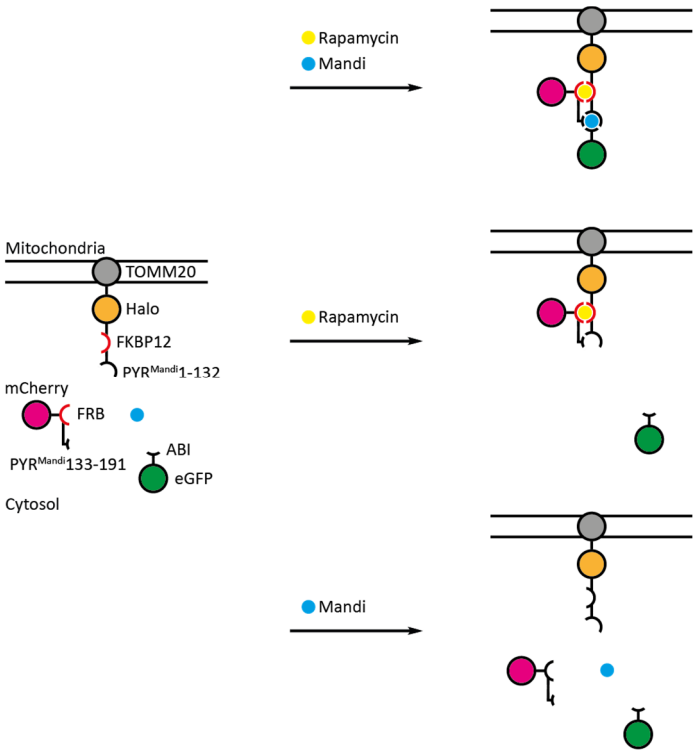

Figure 74: Schematic representation of the used protein constructs and the logic gate colocalization assay for different experimental conditions. In the presence of rapamycin and Mandi, GFP and mCherry are recruited to the outer mitochondrial membrane that is stained via Halo, in the presence of rapamycin only mCherry is recruited and in the presence of Mandi no recruiting occurs.

First, live mammalian cells expressing the respective protein constructs were treated with a high concentration of Mandi (50 µM) and/or rapamycin (5 µM) (Figure 75).

In the presence of both compounds, protein trimerization was indeed induced, both cytosolic fluorescent fusion proteins were recruited to the outer mitochondrial membrane where the third interacting fusion protein was located. The induction of protein proximity can already be detected after 30 min but especially the recruiting of the ABI protein increases within 2 h upon addition (Figure 76). This suggest that rapamycin induced proximity of FKBP12 and FRB and thus of PYR^{Mandi}1-132 and PYR^{Mandi}133-191 occurs faster than the reconstitution of a functional PYR^{Mandi} receptor protein and recruiting of the receiver protein ABI in the presence of Mandi. As expected, addition of rapamycin alone results only in the recruiting of the mCherry-FRB-PYR^{Mandi}133-191 fusion protein was recruited to the outer mitochondrial membrane, where the TOMM20-Halo-FKBP12-PYR^{Mandi}1-132 is located. In the presence of Mandi only and in the DMSO control (absence of both, Mandi and rapamycin) no effect on protein localization was observed. The design of the logic gate could be successfully implemented to live mammalian cells. When the spilt PYR^{Mandi} fragments are forced into proximity they can reconstitute an active receptor protein that is able to recruit ABI in the presence of Mandi.

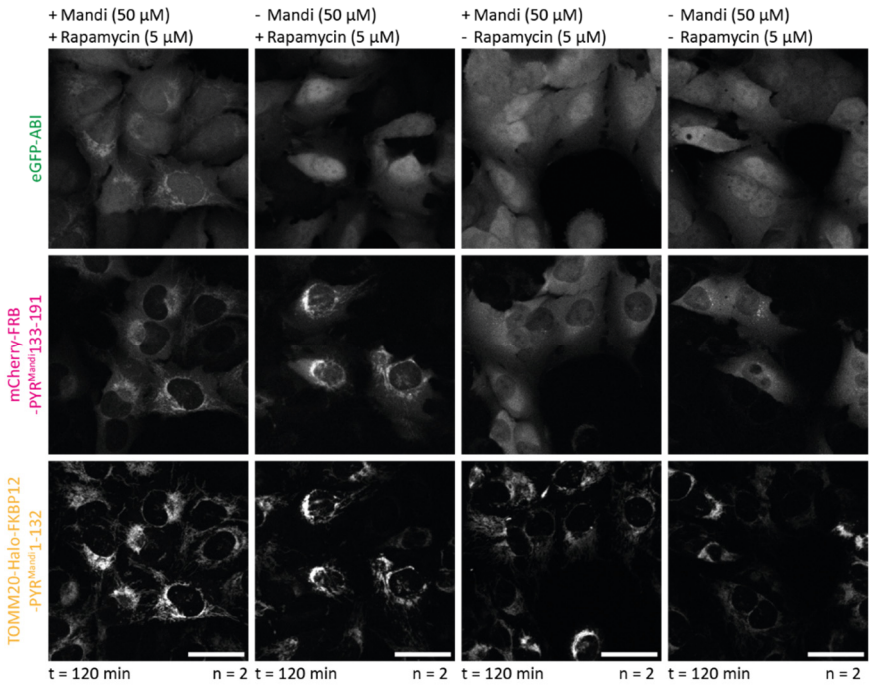

Figure 75: Split PYR^{Mandi} can be successfully used to construct a logic gate colocalization assay in cellulo. In the presence of rapamycin and Mandi, GFP and mCherry are recruited to the outer mitochondrial membrane, in the presence of rapamycin only mCherry is recruited and in the presence of Mandi no recruiting occurs. Confocal microscopy images of U2OS FlpIN cells stably expressing TOMM20-Halo-FKBP12-PYR^{Mandi}1-132, mCherry-FRB-PYR^{Mandi}133-191 and eGFP-ABI 120 min post addition of 50 µM Mandi and/or 5 µM rapamycin and DMSO control. Halo was stained with SiR-Halo. Indicated number n of replicates. Scale bars at 40 µm.

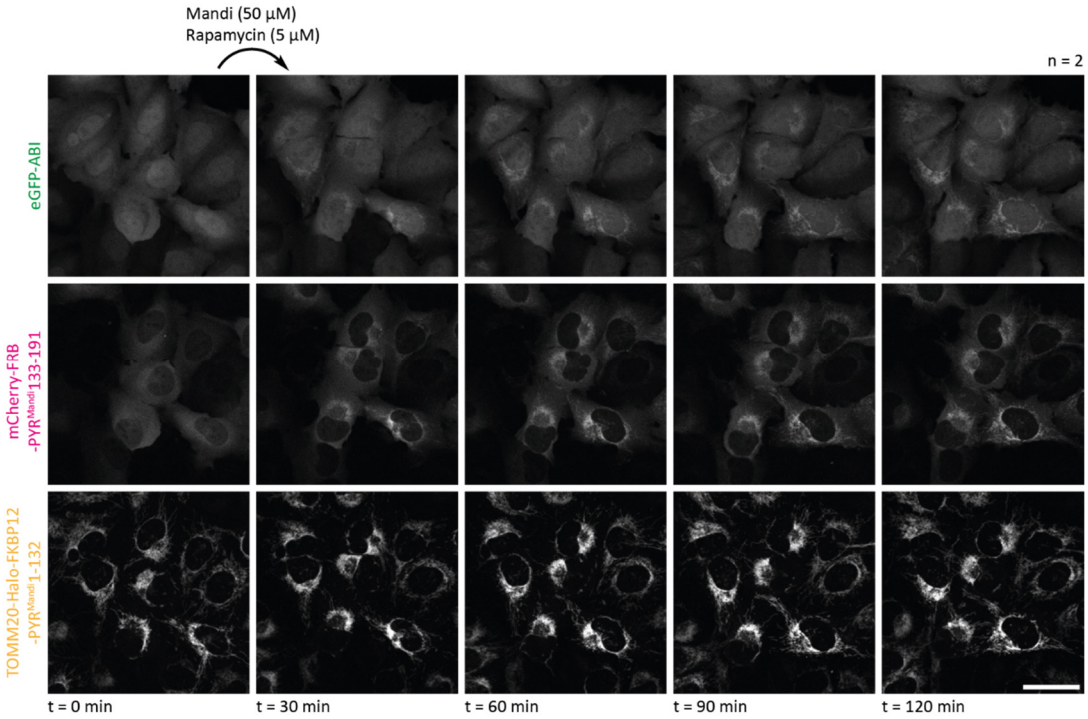

Figure 76: Time course of logic gate colocalization assay with micromolar concentrations of Mandi and rapamycin. Confocal microscopy images of U2OS FlpIN cells stably expressing TOMM20-Halo-FKBP12-PYR^{Mandi}1-132, mCherry-FRB-PYR^{Mandi}133-191 and eGFP-ABI before and at different timepoints post addition of 50 µM Mandi and 5 µM rapamycin. Halo was stained with SiR-Halo. Indicated number n of replicates. Scale bar at 40 µm.

In further experiments, I investigated whether the concentration of Mandi and rapamycin can be lowered (Figure 77). Rapamycin was titrated in the absence of Mandi, revealing that its concertation can be lowered to 5 nM without losing the capability to induce protein proximity. Mandi was titrated in the presence of a fixed concentration of rapamycin (5 µM). A concentration of 50 nM Mandi was sufficient to recruit the receiver protein ABI.

Hence, I postulated that a concentration of 5 nM rapamycin in combination with 50 nM Mandi is sufficient to achieve the recruiting of both cytosolic fusion proteins to the outer mitochondrial membrane were the third fusion protein is located. In fact, this effect was observed on a similar timescale (increasing colocalization within 2 h upon addition) as with the 1000-fold higher concentrations of 5 µM rapamycin and 50 µM Mandi (Figure 78). Assuming the rapamycin driven association of the FRB and the FKBP12 fusion proteins is faster than the Mandi driven association, this hints that the association of the split PYR^{Mandi} fragments to form a functional protein is rate limiting, not the binding of Mandi to one of the split PYR^{Mandi} fragments or a pre-associated PYR^{Mandi} protein.

To sum up, the logic gate can be used at low nanomolar concentrations of both CIPs.

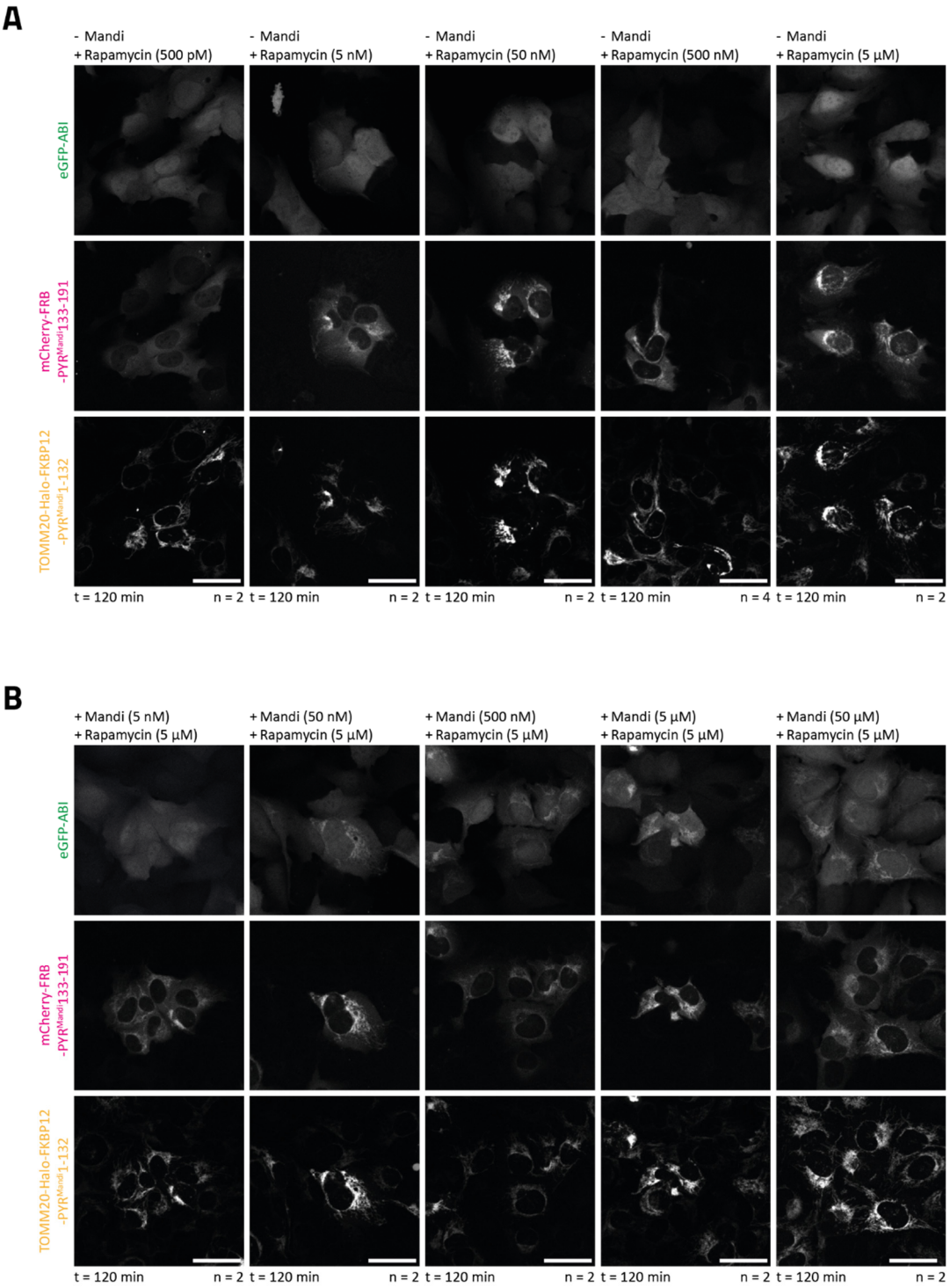

Figure 77: Titration of rapamycin (A) and Mandi (B) in the logic gate colocalization assay. Confocal microscopy images of U2OS FlpIN cells stably expressing TOMM20-Halo-FKBP12-PYR^{Mandi}1-132, mCherry-FRB-PYR^{Mandi}133-191 and eGFP-ABI 120 min post addition of different concentrations of Mandi and rapamycin. Halo was stained with SiR-Halo. Indicated number n of replicates. Scale bars at 40 µm.

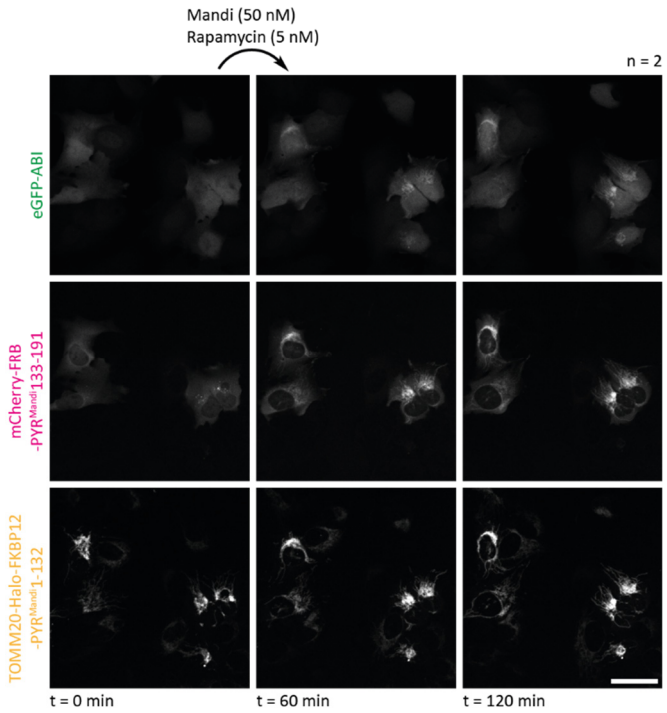

Figure 78: Colocalization of the spit PYR^{Mandi} parts and ABI can be induced at low nanomolar concentrations of Mandi and rapamycin in the logic gate colocalization assay. Confocal microscopy images of U2OS FlpIN cells stably expressing TOMM20-Halo-FKBP12-PYRMandi1-132, mCherry-FRB-PYRMandi133-191 and eGFP-ABI before 60 min and 120 min post addition of 50 nM Mandi and 5 nM rapamycin. Halo was stained with SiR-Halo. Indicated number n of replicates. Scale bar at 40 µm.

Outlook

Prospectively, with this system rapamycin could be used to induce protein trimerization in cells supplemented with Mandi. Moreover, since the split PYR^{Mandi} fragments have to be in spatial proximity to form a functional receptor protein, the system could potentially be used either to dimerize membrane proteins (e.g. membrane receptors) fused to the split PYR^{Mandi} fragments and at the same time recruit another protein fused to ABI there or to recruit ABI fusion proteins to the membrane proteins that already interact. For this application, it has to be investigated if the split PYR^{Mandi} fragments already reconstitute in the absence of Mandi when expressed at the same subcellular membrane localization or if treatment with Mandi forces them together. A FRET assay with different fluorescent proteins expressed as fusion proteins with the split PYR^{Mandi} fragments and anchored to the same subcellular membrane localization would answer this question.

To fulfill user defined properties, the split PYR^{Mandi} fragments could also be further engineered to increase or decrease their affinity toward each other, for example by moving the exact split position some amino acids forward or backward, by introducing extensions to the split PYR^{Mandi} fragments that increase the affinity or by shortening of the split PYR^{Mandi} fragments to decrease the affinity. With these modifications the system can, for example, be optimized for the applications mentioned above.

3.7 Size reduction of ABI

CIPs induce proximity of specific protein domains that can be fused to proteins of interest (POIs). To disturb the POIs as little as possible, it is of interest to keep the interacting protein domains as small as possible. Especially the receiver protein ABI (32.6 kDa) is attractive for size reduction, because the interaction surface to the receptor proteins is small compared to the overall size of the protein (Figure 7, Figure 79). Making ABI smaller is challenging because there is no continuous amino acid sequence that covers the whole interaction surface to the receptor protein. Amino acids contributing to the interaction to the receptor protein are located throughout the whole protein.

The receptor protein PYR^{Mandi} (21.5 kDa) is not suitable for large size reduction, since the whole protein scaffold is responsible for forming a binding pocket for Mandi. Moreover, PYR^{Mandi} is already one third smaller than ABI (Figure 7, Figure 79).

In 2023, a unimolecular FRET-based biosensor for sensing ABA was published, relying on ABA induced proximity of the receptor protein PYL1 and ABIaid, a fragment of the receiver protein ABI1 (amino acids 279-327 of ABI1, 5.4 kDa) that covers a part of the interaction surface to the receptor protein (Figure 79).[81]

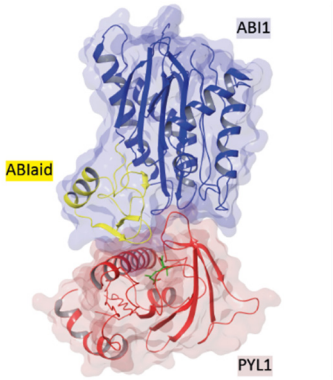

Figure 79: Crystal structure of the PYL1-ABA-ABI1 complex (pdb: 3JRQ) with the ABIaid domain (amino acids 279-327 of ABI1) marked in yellow.

Based on this finding, I investigated whether ABIaid can be used instead of ABI for the induction of protein proximity in live mammalian cells in combination with the receptor protein PYR^{Mandi} and the CIP Mandi. For this, I used a fluorescence colocalization assay with ABIaid, expressed as fusion protein with eGFP in the cytosol and PYR^{Mandi} fused to mCherry and TOMM20, localizing the protein construct to the outer mitochondrial membrane pointing inside the cytosol. Fluorescence colocalization at the outer mitochondrial membrane would indicate the induction of protein proximity (Figure 80).

However, upon treatment with a high concentration of Mandi (50 µM) no induction of protein proximity was observed, just as in the negative control without Mandi treatment (Figure 81). Consequently, ABI cannot be reduced in size to ABIaid while at the same maintaining its ability to be recruited to PYR^{Mandi} in the presence of Mandi.

Presumably, ABIaid could only be recruited to the receptor protein in the ABA biosensor[81] because the unimolecular sensor design already forces the proteins in spatial proximity.

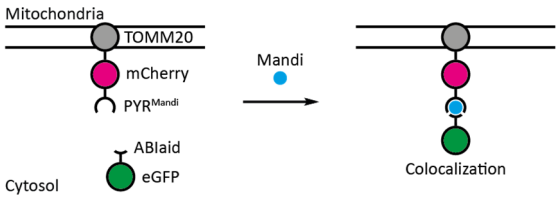

Figure 80: Schematic representation of the used protein constructs and the colocalization assay to investigate ABIaid.

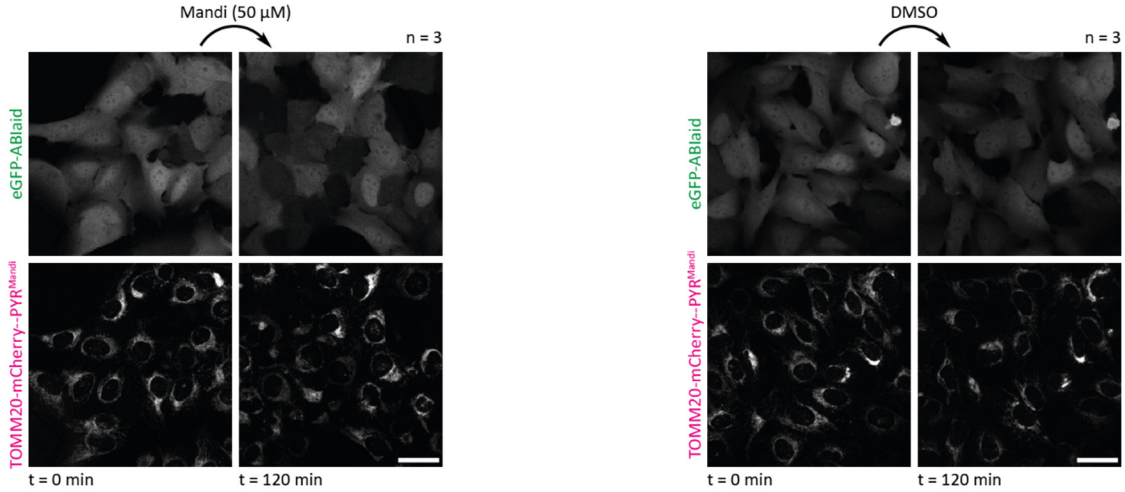

Figure 81: Mandi does not induce protein proximity between PYR^{Mandi} and ABIaid in cellulo. Confocal microscopy images of U2OS FlpIN cells stably expressing TOMM20-mCherry-PYR^{Mandi} and eGFP-ABIaid before and 120 min post addition of 50 µM Mandi and DMSO control. Indicated number n of replicates. Scale bars at 40 µm.

Outlook

A potential future strategy to reduce the size of the receiver protein would be to screen a library of nanobodies that have a smaller size (typically around 15 kDa)[82] than ABI (32.6 kDa) against the receptor protein PYR^{Mandi}. Since PYR^{Mandi} undergoes a conformational change upon binding of Mandi, selections could be performed in the presence or absence of Mandi to identify nanobodies that bind PYR^{Mandi} in a similar way to ABI. As technique to select a nanobody phage display[83] could be used.

Smaller receiver proteins could likely be used similar to ABI in combination with both, the receptor protein PYR^{Mandi} in combination with Mandi as CIP or with the receptor protein PYL in combination with ABA or OP as CIPs.

4 Conclusion

4.1 Summary

In this work, I investigated different strategies to precisely control protein proximity by chemical modification of CIPs and engineering of the interacting protein domains for applications in live mammalian cells and in vivo.

To obtain an antagonist for the CIP Mandi, I designed, synthesized and screened potential antagonists that I hypothesized would bind to the Mandi receptor protein PYR^{Mandi} but block the recruiting of the receiver protein ABI. This led to identification of the Mandi antagonist Mandi-Dopa-C6-Indole that is able to reverse protein proximity previously induced by Mandi in live mammalian cells when applied in a 100-fold excess. For fluorescent, noncovalent labeling of PYR^{Mandi} this scaffold could not be used since the binding affinity is too low. To increase the binding affinity of this class of Mandi derivatives, a screen of a larger library of compounds or rational compound design based on a crystal structure of Mandi-Dopa-C6-Indole bound to PYR^{Mandi} would constitute a starting point for future studies.

The photocaged derivative of Mandi, pMandi, puts the induction of protein proximity under light control and releases the active CIP upon irradiation. When I performed locally confined irradiation of live mammalian cells treated with pMandi, protein proximity was induced immediately, but reversed over time due to the diffusion of Mandi out of the irradiated area diluting its temporarily elevated local concentration. This characteristic allowed several cycles of reversible photoactivation. Upon strong and nonlocally confined irradiation converting a larger amount of pMandi to Mandi, protein proximity was induced that persisted over time in live mammalian cells. pMandi also enables to induce protein proximity upon irradiation in vivo as I showed in live medaka embryos. The low working concentration of pMandi (500 nM in live mammalian cells and 5 µM in live medaka embryos) make this photoactivatable CIP attractive for an application in live cells and in vivo. However, the high permeability of Mandi limits a spatial control over the induction of protein proximity.

In a next step, I aimed to design photocaged derivatives of Mandi that release an active polar molecule upon irradiation that is trapped intracellularly in order to achieve single-cell resolution upon photoactivation. Since this approach was not successful with Mandi derivatives because either the released molecule was not active or not trapped inside the cells, I identified the ABA agonist OP, that was developed in plant research that already has a polar carboxylic acid moiety, as an attractive candidate and repurposed and established it as CIP. Upon treatment with the AM ester of OP, protein proximity of the ABA receptor protein PYL and the receiver protein ABI is induced in live mammalian cells at a low nanomolar concentration (5 nM within 30 min and 50 nM within 5 min) and in live medaka embryos at a sub micromolar concentration (500 nM) which are similar working concentrations to the CIP Mandi. The photocaged derivative of OP, pOP, enables the induction of protein proximity in live mammalian cells with precise spatiotemporal control up to single-cell

resolution at a sub-micromolar working concentration (500 nM). This makes the manipulation of individual cells in the same sample possible. In live medaka embryos pOP is not applicable, protein proximity is induced upon addition of pOP also without irradiation, most likely the ester bond linking the photocage to OP is instable in vivo. A more stable variant of pOP is to be developed as I proposed by attaching the photocage via a linkage that is stable in vivo.

To expand the CIP system based on Mandi from the induction of proximity of two protein to the induction of proximity of three proteins (trimerization), I split the receptor protein PYR^{Mandi} into two fragments at different split sites and identified the split parts PYR^{Mandi}1-132 and PYR^{Mandi}133-191, that together are able to recruit the receiver protein ABI in the presence of Mandi. In live mammalian cells, the split PYR^{Mandi} fragments only reconstitute to a functional receptor protein when spatial proximity is given and thus this system cannot be used to induce trimerization for proteins that are far apart in live mammalian cells. In combination with the CIP rapamycin a logic gate system was constructed where the proximity of the split PYR^{Mandi} fragments is induced by rapamycin trigger association of FRB and FKBP12.

I further investigated, whether the receiver protein ABI can be reduced in size. However, size reduction completely abolished the recruiting to the receptor protein PYR^{Mandi} upon treatment with Mandi in live mammalian cells. Prospectively, to obtain a smaller receiver protein nanobodies could be screened that bind the PYR^{Mandi}-Mandi complex.

4.2 Future perspective

CIPs are a widely used tool to manipulate and investigate biological processes that rely on spatial proximity in live cells and in vivo.[2] The plant hormone-based CIPs investigated in this work, Mandi (literature[54] reported and further investigated in this work) and OP (established in this work), act via the molecular ratchet mechanism, are bioorthogonal, require low working concentration and are therefore well suited for an application in vivo. Other existing CIPs do not fulfill these criteria (see Section 1.3). To introduce a further control over the induction of protein proximity several strategies were explored in this work. The presented development of antagonists for Mandi is a significant step towards the reversion of induced interactions in complex biological systems where protein proximity cannot be reversed by washing out the CIP. Further, the investigated photocaged derivatives of Mandi and OP hold the potential to manipulate cellular processes with high specificity and spatiotemporal precision and pave the way towards the application of photocaged CIPs in complex living organisms.

Nevertheless, there is still further room for conceptual improvements to the CIP systems:
The chemical induction of protein proximity with Mandi as CIP relies on noncovalent interactions that can be reversed by withdrawal of the active CIP or treatment with an antagonist. However, for some applications it is of interest to chemically induce protein proximity that persists, e.g. for photoactivation in single cells in tissue culture and in vivo or when subsequent washing steps are required. Having such a system would allow photoactivation with pMandi in single cells without any reversion over time and can also be used for pOP, when the protein proximity has to be more persistent than it can be achieved with intracellular trapping via a polar carboxylic acid moiety. A system with this properties could be achieved by fusing the SpyTag/SpyCatcher system[84] to PYR^{Mandi}/PYL and ABI. The SpyTag peptide spontaneously reacts with the SpyCatcher protein to form a covalent isopeptide bond when SpyTag and SpyCatcher are in proximity to each other. Upon chemically induced proximity of PYR^{Mandi}/PYL-SpyTag and ABI-SpyCatcher (or PYR^{Mandi}/PYL-SpyCatcher and ABI-SpyTag) fusion proteins, SpyTag and SpyCatcher would undergo a covalent reaction linking both fusion proteins permanently together (Figure 82).

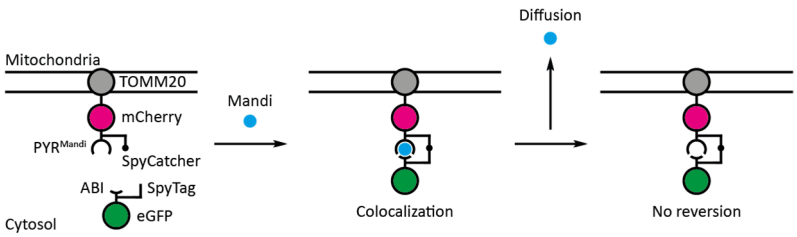

Figure 82: Schematic representation of the proposed protein constructs and a colocalization assay to investigate Mandi induced protein proximity that is irreversible by fusing the SpyTag/SpyCatcher system to PYR^{Mandi} and ABI. Addition of Mandi induces protein proximity of the PYR^{Mandi} fusion protein and the ABI fusion protein leading to a covalent reaction of SpyTag with SpyCatcher. Withdrawal of Mandi does not lead to a reversion of the induced protein proximity since both fusion proteins are covalently linked to each other. For simplification, PYR^{Mandi}/Mandi is displayed but can be replaced by PYL/OP.

Another option to achieve precise spatiotemporal control over the induction of protein proximity using CIPs would be to attach the photocage not to the CIP but to one of the interacting proteins, preferably to PYR^{Mandi}/PYL, the protein with the binding pocket for the CIP. The interacting proteins are able not diffuse out of the cells after photoactivation allowing single-cell resolution. The native CIP would be supplied and only induce protein proximity upon irradiation and cleavage of the photocage from the protein (Figure 83). The induction of protein proximity would remain reversible by washing the CIP out or applying an antagonist. However, this approach requires genetic code expansion to introduce a photocaged amino acid to the protein. Nevertheless, a similar approach was used in the design of a photocaged SpyTag where a photocaged lysine was introduced to block the interaction to the SpyCatcher protein.[85]

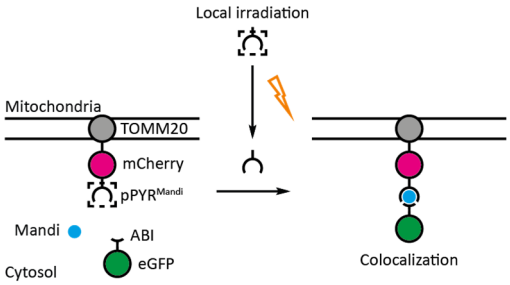

Figure 83: Schematic representation of the proposed protein constructs and a colocalization assay for the investigation of photocaged PYR^{Mandi} (pPYR^{Mandi}). Upon local irradiation the photocage is cleaved from PYR^{Mandi} and protein proximity is induced in the presence of Mandi. For simplification PYR^{Mandi}/Mandi is displayed but can be replaced by PYL/OP.

To optimize photoactivation with CIPs, different photolabile protecting groups could be attached to the active molecule.[86] This would be especially interesting for the use of two different photocaged CIPs with orthogonal photolabile protecting groups in combination to induce two different processes upon irradiation with light of different wavelengths. One photocaged CIP could be activated upon irradiation with a long wavelength while the other photocaged CIP stays inactive and is only converted into its active form upon irradiation at a shorter wavelength.

Besides introducing modifications to an already existing CIP system, there is also the possibility to design a CIP system around a ligand that fulfills user defined properties. It was reported that the ABA-based CIP system can be engineered by mutating the interacting proteins to respond to various different ligands.[65,66,68] This could be used to first design a molecule with e.g. low toxicity, good permeability, a moiety to attach photolabile protecting groups or to allow intracellular trapping, with good solubility, easy accessibility etc. and then develop the proteins that are brought into proximity upon treatment with this ligand. This approach could also facilitate the application of CIPs in medicine by repurposing compounds with good pharmacological properties as CIPs. That the application of CIPs can be beneficial for medical treatments has been demonstrated in the implementation of CIP-based on- and off-switches to CAR T cell therapy.

5 Materials and methods

5.1 Chemicals and synthesis

5.1.1 General experimental conditions and analytical methods

Chemicals and reagents

The used chemicals were obtained from commercial vendors (Sigma-Aldrich, Carl Roth GmbH + Co. KG, TCI Deutschland GmbH, Merck KGaA, Acros Organics or abcr GmbH) and used without further purification. Anhydrous solvents were stored over molecular sieve. Water was purified prior usage with the Milli-Q system (Merck KGaA).

Synthesis conditions

All reactions with water or oxygen sensitive reagents or intermediates were performed under argon atmosphere and in anhydrous solvents. Standard Schlenk-techniques were used.

Chromatography

For reaction control and analysis thin layer chromatography (TLC) was performed using polyester plates with silica gel 60 and fluorescence indicator (Macherey-Nagel POLYGRAM® SIL G/UV_{254}). Compound were visualized with UV light (254 nm or 365 nm) or common staining reagents. Moreover, liquid chromatography – mass spectrometry (LC-MS) was conducted on a LCMS-2020 system from SHIMADZU (acetonitrile:water gradient + 0.1 % formic acid) equipped with a C18 1.9 µm, 2.1 x 50 mm column (Supelco®) and a SPD-20AV UV-VIS photodiode array detector for product visualization.

Column chromatography was performed on the flash column chromatography Isolera™ One from Biotage® with SiliaSep columns (silica gel 40 µm to 63 µm) from SILICYCLE.

For preparative high performance liquid chromatography (HPLC) the system Alliance® e2695 (Waters™) or the system UltiMate 3000 (Thermo Fisher Scientific Inc.) was used. Both systems were connected to C18 columns from Supelco® with the sizes 5 µm, 10 x 250 mm (flow rate 4 ml/min) or 5 µm, 21.2 x 250 mm (flow rate 8 ml/min. Fractions were collected with an automated fraction collector based on the absorption maxima of the purified compounds.

Nuclear magnetic resonance spectroscopy

Nuclear magnetic resonance (NMR) spectra were recorded on Bruker Avance III HD spectrometer system equipped with a Bruker AscendTM 400 magnet (field strength: 9.4 T, ^{1}H-NMR frequency: 400.15 MHz, $^{13}C\{^{1}H\}$-NMR frequency: 100.62 MHz) at 298.15 K. Chemical shifts δ are reported in ppm, internally referenced to the residual ^{1}H-NMR signal of the solvent (e.g. chloroform at δ = 7.26 ppm, methanol at δ = 3.31 ppm) in ^{1}H-NMR spectra and to the ^{13}C-isotopes of the solvent (e.g. deuterated chloroform at δ = 77.16 ppm, deuterated methanol at δ = 49.00 ppm) in ^{13}C-NMR spectra.[87] The

multiplicity is given with the following abbreviations: s = singlet, d = doublet, t = triplet, q = quartet, qui = quintet, dd = doublet of doublet, br s = broad singlet etc. coupling constants *J* are given in Hz. NMR spectra were analyzed with the software MestReNova v14.1.0-24037.

Mass spectrometry

Mass spectrometry (MS) measurements were performed with electrospray ionisation (ESI) in positive (+) or in negative (-) mode by the mass spectrometry core facility of the Max Planck Institute for Medical Research on a Bruker maXis II™ ETD mass spectrometer. As solvent acetonitrile was used.

5.1.2 Purchased compounds for direct use

(+)-(*S*)-Abscisic acid (ABA), mandipropamid (Mandi) and rapamycin were purchased from Sigma-Aldrich as analytical standard and used without further purification.

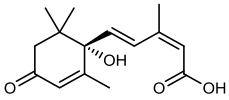

ABA

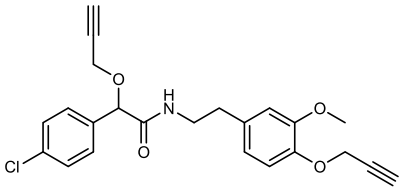

Mandi

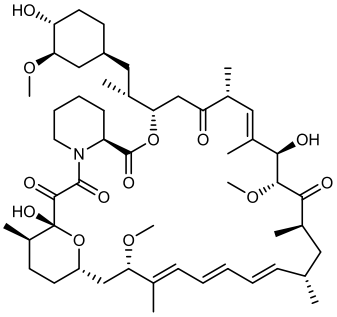

Rapamycin

SiR-Halo and Halo-CPY were obtained from our lab stock.

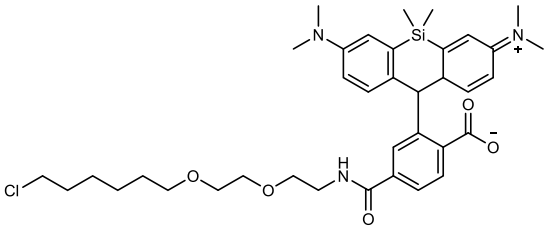

SiR-Halo

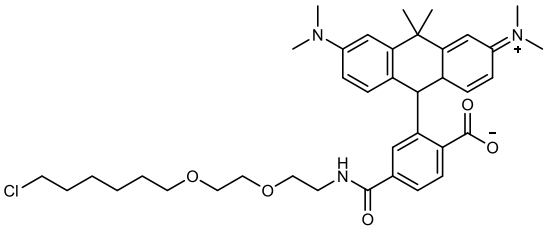

Halo-CPY

5.1.3 Synthesis

Mandi-Dopa-Cn

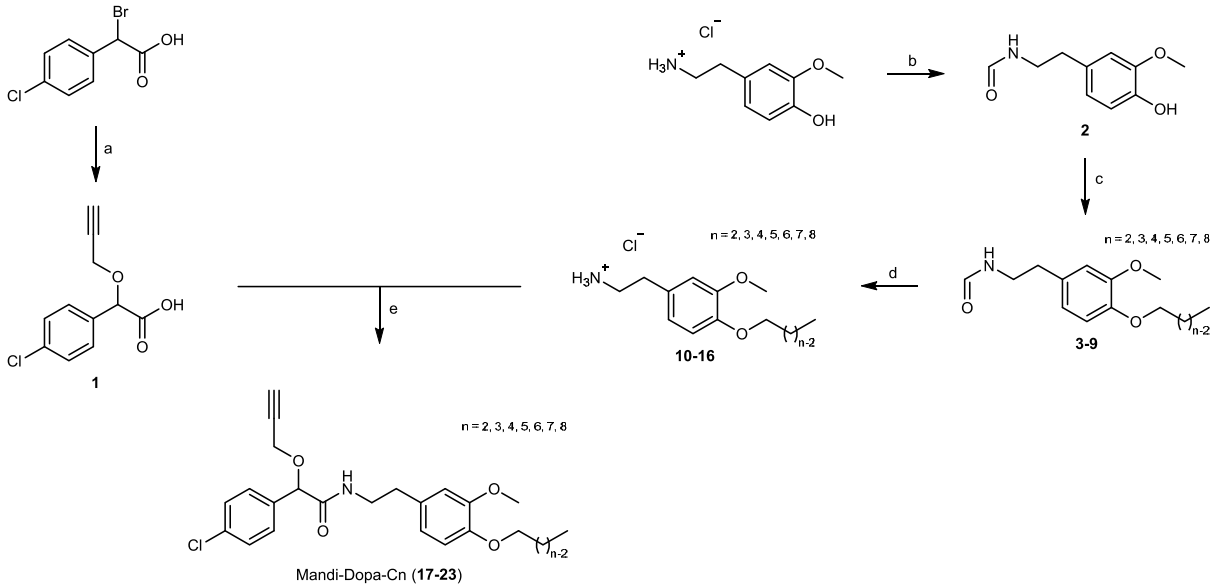

Conditions: a: propargyl alcohol, KOH, rt, 2 h; b: Ac_2O, formic acid, 70 °C, 2 h; c: alkyl bromide, NaOMe, 3 – 4 h, 65 °C or alkyl bromide, K_2CO_3, KI, rt, 22 h; d: HCl, rt, 45 – 92 h; e: HATU, HOBt, DIPEA, rt, 20 – 21 h.

2-(4-Chlorophenyl)-2-(prop-2-yn-1-yloxy)acetic acid (1)

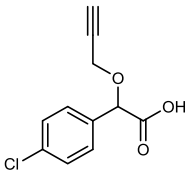

2-(4-Chlorophenyl)-2-(prop-2-yn-1-yloxy)acetic acid (**1**) was synthesized during my master's thesis[79] as described in literature[76]:

Potassium hydroxide (1.32 g, 24.0 mmol, 3.00 eq.) and prop-2-yn-1-ol (propargyl alcohol) (0.95 ml, 899 mg, 16.0 mmol, 2.00 eq) were suspended in chlorobenzene (6 ml). Then, a solution 2-bromo-2-(4-chlorophenyl)acetic acid (2.00 g, 8.02 mmol, 1.00 eq.) in chlorobenzene (8 ml) was added dropwise. The reaction mixture was stirred for 2 h at room temperature. Hydrochloric acid (1.00 M, 20.0 ml) was added and the layers were separated. The aqueous layer was extracted with dichloromethane (3 x 50 ml) and the combined organic layer was dried over sodium sulphate. The solvent was removed under reduced pressure and the obtained residue was dried in vacuo. The product was obtained as slightly yellow solid (1.62 g, 7.20 mmol, 90 %).

^{1}H-NMR (400.15 MHz, $CDCl_3$): δ = 7.41-7.36 (m, 4H), 5.21 (s, 1H), 4.36 – 4.11 (m, 2H), 2.52 (s, 1H) ppm.

^{13}C-NMR (100.62 MHz, $CDCl_3$): δ = 173.5, 135.5, 133.1, 129.3, 129.1, 77.8, 76.6, 56.6 ppm.

HRMS (ESI(-), CH_3CN): *m/z* 223.0166 $[M-H]^-$, calculated for $C_{11}H_8O_3Cl^-$: *m/z* 223.0156.

_N_-(4-Hydroxy-3-methoxyphenethyl)formamide (2)

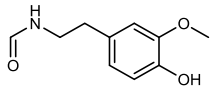

_N_-(4-Hydroxy-3-methoxyphenethyl)formamide (**2**) was synthesized during my master's thesis[79] as described in literature[75]:

Acetic anhydride (3.46 ml, 3.76 g, 36.8 mmol, 15.0 eq.) was cooled to 0 °C and formic acid (1.85 ml, 2.26 g, 49.1 mmol, 20.0 eq.) was added dropwise. The mixture was stirred for 2 h at 55 °C and subsequently cooled to 0 °C again. Then, tetrahydrofuran (5 ml) and 2-(4-hydroxy-3-methoxyphenyl)ethan-1-aminium chloride (3-Methoxytyramine hydrochloride) (500 mg, 2.45 mmol, 1.00 eq.) were added and the reaction mixture was stirred for 2 h at 70 °C. The solvent was removed in vacuo and the crude product was purified by column chromatography (silica gel, dichloromethane:ethyl acetate gradient). The product was obtained in mixture with side products as slightly yellow liquid (444 mg, 1.89 mmol, 77 %) and used in the next synthetic step without further purification.

^{1}H-NMR (400.15 MHz, $CDCl_3$): δ = 8.08 (d, J = 6.8 Hz, 1H), 6.96-6.67 (m, 3H), 5.86 – 5.64 (m, 1H), 3.87-3.81 (m, 3H), 3.57 – 3.52 (m, 2H), 2.84 – 2.74 (m, 2H) ppm.

HRMS (ESI(+), CH_3CN): *m/z* 196.0968 $[M+H]^+$, calculated for $C_{10}H_{14}NO_3^+$: *m/z* 196.0968.

The following side products could be identified:

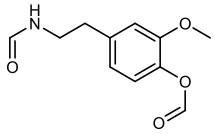

HRMS (ESI(+), CH_3CN): *m/z* 224.0916 $[M+H]^+$, calculated for $C_{11}H_{14}NO_4^+$: *m/z* 224.0917.

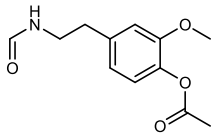

HRMS (ESI(+), CH_3CN): *m/z* 238.1071 $[M+H]^+$, calculated for $C_{12}H_{16}NO_4^+$: *m/z* 238.1074.

_N_-(4-Ethoxy-3-methoxyphenethyl)formamide (3)

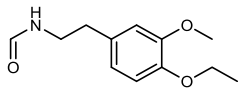

_N_-(4-Hydroxy-3-methoxyphenethyl)formamide (**2**) (100 mg, 512 µmol, 1.00 eq.) was dissolved in anhydrous methanol (1 ml) and a solution of sodium methoxide (27.7 mg, 512 µmol, 1.00 eq.) in methanol (25 wt%, 4.37 M, 114 µl) was added. Then, bromoethane (38.2 µl, 512 µmol, 1.00 eq.) was added and the reaction mixture was stirred for 4 h at 65 °C. The solvent removed under reduced pressure, water (1 ml) was added and the mixture was extracted with dichloromethane (2 ml). The solvent was removed under reduced pressure and the crude product was purified by preparative reverse phase HPLC (C18, acetonitrile:water gradient + 0.1 % TFA). The product was obtained as white solid (40.9 mg, 184 µmol, 36 %).

^{1}H-NMR (400.15 MHz, $CDCl_3$): δ = 8.12 (s, 1H), 6.80 (d, *J* = 8.7 Hz, 1H), 6.71 – 6.66 (m, 2H), 5.71 (s, 1H), 4.06 (q, *J* = 7.0 Hz, 2H), 3.85 (s, 3H), 3.54 (q, *J* = 6.7 Hz, 2H), 2.77 (t, *J* = 6.9 Hz, 2H), 1.44 (t, *J* = 7.0 Hz, 3H) ppm.

^{13}C-NMR (100.62 MHz, $CDCl_3$): δ = 161.3, 149.5, 147.2, 131.0, 120.8, 113.1, 112.3, 64.5, 56.1, 39.4, 35.2, 14.9 ppm.

HRMS (ESI(+), CH_3CN): *m/z* 224.1278 $[M+H]^+$, calculated for $C_{12}H_{18}NO_3^+$: *m/z* 224.1281.

_N_-(3-Methoxy-4-propoxyphenethyl)formamide (4)

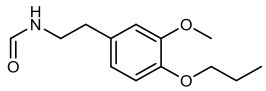

N-(4-Hydroxy-3-methoxyphenethyl)formamide (**2**) (100 mg, 512 µmol, 1.00 eq.) was dissolved in anhydrous methanol (1 ml) and a solution of sodium methoxide (27.7 mg, 512 µmol, 1.00 eq.) in methanol (25 wt%, 4.37 M, 114 µl) was added. Then, 1-bromopropane (46.6 µl, 512 µmol, 1.00 eq.) was added and the reaction mixture was stirred for 4 h at 65 °C. The solvent removed under reduced pressure, water (1 ml) was added and the mixture was extracted with dichloromethane (2 ml). The solvent was removed under reduced pressure and the crude product was purified by preparative reverse phase HPLC (C18, acetonitrile:water gradient + 0.1 % TFA). The product was obtained as white solid (38.7 mg, 163 µmol, 32 %).

^{1}H-NMR (400.15 MHz, $CDCl_3$): δ = 8.11 (s, 1H), 6.80 (d, *J* = 8.7 Hz, 1H), 6.70 – 6.66 (m, 2H), 5.77 (s, 1H), 3.93 (t, *J* = 6.8 Hz, 2H), 3.83 (s, 3H), 3.53 (q, *J* = 6.7 Hz, 2H), 2.76 (t, *J* = 6.9 Hz, 2H), 1.83 (h, *J* = 7.2 Hz, 2H), 1.01 (t, *J* = 7.4 Hz, 3H) ppm.

^{13}C-NMR (100.62 MHz, $CDCl_3$): δ = 161.3, 149.6, 147.4, 131.0, 120.8, 113.3, 112.5, 70.7, 56.1, 39.4, 35.1, 22.6, 10.5 ppm.

HRMS (ESI(+), CH_3CN): *m/z* 238.1436 $[M+H]^+$, calculated for $C_{13}H_{20}NO_3^+$: *m/z* 238.1438.

_N_-(4-Butoxy-3-methoxyphenethyl)formamide (5)

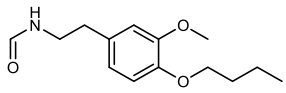

N-(4-Hydroxy-3-methoxyphenethyl)formamide (**2**) (100 mg, 512 µmol, 1.00 eq.) was dissolved in anhydrous methanol (1 ml) and a solution of sodium methoxide (27.7 mg, 512 µmol, 1.00 eq.) in methanol (25 wt%, 4.37 M, 114 µl) was added. Then, 1-bromobutane (55.3 µl, 512 µmol, 1.00 eq.) was added and the reaction mixture was stirred for 4 h at 65 °C. The solvent removed under reduced pressure, water (1 ml) was added and the mixture was extracted with dichloromethane (2 ml). The solvent was removed under reduced pressure and the crude product was purified by preparative reverse phase HPLC (C18, acetonitrile:water gradient + 0.1 % TFA). The product was obtained as white solid (45.3 mg, 180 µmol, 35 %).

^{1}H-NMR (400.15 MHz, $CDCl_3$): δ = 8.15 (s, 1H), 6.82 (d, *J* = 8.7 Hz, 1H), 6.72 – 6.67 (m, 2H), 5.49 (s, 1H), 4.00 (t, *J* = 6.8 Hz, 2H), 3.86 (s, 3H), 3.57 (q, *J* = 6.4 Hz, 2H), 2.79 (t, *J* = 6.9 Hz, 2H), 1.85 – 1.78 (m, 2H), 1.54 – 1.44 (m, 2H), 0.97 (t, *J* = 7.4 Hz, 3H) ppm.

^{13}C-NMR (100.62 MHz, $CDCl_3$): δ = 161.3, 149.8, 146.3, 130.9, 120.8, 113.3, 112.5, 69.0, 56.2, 39.4, 35.2, 31.4, 20.1, 12.7 ppm.

HRMS (ESI(+), CH_3CN): *m/z* 252.1595 $[M+H]^+$, calculated for $C_{14}H_{22}NO_3^+$: *m/z* 252.1594.

_N_-(3-Methoxy-4-(pentyloxy)phenethyl)formamide (6)

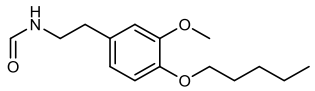

N-(4-Hydroxy-3-methoxyphenethyl)formamide (**2**) (20.0 mg, 86.3 µmol, 1.00 eq.) was dissolved in anhydrous methanol (1 ml) and a solution of sodium methoxide (11.7 mg, 216 µmol, 2.50 eq.) in methanol (25 wt%, 4.37 M, 48 µl) was added. Then, 1-bromopentane (53.9 µl, 432 µmol, 5.00 eq.) was added and the reaction mixture was stirred for 3 h at 65 °C. The solvent removed under reduced pressure, water (1 ml) was added and the mixture was extracted with dichloromethane (2 ml). The solvent was removed under reduced pressure and the crude product was purified by preparative reverse phase HPLC (C18, acetonitrile:water gradient + 0.1 % TFA). The product was obtained as colorless liquid (3.90 mg, 14.7 µmol, 17 %).

^{1}H-NMR (400.15 MHz, $CDCl_3$): δ = 8.15 (d, *J* = 1.2 Hz, 1H), 6.82 (d, *J* = 8.7 Hz, 1H), 6.72 – 6.67 (m, 2H), 5.50 (s, 1H), 3.99 (t, *J* = 6.9 Hz, 2H), 3.86 (s, 3H), 3.56 (q, *J* = 6.6 Hz, 2H), 2.78 (t, *J* = 6.9 Hz, 2H), 1.87 – 1.80 (m, 2H), 1.46 – 1.35 (m, 4H), 0.92 (t, *J* = 7.1 Hz, 3H) ppm.

^{13}C-NMR (100.62 MHz, $CDCl_3$): δ = 161.3, 149.7, 147.6, 130.9, 120.8, 113.3, 112.5, 69.3, 56.2, 39.4, 35.2, 29.1, 28.3, 22.6, 14.2 ppm.

HRMS (ESI(+), CH_3CN): *m/z* 266.1751 $[M+H]^+$, calculated for $C_{15}H_{24}NO_3^+$: *m/z* 266.1751.

_N_-(4-(Hexyloxy)-3-methoxyphenethyl)formamide (7)

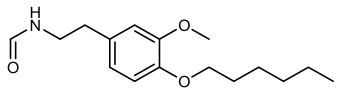

N-(4-Hydroxy-3-methoxyphenethyl)formamide (**2**) (100 mg, 512 µmol, 1.00 eq.) was dissolved in anhydrous methanol (1 ml) and a solution of sodium methoxide (27.7 mg, 512 µmol, 1.00 eq.) in methanol (25 wt%, 4.37 M, 114 µl) was added. Then, 1-bromohexane (72.3 µl, 512 µmol, 1.00 eq.) was added and the reaction mixture was stirred for 4 h at 65 °C. The solvent removed under reduced pressure, water (1 ml) was added and the mixture was extracted with dichloromethane (2 ml). The solvent was removed under reduced pressure and the crude product was purified by preparative reverse phase HPLC (C18, acetonitrile:water gradient + 0.1 % TFA). The product was obtained as white solid (35.1 mg, 126 µmol, 25 %).

^{1}H-NMR (400.15 MHz, $CDCl_3$): δ = 8.15 (s, 1H), 6.82 (d, *J* = 8.6 Hz, 1H), 6.73 – 6.67 (m, 2H), 5.51 (s, 1H), 3.99 (t, *J* = 6.9 Hz, 2H), 3.86 (s, 3H), 3.57 (q, *J* = 6.6 Hz, 2H), 2.79 (t, *J* = 6.9 Hz, 2H), 1.88 – 1.79 (m, 2H), 1.47 – 1.25 (m, 6H), 0.90 (d, *J* = 7.2 Hz, 3H) ppm.

^{13}C-NMR (100.62 MHz, $CDCl_3$): δ = 161.4, 149.7, 147.5, 130.9, 120.8, 113.2, 112.4, 69.3, 56.2, 39.4, 35.2, 31.7, 29.3, 25.8, 22.8, 14.2 ppm.

HRMS (ESI(+), CH_3CN): *m/z* 280.1901 $[M+H]^+$, calculated for $C_{16}H_{26}NO_3^+$: *m/z* 280.1907.

_N_-(4-(Heptyloxy)-3-methoxyphenethyl)formamide (8)

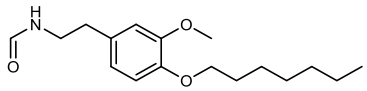

N-(4-Hydroxy-3-methoxyphenethyl)formamide (**2**) (20.0 mg, 86.3 µmol, 1.00 eq.) was dissolved in anhydrous dimethylformamide (1 ml) and potassium carbonate (42.5 mg, 307 µmol, 3.00 eq.) and potassium iodide (8.50 mg, 51.2 µmol, 0.50 eq.) were added. Then, 1-bromoheptane (24.1 µl, 154 µmol, 1.50 eq.) was added and the reaction mixture was stirred for 22 h at room temperature. The solvent removed under reduced pressure, saturated aqueous ammonium chloride solution (1 ml) was added and the mixture was extracted with dichloromethane (2 ml). The solvent was removed under reduced pressure and the crude product was purified by preparative reverse phase HPLC (C18, acetonitrile:water gradient + 0.1 % TFA). The product was obtained as white solid (7.60 mg, 25.9 µmol, 25 %).

^{1}H-NMR (400.15 MHz, $CDCl_3$): δ = .15 (s, 1H), 6.82 (d, *J* = 8.7 Hz, 1H), 6.72 – 6.67 (m, 2H), 5.49 (s, 1H), 3.98 (t, *J* = 6.9 Hz, 2H), 3.86 (s, 3H), 3.56 (q, *J* = 6.7 Hz, 2H), 2.78 (t, *J* = 6.9 Hz, 2H), 1.83 (p, *J* = 6.9 Hz, 2H), 1.46 – 1.25 (m, 8H), 0.89 (t, *J* = 6.8 Hz, 3H) ppm.

^{13}C-NMR (100.62 MHz, $CDCl_3$): δ = 161.3, 149.7, 147.6, 130.9, 120.8, 113.3, 112.5, 69.3, 56.2, 39.4, 35.2, 31.9, 29.4, 29.2, 26.1, 22.8, 14.2 ppm.

HRMS (ESI(+), CH_3CN): *m/z* 294.2064 $[M+H]^+$, calculated for $C_{17}H_{28}NO_3^+$: *m/z* 294.2064.

_N_-(3-Methoxy-4-(octyloxy)phenethyl)formamide (9)

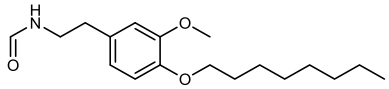

N-(4-Hydroxy-3-methoxyphenethyl)formamide (**2**) (100 mg, 512 µmol, 1.00 eq.) was dissolved in anhydrous methanol (1 ml) and a solution of sodium methoxide (27.7 mg, 512 µmol, 1.00 eq.) in methanol (25 wt%, 4.37 M, 114 µl) was added. Then, 1-bromooctane (89.1 µl, 512 µmol, 1.00 eq.) was added and the reaction mixture was stirred for 4 h at 65 °C. The solvent removed under reduced pressure, water (1 ml) was added and the mixture was extracted with dichloromethane (2 ml). The solvent was removed under reduced pressure and the crude product was purified by preparative

reverse phase HPLC (C18, acetonitrile:water gradient + 0.1 % TFA). The product was obtained as white solid (39.2 mg, 128 µmol, 25 %).

^{1}H-NMR (400.15 MHz, $CDCl_3$): δ = 8.15 (s, 1H), 6.82 (d, *J* = 8.6 Hz, 1H), 6.72 – 6.67 (m, 2H), 5.51 (s, 1H), 3.98 (t, *J* = 6.9 Hz, 2H), 3.86 (s, 3H), 3.57 (q, *J* = 6.6 Hz, 2H), 2.79 (t, *J* = 6.9 Hz, 2H), 1.86 – 1.79 (m, 2H), 1.46 – 1.28 (m, 10H), 0.88 (t, *J* = 6.6 Hz, 3H) ppm.

^{13}C-NMR (100.62 MHz, $CDCl_3$): δ = 161.4, 149.7, 147.5, 130.9, 120.8, 113.2, 112.4, 69.3, 56.2, 39.4, 35.2, 32.0, 29.5, 29.4, 29.3, 26.1, 22.8, 14.3 ppm.

HRMS (ESI(+), CH_3CN): *m/z* 308.2115 $[M+H]^+$, calculated for $C_{18}H_{30}NO_3^+$: *m/z* 308.2220.

2-(4-Ethoxy-3-methoxyphenyl)ethan-1-aminium chloride (10)

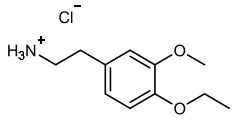

N-(4-Ethoxy-3-methoxyphenethyl)formamide (**3**) (40.9 mg, 184 µmol, 1.00 eq.) was dissolved in methanol (1 ml) and a solution of hydrochloric acid (66.8 mg, 1.83 mmol, 10.00 eq.) in methanol (1.25 M, 1.47 ml) was added. The reaction mixture was stirred for 92 h at room temperature. The solvent was removed under reduced pressure and the product was obtained as white solid (41.2 mg, 178 µmol, 97 %).

^{1}H-NMR (400.15 MHz, CD_3OD): δ = 6.91 – 6.87 (m, 2H), 6.81 (dd, *J* = 8.2, 2.0 Hz, 1H), 4.03 (q, *J* = 7.0 Hz, 2H), 3.84 (s, 3H), 3.17 (t, *J* = 7.7 Hz, 2H), 2.93 – 2.90 (m, 2H), 1.38 (t, *J* = 7.0 Hz, 2H) ppm.

^{13}C-NMR (100.62 MHz, CD_3OD): δ = 151.1, 148.9, 130.7, 122.2, 115.0, 113.9, 65.7, 56.5, 42.1, 34.1, 15.2 ppm.

HRMS (ESI(+), CH_3CN): *m/z* 196.1327 $[M]^+$, calculated for $C_{11}H_{18}NO_2^+$: *m/z* 196.1332.

2-(3-Methoxy-4-propoxyphenyl)ethan-1-aminium chloride (11)

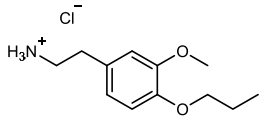

N-(3-Methoxy-4-propoxyphenethyl)formamide (**4**) (38.7 mg, 163 µmol, 1.00 eq.) was dissolved in methanol (1 ml) and a solution of hydrochloric acid (59.4 mg, 1.63 mmol, 10.00 eq.) in methanol (1.25 M, 1.30 ml) was added. The reaction mixture was stirred for 92 h at room temperature. The solvent was removed under reduced pressure and the product was obtained as white solid (39.9 mg, 162 µmol, 100 %).

^{1}H-NMR (400.15 MHz, CD_3OD): δ = 6.91 – 6.89 (m, 2H), 6.80 (dd, *J* = 8.1, 2.0 Hz, 1H), 3.93 (t, *J* = 6.6 Hz, 2H), 3.84 (s, 3H), 3.16 (t, *J* = 7.6 Hz, 2H), 2.93 – 2.89 (m, 2H), 1.83 – 1.74 (m, 2H), 1.03 (t, *J* = 7.4 Hz, 3H) ppm.

^{13}C-NMR (100.62 MHz, CD_3OD): δ = 151.2, 149.2, 130.6, 122.2, 115.1, 114.0, 71.9, 56.6, 42.1, 34.1, 23.6, 10.8 ppm.

HRMS (ESI(+), CH_3CN): *m/z* 210.1486 $[M]^+$, calculated for $C_{12}H_{20}NO_2^+$: *m/z* 210.1489.

2-(4-Butoxy-3-methoxyphenyl)ethan-1-aminium chloride (12)

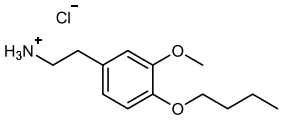

N-(4-Butoxy-3-methoxyphenethyl)formamide (**5**) (45.3 mg, 180 µmol, 1.00 eq.) was dissolved in methanol (1 ml) and a solution of hydrochloric acid (65.8 mg, 1.80 mmol, 10.00 eq.) in methanol (1.25 M, 1.44 ml) was added. The reaction mixture was stirred for 92 h at room temperature. The solvent was removed under reduced pressure and the product was obtained as white solid (45.3 mg, 174 µmol, 97 %).

^{1}H-NMR (400.15 MHz, CD_3OD): δ = 6.91 – 6.89 (m, 2H), 6.80 (dd, *J* = 8.1, 2.0 Hz, 1H), 3.97 (t, *J* = 6.5 Hz, 2H), 3.84 (s, 3H), 3.16 (t, *J* = 7.7 Hz, 2H), 2.93 – 2.89 (m, 2H), 1.78 – 1.71 (m, 2H), 1.54 – 1.45 (m, 2H), 0.97 (t, *J* = 7.4 Hz, 3H) ppm.

^{13}C-NMR (100.62 MHz, CD_3OD): δ = 151.2, 149.2, 130.6, 122.2, 115.1, 114.0, 70.0, 56.6, 42.1, 34.1, 32.5, 20.3, 14.2 ppm.

HRMS (ESI(+), CH_3CN): *m/z* 224.1638 $[M]^+$, calculated for $C_{13}H_{22}NO_2^+$: *m/z* 224.1645.

2-(3-Methoxy-4-(pentyloxy)phenyl)ethan-1-aminium chloride (13)

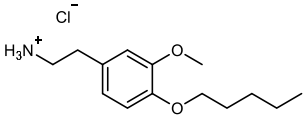

N-(3-Methoxy-4-(pentyloxy)phenethyl)formamide (**6**) (3.90 mg, 14.7 µmol, 1.00 eq.) was dissolved in methanol (1 ml) and a solution of hydrochloric acid (10.9 mg, 297 µmol, 20.00 eq.) in methanol (1.25 M, 235 µl) was added. The reaction mixture was stirred for 45 h at room temperature. The solvent was removed under reduced pressure and the product was obtained as white solid (2.20 mg, 8.04 µmol, 55 %).

^{1}H-NMR (400.15 MHz, $CDCl_3$): δ = 7.84 (s, 3H), 6.81 (d, *J* = 8.6 Hz, 1H), 6.73 – 6.71 (m, 2H), 3.96 (t, *J* = 6.9 Hz, 2H), 3.84 (s, 3H), 3.19 (s, 2H), 2.92 (t, *J* = 7.0 Hz, 2H), 1.83 – 1.78 (m, 2H), 1.43 – 1.35 (m, 4H), 0.92 (t, *J* = 7.1 Hz, 3H) ppm.

^{13}C-NMR (100.62 MHz, $CDCl_3$): δ = 149.9, 148.2, 128.0, 121.0, 113.6, 112.7, 69.3, 56.2, 41.4, 33.2, 29.0, 28.2, 22.6, 14.1 ppm.

HRMS (ESI(+), CH_3CN): *m/z* 238.1801 $[M]^+$, calculated for $C_{14}H_{24}NO_2^+$: *m/z* 238.1802.

2-(4-(Hexyloxy)-3-methoxyphenyl)ethan-1-aminium chloride (14)

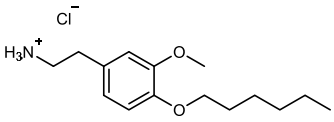

N-(4-(Hexyloxy)-3-methoxyphenethyl)formamide (**7**) (35.1 mg, 126 µmol, 1.00 eq.) was dissolved in methanol (1 ml) and a solution of hydrochloric acid (45.8 mg, 1.26 mmol, 10.00 eq.) in methanol (1.25 M, 1.00 ml) was added. The reaction mixture was stirred for 92 h at room temperature. The solvent was removed under reduced pressure and the product was obtained as white solid (35.0 mg, 122 µmol, 97 %).

^{1}H-NMR (400.15 MHz, CD_3OD): δ = 6.91 – 6.89 (m, 2H), 6.80 (dd, *J* = 8.2, 2.0 Hz, 1H), 3.96 (t, *J* = 6.5 Hz, 2H), 3.84 (s, 3H), 3.16 (t, *J* = 7.7 Hz, 2H), 2.93 – 2.89 (m, 2H), 1.80 – 1.73 (m, 2H), 1.51 – 1.43 (m, 2H), 1.36 – 1.33 (m, 4H), 0.94 – 0.90 (m, 3H) ppm.

^{13}C-NMR (100.62 MHz, CD_3OD): δ = 151.2, 149.2, 130.6, 122.2, 115.1, 114.0, 70.3, 56.6, 42.1, 34.1, 32.8, 30.4, 26.8, 23.7, 14.4 ppm.

HRMS (ESI(+), CH_3CN): *m/z* 252.1956 $[M]^+$, calculated for $C_{15}H_{26}NO_2^+$: *m/z* 252.1958.

2-(4-(Heptyloxy)-3-methoxyphenyl)ethan-1-aminium chloride (15)

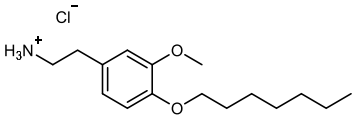

N-(4-(Heptyloxy)-3-methoxyphenethyl)formamide (**8**) (7.60 mg, 25.9 µmol, 1.00 eq.) was dissolved in methanol (1 ml) and a solution of hydrochloric acid (18.9 mg, 518 µmol, 20.00 eq.) in methanol (1.25 M, 414 µl) was added. The reaction mixture was stirred for 67 h at room temperature. The solvent was removed under reduced pressure and the product was obtained as white solid (5.70 mg, 18.9 µmol, 78 %).

^{1}H-NMR (400.15 MHz, $CDCl_3$): δ = 7.85 (s, 3H), 6.81 (d, *J* = 8.6 Hz, 1H), 6.73 – 6.71 (m, 2H), 3.96 (t, *J* = 6.9 Hz, 2H), 3.84 (s, 3H), 3.19 (s, 2H), 2.92 (t, *J* = 7.0 Hz, 2H), 1.81 (p, *J* = 6.9 Hz, 2H), 1.45 – 1.25 (m, 8H), 0.88 (d, *J* = 6.9 Hz, 3H) ppm.

^{13}C-NMR (100.62 MHz, $CDCl_3$): δ = 149.9, 148.2, 128.0, 121.0, 113.6, 112.7, 69.3, 56.2, 41.3, 33.3, 31.9, 29.3, 29.2, 26.1, 22.7, 14.2 ppm.

HRMS (ESI(+), CH_3CN): *m/z* 266.2113 $[M]^+$, calculated for $C_{16}H_{28}NO_2^+$: *m/z* 266.2115.

2-(3-Methoxy-4-(octyloxy)phenyl)ethan-1-aminium chloride (16)

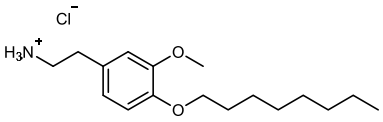

N-(3-Methoxy-4-(octyloxy)phenethyl)formamide (**9**) (39.2 mg, 128 µmol, 1.00 eq.) was dissolved in methanol (1 ml) and a solution of hydrochloric acid (46.5 mg, 1.28 mmol, 10.00 eq.) in methanol (1.25 M, 1.02 ml) was added. The reaction mixture was stirred for 92 h at room temperature. The solvent was removed under reduced pressure and the product was obtained as white solid (40.1 mg, 127 µmol, 100 %).

^{1}H-NMR (400.15 MHz, CD_3OD): δ = 6.91 – 6.89 (m, 2H), 6.80 (dd, *J* = 8.2, 1.9 Hz, 1H), 3.96 (t, *J* = 6.5 Hz, 2H), 3.84 (s, 3H), 3.16 (t, *J* = 7.6 Hz, 2H), 2.93 – 2.89 (m, 2H), 1.80 – 1.73 (m, 2H), 1.49 – 1.43 (m, 2H), 1.38 – 1.31 (m, 8H), 0.92 – 0.89 (m, 3H) ppm.

^{13}C-NMR (100.62 MHz, CD_3OD): δ = 151.2, 149.2, 130.6, 122.2, 115.1, 114.0, 70.3, 56.6, 42.1, 34.1, 33.0, 30.5, 30.4, 30.4, 27.1, 23.7, 14.4 ppm.

HRMS (ESI(+), CH_3CN): *m/z* 280.2267 $[M]^+$, calculated for $C_{17}H_{30}NO_2^+$: *m/z* 280.2271.

Mandi-Dopa-C2 (17)

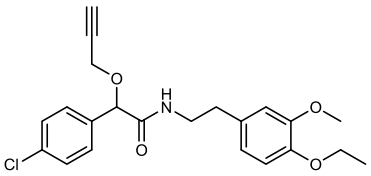

2-(4-Ethoxy-3-methoxyphenyl)ethan-1-aminium chloride (**10**) (41.2 mg, 178 µmol, 1.00 eq.) was dissolved in anhydrous dimethylformamide (1 ml). Then, 2-(4-chlorophenyl)-2-(prop-2-yn-1-yloxy)acetic acid (**1**) (39.9 mg, 178 µmol, 1.00 eq.), HATU (74.4 mg, 196 µmol, 1.10 eq.), 1-hydroxy-6-(trifluoromethyl)benzotriazole (HOBt) (43.3 mg, 213 µmol, 1.20 eq.) and *N*,*N*-diisopropylethylamine (DIPEA) (73.5 µl, 445 µmol, 2.50 eq.) were added. The reaction mixture was stirred for 20 h at room temperature. The solvent was removed under reduced pressure, saturated aqueous ammonium chloride solution (1 ml) was added and extracted with dichloromethane (2 ml). The solvent removed under reduced pressure. The solvent was removed under reduced pressure and the crude product was purified by preparative reverse phase HPLC (C18, acetonitrile:water gradient + 0.1 % TFA). The product was obtained as white solid (40.5 mg, 101 µmol, 71 %).

^{1}H-NMR (400.15 MHz, $CDCl_3$): δ = 7.31 (d, *J* = 8.7 Hz, 2H), 7.26 (d, *J* = 8.5 Hz, 2H), 6.79 (d, *J* = 8.0 Hz, 1H), 6.75 (t, *J* = 5.9 Hz, 1H), 6.70 – 6.66 (m, 2H), 4.96 (s, 1H), 4.20 – 3.94 (m, 4H), 3.83 (s, 3H), 3.60 – 3.45 (m, 2H), 2.79 – 2.75 (m, 2H), 2.47 (t, *J* = 2.4 Hz, 1H), 1.46 (t, *J* = 7.0 Hz, 3H) ppm.

^{13}C-NMR (100.62 MHz, $CDCl_3$): δ = 169.6, 149.5, 147.1, 134.8, 134.7, 131.2, 128.9, 128.8, 120.8, 113.0, 112.3, 79.8, 78.2, 76.0, 64.5, 56.5, 56.0, 40.4, 35.3, 15.0 ppm.

HRMS (ESI(+), CH_3CN): *m/z* 402.1466 $[M+H]^+$, calculated for $C_{22}H_{25}NO_4Cl^+$: *m/z* 402.1467.

Mandi-Dopa-C3 (18)

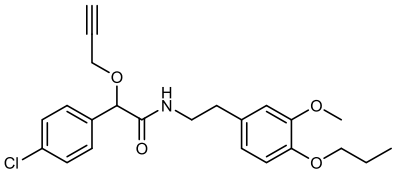

2-(3-Methoxy-4-propoxyphenyl)ethan-1-aminium chloride (**11**) (39.9 mg, 162 µmol, 1.00 eq.) was dissolved in anhydrous dimethylformamide (1 ml). Then, 2-(4-chlorophenyl)-2-(prop-2-yn-1-yloxy)acetic acid (**1**) (36.5 mg, 162 µmol, 1.00 eq.), HATU (67.9 mg, 179 µmol, 1.10 eq.), 1-hydroxy-6-(trifluoromethyl)benzotriazole (HOBt) (39.6 mg, 195 µmol, 1.20 eq.) and *N*,*N*-diisopropylethylamine (DIPEA) (67.1 µl, 406 µmol, 2.50 eq.) were added. The reaction mixture was stirred for 20 h at room temperature. The solvent was removed under reduced pressure, saturated aqueous ammonium chloride solution (1 ml) was added and extracted with dichloromethane (2 ml). The solvent removed under reduced pressure. The solvent was removed under reduced pressure and the crude product was purified by preparative reverse phase HPLC (C18, acetonitrile:water gradient + 0.1 % TFA). The product was obtained as white solid (39.3 mg, 94.5 µmol, 58 %).

^{1}H-NMR (400.15 MHz, $CDCl_3$): δ = 7.31 (d, *J* = 8.5 Hz, 2H), 7.25 (d, *J* = 8.6 Hz, 2H), 6.81 – 6.79 (m, 2H), 6.70 – 6.66 (m, 2H), 4.98 (s, 1H), 4.20 – 3.94 (m, 4H), 3.83 (s, 3H), 3.62 – 3.46 (m, 2H), 2.79 – 2.75 (m, 2H), 2.48 (t, *J* = 2.4 Hz, 1H), 1.91 – 1.82 (m, 2H), 1.04 (t, *J* = 7.5 Hz, 3H) ppm.

^{13}C-NMR (100.62 MHz, $CDCl_3$): δ = 170.0, 149.6, 147.4, 134.8, 134.7, 131.1, 129.0, 128.9, 120.9, 113.3, 112.6, 79.7, 78.2, 76.1, 70.8, 56.5, 56.1, 40.5, 35.3, 22.7, 10.6 ppm.

HRMS (ESI(+), CH_3CN): *m/z* 416.1620 $[M+H]^+$, calculated for $C_{23}H_{27}NO_4Cl^+$: *m/z* 416.1623.

Mandi-Dopa-C4 (19)

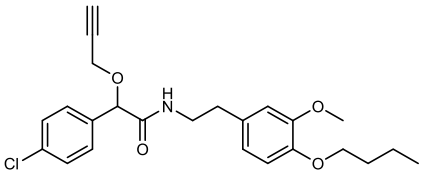

2-(4-Butoxy-3-methoxyphenyl)ethan-1-aminium chloride (**12**) (45.3 mg, 174 µmol, 1.00 eq.) was dissolved in anhydrous dimethylformamide (1 ml). Then, 2-(4-chlorophenyl)-2-(prop-2-yn-1-yloxy)acetic acid (**1**) (39.2 mg, 174 µmol, 1.00 eq.), HATU (72.9 mg, 192 µmol, 1.10 eq.), 1-hydroxy-6-(trifluoromethyl)benzotriazole (HOBt) (42.5 mg, 209 µmol, 1.20 eq.) and *N*,*N*-diisopropylethylamine (DIPEA) (72.1 µl, 436 µmol, 2.50 eq.) were added. The reaction mixture was stirred for 20 h at room temperature. The solvent was removed under reduced pressure, saturated aqueous ammonium chloride solution (1 ml) was added and extracted with dichloromethane (2 ml). The solvent removed under reduced pressure. The solvent was removed under reduced pressure and the crude product was purified by preparative reverse phase HPLC (C18, acetonitrile:water gradient + 0.1 % TFA). The product was obtained as white solid (48.8 mg, 114 µmol, 65 %).

^{1}H-NMR (400.15 MHz, $CDCl_3$): δ = 7.32 (d, *J* = 8.6 Hz, 2H), 7.26 (d, *J* = 8.5 Hz, 2H), 6.80 (d, *J* = 8.0 Hz, 1H), 6.76 (t, *J* = 6.0 Hz, 1H), 6.70 – 6.66 (m, 2H), 4.97 (s, 1H), 4.21 – 3.94 (m, 4H), 3.83 (s, 3H), 3.61 – 3.45 (m, 2H), 2.79 – 2.75 (m, 2H), 2.47 (t, *J* = 2.4 Hz, 1H), 1.86 – 1.79 (m, 2H), 1.55 – 1.45 (m, 2H), 0.98 (t, *J* = 7.4 Hz, 3H) ppm.

^{13}C-NMR (100.62 MHz, $CDCl_3$): δ = 169.7, 149.6, 147.5, 134.8, 134.8, 131.2, 129.0, 128.9, 120.9, 113.3, 112.5, 79.8, 78.2, 76.0, 69.0, 56.5, 56.1, 40.4, 35.3, 31.4, 19.4, 14.0 ppm.

HRMS (ESI(+), CH_3CN): *m/z* 430.1778 $[M+H]^+$, calculated for $C_{24}H_{29}NO_4Cl^+$: *m/z* 430.1780.

Mandi-Dopa-C5 (20)

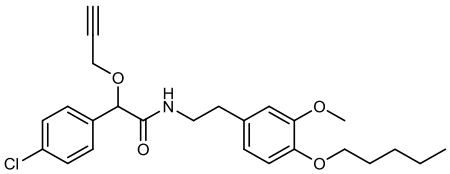

2-(3-Methoxy-4-(pentyloxy)phenyl)ethan-1-aminium chloride (**13**) (2.20 mg, 8.04 µmol, 1.00 eq.) was dissolved in anhydrous dimethylformamide (1 ml). Then, 2-(4-chlorophenyl)-2-(prop-2-yn-1-yloxy)acetic acid (**1**) (1.80 mg, 8.04 µmol, 1.00 eq.), HATU (3.36 mg, 8.84 µmol, 1.10 eq.), 1-hydroxy-6-(trifluoromethyl)benzotriazole (HOBt) (1.48 mg, 9.64 µmol, 1.20 eq.) and *N*,*N*-diisopropylethylamine (DIPEA) (3.32 µl, 20.1 µmol, 2.50 eq.) were added. The reaction mixture was stirred for 21 h at room temperature. The solvent was removed under reduced pressure, saturated aqueous ammonium chloride solution (1 ml) was added and extracted with dichloromethane (2 ml). The solvent removed under reduced pressure. The solvent was removed under reduced pressure and the crude product was purified by preparative reverse phase HPLC (C18, acetonitrile:water gradient + 0.1 % TFA). The product was obtained as white solid (1.20 mg, 2.70 µmol, 34 %).

^{1}H-NMR (400.15 MHz, $CDCl_3$): δ = 7.32 (d, *J* = 8.5 Hz, 2H), 7.27 (d, *J* = 5.1 Hz, 2H), 6.80 (d, *J* = 8.0 Hz, 1H), 6.76 (t, *J* = 5.6 Hz, 1H), 6.69 – 6.67 (m, 2H), 4.97 (s, 1H), 4.21 – 3.95 (m, 4H), 3.83 (s, 3H), 3.61 – 3.45 (m, 2H), 2.79 – 2.75 (m, 2H), 2.47 (t, *J* = 2.3 Hz, 1H), 1.88 – 1.81 (m, 2H), 1.47 – 1.36 (m, 4H), 0.93 (t, *J* = 7.1 Hz, 3H) ppm.

^{13}C-NMR (100.62 MHz, $CDCl_3$): δ = 169.7, 149.6, 147.5, 134.8, 134.8, 131.2, 129.0, 128.9, 120.9, 113.3, 112.5, 79.8, 78.2, 76.0, 69.3, 56.5, 56.2, 40.4, 35.3, 29.1, 28.3, 22.6, 14.2 ppm.

HRMS (ESI(+), CH_3CN): *m/z* 444.1934 $[M+H]^+$, calculated for $C_{25}H_{31}NO_4Cl^+$: *m/z* 444.1936.

Mandi-Dopa-C6 (21)

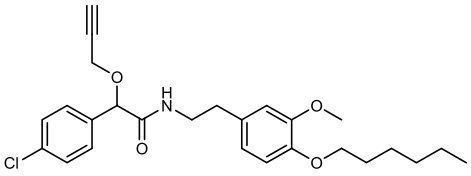

2-(4-(Hexyloxy)-3-methoxyphenyl)ethan-1-aminium chloride (**14**) (35.0 mg, 122 µmol, 1.00 eq.) was dissolved in anhydrous dimethylformamide (1 ml). Then, 2-(4-chlorophenyl)-2-(prop-2-yn-1-yloxy)acetic acid (**1**) (27.3 mg, 122 µmol, 1.00 eq.), HATU (50.9 mg, 134 µmol, 1.10 eq.), 1-hydroxy-6-(trifluoromethyl)benzotriazole (HOBt) (29.6 mg, 146 µmol, 1.20 eq.) and *N*,*N*-diisopropylethylamine (DIPEA) (50.2 µl, 304 µmol, 2.50 eq.) were added. The reaction mixture was stirred for 20 h at room temperature. The solvent was removed under reduced pressure, saturated aqueous ammonium chloride solution (1 ml) was added and extracted with dichloromethane (2 ml). The solvent removed under reduced pressure. The solvent was removed under reduced pressure and the crude product was purified by preparative reverse phase HPLC (C18, acetonitrile:water gradient + 0.1 % TFA). The product was obtained as white solid (31.4 mg, 68.6 µmol, 56 %).

^{1}H-NMR (400.15 MHz, $CDCl_3$): δ = 7.32 (d, *J* = 8.6 Hz, 2H), 7.26 (d, *J* = 8.5 Hz, 2H), 6.80 (d, *J* = 8.0 Hz, 2H), 6.75 (t, *J* = 6.0 Hz, 1H), 6.70 – 6.66 (m, 2H), 4.96 (s, 1H), 4.21 – 3.94 (m, 4H), 3.83 (s, 3H), 3.61 – 3.45 (m, 2H), 2.79 – 2.75 (m, 2H), 2.47 (t, *J* = 2.4 Hz, 1H), 1.87 – 1.80 (m, 2H), 1.50 – 1.32 (m, 6H), 0.92 – 0.88 (m, 3H) ppm.

^{13}C-NMR (100.62 MHz, $CDCl_3$): δ = 169.6, 149.6, 147.4, 134.8, 134.7, 131.2, 128.9, 128.8, 120.9, 113.3, 112.5, 79.8, 78.2, 76.0, 69.3, 56.5, 56.1, 40.4, 35.3, 31.7, 29.3, 25.8, 22.7, 14.2 ppm.

HRMS (ESI(+), CH_3CN): *m/z* 458.2088 $[M+H]^+$, calculated for $C_{26}H_{33}NO_4Cl^+$: *m/z* 458.2093.

Mandi-Dopa-C7 (22)

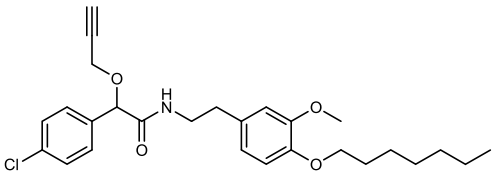

2-(4-(Heptyloxy)-3-methoxyphenyl)ethan-1-aminium chloride (**15**) (5.70 mg, 18.9 µmol, 1.00 eq.) was dissolved in anhydrous dimethylformamide (1 ml). Then, 2-(4-chlorophenyl)-2-(prop-2-yn-1-yloxy)acetic acid (**1**) (4.24 mg, 18.9 µmol, 1.00 eq.), HATU (7.90 mg, 20.8 µmol, 1.10 eq.), 1-hydroxy-6-(trifluoromethyl)benzotriazole (HOBt) (3.47 mg, 22.7 µmol, 1.20 eq.) and *N*,*N*-diisopropylethylamine (DIPEA) (7.80 µl, 47.2 µmol, 2.50 eq.) were added. The reaction mixture was stirred for 21 h at room temperature. The solvent was removed under reduced pressure, saturated aqueous ammonium chloride solution (1 ml) was added and extracted with dichloromethane (2 ml). The solvent removed under reduced pressure. The solvent was removed under reduced pressure and the crude product was

purified by preparative reverse phase HPLC (C18, acetonitrile:water gradient + 0.1 % TFA). The product was obtained as white solid (3.80 mg, 8.05 µmol, 43 %).

^{1}H-NMR (400.15 MHz, $CDCl_3$): δ = 7.32 (d, *J* = 8.6 Hz, 2H), 7.26 (d, *J* = 8.5 Hz, 2H), 6.80 (d, *J* = 8.0 Hz, 1H), 6.75 (t, *J* = 5.6 Hz, 1H), 6.70 – 6.66 (m, 1H), 4.97 (s, 1H), 4.21 – 3.95 (m, 4H), 3.83 (s, 3H), 3.61 – 3.45 (m, 2H), 2.79 – 2.75 (m, 2H), 2.47 (t, *J* = 2.4 Hz, 1H), 1.87 – 1.80 (m, 2H), 1.49 – 1.25 (m, 8H), 0.90 – 0.87 (m, 3H) ppm.

^{13}C-NMR (100.62 MHz, $CDCl_3$): δ = 169.7, 149.6, 147.5, 134.8, 134.8, 131.2, 129.0, 128.9, 120.9, 113.3, 112.5, 79.8, 78.2, 76.0, 69.3, 56.5, 56.1, 40.4, 35.3, 31.9, 29.4, 29.2, 26.1, 22.8, 14.2 ppm.

HRMS (ESI(+), CH_3CN): *m/z* 472.2249 $[M+H]^+$, calculated for $C_{27}H_{35}NO_4Cl^+$: *m/z* 471.2249.

Mandi-Dopa-C8 (23)

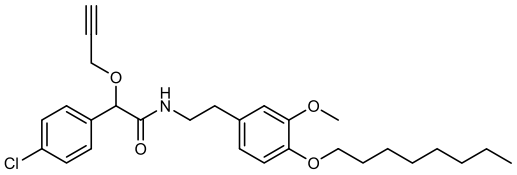

2-(3-Methoxy-4-(octyloxy)phenyl)ethan-1-aminium chloride (**16**) (40.1 mg, 127 µmol, 1.00 eq.) was dissolved in anhydrous dimethylformamide (1 ml). Then, 2-(4-chlorophenyl)-2-(prop-2-yn-1-yloxy)acetic acid (**1**) (28.5 mg, 127 µmol, 1.00 eq.), HATU (53.1 mg, 140 µmol, 1.10 eq.), 1-hydroxy-6-(trifluoromethyl)benzotriazole (HOBt) (30.9 mg, 152 µmol, 1.20 eq.) and *N*,*N*-diisopropylethylamine (DIPEA) (52.5 µl, 317 µmol, 2.50 eq.) were added. The reaction mixture was stirred for 20 h at room temperature. The solvent was removed under reduced pressure, saturated aqueous ammonium chloride solution (1 ml) was added and extracted with dichloromethane (2 ml). The solvent removed under reduced pressure. The solvent was removed under reduced pressure and the crude product was purified by preparative reverse phase HPLC (C18, acetonitrile:water gradient + 0.1 % TFA). The product was obtained as white solid (24.7 mg, 50.8 µmol, 40 %).

^{1}H-NMR (400.15 MHz, $CDCl_3$): δ = 7.32 (d, *J* = 8.5 Hz, 2H), 7.26 (d, *J* = 8.5 Hz, 2H), 6.80 (d, *J* = 8.0 Hz, 1H), 6.75 (t, *J* = 5.9 Hz, 1H), 6.70 – 6.66 (m, 2H), 4.97 (s, 1H), 4.21 – 3.95 (m, 4H), 3.83 (s, 3H), 3.61 – 3.45 (m, 2H), 2.79 – 2.75 (m, 2H), 2.47 (t, *J* = 2.4 Hz, 1H), 1.87 – 1.80 (m, 2H), 1.49 – 1.28 (m, 10H), 0.90 – 0.86 (m, 3H) ppm.

^{13}C-NMR (100.62 MHz, $CDCl_3$): δ = 169.6, 149.6, 147.5, 134.9, 134.8, 131.2, 129.0, 128.9, 120.9, 113.3, 112.5, 79.8, 78.2, 76.0, 69.3, 56.5, 56.1, 40.4, 35.3, 32.0, 29.5, 29.4, 26.1, 22.8, 14.2 ppm.

HRMS (ESI(+), CH_3CN): *m/z* 486.2404 $[M+H]^+$, calculated for $C_{28}H_{37}NO_4Cl^+$: *m/z* 486.2406.

Mandi-MS-Cn: strategy 1

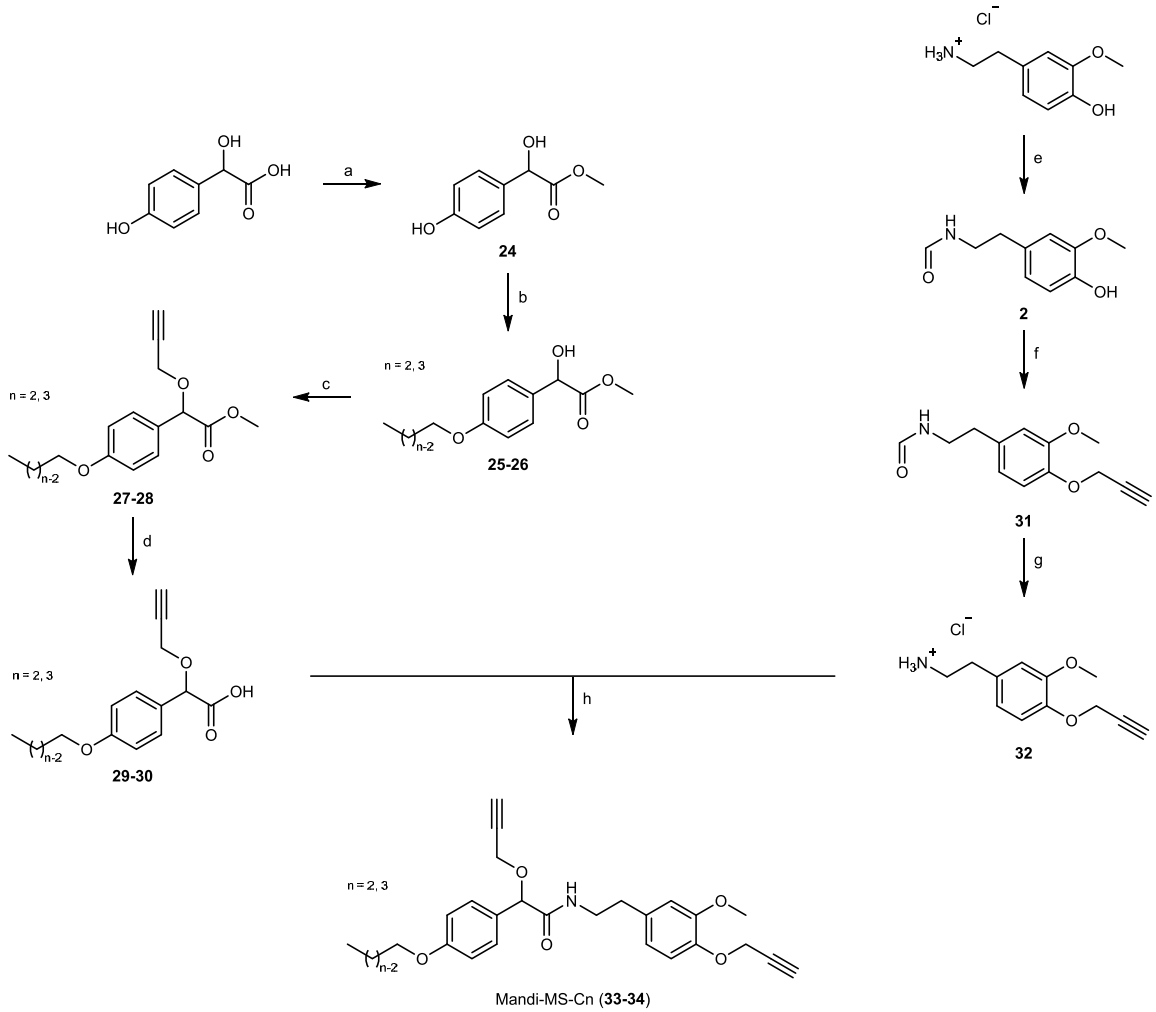

Conditions: a: MeOH, H_2SO_4, rt, 21 h; b: alkyl bromide, K_2CO_3, KI, rt, 67 h; c: propargyl bromide, NaH, 0 °C -> rt, 2 h; d: NaOH, rt, 16 h; e: Ac_2O, formic acid, 70 °C, 2 h; f: propargyl bromide, NaOMe, 4 h, 65 °C; g: HCl, rt, 91 h; h: HATU, HOBt, DIPEA, rt, 71 h.

Methyl 2-hydroxy-2-(4-hydroxyphenyl)acetate (24)

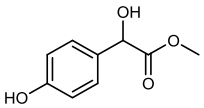

Methyl 2-hydroxy-2-(4-hydroxyphenyl)acetate (**24**) was synthesized during my master's thesis[79] as described in literature[88]:

2-Hydroxy-2-(4-hydroxyphenyl)acetic acid monohydrate (4-hydroxymandelic acid monohydrate) (1.00 g, 5.37 mmol, 1.00 eq.) was dissolved in methanol (10 ml). The red solution was cooled to 0 °C and sulfuric acid (315 µl, 5.90 mmol, 1.10 eq.) was added dropwise. The reaction mixture was stirred for 21 h at room temperature. Then, saturated aqueous sodium hydrogencarbonate solution (20 ml) were added and the mixture was extracted with dichloromethane (5 x 10 ml). The combined organic

layer was dried over sodium sulphate and the solvent was removed under reduced pressure. The product was obtained was pink solid (450 mg, 2.47 mmol, 46 %).

^{1}H-NMR (400.15 MHz, CD_3OD): δ = 7.23 (d, *J* = 8.4 Hz, 2H), 6.76 (d, *J* = 8.7 Hz, 2H), 5.08 (s, 1H), 3.68 (s, 3H) ppm.

^{13}C-NMR (100.62 MHz, CD_3OD): δ = 175.3, 158.8, 131.2, 129.3, 116.2, 74.0, 52.6 ppm.

HRMS (ESI(+), CH_3CN): *m/z* 205.0469 $[M+Na]^+$, calculated for $C_9H_{10}O_4Na^+$: *m/z* 205.0471.

Methyl 2-(4-ethoxyphenyl)-2-hydroxyacetate (25)

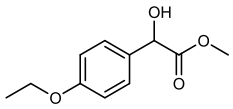

Methyl 2-hydroxy-2-(4-hydroxyphenyl)acetate (**24**) (150 mg, 823 µmol, 1.00 eq.) was dissolved in anhydrous dimethylformamide (1 ml). Then, potassium carbonate (341 mg, 2.47 mmol, 3.00 eq.), potassium iodide (68.3 mg, 412 µmol, 0.50 eq.) and ethyl bromide (91.6 µl, 1.24 mmol, 1.50 eq.) were added. The reaction mixture was stirred for 67 h at room temperature. Thereafter, saturated aqueous ammonium chloride solution (10 ml) was added and the mixture was extracted with dichloromethane (4 x 10 ml). The combined organic layer was dried over sodium sulphate and the solvent was removed under reduced pressure. The crude product was purified by preparative reverse phase HPLC (C18, acetonitrile:water gradient + 0.1 % TFA). The product was obtained as white solid (52.8 mg, 251 µmol, 31 %).

^{1}H-NMR (400.15 MHz, $CDCl_3$): δ = 7.31 (d, *J* = 8.6 Hz, 2H), 6.88 (d, *J* = 8.7 Hz, 2H), 5.12 (s, 1H), 4.03 (q, *J* = 7.0 Hz, 2H), 3.75 (s, 3H), 1.40 (t, *J* = 7.0 Hz, 3H) ppm.

^{13}C-NMR (100.62 MHz, $CDCl_3$): δ = 174.5, 159.3, 130.4, 128.0, 114.7, 72.6, 63.6, 53.1, 14.9 ppm.

HRMS (ESI(+), CH_3CN): *m/z* 233.0784 $[M+Na]^+$, calculated for $C_{11}H_{14}O_4Na^+$: *m/z* 233.0784.

Methyl 2-hydroxy-2-(4-propoxyphenyl)acetate (26)

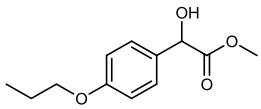

Methyl 2-hydroxy-2-(4-hydroxyphenyl)acetate (**24**) (150 mg, 823 µmol, 1.00 eq.) was dissolved in anhydrous dimethylformamide (1 ml). Then, potassium carbonate (341 mg, 2.47 mmol, 3.00 eq.), potassium iodide (68.3 mg, 412 µmol, 0.50 eq.) and 1-bromopropane (113 µl, 1.24 mmol, 1.50 eq.) were added. The reaction mixture was stirred for 67 h at room temperature. Thereafter, saturated aqueous ammonium chloride solution (10 ml) was added and the mixture was extracted with dichloromethane (4 x 10 ml). The combined organic layer was dried over sodium sulphate and the solvent was removed under reduced pressure. The crude product was purified by preparative reverse

phase HPLC (C18, acetonitrile:water gradient + 0.1 % TFA). The product was obtained as white solid (34.5 mg, 154 µmol, 19 %).

^{1}H-NMR (400.15 MHz, $CDCl_3$): δ = 7.31 (d, *J* = 8.4 Hz, 2H), 6.88 (d, *J* = 8.7 Hz, 2H), 5.12 (s, 1H), 3.91 (t, *J* = 6.6 Hz, 2H), 3.75 (s, 3H), 1.84 – 1.75 (m, 2H), 1.03 (t, *J* = 7.4 Hz, 3H) ppm.

^{13}C-NMR (100.62 MHz, $CDCl_3$): δ = 174.5, 159.5, 130.3, 128.0, 114.7, 72.6, 69.7, 53.1, 22.7, 10.6 ppm.

HRMS (ESI(+), CH_3CN): *m/z* 247.0940 $[M+Na]^+$, calculated for $C_{12}H_{16}O_4Na^+$: *m/z* 247.0941.

Methyl 2-(4-ethoxyphenyl)-2-(prop-2-yn-1-yloxy)acetate (27)

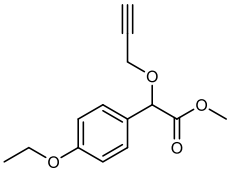

Methyl 2-(4-ethoxyphenyl)-2-hydroxyacetate (**25**) (52.8 mg, 251 µmol, 1.00 eq.) was dissolved in anhydrous tetrahydrofuran (5 ml), cooled to 0 °C and sodium hydride (60 %, 11.1 mg, 276 µmol, 1.10 eq.) was added slowly. Then, a solution of 3-bromoprop-1-yne (propargyl bromide) (41.1 mg, 276 µmol, 1.10 eq.) in xylene (80 wt%, 30.7 µl) was added dropwise at 0 °C. The reaction mixture was stirred for 2 h at room temperature. Saturated aqueous ammonium chloride solution (10 ml) was added and the mixture was extracted with dichloromethane (3 x 10 ml). The combined organic layer was dried over sodium sulphate and the solvent was removed under reduced pressure. The crude product was purified by preparative reverse phase HPLC (C18, acetonitrile:water gradient + 0.1 % TFA). The product was obtained as colorless liquid (10.7 mg, 43.1 µmol, 17 %).

^{1}H-NMR (400.15 MHz, $CDCl_3$): δ = 7.35 (d, *J* = 8.7 Hz, 2H), 6.88 (d, *J* = 8.7 Hz, 2H), 5.15 (s, 1H), 4.30 – 4.08 (m, 2H), 4.03 (q, *J* = 7.0 Hz, 2H), 3.72 (s, 3H), 2.47 (t, *J* = 2.4 Hz, 1H), 1.41 (t, *J* = 7.0 Hz, 3H) ppm.

^{13}C-NMR (100.62 MHz, $CDCl_3$): δ = 171.1, 159.7, 129.2, 127.3, 114.8, 78.7, 78.3, 75.7, 63.6, 56.0, 52.5, 14.9 ppm.

HRMS (ESI(+), CH_3CN): *m/z* 271.0938 $[M+Na]^+$, calculated for $C_{14}H_{16}O_4Na^+$: *m/z* 271.0941.

Methyl 2-(prop-2-yn-1-yloxy)-2-(4-propoxyphenyl)acetate (28)

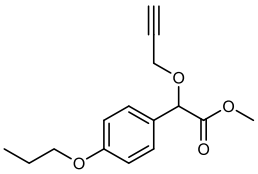

Methyl 2-hydroxy-2-(4-propoxyphenyl)acetate (**26**) (34.5 mg, 154 µmol, 1.00 eq.) was dissolved in anhydrous tetrahydrofuran (5 ml), cooled to 0 °C and sodium hydride (60 %, 6.77 mg, 169 µmol, 1.10 eq.) was added slowly. Then, a solution of 3-bromoprop-1-yne (propargyl bromide) (25.2 mg, 169 µmol, 1.10 eq.) in xylene (80 wt%, 18.8 µl) was added dropwise at 0 °C. The reaction mixture was stirred for 2 h at room temperature. Saturated aqueous ammonium chloride solution (10 ml) was

added and the mixture was extracted with dichloromethane (3 x 10 ml). The combined organic layer was dried over sodium sulphate and the solvent was removed under reduced pressure. The crude product was purified by preparative reverse phase HPLC (C18, acetonitrile:water gradient + 0.1 % TFA). The product was obtained as colorless liquid (4.20 mg, 16.0 µmol, 10 %).

^{1}H-NMR (400.15 MHz, $CDCl_3$): δ = 7.35 (d, *J* = 8.7 Hz, 1H), 6.89 (d, *J* = 8.7 Hz, 1H), 5.16 (s, 1H), 4.31 – 4.07 (m, 2H), 3.92 (t, *J* = 6.6 Hz, 2H), 3.72 (s, 3H), 2.47 (t, *J* = 2.4 Hz, 1H), 1.87 – 1.73 (m, 1H), 1.03 (t, *J* = 7.4 Hz, 3H) ppm.

^{13}C-NMR (100.62 MHz, $CDCl_3$): δ = 171.1, 159.9, 129.2, 127.2, 114.9, 78.8, 78.3, 75.7, 69.7, 56.0, 52.5, 22.7, 10.7 ppm.

HRMS (ESI(+), CH_3CN): *m/z* 285.1091 $[M+Na]^+$, calculated for $C_{15}H_{18}O_4Na^+$: *m/z* 285.1097.

2-(4-Ethoxyphenyl)-2-(prop-2-yn-1-yloxy)acetic acid (29)

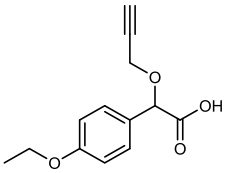

Methyl 2-(4-ethoxyphenyl)-2-(prop-2-yn-1-yloxy)acetate (**27**) (10.7 mg, 43.1 µmol, 1.00 eq.) was dissolved in anhydrous tetrahydrofuran (1 ml) and aqueous sodium hydroxide (6.90 mg, 172.4 µmol, 4.00 eq.) solution (2.00 M, 172 µl) was added. The reaction mixture was stirred for 16 h at room temperature. Then, aqueous acetic acid (2.00 M) was added until pH 3 was reached, the mixture was extracted with dichloromethane (3 x 10 ml) and the combined organic layer was dried over sodium sulphate. The solvent was removed under reduced pressure and the product was obtained as colorless liquid (8.80 mg, 37.6 µmol, 87 %)

^{1}H-NMR (400.15 MHz, $CDCl_3$): δ = 7.35 (d, *J* = 8.7 Hz, 2H), 6.90 (d, *J* = 8.7 Hz, 2H), 5.17 (s, 1H), 4.32 – 4.06 (m, 2H), 4.03 (q, *J* = 7.0 Hz, 2H), 2.50 (t, *J* = 2.4 Hz, 1H), 1.41 (t, *J* = 7.0 Hz, 3H) ppm.

^{13}C-NMR (100.62 MHz, $CDCl_3$): δ = 173.8, 160.0, 129.3, 126.4, 115.0, 78.2, 77.9, 76.2, 63.7, 56.1, 14.9 ppm.

HRMS (ESI(+), CH_3CN): *m/z* 257.0785 $[M+Na]^+$, calculated for $C_{13}H_{14}O_4Na^+$: *m/z* 257.0784.

2-(Prop-2-yn-1-yloxy)-2-(4-propoxyphenyl)acetic acid (30)

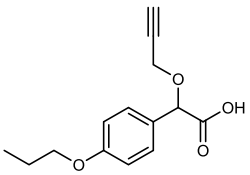

Methyl 2-(prop-2-yn-1-yloxy)-2-(4-propoxyphenyl)acetate (**28**) (4.20 mg, 16.0 µmol, 1.00 eq.) was dissolved in anhydrous tetrahydrofuran (1 ml) and aqueous sodium hydroxide (2.56 mg, 64.0 µmol, 4.00 eq.) solution (2.00 M, 64.0 µl) was added. The reaction mixture was stirred for 16 h at room

temperature. Then, aqueous acetic acid (2.00 M) was added until pH 3 was reached, the mixture was extracted with dichloromethane (3 x 10 ml) and dried over sodium sulphate. The solvent was removed under reduced pressure and the product was obtained as colorless liquid (3.60 mg, 14.5 µmol, 91 %)

^{1}H-NMR (400.15 MHz, $CDCl_3$): δ = 7.34 (d, *J* = 8.7 Hz, 2H), 6.90 (d, *J* = 8.7 Hz, 2H), 5.17 (s, 1H), 4.32 – 4.06 (m, 2H), 3.92 (t, *J* = 6.5 Hz, 2H), 2.50 (t, *J* = 2.4 Hz, 1H), 1.85 – 1.76 (m, 2H), 1.03 (t, *J* = 7.4 Hz, 3H) ppm.

^{13}C-NMR (100.62 MHz, $CDCl_3$): δ = 173.0, 160.2, 129.3, 126.3, 115.0, 78.2, 77.9, 76.2, 69.7, 56.1, 22.7, 10.6 ppm.

HRMS (ESI(+), CH_3CN): *m/z* 271.0939 $[M+Na]^+$, calculated for $C_{14}H_{16}O_4Na^+$: *m/z* 271.0941.

_N_-(3-Methoxy-4-(prop-2-yn-1-yloxy)phenethyl)formamide (31)

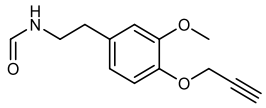

N-(3-Methoxy-4-(prop-2-yn-1-yloxy)phenethyl)formamide (**31**) was synthesized during my master's thesis[79] as described in literature[75]:

N-(4-Hydroxy-3-methoxyphenethyl)formamide (**2**) (227 mg, 1.42 mmol, 1.00 eq.) was dissolved in anhydrous methanol (3.3 ml). Then, a solution of sodium methoxide (76.5 mg, 1.42 mmol, 1.00 eq.) in methanol (25 wt%, 4.37 M, 324 µl) and a solution of 3-bromoprop-1-yne (propargyl bromide) (168 mg, 1.42 mmol, 1.00 eq.) in xylene (80 wt%, 157 µl) were added. The reaction mixture was stirred for 4 h at 65 °C. The solvent was removed in vacuo and ethyl acetate (10 ml) was added to the residue. The organic layer was washed with water (2 x 10 ml) and dried over sodium sulphate. The solvent was removed under reduced pressure and the crude product was purified by column chromatography (silica gel, dichloromethane:ethyl acetate gradient). The product was obtained as slightly yellow liquid (142 mg, 609 µmol, 43 %).

^{1}H-NMR (400.15 MHz, $CDCl_3$): δ = 8.15 (s, 1H), 6.98 (d, *J* = 8.6 Hz, 1H), 6.74 – 6.70 (m, 2H), 5.55 (s, 1H), 4.74 (d, *J* = 2.4 Hz, 2H), 3.87 (s, 3H), 3.57 (q, *J* = 6.7 Hz, 2H), 2.80 (t, *J* = 6.9 Hz, 2H), 2.50 (t, *J* = 2.4 Hz, 1H) ppm.

^{13}C-NMR (100.62 MHz, $CDCl_3$): δ = 161.3, 150.0, 145.7, 132.6, 120.7, 114.9, 112.5, 78.8, 75.9, 57.0, 56.1, 39.4, 35.3 ppm.

HRMS (ESI(+), CH_3CN): *m/z* 234.1125 $[M+H]^+$, calculated for $C_{13}H_{16}NO_3^+$: *m/z* 234.1125.

2-(3-Methoxy-4-(prop-2-yn-1-yloxy)phenyl)ethan-1-aminium chloride (32)

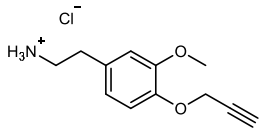

2-(3-Methoxy-4-(prop-2-yn-1-yloxy)phenyl)ethan-1-aminium chloride (**32**) was synthesized during my master's thesis[79] as described in literature[70]:

N-(3-Methoxy-4-(prop-2-yn-1-yloxy)phenethyl)formamide (**31**) (562 mg, 2.41 mmol, 1.00 eq.) was dissolved in anhydrous methanol (15 ml) and a solution of hydrogen chloride (264 mg, 1.83 mmol, 3.00 eq.) in methanol (1.25 M, 5.78 ml) was added. The reaction mixture was stirred for 91 h at room temperature. The solvent was removed under reduced pressure and the residue was dissolved in methanol (5 ml). Then, diethyl ether (20 ml) was added resulting in the formation of a precipitate. The solvent was pipetted off and the residue was died in vacuo. The product was obtained as slightly brown solid (415 mg, 1.72 mmol, 71 %).

^{1}H-NMR (400.15 MHz, CD_3OD): δ = 7.03 (d, *J* = 8.2 Hz, 1H), 6.91 (d, *J* = 2.0 Hz, 1H), 6.81 (dd, *J* = 8.2 Hz, *J* = 2.0 Hz, 1H), 4.73 (d, *J* = 2.4 Hz, 2H), 4.58 (s, 3H), 3.85 (s, 3H), 3.16 (t, *J* = 7.6 Hz, 2H), 2.93 – 2.88 (m, 3H) ppm.

^{13}C-NMR (100.62 MHz, CD_3OD): δ = 151.7, 147.6, 132.0, 122.0, 116.9, 114.0, 79.8, 76.9, 57.9, 56.5, 42.0, 34.3 ppm.

HRMS (ESI(+), CH_3CN): *m/z* 206.1174 $[M+H]^+$, calculated for $C_{12}H_{16}NO_2^+$: *m/z* 206.1176.

Mandi-MS-C2 (33)

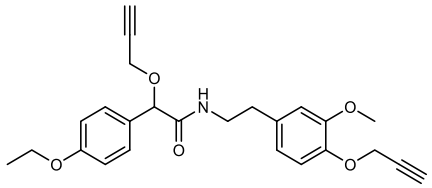

2-(4-Ethoxyphenyl)-2-(prop-2-yn-1-yloxy)acetic acid (**29**) (8.80 mg, 37.6 µmol, 1.00 eq.) was dissolved in anhydrous dimethylformamide (1 ml) and 2-(3-methoxy-4-(prop-2-yn-1-yloxy)phenyl)ethan-1-aminium chloride (**32**) (9.08 mg, 37.6 µmol, 1.00 eq.), HATU (15.7 mg, 41.3 µmol, 1.10 eq.), 1-hydroxybenzotriazole (HOBt) (6.90 mg, 45.1 µmol, 1.20 eq.) and *N*,*N*-diisopropylethylamine (DIPEA) (15.5 µl, 93.9 µmol, 2.50 eq.) were added. The reaction mixture was stirred for 71 h at room temperature. Then, saturated aqueous ammonium chloride solution (1 ml) was added an the mixture was extracted with dichloromethane (2 ml). The solvent as removed under reduced pressure and the crude product was purified by preparative reverse phase HPLC (C18, acetonitrile:water gradient + 0.1 % TFA). The product was obtained as white liquid (8.10 mg, 19.2 µmol, 51 %).

^{1}H-NMR (400.15 MHz, $CDCl_3$): δ = 7.21 (d, *J* = 8.6 Hz, 2H), 6.97 (d, *J* = 7.9 Hz, 1H), 6.85 (d, *J* = 8.7 Hz, 2H), 6.80 (t, *J* = 6.0 Hz, 1H), 6.74 – 6.71 (m, 2H), 4.94 (s, 1H), 4.75 (d, *J* = 2.4 Hz, 2H), 4.17 – 3.91 (m, 2H),

4.02 (q, *J* = 7.0 Hz, 2H), 3.83 (s, 3H), 3.64 – 3.47 (m, 2H), 2.82 – 2.78 (m, 2H), 2.51 (t, *J* = 2.4 Hz, 1H), 2.46 (t, *J* = 2.4 Hz, 1H), 1.40 (t, *J* = 7.0 Hz, 3H) ppm.

^{13}C-NMR (100.62 MHz, $CDCl_3$): δ = 170.5, 159.5, 149.9, 145.6, 133.0, 129.0, 128.0, 120.8, 114.8, 114.8, 112.5, 80.1, 78.9, 78.7, 75.8, 75.6, 63.6, 57.0, 56.0, 56.0, 40.3, 35.4, 14.9 ppm.

HRMS (ESI(+), CH_3CN): *m/z* 422.1963 $[M+H]^+$, calculated for $C_{25}H_{28}NO_5^+$: *m/z* 422.1962.

Mandi-MS-C3 (34)

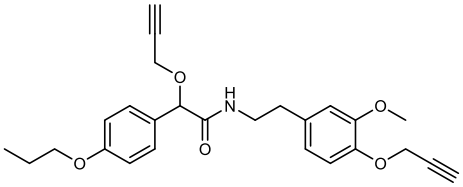

2-(Prop-2-yn-1-yloxy)-2-(4-propoxyphenyl)acetic acid (**30**) (7.70 mg, 31.0 µmol, 1.00 eq.) was dissolved in anhydrous dimethylformamide (**32**) (1 ml) and 2-(3-methoxy-4-(prop-2-yn-1-yloxy)phenyl)ethan-1-aminium chloride (7.50 mg, 31.0 µmol, 1.00 eq.), HATU (13.0 mg, 34.1 µmol, 1.10 eq.), 1-hydroxybenzotriazole (HOBt) (5.70 mg, 37.2 µmol, 1.20 eq.) and *N*,*N*-diisopropylethylamine (DIPEA) (12.8 µl, 77.5 µmol, 2.50 eq.) were added. The reaction mixture was stirred for 71 h at room temperature. Then, saturated aqueous ammonium chloride solution (1 ml) was added an the mixture was extracted with dichloromethane (2 ml). The solvent as removed under reduced pressure and the crude product was purified by preparative reverse phase HPLC (C18, acetonitrile:water gradient + 0.1 % TFA). The product was obtained as white liquid (1.90 mg, 4.36 µmol, 14 %).

^{1}H-NMR (400.15 MHz, $CDCl_3$): δ = 7.21 (d, *J* = 8.6 Hz, 2H), 6.98 (d, *J* = 7.9 Hz, 1H), 6.86 (d, *J* = 8.7 Hz, 2H), 6.78 (t, *J* = 6.0 Hz, 1H), 6.74 – 6.71 (m, 2H), 4.94 (s, 1H), 4.75 (d, *J* = 2.4 Hz, 2H), 4.17 – 3.92 (m, 2H), 3.91 (t, *J* = 6.6 Hz, 2H), 3.84 (s, 3H), 3.63 – 3.47 (m, 2H), 2.82 – 2.78 (m, 2H), 2.51 (t, *J* = 2.4 Hz, 1H), 2.46 (t, *J* = 2.4 Hz, 1H), 1.84 – 1.75 (m, 2H), 1.03 (t, *J* = 7.4 Hz, 3H) ppm.

^{13}C-NMR (100.62 MHz, $CDCl_3$): δ = 170.8, 159.8, 149.9, 145.6, 132.9, 129.0, 127.7, 120.8, 114.8, 112.5, 80.0, 78.9, 78.6, 75.9, 75.6, 69.7, 57.0, 56.0, 56.0, 40.4, 35.4, 22.7, 10.7 ppm.

HRMS (ESI(+), CH_3CN): *m/z* 436.2119 $[M+H]^+$, calculated for $C_{26}H_{30}NO_5^+$: *m/z* 436.2118.

Mandi-MS-Cn: strategy 2

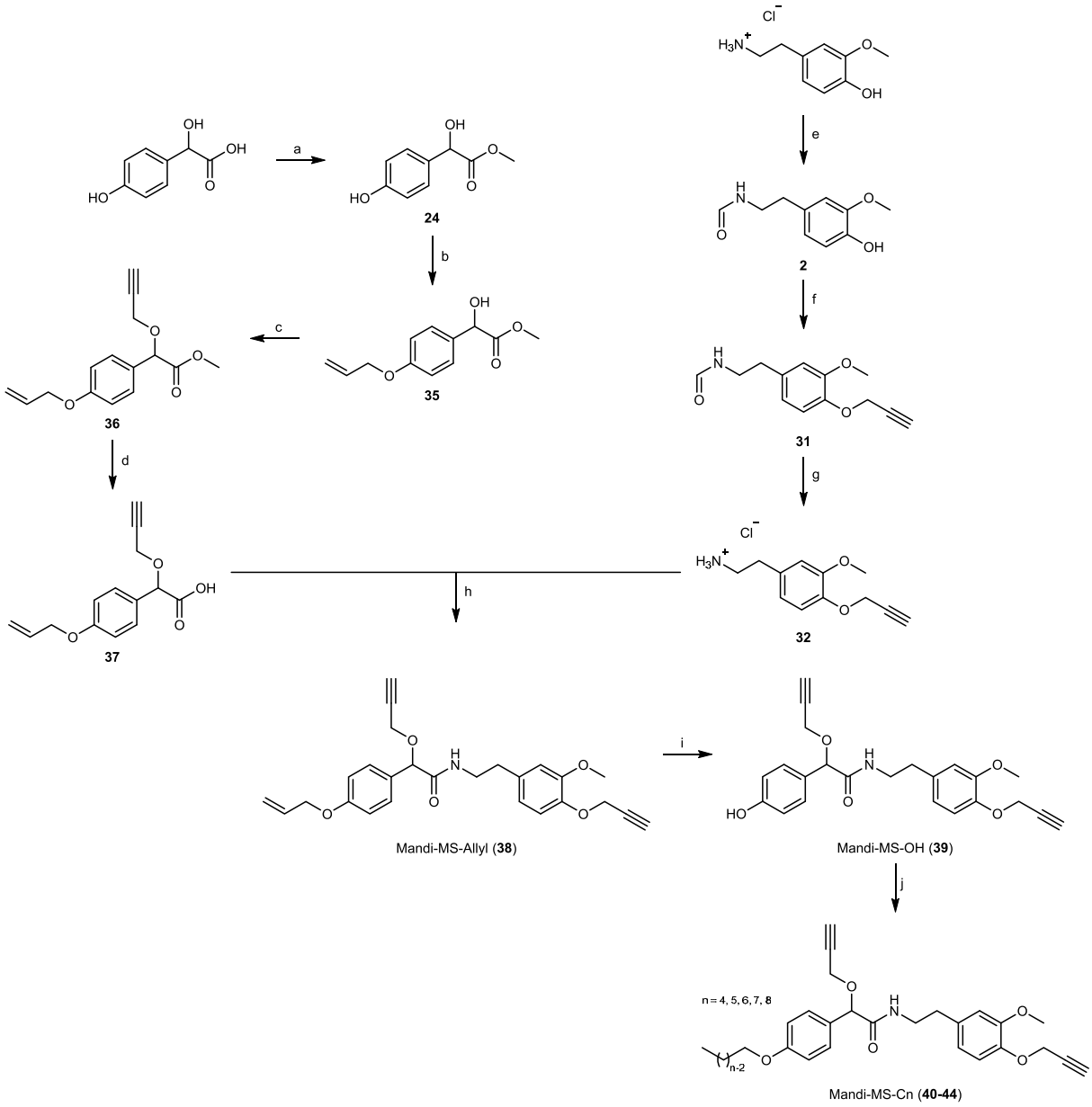

Conditions: a: MeOH, H_2SO_4, rt, 21 h; b: allyl bromide, K_2CO_3, KI, rt, 70 h; c: 3-bromoprop-1-yne, NaH, 0 °C -> rt, 3 h; d: NaOH, rt, 3 h; e: Ac_2O, formic acid, 70 °C, 2 h; f: 3-bromoprop-1-yne, NaOMe, 4 h, 65 °C; g: HCl, rt, 91 h; h: HATU, HOBt, DIPEA, rt, 19 h; i: $Pd(PPh_3)_4$, K_2CO_3, rt, 2 h; j: alkyl bromide, K_2CO_3, KI, rt, 17 – 72 h.

Methyl 2-(4-(allyloxy)phenyl)-2-hydroxyacetate (35)

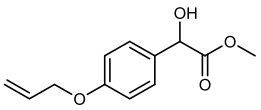

Methyl 2-(4-(allyloxy)phenyl)-2-hydroxyacetate (**35**) was synthesized during my master's thesis[79]:

Methyl 2-hydroxy-2-(4-hydroxyphenyl)acetate (**24**) (200 mg, 1.10 mmol, 1.00 eq.) was dissolved in anhydrous dimethylformamide (3 ml) and potassium carbonate (455 mg, 3.29 mmol, 3.00 eq.) and potassium iodide (91.1 mg, 549 µmol, 0.50 eq.) were added. Then, 3-bromo-1-propene (allyl bromide) (143 µl, 1.65 mmol, 1.50 eq.) was added dropwise and the reaction mixture was stirred for 70 h at room temperature. Saturated aqueous ammonium chloride solution (10 ml) was added and the mixture was extracted with dichloromethane (3 x 10 ml). The combined organic layer was washed with brine (10 ml) and dried over sodium sulphate. The solvent was removed under reduced pressure and the crude product was purified by column chromatography (silica gel, dichloromethane:methanol gradient). The product was obtained slightly yellow liquid (127 mg, 573 µmol, 52 %).

^{1}H-NMR (400.15 MHz, $CDCl_3$): δ = 7.32 (d, *J* = 8.5 Hz, 2H), 6.91 (d, *J* = 8.8 Hz, 2H), 6.09 – 6.00 (m, 1H), 5.41 (dq, *J* = 17.3, 1.6 Hz, 1H), 5.29 (dq, *J* = 10.5, 1.4 Hz, 1H), 5.12 (d, *J* = 5.6 Hz, 1H), 4.54 (dt, *J* = 5.3, 1.5 Hz, 2H), 3.76 (s, 3H), 3.33 (d, *J* = 5.6 Hz, 1H) ppm.

^{13}C-NMR (100.62 MHz, $CDCl_3$): δ = 174.5, 159.0, 133.2, 130.7, 128.0, 117.9, 115.0, 72.6, 69.0, 53.1 ppm.

HRMS (ESI(+), CH_3CN): *m/z* 245.0782 $[M+Na]^+$, caluclated for $C_{12}H_{14}O_4Na^+$: *m/z* 245.0784.

Methyl 2-(4-(allyloxy)phenyl)-2-(prop-2-yn-1-yloxy)acetate (36)

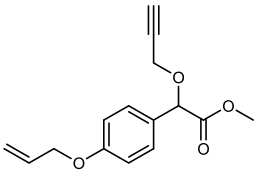

Methyl 2-(4-(allyloxy)phenyl)-2-(prop-2-yn-1-yloxy)acetate (**36**) was synthesized during my master's thesis[79]:

Methyl 2-(4-(allyloxy)phenyl)-2-hydroxyacetate (**35**) (127 mg, 573 µmol, 1.00 eq.) was dissolved in anhydrous tetrahydrofuran (5 ml) and cooled to 0 °C. Then, sodium hydride (60 %, 34.4 mg, 860 µmol, 1.50 eq.) was added slowly. Thereafter, a solution of 3-bromo-1-propyne (propargyl bromide) (128 mg, 860 µmol, 1.50 eq.) in xylene (80 wt%, 95.4 µl) was added dropwise and the reaction mixture was stirred for 3 h at room temperature. Saturated aqueous ammonium chloride solution (10 ml) was added and the mixture was extracted with dichloromethane (3 x 10 ml). The combined organic layer was dried over sodium sulphate. The solvent as removed under reduced pressure and the crude product was purified by preparative reverse phase HPLC (C18, acetonitrile:water gradient + 0.1 % TFA). The product was obtained as colorless liquid (21.8 mg, 83.8 µmol, 15 %).

^{1}H-NMR (400.15 MHz, $CDCl_3$): δ = 7.36 (d, *J* = 8.7 Hz, 2H), 6.91 (d, *J* = 8.7 Hz, 2H), 6.09 – 5.99 (m, 1H), 5.41 (dd, *J* = 17.3, 1.5 Hz, 1H), 5.29 (dd, *J* = 10.5, 1.4 Hz, 1H), 5.16 (s, 1H), 4.53 (dt, *J* = 5.3, 1.4 Hz, 2H), 4.30 – 4.09 (m, 2H), 3.72 (s, 3H), 2.47 (t, *J* = 2.4 Hz, 1H) ppm.

^{13}C-NMR (100.62 MHz, $CDCl_3$): δ = 171.0, 159.4, 133.2, 129.2, 127.7, 118.0, 115.1, 78.7, 78.3, 75.7, 69.0, 56.1, 52.5 ppm.

HRMS (ESI(+), CH_3CN): *m/z* 278.1385 $[M+NH_4]^+$, calculated for $C_{15}H_{20}NO_4^+$: *m/z* 278.1387.

2-(4-(Allyloxy)phenyl)-2-(prop-2-yn-1-yloxy)acetic acid (37)

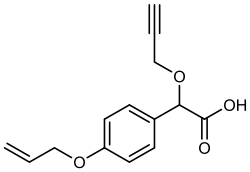

2-(4-(Allyloxy)phenyl)-2-(prop-2-yn-1-yloxy)acetic acid (**37**) was synthesized during my master's thesis[79]:

Methyl 2-(4-(allyloxy)phenyl)-2-(prop-2-yn-1-yloxy)acetate (**36**) (21.8 mg, 83.8 µmol, 2.00 eq.) was dissolved in anhydrous tetrahydrofuran (1 ml) and aqueous sodium hydroxide (6.70 mg, 168 µmol, 4.00 eq.) solution (1.00 M, 168 µl) was added at 0 °C. The reaction mixture was stirred for 3 h at room temperature. Then, aqueous acetic acid (2.00 M) was added until pH 3 was reached, the mixture was extracted with dichloromethane (3 x 10 ml) and the combined organic layer was dried over sodium sulphate. The solvent was removed under reduced pressure and the product was obtained as white solid (15.8 mg, 64.2 µmol, 77 %).

^{1}H-NMR (400.15 MHz, $CDCl_3$): δ = 7.35 (d, *J* = 8.7 Hz, 2H), 6.92 (d, *J* = 8.7 Hz, 2H), 6.09 – 5.99 (m, 1H), 5.41 (dd, *J* = 17.3, 1.5 Hz, 1H), 5.29 (dd, *J* = 10.5, 1.4 Hz, 1H), 5.17 (s, 1H), 4.54 (dt, *J* = 5.3, 1.6 Hz, 2H), 4.32 – 4.07 (m, 2H), 2.50 (t, *J* = 2.4 Hz, 1H) ppm.

^{13}C-NMR (100.62 MHz, $CDCl_3$): δ = 174.3, 159.6, 133.1, 129.3, 126.8, 118.0, 115.2, 78.2, 77.9, 76.2, 69.0, 56.1 ppm.

HRMS (ESI(+), CH3CN): *m/z* 264.1231 $[M+NH_4]^+$, calculated for $C_{14}H_{18}NO_4^+$: *m/z* 264.1230.

Mandi-MS-Allyl (38)

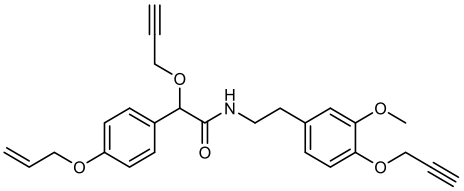

Mandi-MS-Allyl (**38**) was synthesized during my master's thesis[79]:

2-(4-(Allyloxy)phenyl)-2-(prop-2-yn-1-yloxy)acetic acid (**37**) (15.8 mg, 64.1 µmol, 1.20 eq.) was dissolved in anhydrous dimethylformamide (2 ml) and 2-(3-methoxy-4-(prop-2-yn-1-yloxy)phenyl)ethan-1-aminium chloride (**32**) (15.5 mg, 64.1 µmol, 1.00 eq.) was added. The solution

was cooled to 0°C and HATU (26.8 mg, 70.6 µmol, 1.10 eq.), 1-hydroxybenzotriazole hydrate (HOBt) (11.8 mg, 77.0 µmol, 1.20 eq.) and *N*,*N*-diisopropylethylamine (DIPEA) (26.5 µl, 20.7 mg, 160 µmol, 2.50 eq.) were added. The reaction mixture was stirred for 19 h at room temperature. The solvent was removed in vacuo and the residue was dissolved in dichloromethane (10 ml). The organic layer was washed with saturated aqueous sodium hydrogencarbonate solution (10 ml), saturated aqueous ammonium chloride solution (10 ml) and brine (10 ml) and dried over sodium sulphate. The solvent as removed under reduced pressure and the crude product was purified by preparative reverse phase HPLC (C18, acetonitrile:water gradient + 0.1 % TFA). The product was obtained as white solid (17.0 mg, 39.2 µmol, 61 %).

^{1}H-NMR (400.15 MHz, $CDCl_3$): δ = 7.22 (d, *J* = 8.7 Hz, 2H), 6.98 (d, *J* = 8.0 Hz, 1H), 6.88 (d, *J* = 8.7 Hz, 2H), 6.80 (t, *J* = 5.7 Hz, 1H), 6.74 – 6.71 (m, 2H), 6.09 – 5.99 (m, 1H), 5.41 (dd, *J* = 17.3, 1.6 Hz, 1H), 5.28 (dd, *J* = 10.5, 1.4 Hz, 1H), 4.94 (s, 1H), 4.75 (d, *J* = 2.4 Hz, 2H), 4.53 (dt, *J* = 5.3, 1.5 Hz, 2H), 4.17 – 3.92 (m, 2H), 3.84 (s, 3H), 3.65 – 3.47 (m, 2H), 2.80 (td, *J* = 6.9, 1.9 Hz, 2H), 2.51 (t, *J* = 2.4 Hz, 1H), 2.46 (t, *J* = 2.4 Hz, 1H) ppm.

^{13}C-NMR (100.62 MHz, $CDCl_3$): δ = 170.5, 159.2, 149.9, 145.6, 133.3, 133.0, 129.0, 128.3, 120.8, 117.9, 115.1, 114.8, 112.5, 80.1, 78.9, 78.6, 75.8, 75.6, 69.0, 57.0, 56.0, 40.4, 35.4 ppm.

HRMS (ESI(+), CH_3CN): *m/z* 434.1959 $[M+H]^+$, calculated for $C_{26}H_{28}NO_5^+$: *m/z* 434.1962.

Mandi-MS-OH (39)

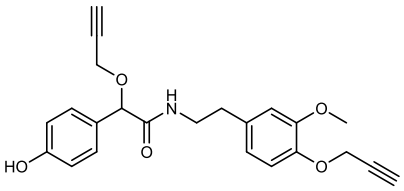

Mandi-MS-OH (**39**) was synthesized during my master's thesis[79]:

Mandi-MS-Allyl (**38**) (5.00 mg, 11.5 µmol, 1.00 eq.) was dissolved in anhydrous methanol (2 ml) and tetrakis(triphenylphosphine)palladium(0) (1.33 mg, 1.15 µmol, 0.10 eq.) as well as potassium carbonate (4.78 mg, 34.6 µmol, 3.00 eq.) were added. The reaction mixture was stirred for 2 h at room temperature. Then, dichloromethane (10 ml) was added and the organic layer was washed with saturated aqueous ammonium chloride solution (10 ml). The aqueous layer was extracted with dichloromethane (3 x 10 ml) and the combined organic layer was washed with brine (10 ml) and dried over sodium sulphate. The solvent as removed under reduced pressure and the crude product was purified by preparative reverse phase HPLC (C18, acetonitrile:water gradient + 0.1 % TFA). The product was obtained as white solid (2.10 mg, 5.34 µmol, 46 %).

^{1}H-NMR (400.15 MHz, $CDCl_3$): δ = 7.03 (d, *J* = 8.5 Hz, 2H), 6.99 (d, *J* = 7.9 Hz, 1H), 6.93 (t, *J* = 5.9 Hz, 1H), 6.76 – 6.73 (m, 2H), 6.59 (d, *J* = 8.5 Hz, 2H), 4.91 (s, 1H), 4.76 (d, *J* = 2.4 Hz, 2H), 4.15 – 3.87 (m, 2H),

3.85 (s, 3H), 3.68 – 3.50 (m, 2H), 2.83 (td, *J* = 6.9, 3.7 Hz, 2H), 2.51 (t, *J* = 2.4 Hz, 1H), 2.46 (t, *J* = 2.4 Hz, 1H) ppm.

^{13}C-NMR (100.62 MHz, $CDCl_3$): δ = 171.1, 156.9, 149.9, 145.6, 132.9, 129.3, 127.1, 120.8, 115.9, 114.8, 112.6, 80.0, 78.9, 78.6, 75.9, 75.6, 57.0, 56.0, 55.7, 40.4, 35.4 ppm.

HRMS (ESI(+), CH_3CN): *m/z* 416.1468 $[M+Na]^+$, calculated for $C_{23}H_{23}NO_5Na^+$: *m/z* 416.1468.

Mandi-MS-C4 (40)

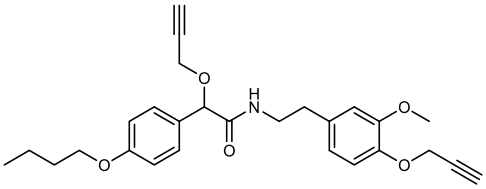

Mandi-MS-OH (**39**) (5.00 mg, 12.7 µmol, 1.00 eq.) was dissolved in anhydrous dimethylformamide (1 ml) and potassium carbonate (5.27 mg, 38.1 µmol, 3.00 eq.), potassium iodide (1.05 mg, 6.35 µmol, 0.50 eq.) and 1-bromobutane (6.86 µl, 63.5 µmol, 5.00 eq.) were added. The reaction mixture was stirred for 72 h at room temperature. Then, the solvent was removed under reduced pressure and saturated aqueous ammonium chloride solution (1 ml) was added and the mixture was extracted with dichloromethane (2 ml). The solvent as removed under reduced pressure and the crude product was purified by preparative reverse phase HPLC (C18, acetonitrile:water gradient + 0.1 % TFA). The product was obtained as white solid (2.60 mg, 5.78 µmol, 46 %).

^{1}H-NMR (400.15 MHz, $CDCl_3$): δ = 7.21 (d, *J* = 8.6 Hz, 2H), 6.98 (d, *J* = 7.9 Hz, 1H), 6.86 (d, *J* = 8.7 Hz, 2H), 6.80 (t, *J* = 6.0 Hz, 1H), 6.74 – 6.71 (m, 2H), 4.94 (s, 1H), 4.75 (d, *J* = 2.4 Hz, 2H), 4.17 – 3.91 (m, 4H), 3.84 (s, 3H), 3.63 – 3.47 (m, 2H), 2.82 – 2.78 (m, 2H), 2.50 (t, *J* = 2.4 Hz, 1H), 2.46 (t, *J* = 2.4 Hz, 1H), 1.79 – 1.74 (m, 2H), 1.53 – 1.43 (m, 2H), 0.97 (t, *J* = 7.4 Hz, 3H) ppm.

^{13}C-NMR (100.62 MHz, $CDCl_3$): δ = 170.5, 159.7, 149.9, 145.6, 133.0, 129.0, 127.9, 120.8, 114.8, 114.8, 112.6, 80.1, 78.9, 78.7, 75.8, 75.6, 67.9, 57.0, 56.0, 56.0, 40.4, 35.5, 31.4, 19.4, 14.0 ppm.

HRMS (ESI(+), CH_3CN): *m/z* 472.2089 $[M+Na]^+$, calculated for $C_{27}H_{31}NO_5Na^+$: *m/z* 472.2094.

Mandi-MS-C5 (41)

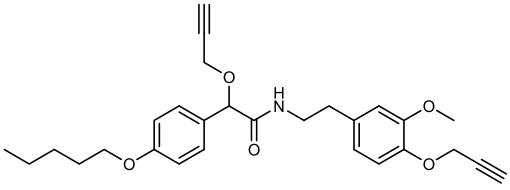

Mandi-MS-OH (**39**) (10.0 mg, 25.4 µmol, 1.00 eq.) was dissolved in anhydrous dimethylformamide (1 ml) and potassium carbonate (10.5 mg, 76.3 µmol, 3.00 eq.), potassium iodide (2.11 mg, 12.7 µmol, 0.50 eq.) and 1-bromopentane (31.7 µl, 254 µmol, 10.0 eq.) were added. The reaction mixture was stirred for 17 h at room temperature. Then, the solvent was removed under reduced pressure and

saturated aqueous ammonium chloride solution (1 ml) was added and the mixture was extracted with dichloromethane (2 ml). The solvent as removed under reduced pressure and the crude product was purified by preparative reverse phase HPLC (C18, acetonitrile:water gradient + 0.1 % TFA). The product was obtained as white solid (4.80 mg, 10.4 µmol, 41 %).

^{1}H-NMR (400.15 MHz, $CDCl_3$): δ = 7.21 (d, *J* = 8.7 Hz, 2H), 6.98 (d, *J* = 7.9 Hz, 1H), 6.86 (d, *J* = 8.7 Hz, 2H), 6.79 (t, *J* = 6.0 Hz, 1H), 6.74 – 6.71 (m, 2H), 4.94 (s, 1H), 4.75 (d, *J* = 2.4 Hz, 2H), 4.17 – 3.92 (m, 4H), 3.84 (s, 3H), 3.63 – 3.47 (m, 2H), 2.82 – 2.78 (m, 2H), 2.50 (t, *J* = 2.4 Hz, 1H), 2.46 (t, *J* = 2.4 Hz, 1H), 1.81 – 1.74 (m, 2H), 1.45 – 1.25 (m, 4H), 0.94 – 0.91 (m, 3H) ppm.

^{13}C-NMR (100.62 MHz, $CDCl_3$): δ = 170.5, 159.7, 149.9, 145.6, 133.0, 129.0, 127.9, 120.8, 114.8, 114.8, 112.6, 80.2, 78.9, 78.7, 75.8, 75.6, 68.2, 57.0, 56.0, 56.0, 40.4, 35.5, 29.1, 28.3, 22.6, 14.2 ppm.

HRMS (ESI(+), CH_3CN): *m/z* 486.2246 $[M+Na]^+$, calculated for $C_{28}H_{33}NO_5Na^+$: *m/z* 486.2251.

Mandi-MS-C6 (42)

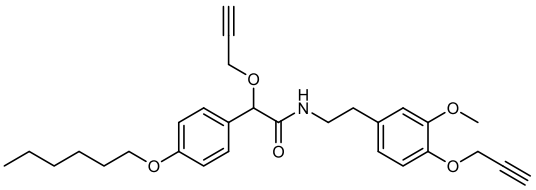

Mandi-MS-OH (**39**) (10.0 mg, 25.4 µmol, 1.00 eq.) was dissolved in anhydrous dimethylformamide (1 ml) and potassium carbonate (10.5 mg, 76.3 µmol, 3.00 eq.), potassium iodide (2.11 mg, 12.7 µmol, 0.50 eq.) and 1-bromohexane (35.9 µl, 254 µmol, 10.0 eq.) were added. The reaction mixture was stirred for 17 h at room temperature. Then, the solvent was removed under reduced pressure and saturated aqueous ammonium chloride solution (1 ml) was added and the mixture was extracted with dichloromethane (2 ml). The solvent as removed under reduced pressure and the crude product was purified by preparative reverse phase HPLC (C18, acetonitrile:water gradient + 0.1 % TFA). The product was obtained as white solid (5.40 mg, 11.3 µmol, 44 %).

^{1}H-NMR (400.15 MHz, $CDCl_3$): δ = 7.21 (d, *J* = 8.7 Hz, 2H), 6.98 (d, *J* = 7.9 Hz, 1H), 6.86 (d, *J* = 8.7 Hz, 2H), 6.78 (t, *J* = 6.1 Hz, 1H), 6.74 – 6.71 (m, 2H), 4.94 (s, 1H), 4.75 (d, *J* = 2.4 Hz, 2H), 4.17 – 3.92 (m, 4H), 3.84 (s, 3H), 3.63 – 3.47 (m, 2H), 2.82 – 2.78 (m, 2H), 2.50 (t, *J* = 2.4 Hz, 1H), 2.46 (t, *J* = 2.4 Hz, 1H), 1.80 – 1.73 (m, 2H), 1.48 – 1.25 (m, 6H), 0.92 – 0.88 (m, 2H) ppm.

^{13}C-NMR (100.62 MHz, $CDCl_3$): δ = 170.5, 159.7, 149.9, 145.6, 133.0, 128.9, 127.9, 120.8, 114.8, 114.8, 112.6, 80.2, 78.9, 78.7, 75.8, 75.6, 68.2, 57.0, 56.0, 56.0, 40.4, 35.5, 31.7, 29.3, 25.9, 22.8, 14.2 ppm.

HRMS (ESI(+), CH_3CN): *m/z* 500.2403 $[M+Na]^+$, calculated for $C_{29}H_{35}NO_5Na^+$: *m/z* 500.2407.

Mandi-MS-C7 (43)

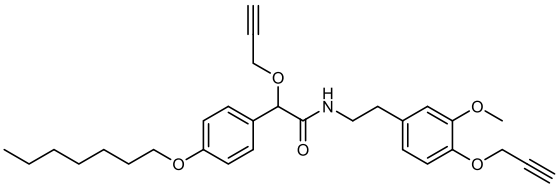

Mandi-MS-OH (**39**) (10.0 mg, 25.4 µmol, 1.00 eq.) was dissolved in anhydrous dimethylformamide (1 ml) and potassium carbonate (10.5 mg, 76.3 µmol, 3.00 eq.), potassium iodide (2.11 mg, 12.7 µmol, 0.50 eq.) and 1-bromoheptane (39.9 µl, 254 µmol, 10.0 eq.) were added. The reaction mixture was stirred for 17 h at room temperature. Then, the solvent was removed under reduced pressure and saturated aqueous ammonium chloride solution (1 ml) was added and the mixture was extracted with dichloromethane (2 ml). The solvent as removed under reduced pressure and the crude product was purified by preparative reverse phase HPLC (C18, acetonitrile:water gradient + 0.1 % TFA). The product was obtained as white solid (6.00 mg, 12.2 µmol, 48 %).

^{1}H-NMR (400.15 MHz, $CDCl_3$): δ = 7.21 (d, *J* = 8.7 Hz, 2H), 6.98 (d, *J* = 7.9 Hz, 1H), 6.86 (d, *J* = 8.7 Hz, 2H), 6.78 (t, *J* = 6.1 Hz, 1H), 6.74 – 6.71 (m, 2H), 4.94 (s, 1H), 4.75 (d, *J* = 2.4 Hz, 2H), 4.17 – 3.91 (m, 4H), 3.84 (s, 3H), 3.63 – 3.47 (m, 2H), 2.82 – 2.78 (m, 2H), 2.50 (t, *J* = 2.4 Hz, 1H), 2.46 (t, *J* = 2.4 Hz, 1H), 1.80 – 1.73 (m, 2H), 1.46 – 1.26 (m, 8H), 0.88 (d, *J* = 6.9 Hz, 2H) ppm.

^{13}C-NMR (100.62 MHz, $CDCl_3$): δ = 170.5, 159.7, 149.9, 145.6, 133.0, 128.9, 127.9, 120.8, 114.8, 114.8, 112.6, 80.2, 78.9, 78.7, 75.8, 75.6, 68.2, 57.0, 56.0, 56.0, 40.4, 35.5, 31.9, 29.4, 29.2, 26.1, 22.8, 14.2 ppm.

HRMS (ESI(+), CH_3CN): *m/z* 514.2561 $[M+Na]^+$, calculated for $C_{30}H_{37}NO_5Na^+$: *m/z* 514.2564.

Mandi-MS-C8 (44)

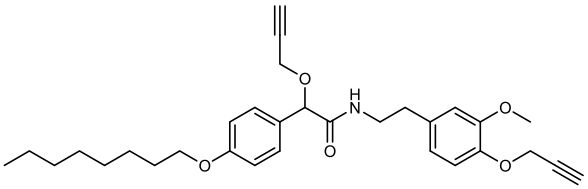

Mandi-MS-OH (**39**) (10.0 mg, 25.4 µmol, 1.00 eq.) was dissolved in anhydrous dimethylformamide (1 ml) and potassium carbonate (10.5 mg, 76.3 µmol, 3.00 eq.), potassium iodide (2.11 mg, 12.7 µmol, 0.50 eq.) and 1-bromooctane (44.2 µl, 254 µmol, 10.0 eq.) were added. The reaction mixture was stirred for 25 h at room temperature. Then, the solvent was removed under reduced pressure and saturated aqueous ammonium chloride solution (1 ml) was added and the mixture was extracted with dichloromethane (2 ml). The solvent as removed under reduced pressure and the crude product was purified by preparative reverse phase HPLC (C18, acetonitrile:water gradient + 0.1 % TFA). The product was obtained as white solid (5.90 mg, 11.7 µmol, 46 %).

^{1}H-NMR (400.15 MHz, $CDCl_3$): δ = 7.21 (d, *J* = 8.7 Hz, 2H), 6.98 (d, *J* = 7.9 Hz, 1H), 6.86 (d, *J* = 8.7 Hz, 2H), 6.79 (t, *J* = 6.0 Hz, 1H), 6.74 – 6.71 (m, 2H), 4.94 (s, 1H), 4.75 (d, *J* = 2.4 Hz, 2H), 4.17 – 3.91 (m, 4H), 3.84 (s, 3H), 3.63 – 3.47 (m, 2H), 2.82 – 2.78 (m, 2H), 2.50 (t, *J* = 2.4 Hz, 1H), 2.46 (t, *J* = 2.4 Hz, 1H), 1.80 – 1.73 (m, 2H), 1.48 – 1.25 (m, 10H), 0.90 – 0.87 (m, 3H) ppm.

^{13}C-NMR (100.62 MHz, $CDCl_3$): δ = 170.5, 159.7, 149.9, 145.6, 133.0, 128.9, 127.9, 120.8, 114.8, 114.8, 112.6, 80.2, 78.9, 78.7, 75.8, 75.6, 68.2, 57.0, 56.0, 56.0, 40.4, 35.5, 32.0, 29.5, 29.4, 29.4, 26.2, 22.8, 14.2 ppm.

HRMS (ESI(+), CH_3CN): *m/z* 528.2715 $[M+Na]^+$, calculated for $C_{31}H_{39}NO_5Na^+$: *m/z* 528.2720.

Mandi-Dopa-Cn-Indole

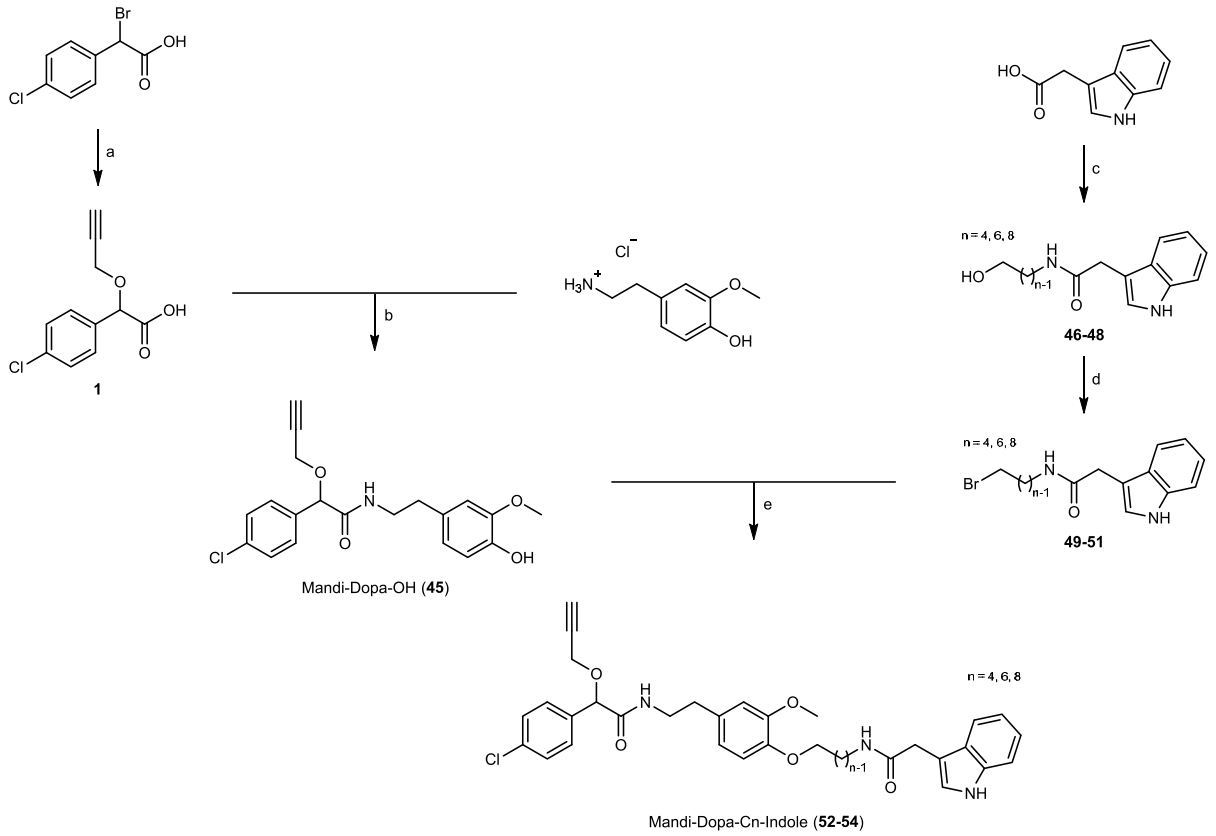

Conditions: a: propargyl alcohol, KOH, rt, 2 h; b: HATU, DIPEA, rt, 68 h; c: amino alkanol, HATU, DIPEA, rt, 18 h; d: CBr_4, PPh_3, rt, 17 – 24 h; e: K_2CO_3, KI, rt, 21 – 22 h.

Mandi-Dopa-OH (45)

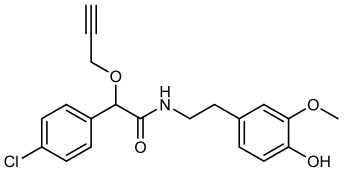

2-(4-Chlorophenyl)-2-(prop-2-yn-1-yloxy)acetic acid (**1**) (200 mg, 890 µmol, 1.00 eq.) was dissolved in anhydrous dimethylformamide (2 ml) and 2-(4-hydroxy-3-methoxyphenyl)ethan-1-aminium chloride (3-Methoxytyramine hydrochloride) (181 mg, 890 µmol, 1.00 eq.), HATU (372 mg, 979 µmol, 1.10 eq.) as well as *N*,*N*-diisopropylethylamine (DIPEA) (368 µl, 2.23 mmol, 2.50 eq.) were added. The reaction mixture was stirred for 68 h at room temperature. Then, the solvent was removed under reduced pressure. The residue was dissolved in dichloromethane (10 ml) and washed with saturated aqueous sodium hydrogencarbonate solution (10 ml) and brine (10 ml). The organic layer was dried over sodium sulphate and the solvent was removed under reduced pressure. The crude product was purified by column chromatography (silica gel, dichloromethane:methanol gradient) and the product was obtained as colorless solid, (264.5 mg, 708 µmol, 79 %).

^{1}H-NMR (400.15 MHz, $CDCl_3$): δ = 7.33 (d, *J* = 8.6 Hz, 2H), 7.27 (d, *J* = 7.9 Hz, 2H), 6.85 (d, *J* = 8.5 Hz, 1H), 6.73 (t, *J* = 5.8 Hz, 1H), 6.67 – 6.64 (m, 2H), 4.96 (s, 1H), 4.21 – 3.95 (m, 2H), 3.83 (s, 3H), 3.62 – 3.44 (m, 2H), 2.83 – 2.71 (m, 2H), 2.47 (t, *J* = 2.4 Hz, 1H) ppm.

^{13}C-NMR (100.62 MHz, $CDCl_3$): δ = 169.6, 146.7, 144.4, 134.9, 134.8, 130.5, 129.0, 128.8, 121.6, 114.5, 111.3, 79.8, 78.3, 76.0, 56.5, 56.0, 40.4, 35.4 ppm.

HRMS (ESI(+), CH_3CN): *m/z* 374.1151 $[M+H]^+$, calculated for $C_{20}H_{21}NO_4Cl^+$: *m/z* 374.1154.

_N_-(4-Hydroxybutyl)-2-(1_H_-indol-3-yl)acetamide (46)

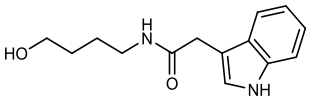

2-(1*H*-Indol-3-yl)acetic acid (50.0 mg, 285 µmol, 1.00 eq.) was dissolved in anhydrous dimethylformamide (1 ml) and HATU (119 mg, 314 µmol, 1.10 eq.), 4-amino-1-butanol (26.5 µl, 285 µmol, 1.00 eq.) as well as *N*,*N*-diisopropylethylamine (DIPEA) (118 µl, 714 µmol, 2.50 eq.) were added. The reaction mixture was stirred for 18 h at room temperature. Then, the solvent was removed under reduced pressure and saturated aqueous ammonium chloride solution (1 ml) was added. The mixture was extracted with dichloromethane (2 x 1 ml). The solvent was removed under reduced pressure and the crude product was purified by preparative reverse phase HPLC (C18, acetonitrile:water gradient + 0.1 % TFA). The product was obtained as off-white liquid (38.2 mg, 155 µmol, 54 %).

^{1}H-NMR (400.15 MHz, CD_3OD): δ = 7.53 (d, *J* = 6.9 Hz, 1H), 7.35 (d, *J* = 8.2 Hz, 1H), 7.16 (s, 1H), 7.12 – 7.08 (m, 1H), 7.03 – 6.99 (m, 1H), 3.64 (s, 2H), 3.50 (t, *J* = 6.1 Hz, 2H), 3.17 (t, *J* = 6.7 Hz, 2H), 1.54 – 1.42 (m, 4H) ppm.

^{13}C-NMR (100.62 MHz, CD_3OD): δ = 175.0, 138.1, 128.5, 124.9, 122.6, 120.0, 119.3, 112.4, 109.3, 62.5, 40.4, 34.0, 30.8, 26.8 ppm.

HRMS (ESI(+), CH_3CN): *m/z* 247.1441 $[M+H]^+$, calculated for $C_{14}H_{19}N_2O_2^+$: *m/z* 247.1441.

_N_-(6-Hydroxyhexyl)-2-(1_H_-indol-3-yl)acetamide (47)

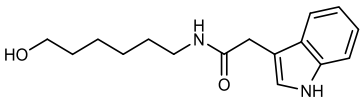

6-Amino-1-hexanol (50.0 mg, 427 µmol, 1.00 eq.) was dissolved in anhydrous dimethylformamide (1 ml) and 2-(1*H*-indol-3-yl)acetic acid (74.7 mg, 427 µmol, 1.00 eq.), HATU (178 mg, 469 µmol, 1.10 eq.) as well as *N*,*N*-diisopropylethylamine (DIPEA) (176 µl, 1.07 mmol, 2.50 eq.) were added. The reaction mixture was stirred for 18 h at room temperature. Then, the solvent was removed under reduced pressure and saturated aqueous ammonium chloride solution (1 ml) was added. The mixture was extracted with dichloromethane (2 x 2 ml). The solvent was removed under reduced pressure and

the crude product was purified by preparative reverse phase HPLC (C18, acetonitrile:water gradient + 0.1 % TFA). The product was obtained as off-white solid (86.0 mg, 313 µmol, 73 %).

^{1}H-NMR (400.15 MHz, CD_3OD): δ = 7.52 (d, J = 7.9 Hz, 1H), 7.35 (d, J = 8.1 Hz, 1H), 7.15 (s, 1H), 7.12 – 7.08 (m, 1H), 7.03 – 6.99 (m, 1H), 3.63 (s, 2H), 3.48 (t, J = 6.6 Hz, 2H), 3.14 (t, J = 7.0 Hz, 2H), 1.48 – 1.39 (m, 4H), 1.31 – 1.18 (m, 4H) ppm.

^{13}C-NMR (100.62 MHz, CD_3OD): δ = 174.9, 138.1, 128.4, 125.0, 122.6, 120.0, 119.3, 112.4, 109.3, 62.8, 40.5, 34.0, 33.5, 30.3, 27.6, 26.5 ppm.

HRMS (ESI(+), CH_3CN): *m/z* 275.1754 $[M+H]^+$, calculated for $C_{16}H_{23}N_2O_2^+$: *m/z* 275.1754.

_N_-(8-Hydroxyoctyl)-2-(1_H_-indol-3-yl)acetamide (48)

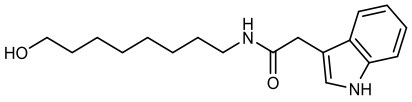

2-(1*H*-Indol-3-yl)acetic acid (50.0 mg, 285 µmol, 1.00 eq.) was dissolved in anhydrous dimethylformamide (1 ml) and HATU (119 mg, 314 µmol, 1.10 eq.), 8-amino-1-octanol (41.5 mg, 285 µmol, 1.00 eq.) as well as *N*,*N*-diisopropylethylamine (DIPEA) (118 µl, 714 µmol, 2.50 eq.) were added. The reaction mixture was stirred for 18 h at room temperature. Then, saturated aqueous ammonium chloride solution (10 ml) was added. The mixture was extracted with dichloromethane (3 x 10 ml) and the combined organic layer was dried over sodium sulphate. The solvent was removed under reduced pressure and the crude product was purified by preparative reverse phase HPLC (C18, acetonitrile:water gradient + 0.1 % TFA). The product was obtained as white solid (70.4 mg, 233 µmol, 82 %).

^{1}H-NMR (400.15 MHz, CD_3OD): δ = 7.53 (dt, J = 7.9, 1.0 Hz, 1H), 7.35 (dt, J = 8.2, 1.0 Hz, 1H), 7.15 (s, 1H), 7.12 – 7.08 (m, 1H), 7.03 – 6.99 (m, 1H), 3.63 (s, 2H), 3.52 (t, J = 6.7 Hz, 2H), 3.13 (t, J = 7.0 Hz, 2H), 1.52 – 1.38 (m, 4H), 1.32 – 1.18 (m, 8H) ppm.

^{13}C-NMR (100.62 MHz, CD_3OD): δ = 174.8, 138.1, 128.5, 124.9, 122.6, 119.9, 119.3, 112.4, 109.4, 63.0, 40.5, 34.1, 33.6, 30.4, 30.3, 27.8, 26.8 ppm.

HRMS (ESI(+), CH_3CN): *m/z* 303.2064 $[M+H]^+$, calculated for $C_{18}H_{27}N_2O_2^+$: *m/z* 303.2067.

_N_-(4-Bromobutyl)-2-(1_H_-indol-3-yl)acetamide (49)

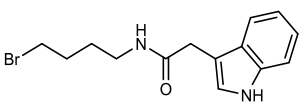

N-(4-Hydroxybutyl)-2-(1*H*-indol-3-yl)acetamide (**46**) (38.2 mg, 155 µmol, 1.00 eq.) was dissolved in anhydrous tetrahydrofuran (2 ml), carbon tetrabromide (61.7 mg, 186 µmol, 1.20 eq.) was added and the mixture was cooled to 0 °C. Then, triphenylphosphine (48.8 mg, 186 µmol, 1.20 eq.) was added in small portions and the reaction mixture was stirred for 24 h at room temperature. The solvent was removed under reduced pressure and the residue was dissolved in dichloromethane (10 ml). The

organic layer was washed with brine (10 ml) and dried over sodium sulphate. The solvent was removed under reduced pressure and the crude product was purified by preparative reverse phase HPLC (C18, acetonitrile:water gradient + 0.1 % TFA). The product was obtained as brown liquid (14.4 mg, 46.6 µmol, 30 %).

^{1}H-NMR (400.15 MHz, CD_3OD): δ = 7.53 (d, *J* = 7.9 Hz, 1H), 7.35 (d, *J* = 8.1 Hz, 1H), 7.17 (s, 1H), 7.12 – 7.08 (m, 1H), 7.04 – 7.00 (m, 1H), 3.64 (s, 2H), 3.37 (t, *J* = 6.7 Hz, 2H), 3.19 (t, *J* = 6.8 Hz, 2H), 1.80 – 1.73 (m, 2H), 1.61 – 1.54 (m, 2H) ppm.

^{13}C-NMR (100.62 MHz, CD_3OD): δ = 175.0, 138.2, 128.5, 125.0, 122.6, 120.0, 119.3, 112.4, 109.4, 39.5, 34.1, 33.8, 31.1, 29.0 ppm.

HRMS (ESI(+), CH_3CN): *m/z* 309.0594 $[M+H]^+$, calculated for $C_{14}H_{18}N_2OBr^+$: *m/z* 309.0597.

_N_-(6-Bromohexyl)-2-(1_H_-indol-3-yl)acetamide (50)

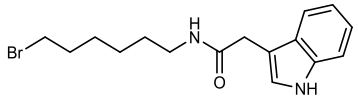

N-(6-Hydroxyhexyl)-2-(1*H*-indol-3-yl)acetamide (**47**) (86.0 mg, 313 µmol, 1.00 eq.) was dissolved in anhydrous tetrahydrofuran (2 ml), carbon tetrabromide (125 mg, 376 µmol, 1.20 eq.) was added and the mixture was cooled to 0 °C. Then, triphenylphosphine (98.7 mg, 376 µmol, 1.20 eq.) was added in small portions and the reaction mixture was stirred for 17 h at room temperature. The solvent was removed under reduced pressure and the residue was dissolved in dichloromethane (10 ml). The organic layer was washed with brine (10 ml) and dried over sodium sulphate. The solvent was removed under reduced pressure and the crude product was purified by preparative reverse phase HPLC (C18, acetonitrile:water gradient + 0.1 % TFA). The product was obtained as brown liquid (23.4 mg, 69.4 µmol, 22 %).

^{1}H-NMR (400.15 MHz, CD_3OD): δ = 7.53 (d, *J* = 7.8 Hz, 1H), 7.35 (d, *J* = 8.1 Hz, 1H), 7.17 (s, 1H), 7.13 – 7.08 (m, 1H), 7.04 – 7.00 (m, 1H), 3.64 (s, 2H), 3.34 (t, *J* = 6.8 Hz, 2H), 3.16 (t, *J* = 6.9 Hz, 2H), 1.76 – 1.69 (m, 2H), 1.47 – 1.40 (m, 2H), 1.39 – 1.32 (m, 2H), 1.25 – 1.17 (m, 2H) ppm.

^{13}C-NMR (100.62 MHz, CD_3OD): δ = 174.9, 138.2, 128.5, 125.0, 122.6, 120.0, 119.4, 112.4, 109.5, 40.3, 34.2, 34.1, 33.8, 30.2, 28.8, 26.9 ppm.

HRMS (ESI(+), CH_3CN): *m/z* 337.0909 $[M+H]^+$, calculated for $C_{16}H_{22}N_2OBr^+$: *m/z* 337.0910.

_N_-(8-Bromooctyl)-2-(1_H_-indol-3-yl)acetamide (51)

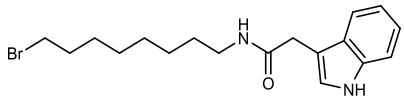

N-(8-Hydroxyoctyl)-2-(1*H*-indol-3-yl)acetamide (**48**) (70.4 mg, 233 µmol, 1.00 eq.) was dissolved in anhydrous tetrahydrofuran (2 ml), carbon tetrabromide (92.6 mg, 279 µmol, 1.20 eq.) was added and the mixture was cooled to 0 °C. Then, triphenylphosphine (73.7 mg, 279 µmol, 1.20 eq.) was added in

small portions and the reaction mixture was stirred for 24 h at room temperature. The solvent was removed under reduced pressure and the residue was dissolved in dichloromethane (10 ml). The organic layer was washed with brine (10 ml) and dried over sodium sulphate. The solvent was removed under reduced pressure and the crude product was purified by preparative reverse phase HPLC (C18, acetonitrile:water gradient + 0.1 % TFA). The product was obtained as brown liquid (8.70 mg, 23.8 µmol, 10 %).

^{1}H-NMR (400.15 MHz, CD_3OD): δ = 7.53 (d, *J* = 7.8 Hz, 1H), 7.35 (d, *J* = 8.1 Hz, 1H), 7.17 (s, 1H), 7.13 – 7.09 (m, 1H), 7.03 – 6.99 (m, 1H), 3.64 (s, 2H), 3.41 (t, *J* = 6.8 Hz, 2H), 3.15 (t, *J* = 6.9 Hz, 2H), 1.83 – 1.76 (m, 2H), 1.47 – 1.33 (m, 4H), 1.26 – 1.20 (m, 6H) ppm.

^{13}C-NMR (100.62 MHz, CD_3OD): δ = 174.9, 138.2, 128.5, 125.0, 122.6, 120.0, 119.4, 112.4, 109.5, 40.4, 34.4, 34.1, 34.0, 30.3, 30.1, 29.7, 29.0, 27.7 ppm.

HRMS (ESI(+), CH_3CN): *m/z* 365.1223 $[M+H]^+$, calculated for $C_{18}H_{26}N_2OBr^+$: *m/z* 365.1223.

Mandi-Dopa-C4-Indole (52)

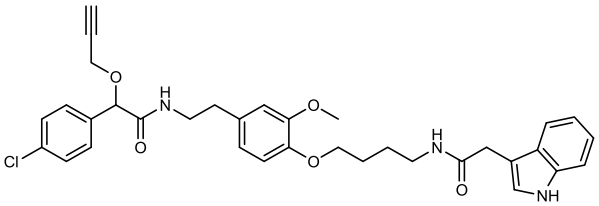

N-(4-Bromobutyl)-2-(1*H*-indol-3-yl)acetamide (**49**) (11.9 mg, 38.5 µmol, 1.00 eq.) was dissolved in anhydrous dimethylformamide (1 ml) and Mandi-Dopa-OH (**45**) (14.4 mg, 38.5 µmol, 1.00 eq.), potassium carbonate (16.0 mg, 116 µmol, 3.00 eq.) as well as potassium iodide (3.20 mg, 19.3 µmol, 0.50 eq.) were added. The reaction mixture was stirred for 22 h at room temperature. Then, the solvent was removed under reduced pressure and saturated ammonium chloride solution (1 ml) was added. The mixture was extracted with dichloromethane (2 x 1 ml) and the solvent was removed under reduced pressure. The crude product was purified by preparative reverse phase HPLC (C18, acetonitrile:water gradient + 0.1 % TFA). The product was obtained as colorless solid (12.0 mg, 19.9 µmol, 52 %).

^{1}H-NMR (400.15 MHz, $CDCl_3$): δ = 8.40 (s, 1H), 7.54 (d, *J* = 6.9 Hz, 1H), 7.37 (d, *J* = 8.2 Hz, 1H), 7.31 (d, *J* = 8.5 Hz, 2H), 7.24 (d, *J* = 8.5 Hz, 2H), 7.20 (dd, *J* = 8.1, 1.2 Hz, 1H), 7.14 – 7.10 (m, 1H), 7.03 (d, *J* = 2.4 Hz, 1H), 6.82 (t, *J* = 6.1 Hz, 1H), 6.68 (d, *J* = 8.6 Hz, 1H), 6.67 – 6.64 (m, 2H), 6.17 (t, *J* = 6.1 Hz, 1H), 4.97 (s, 1H), 4.21 – 3.94 (m, 2H), 3.91 – 3.88 (m, 2H), 3.76 (s, 2H), 3.68 (s, 3H), 3.65 – 3.46 (m, 2H), 3.28 (q, *J* = 6.6 Hz, 2H), 2.83 – 2.71 (m, 2H), 2.49 (t, *J* = 2.4 Hz, 1H), 1.75 – 1.68 (m, 2H), 1.64 – 1.56 (m, 2H) ppm.

^{13}C-NMR (100.62 MHz, $CDCl_3$): δ = 172.8, 169.9, 149.5, 147.0, 136.5, 134.9, 134.7, 131.4, 129.0, 128.9, 127.1, 124.0, 122.7, 120.9, 120.2, 118.7, 113.2, 112.4, 111.6, 108.5, 79.7, 78.2, 76.1, 68.6, 56.5, 55.9, 40.4, 39.5, 35.4, 33.2, 26.4, 26.2 ppm.

HRMS (ESI(+), CH_3CN): *m/z* 602.2411 $[M+H]^+$, calculated for $C_{34}H_{37}N_3O_5Cl^+$: *m/z* 602.2416.

Mandi-Dopa-C6-Indole (53)

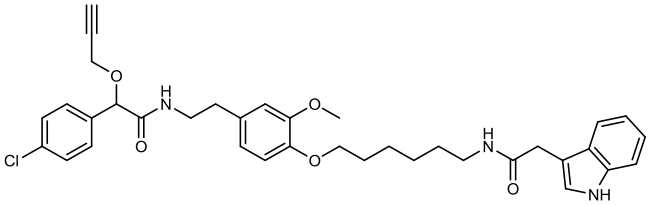

N-(6-Bromohexyl)-2-(1*H*-indol-3-yl)acetamide (**50**) (23.4 mg, 69.4 µmol, 1.00 eq.) was dissolved in anhydrous dimethylformamide (1 ml) and Mandi-Dopa-OH (**45**) (25.9 mg, 69.4 µmol, 1.00 eq.), potassium carbonate (28.8 mg, 208 µmol, 3.00 eq.) as well as potassium iodide (5.76 mg, 34.7 µmol, 0.50 eq.) were added. The reaction mixture was stirred for 21 h at room temperature. Then, the solvent was removed under reduced pressure and saturated ammonium chloride solution (1 ml) was added. The mixture was extracted with dichloromethane (2 x 1 ml) and the solvent was removed under reduced pressure. The crude product was purified by preparative reverse phase HPLC (C18, acetonitrile:water gradient + 0.1 % TFA). The product was obtained as brown liquid (18.5 mg, 29.4 µmol, 42 %).

^{1}H-NMR (400.15 MHz, $CDCl_3$): δ = 8.45 (s, 1H), 7.54 (d, *J* = 7.9 Hz, 1H), 7.38 (d, *J* = 8.2 Hz, 1H), 7.31 (d, *J* = 8.5 Hz, 2H), 7.25 (d, *J* = 8.5 Hz, 2H), 7.21 (d, *J* = 8.0 Hz, 1H), 7.15 (d, *J* = 7.9 Hz, 1H), 7.12 – 7.11 (m, 1H), 6.80 (t, *J* = 6.0 Hz, 1H), 6.76 (d, *J* = 7.9 Hz, 1H), 6.67 (s, 2H), 5.87 (s, 1H), 4.97 (s, 1H), 4.21 – 3.94 (m, 2H), 3.91 (t, *J* = 6.7 Hz, 2H), 3.80 (s, 3H), 3.78 (s, 2H), 3.63 – 3.46 (m, 2H), 3.21 – 3.16 (m, 2H), 2.84 – 2.72 (m, 2H), 2.48 (t, *J* = 2.4 Hz, 1H), 1.75 – 1.68 (m, 2H), 1.42 – 1.32 (m, 4H), 1.26 – 1.16 (m, 2H) ppm.

^{13}C-NMR (100.62 MHz, $CDCl_3$): δ = 172.6, 169.8, 149.6, 147.3, 136.6, 134.8, 134.8, 131.3, 129.0, 128.9, 127.0, 124.1, 122.8, 120.9, 120.3, 118.8, 113.3, 112.6, 111.7, 108.6, 79.7, 78.2, 76.1, 69.0, 56.5, 56.1, 40.5, 39.8, 35.4, 33.1, 29.2, 29.1, 26.6, 25.7 ppm.

HRMS (ESI(+), CH_3CN): *m/z* 630.2719 $[M+H]^+$, calculated for $C_{36}H_{41}N_3O_5Cl^+$: *m/z* 630.2729.

Mandi-Dopa-C8-Indole (54)

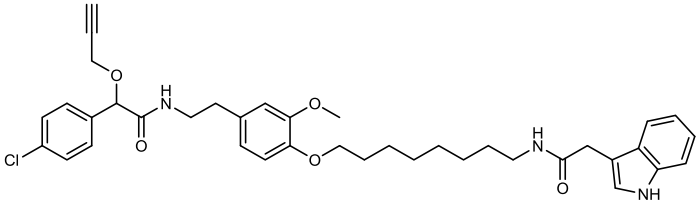

N-(8-Bromooctyl)-2-(1*H*-indol-3-yl)acetamide (**51**) (8.70 mg, 23.8 µmol, 1.00 eq.) was dissolved in anhydrous dimethylformamide (1 ml) and Mandi-Dopa-OH (**45**) (8.90 mg, 23.8 µmol, 1.00 eq.), potassium carbonate (9.87 mg, 71.4 µmol, 3.00 eq.) as well as potassium iodide (1.98 mg, 71.4 µmol, 0.50 eq.) were added. The reaction mixture was stirred for 22 h at room temperature. Then, the solvent was removed under reduced pressure and saturated ammonium chloride solution (1 ml) was

added. The mixture was extracted with dichloromethane (2 x 1 ml) and the solvent was removed under reduced pressure. The crude product was purified by preparative reverse phase HPLC (C18, acetonitrile:water gradient + 0.1 % TFA). The product was obtained as white solid (7.50 mg, 11.4 µmol, 48 %).

^{1}H-NMR (400.15 MHz, $CDCl_3$): δ = 8.58 (s, 1H), 7.54 (d, *J* = 7.9 Hz, 1H), 7.38 (d, *J* = 8.1 Hz, 1H), 7.31 (d, *J* = 8.5 Hz, 2H), 7.25 (d, *J* = 8.0 Hz, 2H), 7.22 (dd, *J* = 8.2, 1.2 Hz, 1H), 7.17 – 7.13 (m, 2H), 6.81 – 6.79 (m, 2H), 6.71 – 6.68 (m, 2H), 5.81 (t, *J* = 6.1 Hz, 1H), 4.98 (s, 1H), 4.21 – 3.94 (m, 4H), 3.81 (s, 3H), 3.78 (s, 2H), 3.63 – 3.46 (m, 2H), 3.18 (q, *J* = 6.7 Hz, 2H), 2.84 – 2.73 (m, 2H), 2.48 (t, *J* = 2.4 Hz, 1H), 1.80 – 1.73 (m, 2H), 1.40 – 1.31 (m, 4H), 1.25 – 1.11 (m, 6H) ppm.

^{13}C-NMR (100.62 MHz, $CDCl_3$): δ = 172.7, 169.9, 149.5, 147.4, 136.6, 134.9, 134.7, 131.2, 129.0, 128.9, 127.0, 124.1, 122.9, 121.0, 120.3, 118.8, 113.2, 112.5, 111.7, 108.6, 79.7, 78.2, 76.1, 69.3, 56.5, 56.1, 40.5, 39.9, 35.3, 33.1, 29.3, 29.3, 29.1, 29.0, 26.8, 26.0 ppm.

HRMS (ESI(+), CH_3CN): *m/z* 658.3034 $[M+H]^+$, calculated for $C_{38}H_{45}N_3O_5Cl^+$: *m/z* 658.3042.

Mandi-Dopa-Cn-FQ

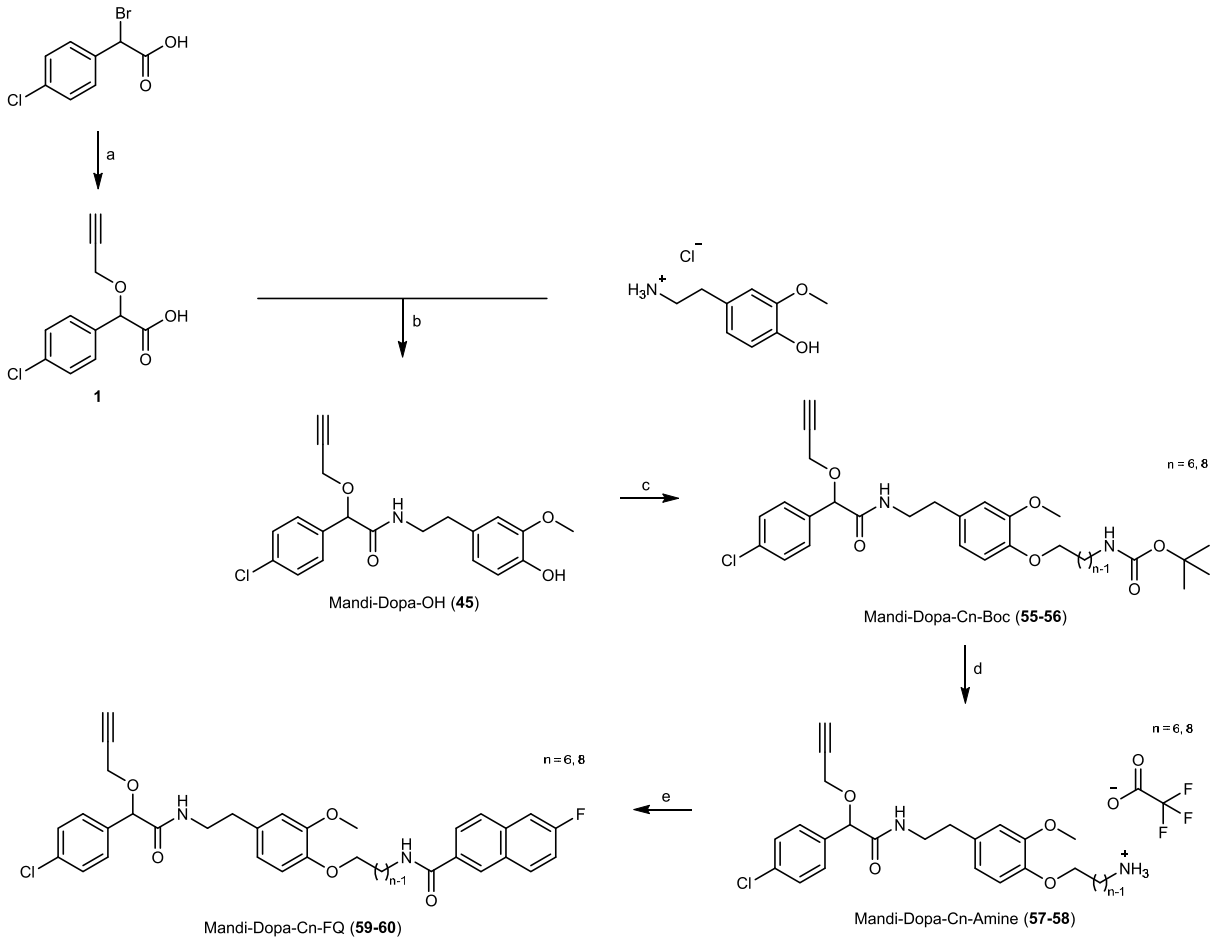

Conditions: a: propargyl alcohol, KOH, rt, 2 h; b: HATU, DIPEA, rt, 68 h; c: Boc-amine alkyl bromide, K_2CO_3, KI, rt, 19 – 96 h; d: TFA, rt, 2 h; e: 6-fluoroquinoline-2-carboxylic acid, HATU, DIPEA, rt, 22 – 23 h.

Mandi-Dopa-C6-Boc (55)

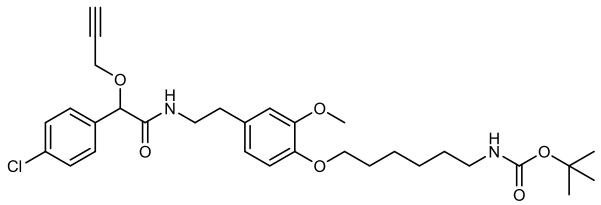

tert-Butyl (6-bromohexyl)carbamate (15.7 µl, 66.9 µmol, 1.00 eq.) was dissolved in anhydrous dimethylformamide (1 ml) and Mandi-Dopa-OH (**45**) (25.0 mg, 66.9 µmol, 1.00 eq.), potassium carbonate (27.7 mg, 201 µmol, 3.00 eq.) as well as potassium iodide (5.55 mg, 33.4 µmol, 0.50 eq.) were added. The reaction mixture was stirred for 19 h at room temperature. Then, saturated aqueous ammonium chloride solution (1 ml) was added and the mixture was extracted with dichloromethane (2 x 1 ml). The solvent was removed under reduced pressure and the crude product was purified by preparative reverse phase HPLC (C18, acetonitrile:water gradient + 0.1 % TFA). The product was obtained as white solid (18.8 mg, 32.8 µmol, 49 %).

^{1}H-NMR (400.15 MHz, $CDCl_3$): δ = 7.31 (d, *J* = 8.6 Hz, 2H), 7.26 (d, *J* = 8.5 Hz, 2H), 6.79 (d, *J* = 8.0 Hz, 1H), 6.75 (t, *J* = 6.0 Hz, 1H), 6.69 – 6.66 (m, 2H), 4.96 (s, 1H), 4.52 (s, 1H), 4.21 – 3.94 (m, 4H), 3.82 (s, 3H), 3.61 – 3.45 (m, 2H), 3.14 – 3.09 (m, 2H), 2.79 – 2.75 (m, 2H), 2.48 (t, *J* = 2.4 Hz, 1H), 1.87 – 1.80 (m, 2H), 1.52 – 1.36 (m, 15H) ppm.

^{13}C-NMR (100.62 MHz, $CDCl_3$): δ = 169.7, 149.6, 147.4, 134.9, 134.8, 131.3, 129.0, 128.9, 120.9, 113.3, 112.5, 79.8, 78.2, 76.0, 69.1, 56.5, 56.1, 40.4, 35.3, 30.1, 29.3, 28.6, 26.7, 25.9 ppm.

HRMS (ESI(+), CH_3CN): *m/z* 573.2730 $[M+H]^+$, calculated for $C_{31}H_{42}N_2O_6Cl^+$: *m/z* 573.2726.

Mandi-Dopa-C8-Boc (56)

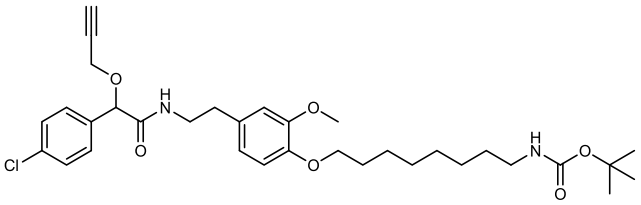

tert-Butyl (8-bromooctyl)carbamate (53.8 µl, 201 µmol, 1.00 eq.) was dissolved in anhydrous dimethylformamide (1 ml) and Mandi-Dopa-OH (**45**) (75.0 mg, 201 µmol, 1.00 eq.), potassium carbonate (83.2 mg, 602 µmol, 3.00 eq.) as well as potassium iodide (16.7 mg, 100 µmol, 0.50 eq.) were added. The reaction mixture was stirred for 96 h at room temperature. Then, saturated aqueous ammonium chloride solution (1 ml) was added and the mixture was extracted with dichloromethane (2 x 1 ml). The solvent was removed under reduced pressure and the crude product was purified by preparative reverse phase HPLC (C18, acetonitrile:water gradient + 0.1 % TFA). The product was obtained as white solid (40.6 mg, 67.5 µmol, 34 %).

^{1}H-NMR (400.15 MHz, $CDCl_3$): δ = 7.31 (d, *J* = 8.5 Hz, 2H), 7.26 (d, *J* = 8.6 Hz, 2H), 6.79 (d, *J* = 8.0 Hz, 1H), 6.75 (t, *J* = 6.0 Hz, 1H), 6.69 – 6.66 (m, 2H), 4.96 (s, 1H), 4.50 (s, 1H), 4.21 – 3.94 (m, 4H), 3.82 (s, 3H), 3.61 – 3.45 (m, 2H), 3.12 – 3.07 (m, 2H), 2.82 – 2.71 (m, 2H), 2.47 (t, *J* = 2.4 Hz, 1H), 1.86 – 1.79 (m, 2H), 1.48 – 1.44 (m, 13H), 1.37 – 1.29 (m, 6H) ppm.

^{13}C-NMR (100.62 MHz, $CDCl_3$): δ = 169.6, 156.1, 149.6, 147.4, 134.9, 134.7, 131.2, 128.9, 128.9, 120.9, 113.3, 112.5, 79.8, 79.1, 78.2, 76.0, 69.2, 56.5, 56.1, 40.7, 40.4, 35.3, 30.2, 29.4, 29.3, 28.6, 26.9, 26.0 ppm.

HRMS (ESI(+), CH_3CN): *m/z* 623.2851 $[M+Na]^+$, calculated for $C_{33}H_{45}N_2O_6ClNa^+$: *m/z* 623.2858.

Mandi-Dopa-C6-Amine (57)

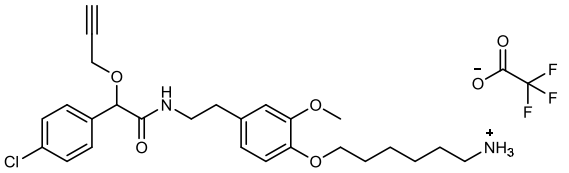

Mandi-Dopa-C6-Boc (**55**) (18.8 mg, 32.8 µmol, 1.00 eq.) was dissolved in chloroform (1 ml) and trifluoracetic acid (1 ml) was added. The reaction mixture was stirred for 2 h at room temperature. The solvent was removed under reduced pressure and successively co-evaporated with toluene (3 x 5 ml). The product was obtained as off-white solid (18.1 mg, 30.8 µmol, 94 %).

^{1}H-NMR (400.15 MHz, $CDCl_3$): δ = 7.90 (s, 3H), 7.31 (d, *J* = 8.5 Hz, 2H), 7.25 (d, *J* = 8.3 Hz, 2H), 6.82 (t, *J* = 6.0 Hz, 1H), 6.77 (d, *J* = 8.1 Hz, 1H), 6.69 – 6.65 (m, 2H), 4.95 (s, 1H), 4.20 – 3.93 (m, 4H), 3.80 (s, 3H), 3.60 – 3.43 (m, 2H), 2.88 (s, 2H), 2.81 – 2.70 (m, 2H), 2.49 (t, *J* = 2.4 Hz, 1H), 1.81 – 1.74 (m, 2H), 1.67 – 1.59 (m, 2H), 1.50 – 1.37 (m, 4H) ppm.

^{13}C-NMR (100.62 MHz, $CDCl_3$): δ = 169.8, 149.5, 147.1, 134.8, 134.8, 131.5, 129.0, 128.9, 121.0, 113.5, 112.6, 79.7, 78.2, 76.1, 68.9, 56.5, 56.1, 40.5, 39.9, 35.4, 28.8, 27.3, 26.0, 25.4 ppm.

HRMS (ESI(+), CH_3CN): *m/z* 473.2202 $[M]^+$, calculated for $C_{26}H_{34}N_2O_4Cl^+$: *m/z* 473.2202.

Mandi-Dopa-C8-Amine (58)

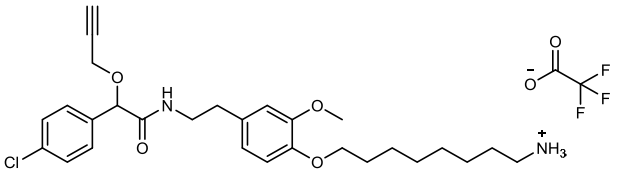

Mandi-Dopa-C8-Boc (**56**) (40.6 mg, 67.5 µmol, 1.00 eq.) was dissolved in chloroform (1 ml) and trifluoracetic acid (1 ml) was added. The reaction mixture was stirred for 2 h at room temperature. The solvent was removed under reduced pressure and successively co-evaporated with toluene (3 x 5 ml). The product was obtained as off-white solid (38.6 mg, 62.8 µmol, 93 %).

^{1}H-NMR (400.15 MHz, $CDCl_3$): δ = 7.83 (s, 3H), 7.31 (d, *J* = 8.5 Hz, 2H), 7.24 (d, *J* = 8.5 Hz, 2H), 6.82 (t, *J* = 6.0 Hz, 1H), 6.78 (d, *J* = 8.1 Hz, 1H), 6.69 – 6.65 (m, 2H), 4.95 (s, 1H), 4.20 – 3.93 (m, 4H), 3.81 (s, 3H), 3.59 – 3.43 (m, 2H), 2.85 (s, 2H), 2.80 – 2.70 (m, 2H), 2.48 (t, *J* = 2. Hz, 1H), 1.83 – 1.76 (m, 2H), 1.61 – 1.58 (m, 2H), 1.46 – 1.39 (m, 2H), 1.35 – 1.25 (m, 6H) ppm.

^{13}C-NMR (100.62 MHz, $CDCl_3$): δ = 169.9, 149.5, 147.3, 134.8, 134.7, 131.2, 129.0, 128.9, 120.9, 113.4, 112.6, 79.7, 78.1, 76.1, 69.1, 56.5, 56.1, 40.5, 40.0, 35.3, 29.1, 29.0, 28.9, 27.5, 26.2, 25.8 ppm.

HRMS (ESI(+), CH_3CN): *m/z* 501.2510 $[M]^+$, calculated for $C_{28}H_{38}N_2O_4Cl^+$: *m/z* 501.2515.

Mandi-Dopa-C6-FQ (59)

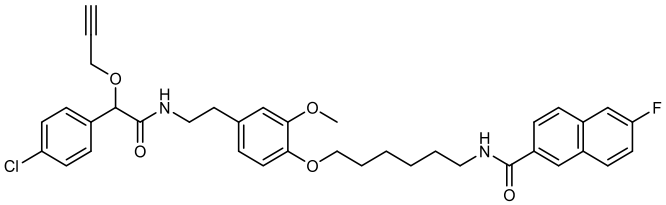

Mandi-Dopa-C6-Amine (**57**) (12.9 mg, 22.0 µmol, 1.00 eq.) was dissolved in anhydrous dimethylformamide (1 ml) and 6-fluoroquinoline-2-carboxylic acid (4.20 mg, 22.0 µmol, 1.00 eq.), HATU (9.19 mg, 24.2 µmol, 1.10 eq.) as well as *N*,*N*-diisopropylethylamine (DIPEA) (9.08 µl, 54.9 µmol, 2.50 eq.) were added. The reaction mixture was stirred for 23 h at room temperature. Then, the solvent was removed under reduced pressure and saturated aqueous ammonium chloride solution (1 ml) was added. The mixture was extracted with dichloromethane (2 x 1 ml) and the solvent was removed under reduced pressure. The crude product was purified by preparative reverse phase HPLC (C18, acetonitrile:water gradient + 0.1 % TFA). The product was obtained as off-white solid (11.1 mg, 17.2 µmol, 78 %).

^{1}H-NMR (400.15 MHz, $CDCl_3$): δ = 8.32 (d, *J* = 8.5 Hz, 1H), 8.27 – 8.23 (m, 2H), 8.11 (dd, *J* = 9.2, 5.3 Hz, 1H), 7.56 – 7.48 (m, 2H), 7.31 (d, *J* = 8.5 Hz, 2H), 7.25 (d, *J* = 8.5 Hz, 2H), 6.80 – 6.76 (m, 2H), 6.69 – 6.65 (m, 2H), 4.97 (s, 1H), 4.21 – 3.94 (m, 2H), 4.01 (t, *J* = 6.7 Hz, 2H), 3.82 (s, 3H), 3.61 – 3.45 (m, 4H), 2.83 – 2.71 (m, 2H), 2.48 (t, *J* = 2.4 Hz, 1H), 1.91 – 1.84 (m, 2H), 1.78 – 1.71 (m, 2H), 1.60 – 1.51 (m, 4H) ppm.

^{13}C-NMR (100.62 MHz, $CDCl_3$): δ = 169.9, 164.4, 162.6, 160.1, 149.7, 149.5, 149.5, 147.4, 143.7, 137.0, 137.0, 134.8, 134.7, 132.4, 132.3, 131.2, 130.3, 130.2, 129.0, 128.9, 120.9, 120.9, 120.6, 119.8, 113.4, 112.5, 111.1, 110.8, 79.7, 78.2, 76.1, 69.1, 56.5, 56.1, 40.5, 39.7, 35.3, 29.8, 29.3, 27.0, 25.9 ppm.

HRMS (ESI(+), CH_3CN): *m/z* 674.2784 $[M+H]^+$, calculated for $C_{38}H_{42}N_3O_5ClF^+$: *m/z* 674.2792.

Mandi-Dopa-C8-FQ (60)

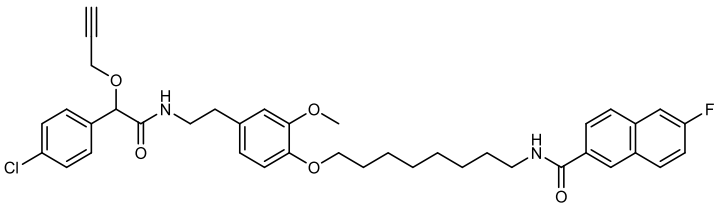

Mandi-Dopa-C8-Amine (**58**) (10.0 mg, 16.3 µmol, 1.00 eq.) was dissolved in anhydrous dimethylformamide (1 ml) and 6-fluoroquinoline-2-carboxylic acid (3.11 mg, 16.3 µmol, 1.00 eq.), HATU (6.80 mg, 17.9 µmol, 1.10 eq.) as well as *N*,*N*-diisopropylethylamine (DIPEA) (6.72 µl, 40.6 µmol, 2.50 eq.) were added. The reaction mixture was stirred for 22 h at room temperature. Then, the solvent was removed under reduced pressure and saturated aqueous ammonium chloride solution (1 ml) was added. The mixture was extracted with dichloromethane (2 x 1 ml) and the solvent was removed under reduced pressure. The crude product was purified by preparative reverse phase HPLC

(C18, acetonitrile:water gradient + 0.1 % TFA). The product was obtained as off-white solid (7.40 mg, 11.0 µmol, 68 %).

^{1}H-NMR (400.15 MHz, $CDCl_3$): δ = 8.33 (d, *J* = 7.7 Hz, 1H), 8.29 – 8.20 (m, 2H), 8.12 (dd, *J* = 9.2, 5.3 Hz, 1H), 7.58 – 7.46 (m, 2H), 7.31 (d, *J* = 8.5 Hz, 2H), 7.25 (d, *J* = 8.6 Hz, 2H), 6.79 (d, *J* = 8.0 Hz, 2H), 6.71 – 6.64 (m, 2H), 4.97 (s, 1H), 4.23 – 3.92 (m, 4H), 3.82 (s, 3H), 3.62 – 3.43 (m, 4H), 2.77 (td, *J* = 6.9, 3.2 Hz, 2H), 2.48 (t, *J* = 2.4 Hz, 1H), 1.83 (q, *J* = 7.1 Hz, 2H), 1.69 (q, *J* = 7.9, 7.1 Hz, 2H), 1.49 – 1.38 (m, 8H) ppm.

^{13}C-NMR (100.62 MHz, $CDCl_3$): δ = 169.9, 164.4, 162.6, 160.1, 149.6, 149.5, 149.5, 147.4, 143.6, 137.1, 137.0, 134.8, 134.7, 132.4, 132.3, 131.2, 130.3, 130.2, 129.0, 128.9, 120.9, 120.6, 119.8, 113.3, 112.5, 111.1, 110.8, 79.7, 78.2, 76.0, 69.2, 56.5, 56.1, 40.5, 39.8, 35.3, 29.8, 29.5, 29.4, 29.4, 27.1, 26.1 ppm.

HRMS (ESI(+), CH_3CN): *m/z* 674.2784 $[M+H]^+$, calculated for $C_{38}H_{42}N_3O_5ClF^+$: *m/z* 674.2792.

Mandi-Dopa-Cn-CPY

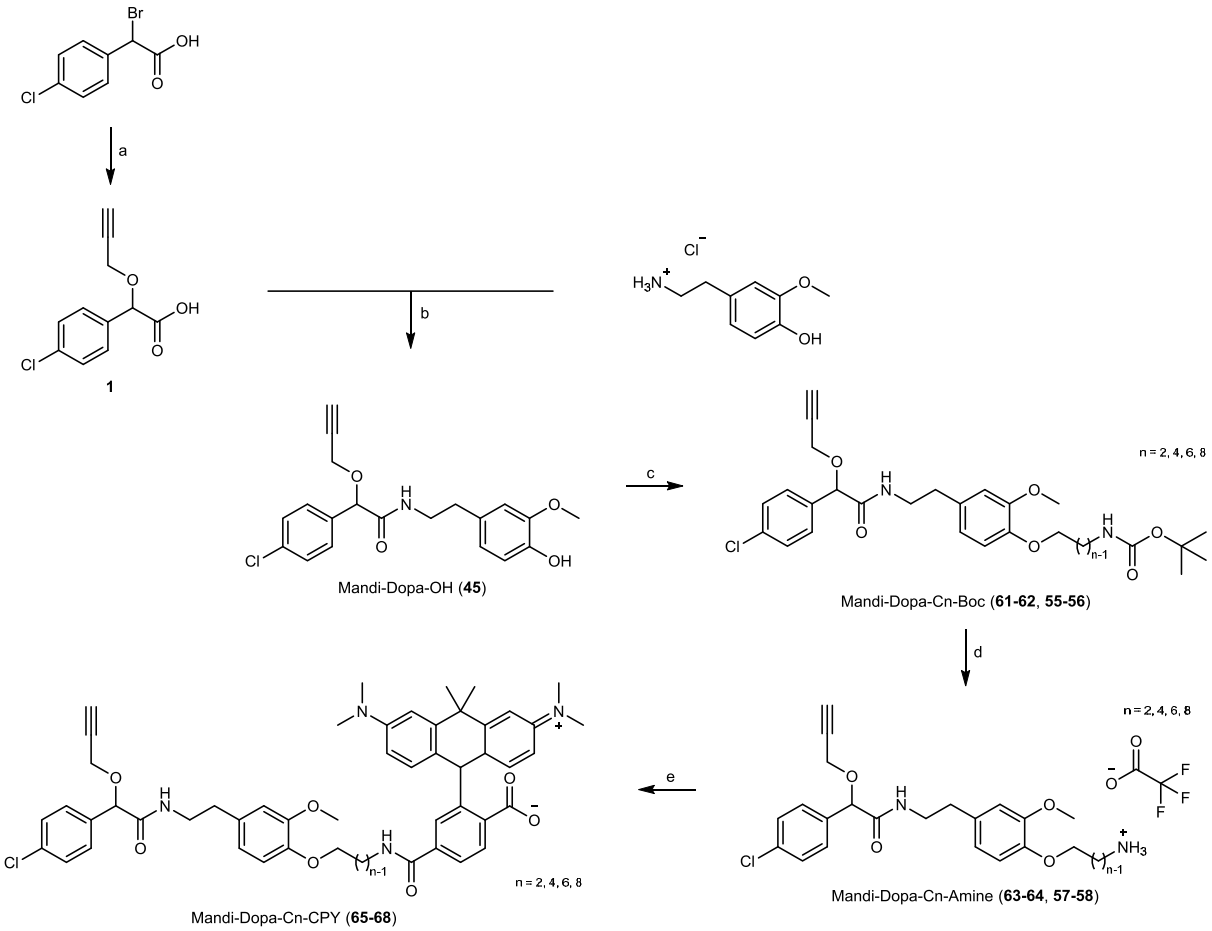

Conditions: a: propargyl alcohol, KOH, rt, 2 h; b: HATU, DIPEA, rt, 68 h; c: Boc-amine alkyl bromide, K_2CO_3, KI, rt, 18 – 40 h; d: TFA, rt, 2 – 3 h; e: CPY-6-COOH, HATU, DIPEA, rt, 19 – 94 h.

Mandi-Dopa-C2-Boc (61)

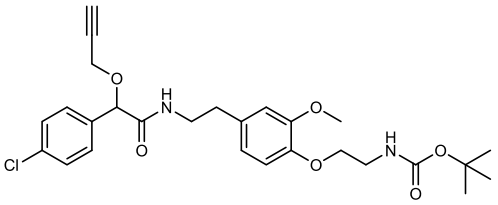

tert-Butyl (2-bromoethyl)carbamate (11.8 µl, 66.9 µmol, 1.00 eq.) was dissolved in anhydrous dimethylformamide (1 ml) and Mandi-Dopa-OH (**45**) (25.0 mg, 66.9 µmol, 1.00 eq.), potassium carbonate (27.7 mg, 201 µmol, 3.00 eq.) as well as potassium iodide (5.55 mg, 33.4 µmol, 0.50 eq.) were added. The reaction mixture was stirred for 40 h at room temperature. The solvent was removed under reduced pressure and the crude product was purified by preparative reverse phase HPLC (C18, acetonitrile:water gradient + 0.1 % TFA). The product was obtained as colorless liquid (16.6 mg, 32.1 µmol, 48 %).

^{1}H-NMR (400.15 MHz, $CDCl_3$): δ = 7.32 (d, *J* = 8.5 Hz, 2H), 7.25 (d, *J* = 8.5 Hz, 2H), 6.87 – 6.82 (m, 2H), 6.71 – 6.67 (m, 2H), 5.25 (s, 1H), 4.99 (s, 1H), 4.21 – 3.94 (m, 2H), 4.06 (t, *J* = 5.2 Hz, 2H), 3.82 (s, 3H), 3.62 – 3.47 (m, 4H), 2.79 (td, *J* = 6.9, 2.6 Hz, 2H), 2.49 (t, *J* = 2.4 Hz, 1H), 1.45 (s, 9H) ppm.

^{13}C-NMR (100.62 MHz, $CDCl_3$): δ = 170.2, 150.0, 146.8, 134.9, 134.5, 132.4, 129.0, 128.9, 121.0, 114.9, 112.6, 79.6, 78.1, 76.1, 69.3, 56.5, 56.0, 40.5, 35.3, 28.5 ppm.

HRMS (ESI(+), CH_3CN): *m/z* 539.1913 $[M+Na]^+$, calculated for $C_{27}H_{33}N_2O_6ClNa^+$: *m/z* 539.1919.

Mandi-Dopa-C4-Boc (62)

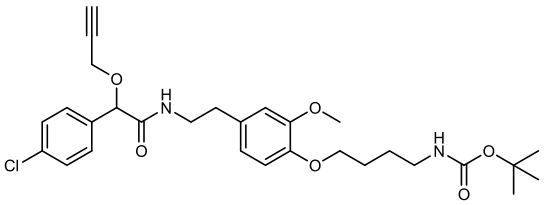

tert-Butyl (2-bromobutyl)carbamate (90 %, 15.2 µl, 66.9 µmol, 1.00 eq.) was dissolved in anhydrous dimethylformamide (1 ml) and Mandi-Dopa-OH (**45**) (25.0 mg, 66.9 µmol, 1.00 eq.), potassium carbonate (27.7 mg, 201 µmol, 3.00 eq.) as well as potassium iodide (5.55 mg, 33.4 µmol, 0.50 eq.) were added. The reaction mixture was stirred for 18 h at room temperature. Then, saturated aqueous ammonium chloride solution (1 ml) was added and the mixture was extracted with dichloromethane (2 x 1 ml). The solvent was removed under reduced pressure and the crude product was purified by preparative reverse phase HPLC (C18, acetonitrile:water gradient + 0.1 % TFA). The product was obtained as colorless liquid (17.0 mg, 31.2 µmol, 47 %).

^{1}H-NMR (400.15 MHz, $CDCl_3$): δ = 7.31 (d, *J* = 8.5 Hz, 2H), 7.26 (d, *J* = 8.5 Hz, 2H), 6.80 – 6.77 (m, 2H), 6.69 – 6.66 (m, 2H), 4.97 (s, 1H), 4.21 – 3.94 (m, 4H), 3.82 (s, 3H), 3.61 – 3.45 (m, 2H), 3.29 (s, 1H), 3.21 – 3.18 (m, 2H), 2.77 (td, *J* = 7.0, 3.1 Hz, 2H), 2.48 (t, *J* = 2.4 Hz, 1H), 1.91 – 1.84 (m, 2H), 1.72 – 1.65 (m, 2H), 1.44 (s, 9H) ppm.

^{13}C-NMR (100.62 MHz, $CDCl_3$): δ = 169.9, 149.6, 147.2, 134.8, 134.7, 131.4, 129.0, 128.9, 120.9, 113.2, 112.4, 79.7, 78.2, 76.1, 68.7, 56.5, 56.0, 40.5, 35.3, 28.6, 26.9, 26.5 ppm.

HRMS (ESI(+), CH_3CN): *m/z* 545.2410 $[M+H]^+$, calculated for $C_{29}H_{38}N_2O_6Cl^+$: *m/z* 545.2413.

Mandi-Dopa-C2-Amine (63)

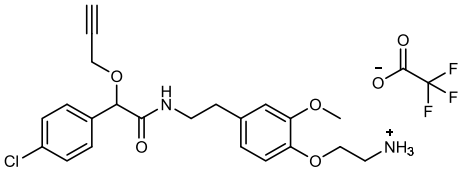

Mandi-Dopa-C2-Boc (**61**) (16.6 mg, 32.1 µmol, 1.00 eq.) was dissolved in chloroform (1 ml) and trifluoracetic acid (1 ml) was added. The reaction mixture was stirred for 2 h at room temperature. The

solvent was removed under reduced pressure and successively co-evaporated with toluene (3 x 5 ml). The product was obtained as off-white solid (12.9 mg, 24.3 µmol, 76 %).

^{1}H-NMR (400.15 MHz, $CDCl_3$): δ = 8.32 (s, 3H), 7.31 (d, *J* = 8.5 Hz, 2H), 7.27 (d, *J* = 7.7 Hz, 2H), 6.85 – 6.82 (m, 2H), 6.69 – 6.66 (m, 2H), 4.96 (s, 1H), 4.21 – 3.94 (m, 4H), 3.76 (s, 3H), 3.54 – 3.45 (m, 2H), 3.30 (s, 2H), 2.76 (t, *J* = 6.9 Hz, 2H), 2.51 (t, *J* = 2.3 Hz, 1H) ppm.

^{13}C-NMR (100.62 MHz, $CDCl_3$): δ = 169.9, 150.2, 145.5, 134.8, 134.7, 134.3, 129.0, 128.9, 121.5, 117.1, 112.8, 79.7, 78.2, 76.1, 67.0, 56.5, 55.9, 40.4, 39.6, 35.5 ppm.

HRMS (ESI(+), CH_3CN): *m/z* 417.1574 $[M]^+$, calculated for $C_{22}H_{26}N_2O_4Cl^+$: *m/z* 417.1576.

Mandi-Dopa-C4-Amine (64)

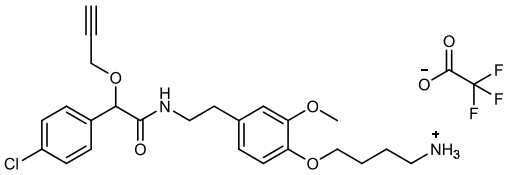

Mandi-Dopa-C4-Boc (**62**) (17.0 mg, 31.2 µmol, 1.00 eq.) was dissolved in chloroform (1 ml) and trifluoracetic acid (1 ml) was added. The reaction mixture was stirred for 3 h at room temperature. The solvent was removed under reduced pressure and successively co-evaporated with toluene (3 x 5 ml). The product was obtained as off-white solid (17.2 mg, 30.8 µmol, 99 %).

^{1}H-NMR (400.15 MHz, $CDCl_3$): δ = 8.08 (s, 3H), 7.31 (d, *J* = 8.5 Hz, 2H), 7.26 (d, *J* = 8.6 Hz, 2H), 6.82 (t, *J* = 6.1 Hz, 1H), 6.75 (d, *J* = 8.0 Hz, 1H), 6.68 – 6.66 (m, 2H), 4.97 (s, 1H), 4.22 – 3.94 (m, 2H), 4.03 (t, *J* = 4.7 Hz, 2H), 3.80 (s, 3H), 3.57 – 3.46 (m, 2H), 3.12 (s, 2H), 2.78 – 2.75 (m, 2H), 2.50 (t, *J* = 2.3 Hz, 1H), 1.99 (s, 4H) ppm.

^{13}C-NMR (100.62 MHz, $CDCl_3$): δ = 169.9, 148.9, 146.0, 134.8, 134.7, 132.3, 129.0, 128.9, 121.0, 112.5, 112.0, 79.7, 78.2, 76.1, 68.6, 56.5, 55.7, 40.4, 40.0, 35.4, 26.4, 25.2 ppm.

HRMS (ESI(+), CH_3CN): *m/z* 445.1886 $[M]^+$, calculated for $C_{24}H_{29}N_2O_4Cl^+$: *m/z* 445.1889.

Mandi-Dopa-C2-CPY (65)

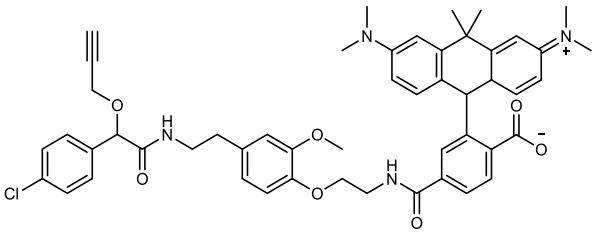

Mandi-Dopa-C2-Amine (**63**) (12.9 mg, 24.3 µmol, 1.00 eq.) was dissolved in anhydrous dimethylformamide (1 ml) and CPY-6-COOH (11.1 mg, 24.3 µmol, 1.00 eq.), HATU (10.2 mg, 26.7 µmol, 1.10 eq.) as well as *N*,*N*-diisopropylethylamine (DIPEA) (10.0 µl, 60.7 µmol, 2.50 eq.). The reaction mixture was stirred for 19 h at room temperature. Then, the solvent removed under reduced pressure and saturated aqueous ammonium chloride solution (1 ml). The mixture was extracted with

dichloromethane (2 x 1 ml) and the solvent was removed under reduced pressure. The crude product was purified by preparative reverse phase HPLC (C18, acetonitrile:water gradient + 0.1 % TFA). The product was obtained as blue solid (14.8 mg, 17.3 µmol, 71 %).

^{1}H-NMR (400.15 MHz, $CDCl_3$): δ = 8.19 (d, *J* = 8.2 Hz, 1H), 8.06 – 7.98 (m, 1H), 7.65 – 7.62 (m, 2H), 7.27 (d, *J* = 5.9 Hz, 2H), 7.24 (s, 2H), 7.15 (s, 2H), 6.90 – 6.84 (m, 4H), 6.70 – 6.64 (m, 4H), 4.97 (s, 1H), 4.20 – 3.93 (m, 4H), 3.80 (q, *J* = 5.5 Hz, 2H), 3.69 (s, 3H), 3.57 – 3.41 (m, 2H), 3.20 (s, 12H), 2.80 – 2.69 (m, 2H), 2.48 (t, *J* = 2.4 Hz, 1H), 1.80 (s, 3H), 1.63 (s, 3H) ppm.

^{13}C-NMR (100.62 MHz, $CDCl_3$): δ = 170.1, 166.9, 166.4, 160.9, 160.5, 160.2, 159.8, 149.9, 146.5, 138.6, 135.3, 134.8, 134.7, 132.9, 130.2, 128.9, 128.1, 127.5, 121.3, 120.5, 117.3, 115.5, 114.4, 113.8, 112.7, 112.0, 79.6, 78.2, 76.1, 68.6, 56.5, 56.0, 41.8, 41.2, 40.5, 39.8, 35.5, 35.3, 32.4 ppm.

HRMS (ESI(+), CH_3CN): *m/z* 855.3514 $[M+H]^+$, calculated for $C_{50}H_{52}N_4O_7Cl^+$: *m/z* 855.3519.

Mandi-Dopa-C4-CPY (66)

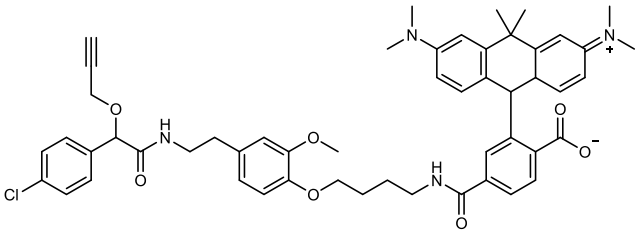

Mandi-Dopa-C4-Amine (**64**) (17.2 mg, 30.8 µmol, 1.00 eq.) was dissolved in anhydrous dimethylformamide (1 ml) and CPY-6-COOH (14.0 mg, 30.8 µmol, 1.00 eq.), HATU (12.9 mg, 33.8 µmol, 1.10 eq.) as well as *N*,*N*-diisopropylethylamine (DIPEA) (12.7 µl, 76.9 µmol, 2.50 eq.). The reaction mixture was stirred for 94 h at room temperature. Then, the solvent removed under reduced pressure and saturated aqueous ammonium chloride solution (1 ml). The mixture was extracted with dichloromethane (2 x 1 ml) and the solvent was removed under reduced pressure. The crude product was purified by preparative reverse phase HPLC (C18, acetonitrile:water gradient + 0.1 % TFA). The product was obtained as blue solid (19.4 mg, 22.0 µmol, 71 %).

^{1}H-NMR (400.15 MHz, $CDCl_3$): δ = 8.13 (d, *J* = 8.2 Hz, 1H), 8.00 (dd, *J* = 8.2, 1.7 Hz, 1H), 7.84 (t, *J* = 5.9 Hz, 1H), 7.69 (s, 1H), 7.28 (d, *J* = 8.7 Hz, 2H), 7.24 (d, *J* = 8.7 Hz, 2H), 7.11 (s, 2H), 6.95 – 6.89 (m, 3H), 6.76 (d, *J* = 8.0 Hz, 1H), 6.67 – 6.64 (m, 4H), 4.97 (s, 1H), 4.20 – 3.93 (m, 2H), 4.01 (t, *J* = 5.8 Hz, 2H), 3.68 (s, 3H), 3.56 – 3.43 (m, 4H), 3.21 (s, 12H), 2.80 – 2.69 (m, 2H), 2.48 (t, *J* = 2.4 Hz, 1H), 1.93 – 1.86 (m, 2H), 1.84 – 1.81 (m, 2H), 1.78 (s, 3H), 1.62 (s, 3H) ppm.

^{13}C-NMR (100.62 MHz, $CDCl_3$): δ = 170.2, 166.8, 166.6, 160.7, 160.3, 160.0, 159.6, 149.3, 146.9, 138.7, 135.9, 134.7, 132.3, 131.5, 130.7, 129.0, 128.9, 128.1, 121.1, 120.1, 117.2, 114.3, 113.7, 113.0, 112.4, 111.7, 79.6, 78.2, 76.1, 68.8, 56.5, 55.9, 41.6, 41.5, 40.6, 39.9, 35.6, 35.2, 32.2, 26.3, 26.1 ppm.

HRMS (ESI(+), CH_3CN): *m/z* 883.3835 $[M+H]^+$, calculated for $C_{52}H_{56}N_4O_7Cl^+$: *m/z* 883.3832.

Mandi-Dopa-C6-CPY (67)

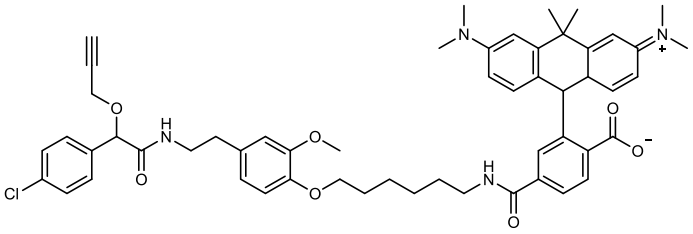

Mandi-Dopa-C6-Amine (**57**) (9.00 mg, 15.3 µmol, 1.00 eq.) was dissolved in anhydrous dimethylformamide (1 ml) and CPY-6-COOH (7.00 mg, 15.3 µmol, 1.00 eq.), HATU (6.41 mg, 16.9 µmol, 1.10 eq.) as well as *N*,*N*-diisopropylethylamine (DIPEA) (6.33 µl, 38.3 µmol, 2.50 eq.). The reaction mixture was stirred for 65 h at room temperature. Then, the solvent removed under reduced pressure and saturated aqueous ammonium chloride solution (1 ml). The mixture was extracted with dichloromethane (2 x 1 ml) and the solvent was removed under reduced pressure. The crude product was purified by preparative reverse phase HPLC (C18, acetonitrile:water gradient + 0.1 % TFA). The product was obtained as blue solid (7.40 mg, 8.11 µmol, 53 %).

^{1}H-NMR (400.15 MHz, $CDCl_3$): δ = 8.10 (d, *J* = 8.1 Hz, 1H), 7.94 (dd, *J* = 8.1, 1.7 Hz, 1H), 7.60 (s, 1H), 7.30 (d, *J* = 8.6 Hz, 2H), 7.25 (d, *J* = 8.6 Hz, 2H), 7.16 (s, 1H), 7.02 (d, *J* = 2.5 Hz, 2H), 6.87 – 6.82 (m, 3H), 6.77 (d, *J* = 8.0 Hz, 1H), 6.68 – 6.60 (m, 4H), 4.96 (s, 1H), 4.20 – 3.94 (m, 4H), 3.79 (s, 3H), 3.61 – 3.45 (m, 2H), 3.42 – 3.35 (m, 2H), 3.18 (s, 12H), 2.81 – 2.70 (m, 2H), 2.47 (t, *J* = 2.4 Hz, 1H), 1.84 – 1.78 (m, 5H), 1.71 (s, 3H), 1.61 (p, *J* = 7.3 Hz, 2H), 1.51 – 1.41 (m, 4H) ppm.

^{13}C-NMR (100.62 MHz, $CDCl_3$): δ = 169.8, 167.6, 166.5, 153.9, 149.6, 147.3, 139.1, 134.9, 134.7, 131.3, 128.9, 128.9, 128.0, 121.5, 121.0, 113.4, 113.1, 112.6, 110.8, 79.7, 78.2, 76.0, 69.1, 56.5, 56.1, 41.2, 40.9, 40.5, 40.4, 35.7, 35.3, 32.5, 29.3, 29.1, 26.7, 25.8 ppm.

HRMS (ESI(+), CH_3CN): *m/z* 911.4140 $[M+H]^+$, calculated for $C_{54}H_{60}N_4O_7Cl^+$: *m/z* 911.4145.

Mandi-Dopa-C8-CPY (68)

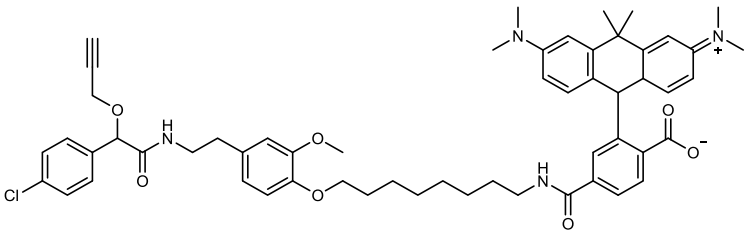

Mandi-Dopa-C8-Amine (**58**) (10.0 mg, 16.3 µmol, 1.00 eq.) was dissolved in anhydrous dimethylformamide (1 ml) and CPY-6-COOH (7.42 mg, 16.3 µmol, 1.00 eq.), HATU (6.80 mg, 17.9 µmol, 1.10 eq.) as well as *N*,*N*-diisopropylethylamine (DIPEA) (6.72 µl, 40.6 µmol, 2.50 eq.). The reaction mixture was stirred for 22 h at room temperature. Then, the solvent removed under reduced pressure and saturated aqueous ammonium chloride solution (1 ml). The mixture was extracted with dichloromethane (2 x 1 ml) and the solvent was removed under reduced pressure. The crude product

was purified by preparative reverse phase HPLC (C18, acetonitrile:water gradient + 0.1 % TFA). The product was obtained as blue solid (9.80 mg, 10.4 µmol, 64 %).

^{1}H-NMR (400.15 MHz, $CDCl_3$): δ = 8.13 (d, *J* = 8.2 Hz, 1H), 7.99 (d, *J* = 8.2 Hz, 1H), 7.64 (s, 1H), 7.36 (s, 1H), 7.30 (d, *J* = 8.5 Hz, 2H), 7.25 (d, *J* = 8.5 Hz, 2H), 7.09 (s, 2H), 6.90 (d, *J* = 9.2 Hz, 2H), 6.83 (t, *J* = 6.0 Hz, 1H), 6.77 (d, *J* = 8.0 Hz, 1H), 6.68 – 6.64 (m, 4H), 4.96 (s, 1H), 4.20 – 3.93 (m, 4H), 3.80 (s, 3H), 3.59 – 3.43 (m, 2H), 3.40 – 3.35 (m, 2H), 3.21 (s, 12H), 2.81 – 2.70 (m, 2H), 2.47 (t, *J* = 2.4 Hz, 1H), 1.83 – 1.76 (m, 5H), 1.66 (s, 3H), 1.60 – 1.54 (m, 2H), 1.44 – 1.39 (m, 2H), 1.32 (s, 6H) ppm.

^{13}C-NMR (100.62 MHz, $CDCl_3$): δ = 169.9, 167.0, 166.6, 149.6, 147.4, 134.8, 134.8, 131.2, 128.9, 128.9, 128.2, 120.9, 113.3, 112.6, 111.2, 79.7, 78.2, 76.1, 69.2, 56.5, 56.1, 41.5, 41.4, 41.3, 40.6, 40.5, 35.7, 35.3, 32.3, 32.2, 29.3, 29.3, 29.3, 29.3, 27.0, 26.0 ppm.

HRMS (ESI(+), CH_3CN): *m/z* 939.4454 $[M+H]^+$, calculated for $C_{56}H_{64}N_4O_7Cl^+$: *m/z* 939.4458.

pMandi

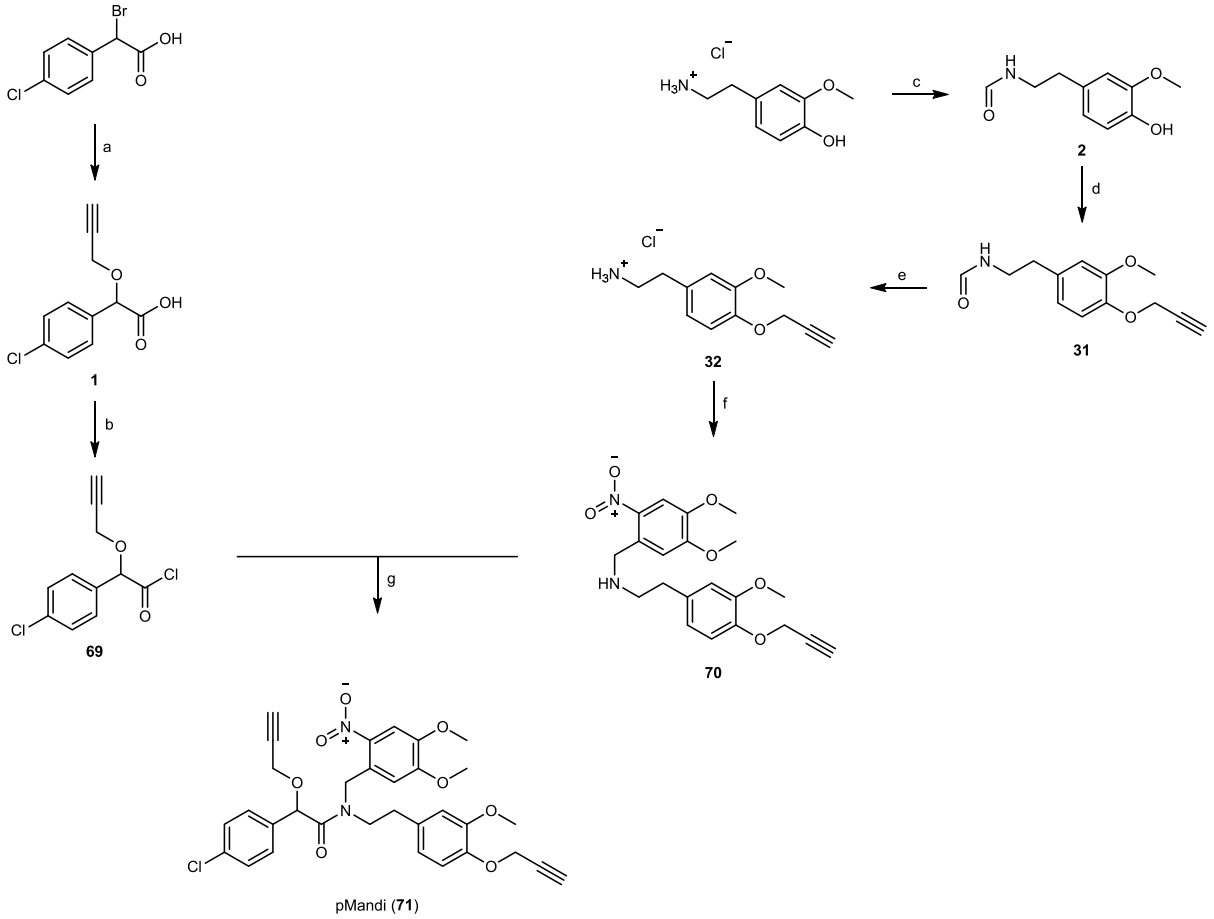

Conditions: a: propargyl alcohol, KOH, rt, 2 h; b: oxalyl chloride, DMF (cat.), 0 °C -> rt, 2 h; c: Ac_2O, formic acid, 70 °C, 2 h; d: propargyl bromide, NaOMe, 65 °C, 4 h; e: HCl, rt, 91 h; f: 1. 4,5-dimethoxy-2-nitrobenzaldehyd, $NaBH(OAc)_3$, rt -> 50 °C, 14 h; g: DIPEA, 0 °C -> rt, 21 h.

2-(4-Chlorophenyl)-2-(prop-2-yn-1-yloxy)acetyl chloride (69)

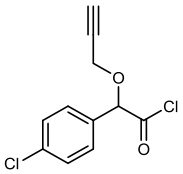

2-(4-Chlorophenyl)-2-(prop-2-yn-1-yloxy)acetyl chloride (**69**) was synthesized during my master's thesis[79]:

2-(4-Chlorophenyl)-2-(prop-2-yn-1-yloxy)acetic acid (**1**) (50.0 mg, 223 µmol, 1.00 eq.) was dried in vacuo for 30 min and subsequently dissolved in anhydrous dichloromethane (1 ml). Then, a drop of anhydrous dimethylformamide (1.72 µl, 22.3 µmol, 0.10 eq.) was added. At 0 °C, a solution of oxalyl chloride (56.5 mg, 445.2 µmol, 2.00 eq.) in dichloromethane (2.00 M, 233 µl) was added dropwise and the reaction mixture was stirred for 15 min at 0 °C and further 2 h at room temperature. The solvent

was removed under reduced pressure. The obtained product (54.1 mg, 223 µmol, 100 %) was used in the next synthetic step without further purification with the assumption of complete conversion.

_N_-(4,5-Dimethoxy-2-nitrobenzyl)-2-(3-methoxy-4-(prop-2-yn-1-yloxy)phenyl)ethan-1-amine (70)

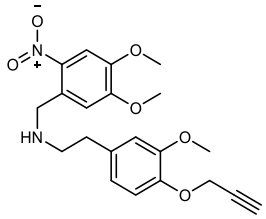

_N_-(4,5-Dimethoxy-2-nitrobenzyl)-2-(3-methoxy-4-(prop-2-yn-1-yloxy)phenyl)ethan-1-amine (**70**) was synthesized during my master's thesis[79]:

2-(3-Methoxy-4-(prop-2-yn-1-yloxy)phenyl)ethan-1-aminium chloride (**32**) (50.0 mg, 207 µmol, 1.00 eq.) was dissolved in anhydrous 1,2-dichloroethane (2 ml). Then, _N_,_N_-diisopropylethylamine (DIPEA) (103 µl, 621 µmol, 3.00 eq.) and 4,5-dimethoxy-2-nitrobenzaldehyd (80 %, 54.6 mg, 207 µmol, 1.00 eq.) were added. The yellow suspension was stirred for 15 min at room temperature and sodium triacetoxyborohydride (92.3 mg, 414 µmol, 2.00 eq.) was added. The reaction mixture was stirred for 14 h at 50 °C. Saturated aqueous sodium hydrogencarbonate solution (5 ml) was added and the resulting mixture was extracted with dichloromethane (3 x 10 ml). The combined organic layer was washed with brine (10 ml) and dried over sodium sulphate. The solvent was removed under reduced pressure and the crude product was purified by preparative reverse phase HPLC (C18, acetonitrile:water gradient + 0.1 % TFA). The product was obtained as brown solid (21.4 mg, 53.4 µmol, 26 %).

^{1}H-NMR (400.15 MHz, $CDCl_3$): δ = 7.56 (s, 1H), 7.14 (s, 1H), 6.99 (d, J = 8.5 Hz, 1H), 6.77 – 6.75 (m, 2H), 4.74 (d, J = 2.4 Hz, 2H), 4.35 (s, 2H), 3.94 (s, 3H), 3.87 (s, 3H), 3.86 (s, 3H), 3.40 (t, J = 7.5 Hz, 2H), 2.95 (t, J = 7.4 Hz, 2H), 2.51 (t, J = 2.4 Hz, 1H) ppm.

^{13}C-NMR (100.62 MHz, $CDCl_3$): δ = 154.2, 150.4, 150.2, 146.3, 141.6, 129.4, 120.7, 120.4, 115.5, 115.1, 112.4, 108.4, 78.5, 76.1, 57.0, 56.8, 56.6, 56.1, 49.7, 49.4, 32.2 ppm.

HRMS (ESI(+), CH_3CN): m/z 401.1704 $[M+H]^+$, calculated for $C_{21}H_{25}N_2O_6^+$: m/z 401.1707.

pMandi (71)

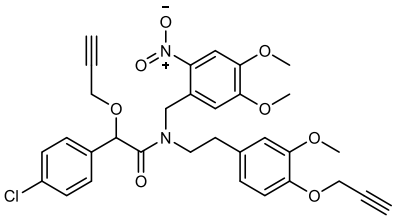

pMandi (**71**) was synthesized during my master's thesis[79]:

N-(4,5-Dimethoxy-2-nitrobenzyl)-2-(3-methoxy-4-(prop-2-yn-1-yloxy)phenyl)ethan-1-amine (**70**) (21.4 mg, 53.4 µmol, 1.00 eq.) was dissolved in anhydrous dichloromethane (1 ml) and *N*,*N*-diisopropylethylamine (DIPEA) (26.5 µl, 160 µmol, 3.00 eq.) was added. At 0 °C, a solution of 2-(4-chlorophenyl)-2-(prop-2-yn-1-yloxy)acetyl chloride (**69**) (13.0 mg, 53.4 µmol, 1.00 eq.) in anhydrous dichloromethane (1 ml) was added dropwise. The reaction mixture was stirred for 21 h at room temperature. Then, hydrochloric acid (1.00 M, 1.00 ml) and dichloromethane (5 ml) were added and the layers were separated. The organic layer was washed a with saturated aqueous sodium hydrogencarbonate solution (5 ml) and dried over sodium sulphate. The solvent was removed under reduced pressure and the crude product was purified by preparative reverse phase HPLC (C18, acetonitrile:water gradient + 0.1 % TFA). The product was obtained as slightly yellow solid (6.90 mg, 11.4 µmol, 21 %).

The NMR spectra show the signals of a 1:1 mixture of the two rotamers.

^{1}H-NMR (400.15 MHz, $CDCl_3$): δ = 7.72 (s, 1H), 7.64 (s, 1H), 7.34 (d, *J* = 2.4 Hz, 4H), 7.26 (d, *J* = 1.8 Hz, 4H), 6.99 (d, *J* = 8.1 Hz, 1H), 6.92 (d, *J* = 8.1 Hz, 1H), 6.73 – 6.66 (m, 5H), 6.42 (s, 1H), 5.35 (s, 1H), 5.30 (s, 1H), 5.07 (d, *J* = 1.9 Hz, 2H), 4.95 (s, 2H), 4.76 (d, *J* = 2.4 Hz, 2H), 4.73 (d, *J* = 2.4 Hz, 2H), 4.29 – 3.98 (m, 4H), 3.96 (s, 3H), 3.93 (s, 3H), 3.86 (s, 3H), 3.82 (s, 3H), 3.78 (s, 3H), 3.71 (s, 3H), 3.67 – 3.56 (m, 2H), 3.54-3.43 (m, 2H), 2.84 (dd, *J* = 11.9 Hz, *J* = 8.1 Hz, 4H), 2.53 (t, *J* = 2.4 Hz, 1H), 2.51-2.49 (m, 2H), 2.33 (t, *J* = 2.4 Hz, 1H) ppm.

^{13}C-NMR (100.62 MHz, $CDCl_3$): δ = 170.5, 170.1, 154.1, 153.9, 150.1, 149.9, 148.2, 148.1, 146.0, 145.7, 141.0, 139.9, 135.4, 135.3, 133.8, 133.3, 132.3, 131.7, 129.6, 129.4, 129.3, 129.2, 127.9, 127.7, 120.8, 120.8, 114.9, 114.8, 112.8, 112.7, 110.1, 109.0, 108.8, 108.4, 78.8, 78.8, 78.7, 78.2, 76.3, 76.2, 76.0, 75.9, 57.0, 57.0, 56.7, 56.5, 56.4, 56.3, 56.3, 56.2, 56.0, 49.9, 49.4, 46.1, 34.8 ppm.

HRMS (ESI(+), CH_3CN): *m/z* 607.1836 $[M+H]^+$, calculated for $C_{32}H_{32}N_2O_8Cl^+$: *m/z* 607.1842.

Mandi-Dopa-Cn-COOH/AM/NV

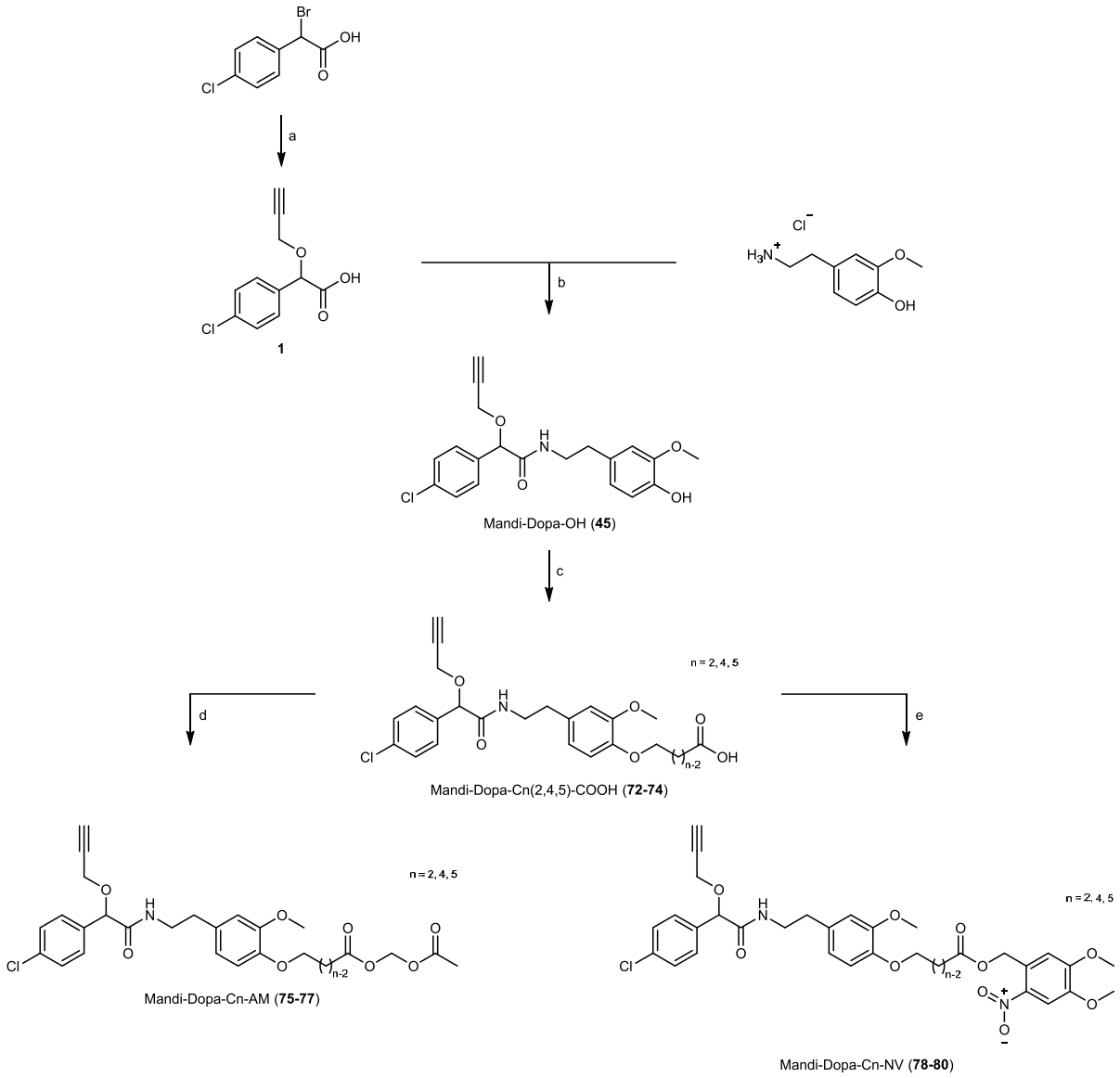

Conditions: a: propargyl alcohol, KOH, rt, 2 h; b: HATU, DIPEA, rt, 68 h; c: 1. methyl bromoalkylate, NaOMe, 21 – 22 h, 65 °C, 2. NaOH, rt, 4 h; d: bromomethyl acetate, DIPEA, rt, 23 – 39 h; e: 1-(bromomethyl)-4,5-dimethoxy-2-nitrobenzene, DIPEA, rt, 23 – 39 h.

Mandi-Dopa-C2-COOH (72)

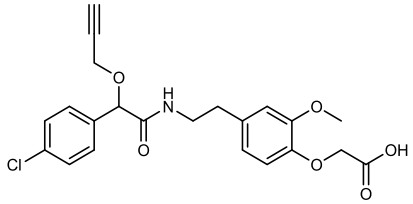

Mandi-Dopa-OH (**45**) (30.0 mg, 80.3 µmol, 1.00 eq.) was dissolved in anhydrous methanol (1 ml) and methyl 2-bromoacetate (22.9 µl, 241 µmol, 3.00 eq.) as well as solution of sodium methoxide (9.54 mg, 177 µmol, 2.20 eq.) in methanol (25 wt%, 4.37 M, 40.4 µl) were added. The reaction mixture was

stirred for 22 h at 65 °C. Then, the solvent was removed under reduced pressure and tetrahydrofuran (1 ml) and aqueous sodium hydroxide solution (1.00 M, 0.50 ml) were added. The reaction mixture was stirred for 4 h at room temperature. Thereafter, hydrochloric acid (1.00 M, 1.00 ml) was added to reach pH 1 and the mixture was extracted with dichloromethane (3 x 5 ml). The combined organic layer was dried over sodium sulphate and the solvent was removed under reduced pressure. The crude product was purified by preparative reverse phase HPLC (C18, acetonitrile:water gradient + 0.1 % TFA). The product was obtained as white solid (9.60 mg, 22.2 µmol, 28 %).

^{1}H-NMR (400.15 MHz, $CDCl_3$): δ = 7.32 (d, *J* = 8.5 Hz, 2H), 7.26 (d, *J* = 8.5 Hz, 2H), 6.84 (d, *J* = 3.5 Hz, 2H), 6.74 (d, *J* = 1.9 Hz, 1H), 6.70 (dd, *J* = 8.1, 2.0 Hz, 1H), 4.99 (s, 1H), 4.65 (s, 2H), 4.21 – 3.94 (m, 2H), 3.85 (s, 3H), 3.61 – 3.47 (m, 2H), 2.82 – 2.78 (m, 2H), 2.49 (t, *J* = 2.4 Hz, 1H) ppm.

^{13}C-NMR (100.62 MHz, $CDCl_3$): δ = 171.3, 170.2, 150.0, 146.0, 134.9, 134.5, 134.3, 129.0, 128.9, 121.3, 116.8, 112.8, 79.7, 78.1, 76.1, 68.2, 56.5, 56.1, 40.4, 35.4 ppm.

HRMS (ESI(+), CH_3CN): *m/z* 432.1203 $[M+H]^+$, calculated for $C_{22}H_{23}NO_6Cl^+$: *m/z* 432.1208.

Mandi-Dopa-C4-COOH (73)

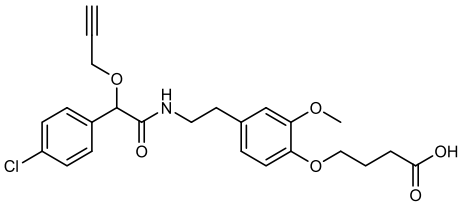

Mandi-Dopa-OH (**45**) (30.0 mg, 80.3 µmol, 1.00 eq.) was dissolved in anhydrous methanol (1 ml) and methyl 4-bromobutyrate (30.4 µl, 241 µmol, 3.00 eq.) as well as solution of sodium methoxide (9.54 mg, 177 µmol, 2.20 eq.) in methanol (25 wt%, 4.37 M, 40.4 µl) were added. The reaction mixture was stirred for 21 h at 65 °C. Then, the solvent was removed under reduced pressure and tetrahydrofuran (1 ml) and aqueous sodium hydroxide solution (1.00 M, 0.50 ml) were added. The reaction mixture was stirred for 4 h at room temperature. Thereafter, hydrochloric acid (1.00 M, 1.00 ml) was added to reach pH 1 and the mixture was extracted with dichloromethane (3 x 5 ml). The combined organic layer was dried over sodium sulphate and the solvent was removed under reduced pressure. The crude product was purified by preparative reverse phase HPLC (C18, acetonitrile:water gradient + 0.1 % TFA). The product was obtained as off-white liquid (15.6 mg, 33.9 µmol, 42 %).

^{1}H-NMR (400.15 MHz, $CDCl_3$): δ = 7.32 (d, *J* = 8.5 Hz, 2H), 7.26 (d, *J* = 8.5 Hz, 2H), 6.82 – 6.78 (m, 2H), 6.70 – 6.66 (m, 2H), 4.98 (s, 1H), 4.21 – 3.94 (m, 2H), 4.06 (t, *J* = 6.2 Hz, 2H), 3.82 (s, 3H), 3.61 – 3.46 (m, 2H), 2.79 – 2.75 (m, 2H), 2.61 (t, *J* = 7.2 Hz, 2H), 2.48 (t, *J* = 2.4 Hz, 1H), 2.19 – 2.12 (m, 2H) ppm.

^{13}C-NMR (100.62 MHz, $CDCl_3$): δ = 177.8, 170.0, 149.8, 147.0, 134.8, 134.7, 131.8, 129.0, 128.9, 120.9, 113.9, 112.6, 79.7, 78.2, 76.1, 68.1, 56.5, 56.1, 40.5, 35.3, 30.6, 24.5 ppm.

HRMS (ESI(+), CH_3CN): *m/z* 460.1524 $[M+H]^+$, calculated for $C_{24}H_{27}NO_6Cl^+$: *m/z* 460.1521.

Mandi-Dopa-C5-COOH (74)

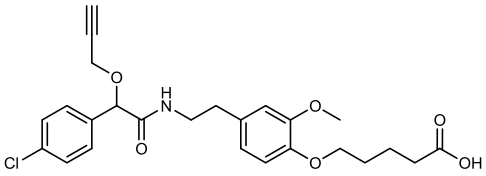

Mandi-Dopa-OH (**45**) (30.0 mg, 80.3 µmol, 1.00 eq.) was dissolved in anhydrous methanol (1 ml) and methyl 5-bromopentanoate (34.5 µl, 241 µmol, 3.00 eq.) as well as solution of sodium methoxide (9.54 mg, 177 µmol, 2.20 eq.) in methanol (25 wt%, 4.37 M, 40.4 µl) were added. The reaction mixture was stirred for 21 h at 65 °C. Then, the solvent was removed under reduced pressure and tetrahydrofuran (1 ml) and aqueous sodium hydroxide solution (1.00 M, 0.50 ml) were added. The reaction mixture was stirred for 4 h at room temperature. Thereafter, hydrochloric acid (1.00 M, 1.00 ml) was added to reach pH 1 and the mixture was extracted with dichloromethane (3 x 5 ml). The combined organic layer was dried over sodium sulphate and the solvent was removed under reduced pressure. The crude product was purified by preparative reverse phase HPLC (C18, acetonitrile:water gradient + 0.1 % TFA). The product was obtained as colorless liquid (19.1 mg, 40.3 µmol, 50 %).

^{1}H-NMR (400.15 MHz, $CDCl_3$): δ = 7.32 (d, *J* = 8.6 Hz, 2H), 7.25 (d, *J* = 8.5 Hz, 2H), 6.83 (t, *J* = 6.4 Hz, 1H), 6.79 (d, *J* = 8.0 Hz, 1H), 6.70 – 6.66 (m, 2H), 4.99 (s, 1H), 4.21 – 3.94 (m, 2H), 4.03 (t, *J* = 6.0 Hz, 2H), 3.82 (s, 3H), 3.62 – 3.47 (m, 2H), 2.80 – 2.76 (m, 2H), 2.49 – 2.45 (m, 3H), 1.93 – 1.82 (m, 4H) ppm.

^{13}C-NMR (100.62 MHz, $CDCl_3$): δ = 178.1, 170.1, 149.7, 147.2, 134.9, 134.6, 131.4, 129.0, 128.9, 120.9, 113.5, 112.6, 79.7, 78.2, 76.1, 68.8, 56.5, 56.1, 40.5, 35.3, 33.7, 28.5, 21.7 ppm.

HRMS (ESI(+), CH_3CN): *m/z* 474.1679 $[M+H]^+$, calculated for $C_{25}H_{29}NO_6Cl^+$: *m/z* 474.1678.

Mandi-Dopa-C2-AM (75)

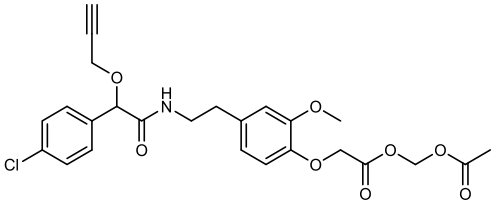

Mandi-Dopa-C2-COOH (**72**) (6.90 mg, 16.0 µmol, 1.00 eq.) was dissolved in anhydrous acetonitrile (1 ml). Then, *N*,*N*-diisopropylethylamine (DIPEA) (3.70 µl, 22.4 µmol, 1.40 eq.) and bromomethyl acetate (2.19 µl, 22.4 µmol, 1.40 eq.) were added. The reaction mixture was stirred for 23 h at room temperature. The solvent was removed under reduced pressure and the crude product was purified by preparative reverse phase HPLC (C18, acetonitrile:water gradient + 0.1 % TFA). The product was obtained as off-white solid (5.40 mg, 10.7 µmol, 67 %).

^{1}H-NMR (400.15 MHz, $CDCl_3$): δ = 7.33 (d, *J* = 8.6 Hz, 2H), 7.27 (d, *J* = 8.6 Hz, 2H), 6.80 – 6.77 (m, 2H), 6.72 (d, *J* = 2.0 Hz, 1H), 6.66 (dd, *J* = 8.1, 2.0 Hz, 1H), 5.83 (s, 2H), 4.97 (s, 1H), 4.72 (s, 2H), 4.21 – 3.94 (m, 2H), 3.84 (s, 3H), 3.60 – 3.46 (m, 2H), 2.84 – 2.73 (m, 2H), 2.49 (t, *J* = 2.4 Hz, 1H), 2.11 (s, 3H) ppm.

^{13}C-NMR (100.62 MHz, $CDCl_3$): δ = 169.9, 169.6, 168.2, 150.0, 145.9, 134.8, 134.7, 133.6, 129.0, 128.9, 120.8, 115.5, 112.9, 79.7, 79.5, 78.2, 76.1, 66.6, 56.5, 56.1, 40.3, 35.3, 20.8 ppm.

HRMS (ESI(+), CH_3CN): *m/z* 504.1420 $[M+H]^+$, calculated for $C_{25}H_{27}NO_8Cl^+$: *m/z* 504.1420.

Mandi-Dopa-C4-AM (76)

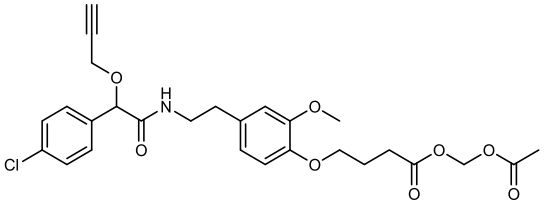

Mandi-Dopa-C4-COOH (**73**) (6.60 mg, 14.4 µmol, 1.00 eq.) was dissolved in anhydrous acetonitrile (1 ml). Then, *N*,*N*-diisopropylethylamine (DIPEA) (3.32 µl, 20.1 µmol, 1.40 eq.) and bromomethyl acetate (1.97 µl, 20.1 µmol, 1.40 eq.) were added. The reaction mixture was stirred for 23 h at room temperature. The solvent was removed under reduced pressure and the crude product was purified by preparative reverse phase HPLC (C18, acetonitrile:water gradient + 0.1 % TFA). The product was obtained as off-white solid (5.50 mg, 10.3 µmol, 72 %).

^{1}H-NMR (400.15 MHz, $CDCl_3$): δ = 7.32 (d, *J* = 8.6 Hz, 2H), 7.27 (d, *J* = 8.6 Hz, 2H), 6.80 (d, *J* = 8.0 Hz, 1H), 6.77 (t, *J* = 5.9 Hz, 1H), 6.70 – 6.66 (m, 2H), 5.75 (s, 2H), 4.97 (s, 1H), 4.21 – 3.95 (m, 2H), 4.05 (t, *J* = 6.2 Hz, 2H), 3.82 (s, 3H), 3.61 – 3.45 (m, 2H), 2.83 – 2.72 (m, 2H), 2.62 (t, *J* = 7.3 Hz, 2H), 2.48 (t, *J* = 2.4 Hz, 1H), 2.19 – 2.13 (m, 2H), 2.10 (s, 3H) ppm.

^{13}C-NMR (100.62 MHz, $CDCl_3$): δ = 172.2, 169.8, 169.7, 149.8, 147.0, 134.8, 131.8, 129.0, 128.9, 120.9, 113.8, 112.6, 79.8, 79.4, 78.2, 76.0, 68.0, 56.5, 56.1, 40.4, 35.3, 30.6, 24.4, 20.9 ppm.

HRMS (ESI(+), CH_3CN): *m/z* 532.1732 $[M+H]^+$, calculated for $C_{27}H_{31}NO_8Cl^+$: *m/z* 532.1733.

Mandi-Dopa-C5-AM (77)

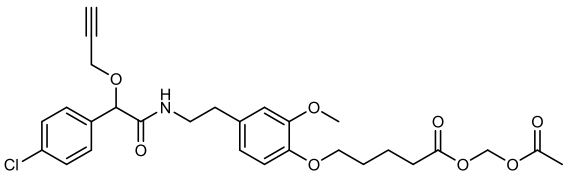

Mandi-Dopa-C5-COOH (**74**) (8.80 mg, 18.6 µmol, 1.00 eq.) was dissolved in anhydrous acetonitrile (1 ml). Then, *N*,*N*-diisopropylethylamine (DIPEA) (4.30 µl, 26.0 µmol, 1.40 eq.) and bromomethyl acetate (2.55 µl, 26.0 µmol, 1.40 eq.) were added. The reaction mixture was stirred for 39 h at room temperature. The solvent was removed under reduced pressure and the crude product was purified by preparative reverse phase HPLC (C18, acetonitrile:water gradient + 0.1 % TFA). The product was obtained as off-white solid (7.20 mg, 13.2 µmol, 71 %).

^{1}H-NMR (400.15 MHz, $CDCl_3$): δ = 7.32 (d, *J* = 8.6 Hz, 2H), 7.27 (d, *J* = 8.6 Hz, 2H), 6.80 – 6.74 (m, 2H), 6.70 – 6.66 (m, 2H), 5.74 (s, 2H), 4.97 (s, 1H), 4.21 – 3.95 (m, 4H), 3.82 (s, 3H), 3.61 – 3.45 (m, 2H), 2.79 – 2.75 (m, 2H), 2.49 – 2.45 (m, 3H), 2.11 (s, 3H), 1.88 – 1.85 (m, 4H) ppm.

^{13}C-NMR (100.62 MHz, $CDCl_3$): δ = 172.3, 169.7, 149.7, 147.2, 134.8, 134.8, 131.6, 129.0, 128.9, 120.9, 113.5, 112.6, 79.8, 79.3, 78.2, 76.0, 68.7, 56.5, 56.1, 40.4, 35.3, 33.7, 28.7, 21.4, 20.9 ppm.

HRMS (ESI(+), CH_3CN): *m/z* 546.1891 $[M+H]^+$, calculated for $C_{28}H_{33}NO_8Cl^+$: *m/z* 546.1889.

Mandi-Dopa-C2-NV (78)

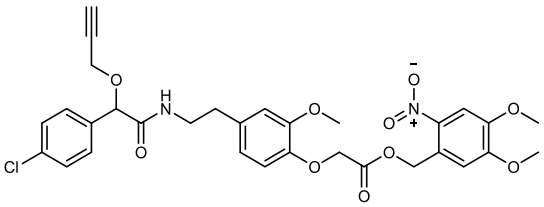

Mandi-Dopa-C2-COOH (**72**) (6.90 mg, 16.0 µmol, 1.00 eq.) was dissolved in anhydrous acetonitrile (1 ml). Then, *N*,*N*-diisopropylethylamine (DIPEA) (3.70 µl, 22.4 µmol, 1.40 eq.) and 1-(bromomethyl)-4,5-dimethoxy-2-nitrobenzene (6.17 mg, 22.4 µmol, 1.40 eq.) were added. The reaction mixture was stirred for 23 h at room temperature. The solvent was removed under reduced pressure and the crude product was purified by preparative reverse phase HPLC (C18, acetonitrile:water gradient + 0.1 % TFA). The product was obtained as off-white solid (6.40 mg, 10.2 µmol, 64 %).

^{1}H-NMR (400.15 MHz, $CDCl_3$): δ = 7.72 (s, 1H), 7.32 (d, *J* = 8.7 Hz, 2H), 7.27 (d, *J* = 8.1 Hz, 2H), 7.01 (s, 1H), 6.80 – 6.76 (m, 2H), 6.72 (d, *J* = 2.0 Hz, 1H), 6.66 (dd, *J* = 8.1, 2.0 Hz, 1H), 5.63 (s, 2H), 4.96 (s, 1H), 4.78 (s, 2H), 4.21 – 3.95 (m, 2H), 3.95 (s, 3H), 3.87 (s, 3H), 3.82 (s, 3H), 3.60 – 3.45 (m, 2H), 2.83 – 2.72 (m, 2H), 2.48 (t, *J* = 2.4 Hz, 1H) ppm.

^{13}C-NMR (100.62 MHz, $CDCl_3$): δ = 169.7, 168.8, 153.7, 149.8, 148.6, 146.0, 140.1, 134.8, 133.4, 129.0, 128.8, 126.4, 120.9, 114.7, 112.8, 110.9, 108.4, 79.8, 78.2, 76.0, 66.9, 64.0, 56.6, 56.6, 56.5, 56.0, 40.3, 35.4 ppm.

HRMS (ESI(+), CH_3CN): *m/z* 627.1742 $[M+H]^+$, calculated for $C_{32}H_{32}N_2O_{10}Cl^+$: *m/z* 627.1740.

Mandi-Dopa-C4-NV (79)

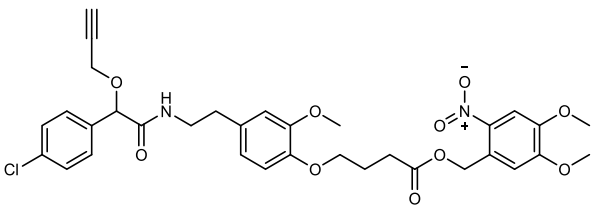

Mandi-Dopa-C4-COOH (**73**) (6.60 mg, 14.4 µmol, 1.00 eq.) was dissolved in anhydrous acetonitrile (1 ml). Then, *N*,*N*-diisopropylethylamine (DIPEA) (3.32 µl, 20.1 µmol, 1.40 eq.) and 1-(bromomethyl)-4,5-dimethoxy-2-nitrobenzene (5.55 mg, 20.1 µmol, 1.40 eq.) were added. The reaction mixture was stirred for 23 h at room temperature. The solvent was removed under reduced pressure and the crude

product was purified by preparative reverse phase HPLC (C18, acetonitrile:water gradient + 0.1 % TFA). The product was obtained as off-white solid (8.00 mg, 12.2 µmol, 85 %).

^{1}H-NMR (400.15 MHz, $CDCl_3$): δ = 7.71 (s, 1H), 7.32 (d, *J* = 8.8 Hz, 2H), 7.27 (d, *J* = 8.5 Hz, 2H), 7.00 (s, 1H), 6.79 (d, *J* = 8.0 Hz, 1H), 6.75 (t, *J* = 6.0 Hz, 1H), 6.69 – 6.65 (m, 2H), 5.53 (s, 2H), 4.96 (s, 1H), 4.21 – 3.95 (m, 2H), 4.07 (t, *J* = 6.1 Hz, 2H), 3.95 (s, 3H), 3.93 (s, 3H), 3.79 (s, 3H), 3.60 – 3.44 (m, 2H), 2.82 – 2.71 (m, 2H), 2.68 (t, *J* = 7.2 Hz, 2H), 2.48 (t, *J* = 2.4 Hz, 1H), 2.23 – 2.17 (m, 2H) ppm.

^{13}C-NMR (100.62 MHz, $CDCl_3$): δ = 172.7, 169.7, 153.6, 149.7, 148.4, 147.0, 140.2, 134.9, 134.8, 131.9, 129.0, 128.9, 127.2, 120.9, 113.8, 112.6, 110.6, 108.4, 79.8, 78.3, 76.0, 68.1, 63.4, 56.6, 56.5, 56.5, 56.0, 40.4, 35.4, 31.0, 24.8 ppm.

HRMS (ESI(+), CH_3CN): *m/z* 655.2047 $[M+H]^+$, calculated for $C_{33}H_{36}N_2O_{10}Cl^+$: *m/z* 655.2053.

Mandi-Dopa-C5-NV (80)

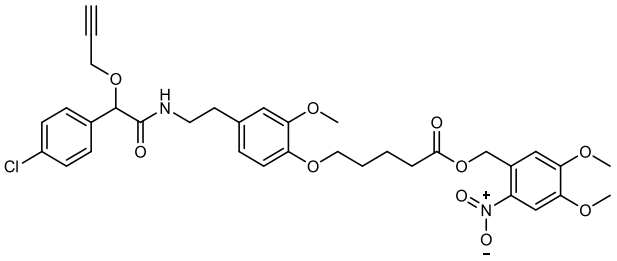

Mandi-Dopa-C5-COOH (**74**) (8.80 mg, 18.6 µmol, 1.00 eq.) was dissolved in anhydrous acetonitrile (1 ml). Then, *N*,*N*-diisopropylethylamine (DIPEA) (4.30 µl, 26.0 µmol, 1.40 eq.) and 1-(bromomethyl)-4,5-dimethoxy-2-nitrobenzene (7.18 mg, 26.0 µmol, 1.40 eq.) were added. The reaction mixture was stirred for 39 h at room temperature. The solvent was removed under reduced pressure and the crude product was purified by preparative reverse phase HPLC (C18, acetonitrile:water gradient + 0.1 % TFA). The product was obtained as off-white solid (10.5 mg, 15.7 µmol, 85 %).

^{1}H-NMR (400.15 MHz, $CDCl_3$): δ = 7.71 (s, 1H), 7.31 (d, *J* = 8.6 Hz, 2H), 7.26 (d, *J* = 8.5 Hz, 2H), 7.00 (s, 1H), 6.79 – 6.74 (m, 2H), 6.69 – 6.65 (m, 2H), 5.51 (s, 2H), 4.96 (s, 1H), 4.21 – 4.00 (m, 4H), 3.95 (d, *J* = 1.0 Hz, 6H), 3.80 (s, 3H), 3.61 – 3.45 (m, 2H), 2.82 – 2.71 (m, 2H), 2.55 – 2.51 (m, 2H), 2.48 (t, *J* = 2.4 Hz, 1H), 1.92 – 1.88 (m, 4H) ppm.

^{13}C-NMR (100.62 MHz, $CDCl_3$): δ = 172.9, 169.7, 153.6, 149.7, 148.4, 147.2, 140.2, 134.8, 134.8, 131.6, 129.0, 128.9, 127.2, 120.9, 113.5, 112.6, 110.7, 108.4, 79.8, 78.2, 76.0, 68.7, 63.3, 56.6, 56.5, 56.1, 40.4, 35.3, 34.0, 28.9, 21.8 ppm.

HRMS (ESI(+), CH_3CN): *m/z* 669.2206 $[M+H]^+$, calculated for $C_{34}H_{38}N_2O_{10}Cl^+$: *m/z* 669.2209.

OP/pOP/OP-AM

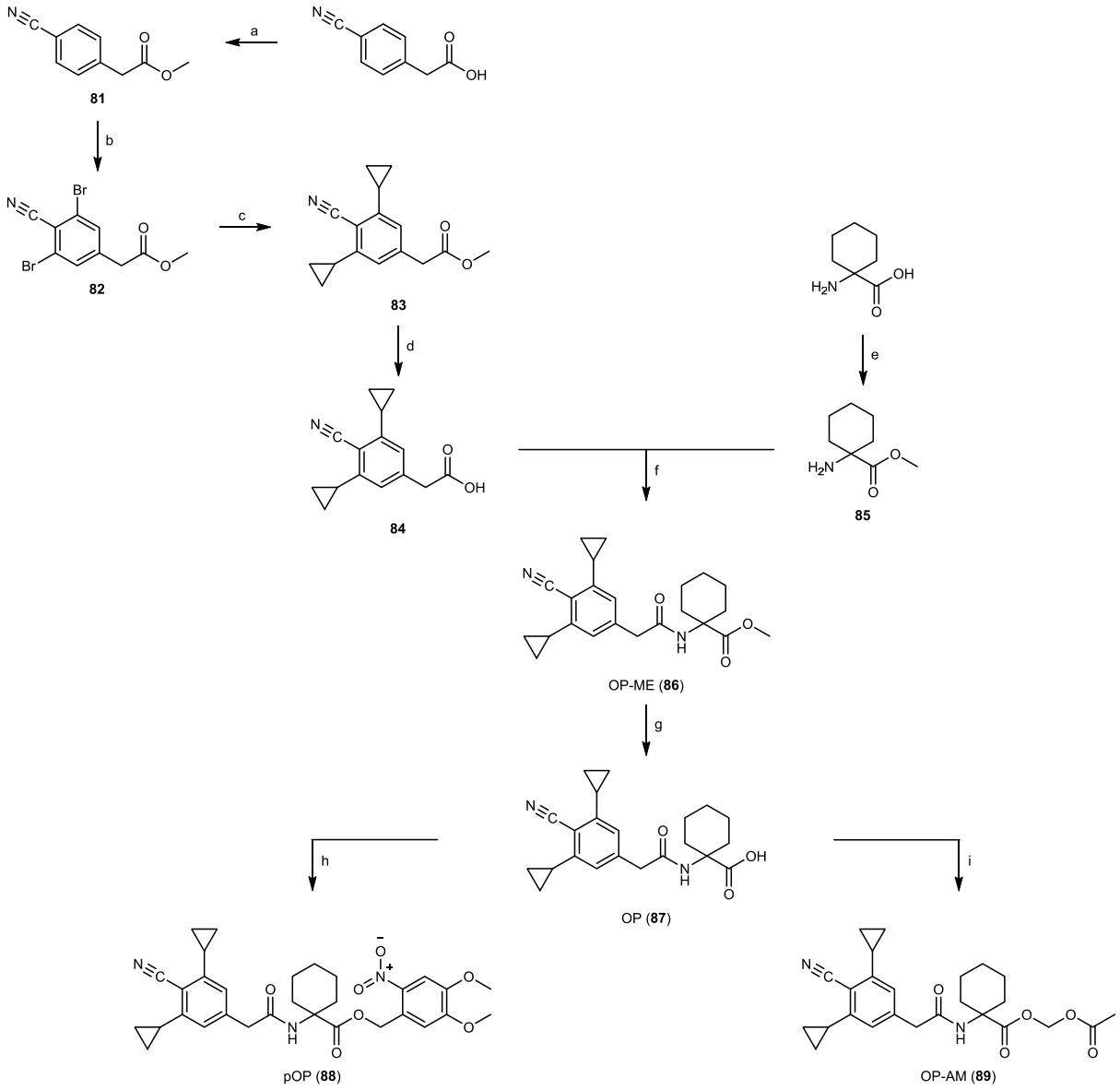

Conditions: a: MeOH, H_2SO_4, 0 °C -> rt, 2 h; b: NBS, pTsOH, $Pd(OAc)_2$, 70 °C, 21 h; c: cyclopropylboronic acid, K_3PO_4, $P(Cy)_3$, $Pd(OAc)_2$, 110 °C, 3 h; d: LiOH, rt, 16 h; e: thionyl chloride, 0 °C -> rt, 72 h; f: EDC, DMAP, rt, 16 h; g: LiOH, 50 °C, 4 h; h: 1-(bromomethyl)-4,5-dimethoxy-2-nitrobenzene, DIPEA, rt, 72 bromomethyl acetate, DIPEA, rt, 72 h.

Methyl 2-(4-cyanophenyl)acetate (81)

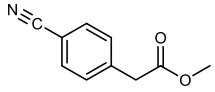

Methyl 2-(4-cyanophenyl)acetate (**81**) was synthesized by Caroline Berrou under my supervision as described in literature[89]:

2-(4-Cyanophenyl)acetic acid (616 mg, 3.82 mmol, 1.00 eq.) was dissolved in methanol (5 ml), the solution was cooled to 0 °C and sulfuric acid (224 µl, 4.20 mmol, 1.10 eq.) was added dropwise. The

reaction mixture was stirred for 1 h at 0 °C and 1 h at room temperature. Then, ice (10 g) and saturated aqueous sodium hydrogencarbonate solution (30 ml) and the mixture was extracted with dichloromethane (4 x 50 ml). The combined organic layer was dried over sodium sulphate and the solvent was removed under reduced pressure. The product was obtained as colorless oil (6.60 mg, 3.57 mmol, 92 %).

^{1}H-NMR (400.15 MHz, $CDCl_3$): δ = 7.63 (d, *J* = 8.3 Hz, 2H), 7.40 (d, *J* = 8.7 Hz, 2H), 3.71 (s, 3H), 3.69 (s, 2H) ppm.

^{13}C-NMR (100.62 MHz, $CDCl_3$): δ = 170.87, 139.37, 132.47, 130.30, 118.80, 111.35, 52.47, 41.18 ppm.

HRMS (ESI(+), CH_3CN): *m/z* 176.0707 $[M+H]^+$, calculated for $C_{10}H_{10}NO_2^+$: *m/z* 176.0706.

Methyl 2-(3,5-dibromo-4-cyanophenyl)acetate (82)

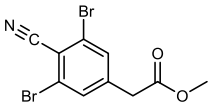

Methyl 2-(3,5-dibromo-4-cyanophenyl)acetate (**82**) was synthesized by Caroline Berrou under my supervision as described in literature[90]:

Methyl 2-(4-cyanophenyl)acetate (**81**) (616 mg, 3.52 mmol, 1.00 eq.) was dissolved in anhydrous 1,2-dichloroethane (8 ml) and *N*-bromosuccinimide (2.50 g, 14.1 mmol, 4.00 eq.), *p*-toluenesulfonic acid monohydrate (669 mg, 3.52 mmol, 1.00 eq.) as well as palladium(II) acetate (78.9 mg, 352 µmol, 0.10 eq.) were added. The reaction mixture was stirred for 21 h at 70 °C. The solvent was removed under reduced pressure and the crude product was purified by column chromatography (silica gel, n-hexane:ethyl acetate gradient). The product was obtained as colorless solid (173 mg, 520 µmol, 15 %).

^{1}H-NMR (400.15 MHz, $CDCl_3$): δ = 7.58 (s, 2H), 3.74 (s, 3H), 3.63 (s, 2H) ppm.

^{13}C-NMR (100.62 MHz, $CDCl_3$): δ = 169.80, 141.39, 132.97, 126.83, 117.78, 115.93, 52.81, 40.38 ppm.

HRMS (ESI(+), CH_3CN): *m/z* 331.8916 $[M+H]^+$, calculated for $C_{10}H_8NO_2Br_2^+$: *m/z* 331.8916.

Methyl 2-(4-cyano-3,5-dicyclopropylphenyl)acetate (83)

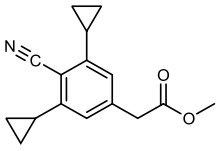

Methyl 2-(4-cyano-3,5-dicyclopropylphenyl)acetate (**83**) was synthesized by Caroline Berrou under my supervision as described in literature[51]:

Methyl 2-(3,5-dibromo-4-cyanophenyl)acetate (**82**) (249 mg, 748 µmol, 1.00 eq.), cyclopropylboronic acid (154 mg, 1.79 mmol, 2.40 eq.), potassium phosphate tribasic (540 mg, 2.54 mmol, 3.40 eq.), tricyclohexyl phosphine (21.0 mg, 74.8 µmol, 0.10 eq.) and palladium(II) acetate (8.39 mg, 37.4 µmol, 0.05 eq.) were added into a Schlenk flask under argon. Then, toluene (3.5 ml) and water (0.2 ml) were added and the reaction mixture was stirred for 3 h at 110 °C. Thereafter, brine (30 ml) was added and

the mixture was extracted with ethyl acetate (3 x 50 ml). The combined organic layer dried over sodium sulphate and the solvent removed under reduced pressure. The crude product was purified by column chromatography (silica gel, n-hexane:ethyl acetate gradient). The product was obtained as colorless oil (165 mg, 650 µmol, 87 %).

^{1}H-NMR (400.15 MHz, $CDCl_3$): δ = 6.64 (s, 2H), 3.69 (s, 3H), 3.54 (s, 2H), 2.32 – 2.24 (m), 1.16 – 1.09 (m, 4H), 0.80 – 0.73 (m, 4H) ppm.

^{13}C-NMR (100.62 MHz, $CDCl_3$): δ = 171.16, 148.41, 138.83, 132.90, 127.06, 125.66, 122.71, 117.67, 113.29, 52.40, 41.47, 14.47, 9.43 ppm.

HRMS (ESI(+), CH_3CN): *m/z* 256.1334 $[M+H]^+$, calculated for $C_{16}H_{18}NO_2^+$: *m/z* 256.1332.

2-(4-Cyano-3,5-dicyclopropylphenyl)acetic acid (84)

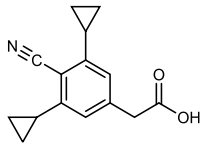

2-(4-Cyano-3,5-dicyclopropylphenyl)acetic acid (**84**) was synthesized by Caroline Berrou under my supervision as described in literature[51]:

Methyl 2-(4-cyano-3,5-dicyclopropylphenyl)acetate (**83**) (144 mg, 564 µmol, 1.00 eq.) was dissolved in methanol (1.5 ml) and water (1.5 ml) was added. Then, lithium hydroxide (67.5 mg, 2.82 mmol, 5.00 eq.) was added and the reaction mixture was stirred for 16 h at room temperature. Thereafter, hydrochloric acid (1.00 M, 5.00 ml) was added and the mixture was extracted with ethyl acetate (3 x 10 ml). The combined organic layer was dried over sodium sulphate and the solvent was removed under reduced pressure. The crude product was purified by column chromatography (silica gel, n-hexane:ethyl acetate gradient). The product was obtained as colorless solid (96.0 mg, 398 µmol, 71 %).

^{1}H-NMR (400.15 MHz, $CDCl_3$): δ = 6.65 (s, 2H), 3.58 (s, 2H), 2.34 – 2.23 (m, 2H), 1.20 – 1.06 (m, 4H), 0.85 – 0.73 (m, 4H) ppm.

^{13}C-NMR (100.62 MHz, $CDCl_3$): δ = 174.77, 148.54, 138.09, 132.96, 127.13, 125.76, 122.79, 117.56, 113.55, 41.04, 14.48, 9.47 ppm.

HRMS (ESI(+), CH_3CN): *m/z* 242.1175 $[M+H]^+$, calculated for $C_{15}H_{16}NO_2^+$: *m/z* 242.1176.

Methyl 1-aminocyclohexane-1-carboxylate (85)

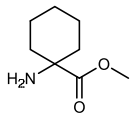

Methyl 1-aminocyclohexane-1-carboxylate (**85**) was synthesized by Caroline Berrou under my supervision as described in literature[91]:

To a solution of 1-aminocyclohexane-1-carboxylic acid (1.00 g, 6.98 mmol, 1.00 eq.) was dissolved in methanol (2 ml) and the solution was cooled to 0 °C. Then, thionyl chloride (1.52 ml, 21.0 mmol, 3.00 eq.) was added dropwise. The reaction mixture was stirred for 72 h at room temperature. The solvent was removed under reduced pressure and the residue was dissolved in water (50 ml). Saturated aqueous sodium carbonate solution (50 ml) was added to reach pH 9 and the mixture was extracted with dichloromethane (3 x 100 ml). The combined organic layer was dried over sodium sulphate and the solvent was removed under reduced pressure. The product was obtained as colorless liquid (1.08 g, 6.86 mmol, 99 %).

^{1}H-NMR (400.15 MHz, CD_3OD): δ = 3.71 (s, 3H), 2.06 – 1.90 (m, 2H), 1.71 – 1.58 (m, 2H), 1.53 – 1.39 (m, 6H) ppm.

^{13}C-NMR (100.62 MHz, CD_3OD): δ = 178.17, 58.44, 52.53, 36.35, 26.39, 23.11 ppm.

HRMS (ESI(+), CH_3CN): *m/z* 158.1175 $[M+H]^+$, calculated for $C_8H_{16}NO_2^+$: *m/z* 158.1176.

OP-ME (86)

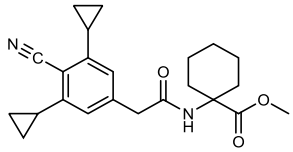

OP-ME (**86**) was synthesized by Caroline Berrou under my supervision as described in literature[51]:

2-(4-Cyano-3,5-dicyclopropylphenyl)acetic acid (**84**) (100 mg, 414 µmol, 1.00 eq.) was dissolved in anhydrous dichloromethane (3 ml) and the solution was cooled to 0 °C. Then, methyl 1-aminocyclohexane-1-carboxylate (**85**) (78.2 mg, 497 µmol, 1.20 eq.), 1-ethyl-3-(3-dimethylaminopropyl)carbodiimide hydrochloride (EDC) (95.3 mg, 497 µmol, 1.20 eq.) and 4-dimethylaminopyridine (DMAP) (60.8 mg, 497 µmol, 1.20 eq.) were added. The reaction mixture was stirred for 16 h at room temperature. Thereafter, brine (30 ml) was added and the mixture was extracted with dichloromethane (3 x 50 ml). The combined organic layer was dried over sodium sulphate. The solvent was removed under reduced pressure and the crude product was purified by column chromatography (silica gel, n-hexane:ethyl acetate gradient). The product was obtained as colorless liquid (141 mg, 371 µmol, 90 %).

^{1}H-NMR (400.15 MHz, $CDCl_3$): δ = 6.65 (s, 2H), 5.29 (s, 1H), 3.68 (s, 3H), 3.48 (s, 2H), 2.32 – 2.24 (m, 2H), 1.99 – 1.90 (m, 2H), 1.86 – 1.75 (m, 2H), 1.65 – 1.56 (m, 2H), 1.29 – 1.20 (m, 4H), 1.16 – 1.05 (m, 4H), 0.81 – 0.71 (m) ppm.

^{13}C-NMR (100.62 MHz, $CDCl_3$): δ = 174.34, 169.24, 148.75, 140.09, 140.07, 133.06, 126.84, 125.34, 122.34, 117.62, 113.18, 113.16, 59.08, 52.50, 43.99, 32.29, 25.12, 21.56, 14.46, 9.56 ppm.

HRMS (ESI(+), CH_3CN): *m/z* 381.2171 $[M+H]^+$, calculated for $C_{23}H_{29}N_2O_3^+$: *m/z* 381.2173.

OP (87)

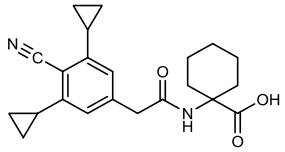

OP (**87**) was synthesized by Caroline Berrou as described in literature[51] under my supervision:

OP-ME (**86**) (61.0 mg, 160 µmol, 1.00 eq.) was dissolved in methanol (5 ml) and water (5 ml) was added. Then, lithium hydroxide (19.2 mg, 805 µmol, 5.00 eq.) was added and the reaction mixture was stirred for 40 h at 50 °C. Thereafter, hydrochloric acid (1.00 M, 10.0 ml) was added and the mixture was extracted with ethyl acetate (3 x 50 ml). The combined organic layers were dried over sodium sulphate. The solvent was removed under reduced pressure and the crude product was purified by preparative reverse phase HPLC (C18, acetonitrile:water gradient + 0.1 % TFA). The product was obtained as colorless liquid (57.0 mg, 155 µmol, 97 %).

^{1}H-NMR (400.15 MHz, CD_3OD): δ = 8.15 (s, 1H), 6.79 (s, 2H), 3.51 (s, 2H), 2.26 – 2.20 (m, 2H), 2.08 – 2.03 (m, 2H), 1.84 – 1.76 (m, 2H), 1.64 – 1.58 (m, 2H), 1.50 – 1.29 (m, 4H), 1.13 – 1.08 (m, 4H), 0.83 – 0.79 (m, 4H) ppm.

^{13}C-NMR (100.62 MHz, CD_3OD): δ = 177.7, 172.6, 149.4, 142.8, 123.3, 118.4, 112.9, 60.3, 60.3, 43.7, 43.7, 33.2, 33.2, 26.4, 22.5, 15.1, 9.7 ppm.

HRMS (ESI(+), CH_3CN): *m/z* 367.2015 $[M+H]^+$, calculated for $C_{22}H_{27}N_2O_3^+$: *m/z* 367.2016.

pOP (88)

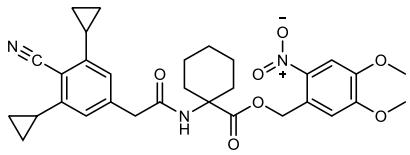

pOP (**88**) was synthesized by Caroline Berrou under my supervision:

OP (**87**) (25.0 mg, 68.2 µmol, 1.00 eq.) was dissolved in anhydrous acetonitrile (6 ml). Then, *N*,*N*-diisopropylethylamine (DIPEA) (12.3 mg, 15.8 µl, 95.5 µmol, 1.40 eq.) and 1-(bromomethyl)-4,5-dimethoxy-2-nitrobenzene (26.4 mg, 95.5 µmol, 1.40 eq.) were added and the reaction mixture was stirred for 72 h at room temperature. The solvent was removed in vacuo and the crude product was

purified by preparative reverse phase HPLC (C18, acetonitrile:water gradient + 0.1 % TFA). The product was obtained as an off-white solid (10.0 mg, 17.8 µmol, 26 %).

^{1}H-NMR (400.15 MHz, $CDCl_3$): δ = 7.70 (s, 1H), 7.06 (s, 1H), 6.61 (s, 2H), 5.56 (s, 2H), 5.54 (s, 1H), 3.97 (s, 3H), 3.96 (s, 3H), 3.49 (s, 2H), 2.30 – 2.23 (m, 2H), 2.07 – 2.03 (m, 2H), 1.90 – 1.83 (m, 2H), 1.68 – 1.59 (m, 2H), 1.32 – 1.19 (m, 4H), 1.14 – 1.09 (m, 4H), 0.75 – 0.71 (m, 4H) ppm.

^{13}C-NMR (100.62 MHz, $CDCl_3$): δ = = 173.7, 169.8, 154.0, 148.9, 148.4, 139.8, 139.7, 127.5, 122.4, 117.5, 113.3, 110.9, 108.2, 64.5, 59.5, 56.9, 56.6, 43.9, 32.4, 25.1, 21.6, 14.5, 9.6 ppm.

HRMS (ESI(+), CH_3CN): *m/z* 562.2549 $[M+H]^+$, calculated for $C_{31}H_{36}N_3O_7^+$: *m/z* 562.2548.

OP-AM (89)

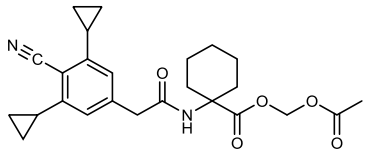

OP-AM (**89**) was synthesized by Caroline Berrou under my supervision:

OP (**88**) (25.0 mg, 68.2 µmol, 1.00 eq.) was dissolved in anhydrous acetonitrile (4 ml) Then, *N*,*N*-diisopropylethylamine (DIPEA) (12.3 mg, 15.8 µl, 95.5 µmol, 1.40 eq.) and bromomethyl acetate (14.6 mg, 9.37 µl, 95.5 µmol, 1.40 eq.) were added and the reaction mixture was stirred for 72 h at room temperature. The solvent was removed in vacuo and the crude product was purified by preparative reverse phase HPLC (C18, acetonitrile:water gradient + 0.1 % TFA). The product was obtained as a colorless solid (8.00 mg, 18.2 µmol, 27 %).

^{1}H-NMR (400.15 MHz, CD_3OD): δ = 8.29 (s, 1H), 6.77 (s, 2H), 5.65 (s, 2H), 3.48 (s, 2H), 2.27 – 2.20 (m, 2H), 1.99 – 1.94 (m, 5H), 1.84 – 1.77 (m, 2H), 1.64 – 1.58 (m, 2H), 1.52 – 1.29 (m, 4H), 1.14 – 1.09 (m, 4H), 0.84 – 0.80 (m, 4H) ppm.

^{13}C-NMR (100.62 MHz, CD_3OD): δ = 174.2, 172.4, 171.1, 149.4, 142.5, 123.5, 118.4, 113.1, 80.6, 60.1, 43.4, 33.1, 26.2, 22.4, 20.5, 15.1, 9.7 ppm.

HRMS (ESI(+), CH_3CN): *m/z* 439.2227 $[M+H]^+$, calculated for $C_{25}H_{31}N_2O_5^+$: *m/z* 439.2227.

ABA-AM

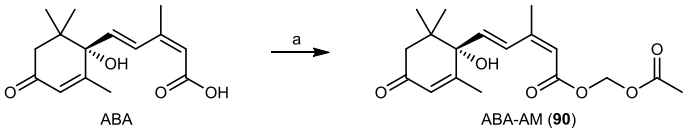

ABA ABA-AM (**90**)

Condition: a: bromomethyl acetate, Et_3N, rt, 24 h.

ABA-AM (90)

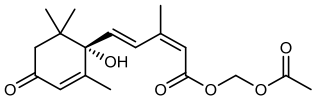

ABA-AM (**90**) was synthesized by Caroline Berrou under my supervision as described in literature[54]: (+)-(*S*)-Abscisic acid (ABA) (10.0 mg, 37.8 µmol, 1.00 eq.) was dissolved in anhydrous acetonitrile (1 ml). Then, bromomethyl acetate (4.82 µl, 49.2 µmol, 1.30 eq.) and triethylamine (6.84 µl, 49.2 µmol, 1.30 eq.) were added and the reaction mixture was stirred for 24 h at room temperature. The solvent was removed under reduced pressure and the crude product was purified by preparative reverse phase HPLC (C18, acetonitrile:water gradient + 0.1 % TFA). The product was obtained as colorless solid (9.60 mg, 28.5 µmol, 76 %).

^{1}H-NMR (400.15 MHz, CD_3OD): δ = 7.80 (d, *J* = 16.1 Hz, 1H), 6.35 (d, *J* = 16.1 Hz, 1H), 5.94 (s, 1H), 5.77 (s, 1H), 5.75 (s, 2H), 2.54 (d, *J* = 17.0 Hz, 1H), 2.20 (d, *J* = 16.9 Hz, 1H), 2.08 (s, 6H), 1.94 (d, *J* = 1.3 Hz, 3H), 1.07 (s, 3H), 1.03 (s, 3H) ppm.

^{13}C-NMR (100.62 MHz, C_2D_6OS): δ = 198.1, 170.3, 164.6, 163.8, 154.6, 140.7, 127.7, 127.0, 116.3, 79.7, 79.3, 50.2, 42.2, 25.1, 24.1, 21.9, 21.5, 19.7 ppm.

HRMS (ESI(+), CH_3CN): *m/z* 337.1650 $[M+H]^+$, calculated for $C_{18}H_{25}O_6^+$: *m/z* 337.1646.

5.1.4 Compound stock preparation

For in vivo, in cellulo or in vitro characterization all compounds were dissolved in DMSO and DMSO stock solutions with 10-fold different concentrations were prepared (e.g. 10 mM, 1 mM…).

5.2 Protein expression

Protein expression was performed by the protein expression and characterization core facility of the Max Planck Institute for Medical Research.

DNA sequences encoding the proteins PYR^{Mandi} and ABI were amplified by PCR and cloned using In-Fusion (Takara Bio) cloning method into pOPINS3C vector (Addgene Plasmid #41115). All constructs were verified by Sanger sequencing (Eurofins).

The vectors were transformed into *E. coli* BL21 CodonPlus(DE3)-RIL (Agilent). Cells were grown at 37 °C in LB medium supplemented with ampicillin (100 µg/ml) and chloramphenicol (30 µg/ml). At an optical density (OD) at 600 nm of 0.8-1.0, cells were transferred to 18 °C and expression was induced with 0.1 mM isopropyl β-D-1-thiogalactopyranoside (IPTG). Cells were harvested after overnight expression by centrifugation, frozen in liquid nitrogen and stored at -80°C until further use. All subsequent purification steps were done at 4 °C.

The cell pellets were resuspended in lysis buffer (50 mM NaH_2PO_4 pH 8.0, 300 mM NaCl, 10 mM imidazole, 10 % (v/v) glycerol) supplemented with complete EDTA-free protease inhibitors (Roche), 1 mg/ml lysozyme, 20 µg/ml DNaseI, 5 mM DTE. The cells were lysed using a sonifier (Branson Ultrasonics) and the lysates were clarified by centrifugation at 47850 g for 1 h at 4 °C. The cleared supernatants were loaded onto a HisTrap FF 5 ml (Cytiva) column pre-equilibrated with lysis buffer. The column was washed with 50 mM NaH_2PO_4 pH 8.0, 300 mM NaCl, 30 mM imidazole, 10 % (v/v) glycerol and the protein was eluted with 50 mM NaH_2PO_4 pH 8.0, 300 mM NaCl, 500 mM imidazole, 10 % (v/v) glycerol. The eluate was supplemented with HRV 3C protease and dialyzed against 20 mM HEPES pH 7.5, 200 mM NaCl, 5 mM $MgCl_2$, 2 mM DTE, 10 % (v/v) glycerol overnight at 4 °C. The cleaved protein was applied onto a subtractive Protino Ni-NTA (Macherey-Nagel) column, the flowthrough was collected, concentrated using Amicon Ultra (Merck Millipore) centrifugal units and loaded onto a HiLoad 16/600 Superdex 200 pg (Cytiva) size-exclusion chromatography column equilibrated with 20 mM HEPES pH 7.5, 200 mM NaCl, 5 mM $MgCl_2$, 2 mM DTE, 10 % (v/v) glycerol. The selected fractions were finally combined and concentrated in 20 mM HEPES pH 7.5, 200 mM NaCl, 5 mM $MgCl_2$, 2 mM DTE, 10 % (v/v) glycerol. Aliquots were flash-frozen in liquid nitrogen and stored at -80 °C. Purified proteins were analyzed by ESI-MS.

Amino acid sequences of the expressed proteins:

PYR^{Mandi}

(UniProtKB entry O49686 – abscisic acid receptor PYR1 (Y58H/K59R/V81I/F108A/S122G/F159L))

GPMPSELTPE ERSELKNSIA EFHTYQLDPG SCSSLHAQRI HAPPELVWSI VRRFDKPQTH
RHFIKSCSVE QNFEMRVGCT RDIIVISGLP ANTSTERLDI LDDERRVTGA SIIGGEHRLT
NYKGVTTVHR FEKENRIWTV VLESYVVDMP EGNSEDDTRM LADTVVKLNL QKLATVAEAM
ARNSGDGSGS QVT

(extra vector-derived residues are underlined)

ABI

(UniProtKB entry P49597 – protein phosphatase 2C 56 – ABI1 (amino acids 126-423, D143A))

GPVPLYGFTS ICGRRPEMEA AVSTIPRFLQ SSSGSMLDGR FDPQSAAHFF GVYDGHGGSQ
VANYCRERMH LALAEEIAKE KPMLCDGDTW LEKWKKALFN SFLRVDSEIE SVAPETVGST
SVVAVVFPSH IFVANCGDSR AVLCRGKTAL PLSVDHKPDR EDEAARIEAA GGKVIQWNGA
RVFGVLAMSR SIGDRYLKPS IIPDPEVTAV KRVKEDDCLI LASDGVWDVM TDEEACEMAR
KRILLWHKKN AVAGDASLLA DERRKEGKDP AAMSAAEYLS KLAIQRGSKD NISVVVVDLK

(extra vector-derived residues are underlined)

5.3 ITC

ITC experiments were performed on a MicroCal PEAQ-ITC (Malvern Panalytical) with the data MicroCal PEAQ-ITC Acquisition Software (v1.41) and analyzed with the MicroCal PEAQ-ITC Analysis Software (v1.41).

One day prior the ITC experiments, aliquots of the protein solutions were thawed and dialyzed against 50 mM HEPES pH 7.3, 50 mM NaCl overnight at 7 °C using a Slide-A-Lyzer MINI Dialysis Unit (10 kDa cutoff, Thermo Fisher Scientific Inc.).

The titration experiments were performed at 35 °C in a series of a single 0.4 µl injection, followed by 18 injections of 2 µl.

Titration experiments with both proteins PYR^{Mandi} and ABI present at the same time, were conducted as forward titrations (ligand into protein):

Titrations of ligand into a 1:1 protein mixture of PYR^{Mandi} and ABI were performed with solutions of 20 µM ligand (from DMSO stock) and 100 µM protein in dialysis buffer with 0.5 % DMSO, respectively. Injections of buffer into the proteins PYR^{Mandi} and ABI were indistinguishable from ligand to buffer and buffer to buffer injections. The mathematical fit was conducted with a fitted offset. The number of binding sites was set to 1 and the ligand concentration was given a fixed number. Hence, the protein concentration (correction for inactive protein), binding enthalpy and binding affinity were treated as variables. The first single 0.4 µl injection was excluded.

Because of lower binding affinity and ligand solubility issues at higher concentrations, titration experiments with only the PYR^{Mandi} protein were conducted as reverse titrations (protein into ligand):

Titrations of PYR^{Mandi} protein into ligand were performed with solutions of 50 µM ligand (from DMSO stock) and 500 µM protein in dialysis buffer with 1 % DMSO, respectively.

Injection of buffer into ligand were indistinguishable from buffer to buffer injections, whereas injections of PYR^{Mandi} protein into buffer were slightly endothermic. The mathematical fit was conducted with a prior correction of the PYR^{Mandi} protein into ligand titration with the corresponding reference titrations. The number of binding sites was set to 1 and the ligand concentration was given a fixed number. Hence, the protein concentration (correction for inactive protein), binding enthalpy and binding affinity were treated as variables. The first single 0.4 µl injection was excluded.

5.4 In vitro irradiation experiments

For in vitro irradiation experiments solutions of the compounds were prepared with a concentration of 20 µM in a 1:1 mixture of acetonitrile and PBS containing 2 % of DMSO. The solutions were prepared from stock solutions in DMSO of a concentration of 1 mM and diluted with equal amounts of acetonitrile and PBS to a total volume of 1 ml.

The UV/Vis measurements were performed with a V-770 UV-Visible-Near Infrared Spectrophotometer (Jasco) in appropriate cuvettes with a total volume of 1 ml.

Irradiation was performed with a SOLIS-365C LED (Thorlabs, nominal wavelength 365 nm, bandwidth (FWHM) 10 nm) and a SOLIS-405C LED (Thorlabs, nominal wavelength 405 nm, bandwidth (FWHM) 14 nm) controlled with a DC2200 driver (Thorlabs) and a photocurrent of 100 mA or 1000 mA.

The light source for irradiation was connected via a light guide to the top of the cuvette that was placed in the spectrometer. The samples were irradiated stepwise und the UV/Vis spectra were recorded between the individual irradiation periods.

For HPLC analysis the whole sample volume was injected into an UltiMate 3000 HPLC system (Thermo Fisher Scientific Inc.) equipped with an Ascentis C18 column (Supleco, 25 cm x 10 mm, 5 µm).

A gradient acetonitrile:water + 0.1 % TFA from 90:10 to 10:90 was used and the absorption was detected from 200 nm to 800 nm over time (bandwidth 2 nm). The HPLC traces are shown at the absorption maxima of the compounds. A flow rate of 4 ml/min was used.

5.5 Cloning and plasmid preparation

For the construction of plasmids, fragments were amplified by PCR from appropriate sources with primers purchased from Sigma-Aldrich. The PCR reaction mixture was digested with DpnI (Thermo Fisher Scientific Inc.), analyzed by agarose gel electrophoresis and purified using the QIAquick PCR Purification Kit (Qiagen). Then, Gibson Assembly was performed and plasmids were purified using the QIAprep Spin Miniprep Kit (Qiagen). The plasmid sequences were validated by Sanger sequencing (Eurofins) using standard and custom-made primers or whole plasmid sequencing (Eurofins). Plasmids marked with (*) were ordered from GeneArt (Thermo Fisher Scientific Inc.).

List of plasmids:

Coding sequence (CDS)	Plasmid backbone
TOMM20-mCherry-PYR^{Mandi}-P2A-eGFP-ABI	pcDNA5/FRT
TOMM20-mCherry-PYL-P2A-eGFP-ABI	pcDNA5/FRT
TOMM20-eGFP-PYR^{Mandi}	pcDNA5/FRT
TOMM20-mCherry-PYR^{Mandi}-P2A-eGFP-ABIaid	pcDNA5/FRT
eGFP-ABI	pcDNA5/FRT
TOMM20-mCherry-PYR^{Mandi}1-132	pcDNA5/FRT
TOMM20-mCherry-PYR^{Mandi}133-191	pcDNA5/FRT
mCherry-PYR^{Mandi}133-191-P2A-eGFP-ABI-P2A-TOMM20-Halo-PYR^{Mandi}1-132	pcDNA5/FRT
mCherry-FRB-PYR^{Mandi}133-191-P2A-eGFP-ABI-P2A-TOMM20-Halo-FKBP12-PYR^{Mandi}1-132	pcDNA5/FRT
PYR^{Mandi}1-86-cLuc-HA (*)	pcDNA3.1(+)
MYC-nLuc-PYR^{Mandi}87-191	pcDNA3.1(+)
PYR^{Mandi}1-102-cLuc-HA (*)	pcDNA3.1(+)
MYC-nLuc-PYR^{Mandi}103-191	pcDNA3.1(+)
PYR^{Mandi}1-114-cLuc-HA (*)	pcDNA3.1(+)
MYC-nLuc-PYR^{Mandi}115-191	pcDNA3.1(+)
PYR^{Mandi}1-132-cLuc-HA (*)	pcDNA3.1(+)
MYC-nLuc-PYR^{Mandi}133-191	pcDNA3.1(+)
PYR^{Mandi}1-149-cLuc-HA (*)	pcDNA3.1(+)
MYC-nLuc-PYR^{Mandi}150-191 (*)	pcDNA3.1(+)
Insert_removed	pcDNA3.1(+)
ABI	pcDNA3.1(+)
eGFP-ABI	pCS2+
Lyn-mCherry-PYR^{Mandi}	pCS2+
Lyn-mCherry-PYL	pCS2+

List of sequences of the gene fragments:

Name	TOMM20
Sequence (5’-3’)	ATGGGTCGGAACAGCGCCATCGCCGCGGGCGTGTGCGGTGCCCTCTTCATAGGGTACTGCATCTACTTTGACCGCAAAAGACGAAGTGACCCCAACTTC
Name	Lyn
Sequence (5’-3’)	ATGGGATGTATTAAATCAAAAAGGAAAGAC

Name	mCherry
Sequence (5’-3’)	ATGGTGAGCAAGGGCGAGGAGGATAACATGGCCATCATCAAGGAGTTCATGCGCTTCAAGG TGCACATGGAGGGCTCCGTGAACGGCCACGAGTTCGAGATCGAGGGCGAGGGCGAGGGCC GCCCCTACGAGGGCACCCAGACCGCCAAGCTGAAGGTGACCAAGGGTGGCCCCCTGCCCTTC GCCTGGGACATCCTGTCCCCTCAGTTCATGTACGGCTCCAAGGCCTACGTGAAGCACCCCGCC GACATCCCCGACTACTTGAAGCTGTCCTTCCCCGAGGGCTTCAAGTGGGAGCGCGTGATGAA CTTCGAGGACGGCGGCGTGGTGACCGTGACCCAGGACTCCTCCCTGCAGGACGGCGAGTTC ATCTACAAGGTGAAGCTGCGCGGCACCAACTTCCCCTCCGACGGCCCCGTAATGCAGAAGAA GACCATGGGCTGGGAGGCCTCCTCCGAGCGGATGTACCCCGAGGACGGCGCCCTGAAGGGC GAGATCAAGCAGAGGCTGAAGCTGAAGGACGGCGGCCACTACGACGCTGAGGTCAAGACC ACCTACAAGGCCAAGAAGCCCGTGCAGCTGCCCGGCGCCTACAACGTCAACATCAAGTTGGA CATCACCTCCCACAACGAGGACTACACCATCGTGGAACAGTACGAACGCGCCGAGGGCCGCC ACTCCACCGGCGGCATGGACGAACTGTACAAG
Name	eGFP
Sequence (5’-3’)	ATGGTGAGCAAGGGCGAGGAGCTGTTCACCGGGGTGGTGCCCATCCTGGTCGAGCTGGACG GCGACGTAAACGGCCACAAGTTCAGCGTGTCCGGCGAGGGCGAGGGCGATGCCACCTACGG CAAGCTGACCCTGAAGTTCATCTGCACCACCGGCAAGCTGCCCGTGCCCTGGCCCACCCTCGT GACCACCCTGACCTACGGCGTGCAGTGCTTCAGCCGCTACCCCGACCACATGAAGCAGCACG ACTTCTTCAAGTCCGCCATGCCCGAAGGCTACGTCCAGGAGCGCACCATCTTCTTCAAGGACG ACGGCAACTACAAGACCCGCGCCGAGGTGAAGTTCGAGGGCGACACCCTGGTGAACCGCAT CGAGCTGAAGGGCATCGACTTCAAGGAGGACGGCAACATCCTGGGGCACAAGCTGGAGTAC AACTACAACAGCCACAACGTCTATATCATGGCCGACAAGCAGAAGAACGGCATCAAGGTGA ACTTCAAGATCCGCCACAACATCGAGGACGGCAGCGTGCAGCTCGCCGACCACTACCAGCAG AACACCCCCATCGGCGACGGCCCCGTGCTGCTGCCCGACAACCACTACCTGAGCACCCAGTC CGCCCTGAGCAAAGACCCCAACGAGAAGCGCGATCACATGGTCCTGCTGGAGTTCGTGACCG CCGCCGGGATCACTCTCGGCATGGACGAGCTGTACAAG
Name	PYR^{Mandi} (PYR1, Y58H/K59R/V81I/F108A/S122G/F159L)
Sequence (5’-3’)	ATGCCATCTGAATTGACCCCTGAGGAACGCTCCGAATTGAAAAATTCAATCGCCGAATTCCAT ACCTATCAGCTCGACCCCGGATCTTGCAGTTCACTGCATGCACAGCGCATCCACGCGCCCCCA GAATTGGTGTGGTCTATCGTTCGCCGCTTTGACAAACCCCAAACGCACCGGCACTTCATAAAG TCATGTTCAGTTGAACAGAATTTCGAAATGCGAGTGGGCTGCACCAGAGATATAATAGTAAT ATCCGGTCTCCCTGCAAATACATCCACGGAGCGACTGGACATACTTGACGATGAAAGAAGAG TTACGGGCGCTTCTATAATTGGGGGCGAACACCGGCTGACTAACTATAAGGGCGTCACAACC GTTCACCGCTTCGAGAAGGAAAACCGCATCTGGACTGTAGTGTTGGAAAGCTATGTAGTGGA TATGCCTGAAGGAAATTCTGAAGACGACACTAGGATGCTTGCGGATACAGTCGTCAAACTTA ACCTCCAGAAACTTGCTACTGTAGCGGAGGCTATGGCCCGGAACTCAGGTGATGGCTCTGGC AGCCAGGTCACG
Name	PYL (PYL1, amino acids 33-209)[52]
Sequence (5’-3’)	ACTCAAGACGAATTCACCCAACTCTCCCAATCAATCGCCGAGTTCCACACGTACCAACTCGGT AACGGCCGTTGCTCATCTCTCCTAGCTCAGCGAATCCACGCGCCGCCGGAAACAGTATGGTC CGTGGTGAGACGTTTCGATAGGCCACAGATTTACAAACACTTCATCAAAAGCTGTAACGTGA GTGAAGATTTCGAGATGCGAGTGGGATGCACGCGCGACGTGAACGTGATAAGTGGATTACC GGCGAATACGTCTCGAGAGAGATTAGATCTGTTGGACGATGATCGGAGAGTGACTGGGTTT AGTATAACCGGTGGTGAACATAGGCTGAGGAATTATAAATCGGTTACGACGGTTCATAGATT TGAGAAAGAAGAAGAAGAAGAAAGGATCTGGACCGTTGTTTTGGAATCTTATGTTGTTGATG TACCGGAAGGTAATTCGGAGGAAGATACGAGATTGTTTGCTGATACGGTTATTAGATTGAAT CTTCAGAAACTTGCTTCGATCACTGAAGCTATGAAC

Name	ABI (ABI1, amino acids 126-423, D143A)
Sequence (5’-3’)	GTGCCTTTGTATGGTTTTACTTCGATTTGTGGAAGAAGACCTGAGATGGAAGCTGCTGTTTCG ACTATACCAAGATTCCTTCAATCTTCCTCTGGTTCGATGTTAGATGGTCGGTTTGATCCTCAAT CCGCCGCTCATTTCTTCGGTGTTTACGACGGCCATGGCGGTTCTCAGGTAGCGAACTATTGTA GAGAGAGGATGCATTTGGCTTTGGCGGAGGAGATAGCTAAGGAGAAACCGATGCTCTGCGA TGGTGATACGTGGCTGGAGAAGTGGAAGAAAGCTCTTTTCAACTCGTTCCTGAGAGTTGACT CGGAGATTGAGTCAGTTGCGCCGGAGACGGTTGGGTCAACGTCGGTGGTTGCCGTTGTTTTC CCGTCTCACATCTTCGTCGCTAACTGCGGTGACTCTAGAGCCGTTCTTTGCCGCGGCAAAACT GCACTTCCATTATCCGTTGACCATAAACCGGATAGAGAAGATGAAGCTGCGAGGATTGAAGC CGCAGGAGGGAAAGTGATTCAGTGGAATGGAGCTCGTGTTTTCGGTGTTCTCGCCATGTCGA GATCCATTGGCGATAGATACTTGAAACCATCCATCATTCCTGATCCGGAAGTGACGGCTGTGA AGAGAGTAAAAGAAGATGATTGTCTGATTTTGGCGAGTGACGGGGTTTGGGATGTAATGAC GGATGAAGAAGCGTGTGAGATGGCAAGGAAGCGGATTCTCTTGTGGCACAAGAAAAACGC GGTGGCTGGGGATGCATCGTTGCTCGCGGATGAGCGGAGAAAGGAAGGGAAAGATCCTGC GGCGATGTCCGCGGCTGAGTATTTGTCAAAGCTGGCGATACAGAGAGGAAGCAAAGACAAC ATAAGTGTGGTGGTGGTTGATTTGAAG
Name	ABIaid (ABI1, amino acids 279-327)
Sequence (5’-3’)	CATAAACCGGATAGAGAAGATGAAGCTGCGAGGATTGAAGCCGCAGGAGGGAAAGTGATT CAGTGGAATGGAGCTCGTGTTTTCGGTGTTCTCGCCATGTCGAGATCCATTGGCGATAGATA CTTGAAACCATCCATCATTCCTGAT
Name	Halo
Sequence (5’-3’)	ATGGGATCCGAAATCGGTACTGGCTTTCCATTCGACCCCCATTATGTGGAAGTCCTGGGCGA GCGCATGCACTACGTCGATGTTGGTCCGCGCGATGGCACCCCTGTGCTGTTCCTGCACGGTA ACCCGACCTCCTCCTACGTGTGGCGCAACATCATCCCGCATGTTGCACCGACCCATCGCTGCA TTGCTCCAGACCTGATCGGTATGGGCAAATCCGACAAACCAGACCTGGGTTATTTCTTCGACG ACCACGTCCGCTTCATGGATGCCTTCATCGAAGCCCTGGGTCTGGAAGAGGTCGTCCTGGTC ATTCACGACTGGGGCTCCGCTCTGGGTTTCCACTGGGCCAAGCGCAATCCAGAGCGCGTCAA AGGTATTGCATTTATGGAGTTCATCCGCCCTATCCCGACCTGGGACGAATGGCCAGAATTTGC CCGCGAGACCTTCCAGGCCTTCCGCACCACCGACGTCGGCCGCAAGCTGATCATCGATCAGA ACGTTTTTATCGAGGGTACGCTGCCGATGGGTGTCGTCCGCCCGCTGACTGAAGTCGAGATG GACCATTACCGCGAGCCGTTCCTGAATCCTGTTGACCGCGAGCCACTGTGGCGCTTCCCAAAC GAGCTGCCAATCGCCGGTGAGCCAGCGAACATCGTCGCGCTGGTCGAAGAATACATGGACT GGCTGCACCAGTCCCCTGTCCCGAAGCTGCTGTTCTGGGGCACCCCAGGCGTTCTGATCCCAC CGGCCGAAGCCGCTCGCCTGGCCAAAAGCCTGCCTAACTGCAAGGCTGTGGACATCGGCCCG GGTCTGAATCTGCTGCAAGAAGACAACCCGGACCTGATCGGCAGCGAGATCGCGCGCTGGC TGTCTACTCTGGAGATTTCCGGT
Name	cLuc (fLuc, amino acids 492-550)
Sequence (5’-3’)	ACCATGACCGAGAAGGAGATCGTGGACTATGTGGCCAGCCAGGTTACAACCGCCAAGAAGC TGCGCGGTGGTGTTGTGTTCGTGGACGAGGTGCCTAAAGGACTGACCGGCAAGTTGGACGC CCGCAAGATCCGCGAGATTCTCATTAAGGCCAAGAAGGGCGGCAAGATCGCCGTG

Name	nLuc (fLuc, amino acids 2-491)
Sequence (5’-3’)	GAAGATGCCAAAAACATTAAGAAGGGCCCAGCGCCATTCTACCCACTCGAAGACGGGACCG CCGGCGAGCAGCTGCACAAAGCCATGAAGCGCTACGCCCTGGTGCCCGGCACCATCGCCTTT ACCGACGCACATATCGAGGTGGACATTACCTACGCCGAGTACTTCGAGATGAGCGTTCGGCT GGCAGAAGCTATGAAGCGCTATGGGCTGAATACAAACCATCGGATCGTGGTGTGCAGCGAG AATAGCTTGCAGTTCTTCATGCCCGTGTTGGGTGCCCTGTTCATCGGTGTGGCTGTGGCCCCA GCTAACGACATCTACAACGAGCGCGAGCTGCTGAACAGCATGGGCATCAGCCAGCCCACCGT CGTATTCGTGAGCAAGAAAGGGCTGCAAAAGATCCTCAACGTGCAAAAGAAGCTACCGATC ATACAAAAGATCATCATCATGGATAGCAAGACCGACTACCAGGGCTTCCAAAGCATGTACAC CTTCGTGACTTCCCATTTGCCACCCGGCTTCAACGAGTACGACTTCGTGCCCGAGAGCTTCGA CCGGGACAAAACCATCGCCCTGATCATGAACAGTAGTGGCAGTACCGGATTGCCCAAGGGC GTAGCCCTACCGCACCGCACCGCTTGTGTCCGATTCAGTCATGCCCGCGACCCCATCTTCGGC AACCAGATCATCCCCGACACCGCTATCCTCAGCGTGGTGCCATTTCACCACGGCTTCGGCATG TTCACCACGCTGGGCTACTTGATCTGCGGCTTTCGGGTCGTGCTCATGTACCGCTTCGAGGAG GAGCTATTCTTGCGCAGCTTGCAAGACTATAAGATTCAATCTGCCCTGCTGGTGCCCACACTA TTTAGCTTCTTCGCTAAGAGCACTCTCATCGACAAGTACGACCTAAGCAACTTGCACGAGATC GCCAGCGGCGGGGCGCCGCTCAGCAAGGAGGTAGGTGAGGCCGTGGCCAAACGCTTCCACC TACCAGGCATCCGCCAGGGCTACGGCCTGACAGAAACAACCAGCGCCATTCTGATCACCCCC GAAGGGGACGACAAGCCTGGCGCAGTAGGCAAGGTGGTGCCCTTCTTCGAGGCTAAGGTG GTGGACTTGGACACCGGTAAGACACTGGGTGTGAACCAGCGCGGCGAGCTGTGCGTCCGTG GCCCCATGATCATGAGCGGCTACGTTAACAACCCCGAGGCTACAAACGCTCTCATCGACAAG GACGGCTGGCTGCACAGCGGCGACATCGCCTACTGGGACGAGGACGAGCACTTCTTCATCGT GGACCGGCTGAAGAGCCTGATCAAATACAAGGGCTACCAGGTAGCCCCAGCCGAACTGGAG AGCATCCTGCTGCAACACCCCAACATCTTCGACGCCGGGGTCGCCGGCCTGCCCGACGACGA TGCCGGCGAGCTGCCCGCCGCAGTCGTCGTGCTGGAACACGGTAAA
Name	FRB (FRAP, amino acids 2020-2113)
Sequence (5’-3’)	GCTATCCTCTGGCATGAGATGTGGCATGAAGGCCTGGAAGAGGCATCTCGTTTGTACTTTGG GGAAAGGAACGTGAAAGGCATGTTTGAGGTGCTGGAGCCCTTGCATGCTATGATGGAACGG GGCCCCCAGACTCTGAAGGAAACATCCTTTAATCAGGCCTATGGTCGAGATTTAATGGAGGC CCAAGAGTGGTGCAGGAAGTACATGAAATCAGGGAATGTCAAGGACCTCCTCCAAGCCTGG GACCTCTATTATCATGTGTTCCGACGAATCTCAAAA
Name	FKBP12
Sequence (5’-3’)	ATGGGAGTGCAGGTGGAAACCATCTCCCCAGGAGACGGGCGCACCTTCCCCAAGCGCGGCC AGACCTGCGTGGTGCACTACACCGGGATGCTTGAAGATGGAAAGAAATTTGATTCCTCCCGG GACAGAAACAAGCCCTTTAAGTTTATGCTAGGCAAGCAGGAGGTGATCCGAGGCTGGGAAG AAGGGGTTGCCCAGATGAGTGTGGGTCAGAGAGCCAAACTGACTATATCTCCAGATTATGCC TATGGTGCCACTGGGCACCCAGGCATCATCCCACCACATGCCACTCTCGTCTTCGATGTGGAG CTTCTAAAACTGGAA
Name	Linker-P2A-Linker
Sequence (5’-3’)	GGCTCTGGTGCCACAAACTTCTCTCTGCTAAAGCAAGCAGGTGATGTTGAAGAAAACCCCGG GCCTGGCGGTTCT
Name	Flexible linker between TOMM20 and mCherry and between Lyn and mCherry
Sequence (5’-3’)	GGATCCGGAGCAAGTGGA

Name	Flexible linker between eGFP and ABI
Sequence (5’-3’)	AGCGCAGGAGGAACGCGT
Name	Flexible linker between mCherry and PYR^{Mandi} and between mCherry and PYL
Sequence (5’-3’)	AGCGCAGGAGGACCA
Name	Flexible linker between eGFP and ABIaid, as well as before and after PYR^{Mandi}X-Y, Halo, FRB, and FKBP12
Sequence (5’-3’)	GGCGGCTCTGGCGGCGGCTCCGGAGGCTCT
Name	MYC-Linker
Sequence (5’-3’)	ATGGAGCAGAAGCTGATCAGCGAGGAGGACCTGGGTTCTGGA
Name	Linker-HA
Sequence (5’-3’)	GGTTCTGGATACCCATACGATGTTCCAGATTACGCT
Name	Stop codon
Sequence (5’-3’)	TAG
Name	Kozak sequence in pCS2+ plasmids
Sequence (5’-3’)	GCTGCCAAC

5.6 Cell culture

5.6.1 General conditions

Cells were grown at 37 °C and 5 % CO_2 in Dulbecco's Modified Eagle Medium (DMEM; Sigma-Aldrich) supplemented with 2 mM L-glutamine, 1 mM sodium pyruvate and 10 % (vol/vol) fetal bovine serum. Cells were routinely passaged after 2 to 3 days or upon reaching 80 % confluency.
Cell experiments were performed at 70 % to 90 % confluency.

5.6.2 Generation of stable cell lines

Stable cell lines were generated with U2OS FlpIN™ TREx™ cells using the Flp-In System (Thermo Fisher Scientific Inc.) according to the manufacturer's protocol.

5.6.3 Transient transfection

Transient transfection was performed with Lipofectamine™ 3000 (Thermo Fisher Scientific Inc.) according to the manufacturer's protocol.

5.6.4 Sample preparation for microscopy

One day prior imaging cells were seeded on microscopy dishes (µ-Slide 8 Well Glass Bottom (ibidi) or µ-Slide 18 Well Glass Bottom (ibidi)) in DMEM without phenol red.
µ-Slide 8 Well Glass Bottom (ibidi):
The medium was exchanged prior imaging with 200 µl DMEM without phenol red. The compounds were diluted from DMSO stocks in DMEM without phenol red to a total volume of 200 µl and this solution was added to the cell suspension at the microscope. The final DMSO fraction was 0.5 %.
µ-Slide 18 Well Glass Bottom (ibidi):
The medium was exchanged prior imaging with 100 µl DMEM without phenol red. The compounds were diluted from DMSO stocks in DMEM without phenol red to a total volume of 100 µl and this solution was added to the cell suspension at the microscope. The final DMSO fraction was 0.5 %.

In experiments where antagonists for Mandi where investigated were performed with cells seeded on µ-Slide 8 Well Glass Bottom (ibidi) microscopy dishes:
The medium was exchanged prior imaging with 100 µl DMEM without phenol red. Then, 100 µl DMEM without phenol red containing Mandi was added yielding a concentration of 100 nM and a DMSO fraction of 0.5 %. After 20 min, 100 µl DMEM without phenol red containing the antagonist (or DMSO only as control) was added, achieving a DMSO fraction of 0.5 % and diluting the concentration of Mandi to 50 nM.

In one experiment, 60 min after addition of antagonist again Mandi in 100 µl DMEM without phenol red was added yielding a final concentration of 1 uM Mandi and a DMSO fraction of 0.5 %

5.6.5 Staining of Halo protein

For staining of cells expressing the Halo protein, cells were incubated with 50 nM SiR-Halo overnight. Prior imaging two further wash steps with DMEM without phenol red were performed.

5.7 Fluorescence microscopy

5.7.1 Confocal fluorescence microscopy

Confocal fluorescence imaging was performed with a SP8 microscope (Leica) equipped with a White Light Laser (WLL, 470 nm to 670 nm) and a 405 nm diode laser for excitation.
For imaging of eGFP excitation was conducted at 488 nm and the emission was detected from 503 nm to 563 nm on a HyD 2 SMD detector (Leica). mCherry was imaged with excitation at 587 nm and the emission was detected from 607 nm to 667 nm on a HyD 4 SMD detector (Leica). The different channels were imaged simultaneously.

Microscopy settings for imaging of live cells

For live-cell imaging a HC PL APO CS2 20x/0.75 DRY objective was used. The following settings were applied: zoom factor 2.00, line average 4, pixel size 142 nm x 142 nm, format 2048 x 2048 pixels, pixel dwell time 787 ns, pinhole 1.2 airy units (67.94 µm).
Irradiation for in cellulo photouncaging of pMandi was conducted at 405 nm with a power of 0.43 mW and normal imaging settings of the whole field of view.
Irradiation for in cellulo photouncaging of pOP was conducted at 405 nm with a power of 2.31 mW and normal imaging settings of a defined region of interest (ROI) or the whole field of view.
Irradiation for in cellulo photouncaging of Mandi-Dopa-Cn-NV was conducted at 405 nm with a power of 1.06 mW and normal imaging settings of the whole field of view.
Imaging was performed at 37 °C.
The pearson coefficient was calculated with the plugin Colocalization_finder (version 1.6) in Fiji ImageJ using the eGFP and mCherry channels of confocal fluorescence microscopy images.

Microscopy settings for imaging of live medaka embryos

For imaging of live medaka embryos a HC PL APO CS2 63x/1.40 OIL objective was used. The following settings were applied: zoom factor 2.00, line average 4, pixel size 90 nm x 90 nm, format 2048 x 2048 pixels, pixel dwell time 787 ns, pinhole 1.2 airy units (114.6 µm).
Irradiation for in vivo photouncaging of pMandi was conducted at 405 nm with a power of 1.10 mW and normal imaging settings of a defined region of interest (ROI) or the whole field of view.
Imaging was performed at 27 °C.

5.7.2 Widefield fluorescence microscopy

For widefield fluorescence imaging a DMi8 microscope from Leica was used, equipped with 4 LEDs (405, 488, 552 and 638 nm) for excitation and dichroic mirrors (409, 493, 573 and 652 nm) for the

detection of the emission. For imaging of eGFP and mCherry excitation prefilters were used (mCherry: 580 nm, eGFP: 490 nm). An HC PL APO 20x/0.80 DRY objective was used.

Irradiation for in cellulo photouncaging of pMandi was conducted at 405 nm with a power of 53 mW. Imaging was performed at 37 °C.

5.8 Medaka embryo experiments

5.8.1 Fish maintenance

Adult medaka (*oryzias latipes*, Cab strain) stocks were raised and maintained as closed stocks at 28 °C on a 14 h:10 h light:dark cycle at Heidelberg University. Fish husbandry and experiments were performed in accordance with the local animal welfare guidelines (Tierschutzgesetz §11, Abs. 1, Nr. 1, husbandry permit number 35-9185.64/BH Wittbrodt). The fish facility is under the supervision of the local representative of the animal welfare agency.

5.8.2 In vitro transcription of mRNA for microinjections

For in vitro transcription of mRNA, first the plasmids pCS2+-eGFP-ABI, pCS2+-Lyn-mCherry-PYR^{Mandi} and pCS2+-Lyn-mCherry-PYL were linearized with HpaI (NEB) according to the manufacturers protocol. Then, the linearized plasmids were purified using the QIAquick PCR Purification Kit (Qiagen) and transcribed in vitro with the mMESSAGE mMACHINE™ SP6 Transcription Kit (Thermo Fisher Scientific Inc.). The mRNA was purified using the RNeasy Mini Kit (Qiagen) and the quality of the mRNA was assessed via agarose gel electrophoresis.

5.8.3 Microinjections

Microinjections were performed by Kaisa Pakari in wild-type Cab embryos at the one-cell stage. Fertilized embryos were injected with 50 ng/µl eGFP-ABI and Lyn-mCherry-PYR^{Mandi} mRNA or 50 ng/µl eGFP-ABI and Lyn-mCherry-PYL mRNA. Injected embryos were maintained in embryo rearing medium (1x ERM: 17 mM NaCl, 40 mM KCl, 0.27 mM $CaCl_2 \cdot 2\ H_2O$, 0.66 mM $MgSO_4 \cdot 7\ H_2O$ and 17 mM HEPES) and incubated at 26 °C. Embryos were screened for eGFP and mCherry expression 1 day after injections using a Nikon SMZ18 stereomicroscope. Only fluorescent positive and properly developed embryos were continued with.

5.8.4 Sample preparation for microscopy

Confocal fluorescence imaging was performed 2 days post fertilization (dpf).[74] Embryos were dechorionated using hatching enzyme and washed with 1x ERM. For imaging embryos were mounted dorsally on 12-well glass-bottom plates (Matek) in 200 µl low melting agarose (1 %) supplemented with 1x Tricaine and covered with 1 ml 1x ERM supplemented with 1x Tricaine. The compounds were diluted from DMSO stocks in 1 ml ERM supplemented with 1x Tricaine and the solution was added to the embedded embryos. The final DMSO fraction was 0.5 %.

5.8.5 Toxicity test of OP-AM, pOP, Mandi and pMandi in medaka embryos

To assess the influence of the compounds OP-AM, pOP, Mandi and pMandi in medaka embryos a toxicity test was performed by Kaisa Pakari.

Of each compound 10 µM DMSO stock solutions were prepared and further diluted in 1x ERM to the final concentration. Wild-type Cab embryos were collected and kept at 26 °C. At 2 dpf embryos were transferred into a 96-well plate and treated with 5 µM of each compound in 1x ERM (final DMSO fraction: 0.1 %) as well as 1x ERM only and 0.1 % DMSO only as controls. The embryos were phenotyped 3 h, 6 h and 24 h after treatment and after hatch. After 24 h of compound incubation the media was exchanged for 1x ERM and refreshed every 24 h until hatch. Phenotypes were assessed by imaging on a Nikon SMZ18 stereomicroscope.

Results

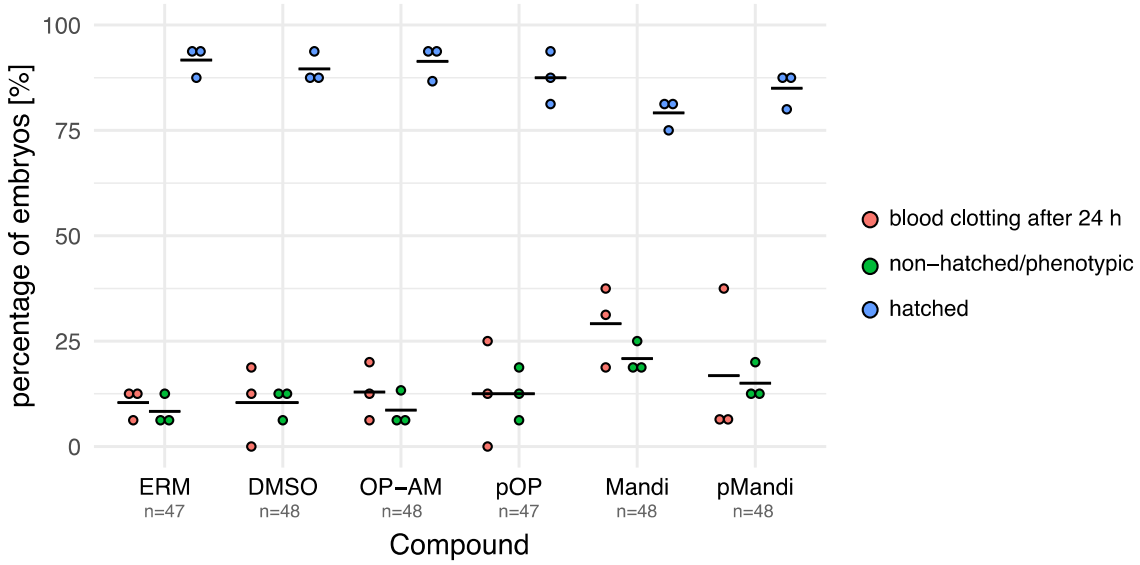

Three independent experiments were performed with 15 to 16 embryos per condition in each experiment. After 3 and 6 h no phenotypes were visible. After 24 h blood clotting was visible in a few embryos (red). Many individuals recovered from the blood clotting after media was changed to 1x ERM after 24 h of compound incubation and hatched (blue). Only a small proportion of the embryos did not hatch or was phenotypic at that timepoint (blue).

Data analysis and Figure creation was conducted by Kaisa Pakari.

5.9 Split PYR^{Mandi} luciferase assay

293 FlpIN™ TREx™ cells (Thermo Fisher Scientific Inc.) were seeded on 96-well plates in 100 µl DMEM without phenol red. On the next day cells were transiently transfected with:

Negative control	Positive control	Split contructs
5 ng pGL 4.75 (rLuc, Promega™)	50 ng pGL4.50 (fLuc2, Promega™)	50 ng pcDNA3.1(+)-PYR^{Mandi}A-B-cLuc-HA
100 ng pcDNA3.1(+)-*Insert_removed*	5 ng pGL 4.75 (rLuc, Promega™)	50 ng pcDNA3.1(+)-MYC-nLuc-PYR^{Mandi}C-D
	50 ng pcDNA3.1(+)-*Insert_removed*	5 ng pGL 4.75 (rLuc, Promega™)

Or:

Negative control	Positive control	Split contructs
5 ng pGL 4.75 (rLuc, Promega™)	50 ng pGL4.50 (fLuc2, Promega™)	50 ng pcDNA3.1(+)-PYR^{Mandi}A-B-cLuc-HA
100 ng pcDNA3.1(+)-*Insert_removed*	5 ng pGL 4.75 (rLuc, Promega™)	50 ng pcDNA3.1(+)-MYC-nLuc-PYR^{Mandi}C-D
50 ng pcDNA3.1(+)-ABI	50 ng pcDNA3.1(+)-*Insert_removed*	5 ng pGL 4.75 (rLuc, Promega™)
	50 ng pcDNA3.1(+)-ABI	50 ng pcDNA3.1(+)-ABI

One day after transfection the cell culture medium was exchanged and cell were incubated with 100 µl DMEM without phenol red containing 50 µM Mandi and 0.5 % DMSO or only 0.5 % DMSO overnight (each 3 wells per condition).

Then, the kit Dual-Glo® Luciferase Assay System (Promega™) was performed and bioluminescence was read out on a Tecan Spark® plate reader.

6 Bibliography

[1] A. Fegan, B. White, J. C. T. Carlson, C. R. Wagner, *Chem. Rev. (Washington, DC, U. S.)* **2010**, *110*, 3315.

[2] B. Z. Stanton, E. J. Chory, G. R. Crabtree, *Science (Washington, DC, U. S.)* **2018**, *359*.

[3] P. J. Steiner, M. A. Bedewitz, A. V. Medina-Cucurella, S. R. Cutler, T. A. Whitehead, *AIChE J.* **2020**, *66*.

[4] E. M. Sletten, C. R. Bertozzi, *Angew. Chem., Int. Ed.* **2009**, *48*, 6974.

[5] P. J. Steiner, S. D. Swift, M. Bedewitz, I. Wheeldon, S. R. Cutler, D. A. Nusinow, T. A. Whitehead, *Biochemistry* **2022**.

[6] a) N. Ankenbruck, T. Courtney, Y. Naro, A. Deiters, *Angew. Chem., Int. Ed.* **2018**, *57*, 2768; b) L. Klewer, Y.-W. Wu, *Chem. - Eur. J.* **2019**, *25*, 12452; c) S. Voß, L. Klewer, Y.-W. Wu, *Curr. Opin. Chem. Biol.* **2015**, *28*, 194; d) C. Brieke, F. Rohrbach, A. Gottschalk, G. Mayer, A. Heckel, *Angew. Chem., Int. Ed.* **2012**, *51*, 8446.

[7] M. Putyrski, C. Schultz, *FEBS Lett.* **2012**, *586*, 2097.

[8] J. Liu, J. D. Farmer, W. S. Lane, J. Friedman, I. Weissman, S. L. Schreiber, *Cell (Cambridge, MA, U. S.)* **1991**, *66*, 807.

[9] D. M. Spencer, T. J. Wandless, S. L. Schreiber, G. R. Crabtree, *Science (Washington, DC, U. S.)* **1993**, *262*, 1019.

[10] E. J. Brown, M. W. Albers, T. B. Shin, K. Ichikawa, C. T. Keith, W. S. Lane, S. L. Schreiber, *Nature (London, U. K.)* **1994**, *369*, 756.

[11] J. Chen, X. F. Zheng, E. J. Brown, S. L. Schreiber, *Proc. Natl. Acad. Sci. U. S. A.* **1995**, *92*, 4947.

[12] J. Choi, J. Chen, S. L. Schreiber, J. Clardy, *Science (Washington, DC, U. S.)* **1996**, *273*, 239.

[13] V. M. Rivera, T. Clackson, S. Natesan, R. Pollock, J. F. Amara, T. Keenan, S. R. Magari, T. Phillips, N. L. Courage, F. Cerasoli et al., *Nat. Med. (N. Y., NY, U. S.)* **1996**, *2*, 1028.

[14] D. A. Holt, J. I. Luengo, D. S. Yamashita, H. J. Oh, A. L. Konialian, H. K. Yen, L. W. Rozamus, M. Brandt, M. J. Bossard, M. A. Levy et al., *J. Am. Chem. Soc.* **1993**, *115*, 9925.

[15] J. F. Amara, T. Clackson, V. M. Rivera, T. Guo, T. Keenan, S. Natesan, R. Pollock, W. Yang, N. L. Courage, D. A. Holt et al., *Proc. Natl. Acad. Sci. U. S. A.* **1997**, *94*, 10618.

[16] S. D. Liberles, S. T. Diver, D. J. Austin, S. L. Schreiber, *Proc. Natl. Acad. Sci. U. S. A.* **1997**, *94*, 7825.

[17] J. H. Bayle, J. S. Grimley, K. Stankunas, J. E. Gestwicki, T. J. Wandless, G. R. Crabtree, *Chem. Biol. (Oxford, U. K.)* **2006**, *13*, 99.

[18] R. Grünberg, T. S. Ferrar, A. M. van der Sloot, M. Constante, L. Serrano, *Nucleic Acids Res.* **2010**, *38*, 2645.

[19] T. Clackson, W. Yang, L. W. Rozamus, M. Hatada, J. F. Amara, C. T. Rollins, L. F. Stevenson, S. R. Magari, S. A. Wood, N. L. Courage et al., *Proc. Natl. Acad. Sci. U. S. A.* **1998**, *95*, 10437.

[20] Z.-Y. Li, K. Otto, R. E. Richard, S. Ni, I. Kirillova, N. Fausto, C. A. Blau, A. Lieber, *Mol. Ther.* **2002**, *5*, 420.

[21] C. J. Buchholz, J. Hartmann, M. Schüßler-Lenz, B. Keller-Stanislawski, *Perspektiven der Onkologie* **2018**, 38.

[22] D. J. Baker, T. Wijshake, T. Tchkonia, N. K. LeBrasseur, B. G. Childs, B. van de Sluis, J. L. Kirkland, J. M. van Deursen, *Nature (London, U. K.)* **2011**, *479*, 232.

[23] C.-Y. Wu, K. T. Roybal, E. M. Puchner, J. Onuffer, W. A. Lim, *Science (Washington, DC, U. S.)* **2015**, *350*, aab4077.

[24] A. V. Karginov, Y. Zou, D. Shirvanyants, P. Kota, N. V. Dokholyan, D. D. Young, K. M. Hahn, A. Deiters, *J. Am. Chem. Soc.* **2011**, *133*, 420.

[25] T. M. Courtney, K. E. Darrah, T. J. Horst, M. Tsang, A. Deiters, *ACS Chem. Biol.* **2021**, *16*, 2434.

[26] K. A. Brown, Y. Zou, D. Shirvanyants, J. Zhang, S. Samanta, P. K. Mantravadi, N. V. Dokholyan, A. Deiters, *Chem. Commun. (Cambridge, U. K.)* **2015**, *51*, 5702.

[27] N. Umeda, T. Ueno, C. Pohlmeyer, T. Nagano, T. Inoue, *J. Am. Chem. Soc.* **2011**, *133*, 12.

[28] A. V. Karginov, F. Ding, P. Kota, N. V. Dokholyan, K. M. Hahn, *Nat. Biotechnol.* **2010**, *28*, 743.

[29] H. D. Wu, M. Kikuchi, O. Dagliyan, A. K. Aragaki, H. Nakamura, N. V. Dokholyan, T. Umehara, T. Inoue, *Nat. Methods* **2020**, *17*, 928.

[30] J.-M. Davière, P. Achard, *Development (Cambridge, U. K.)* **2013**, *140*, 1147.

[31] K. Murase, Y. Hirano, T.-P. Sun, T. Hakoshima, *Nature (London, U. K.)* **2008**, *456*, 459.

[32] T. Miyamoto, R. DeRose, A. Suarez, T. Ueno, M. Chen, T.-P. Sun, M. J. Wolfgang, C. Mukherjee, D. J. Meyers, T. Inoue, *Nat. Chem. Biol.* **2012**, *8*, 465.

[33] G. Grynkiewicz, M. Poenie, R. Y. Tsien, *J. Biol. Chem.* **1985**, *260*, 3440.

[34] B. H. Weinberg, J. H. Cho, Y. Agarwal, N. T. H. Pham, L. D. Caraballo, M. Walkosz, C. Ortega, M. Trexler, N. Tague, B. Law et al., *Nat. Commun.* **2019**, *10*, 4845.

[35] M. Varbanova, S. Yamaguchi, Y. Yang, K. McKelvey, A. Hanada, R. Borochov, F. Yu, Y. Jikumaru, J. Ross, D. Cortes et al., *Plant Cell* **2007**, *19*, 32.

[36] K. M. Schelkle, T. Griesbaum, D. Ollech, S. Becht, T. Buckup, M. Hamburger, R. Wombacher, *Angew. Chem., Int. Ed.* **2015**, *54*, 2825.

[37] M. J. Ziegler, R. Wombacher, *Methods Enzymol.* **2020**, *638*, 259.

[38] a) S. Kepinski, O. Leyser, *Nature (London, U. K.)* **2005**, *435*, 446; b) N. Dharmasiri, S. Dharmasiri, M. Estelle, *Nature (London, U. K.)* **2005**, *435*, 441.

[39] D. Weijers, D. Wagner, *Annu. Rev. Plant Biol.* **2016**, *67*, 539.

[40] K. Nishimura, T. Fukagawa, H. Takisawa, T. Kakimoto, M. Kanemaki, *Nat. Methods* **2009**, *6*, 917.

[41] W. Zhao, H. Nguyen, G. Zeng, D. Gao, H. Yan, F.-S. Liang, *Chem. Sci.* **2018**, *9*, 5822.

[42] K. Daniel, J. Icha, C. Horenburg, D. Müller, C. Norden, J. Mansfeld, *Nat. Commun.* **2018**, *9*, 3297.

[43] N. Kusaka, J. Maisch, P. Nick, K. Hayashi, H. Nozaki, *ChemBioChem* **2009**, *10*, 2195.

[44] K. Hayashi, N. Kusaka, S. Yamasaki, Y. Zhao, H. Nozaki, *Bioorg. Med. Chem. Lett.* **2015**, *25*, 4464.

[45] Q. Delacour, C. Li, M.-A. Plamont, E. Billon-Denis, I. Aujard, T. Le Saux, L. Jullien, A. Gautier, *ACS Chem. Biol.* **2015**, *10*, 1643.

[46] S. R. Cutler, P. L. Rodriguez, R. R. Finkelstein, S. R. Abrams, *Annu. Rev. Plant Biol.* **2010**, *61*, 651.

[47] K.-I. Miyazono, T. Miyakawa, Y. Sawano, K. Kubota, H.-J. Kang, A. Asano, Y. Miyauchi, M. Takahashi, Y. Zhi, Y. Fujita et al., *Nature (London, U. K.)* **2009**, *462*, 609.

[48] a) K. Melcher, L.-M. Ng, X. E. Zhou, F.-F. Soon, Y. Xu, K. M. Suino-Powell, S.-Y. Park, J. J. Weiner, H. Fujii, V. Chinnusamy et al., *Nature (London, U. K.)* **2009**, *462*, 602; b) N. Nishimura, K. Hitomi, A. S. Arvai, R. P. Rambo, C. Hitomi, S. R. Cutler, J. I. Schroeder, E. D. Getzoff, *Science (Washington, DC, U. S.)* **2009**, *326*, 1373.

[49] S.-Y. Park, P. Fung, N. Nishimura, D. R. Jensen, H. Fujii, Y. Zhao, S. Lumba, J. Santiago, A. Rodrigues, T.-F. F. Chow et al., *Science (Washington, DC, U. S.)* **2009**, *324*, 1068.

[50] Y. Ma, I. Szostkiewicz, A. Korte, D. Moes, Y. Yang, A. Christmann, E. Grill, *Science (Washington, DC, U. S.)* **2009**, *324*, 1064.

[51] A. S. Vaidya, J. D. M. Helander, F. C. Peterson, D. Elzinga, W. Dejonghe, A. Kaundal, S.-Y. Park, Z. Xing, R. Mega, J. Takeuchi et al., *Science (Washington, DC, U. S.)* **2019**, *366*.

[52] F.-S. Liang, W. Q. Ho, G. R. Crabtree, *Sci. Signaling* **2011**, *4*, rs2.

[53] a) G. Zeng, R. Zhang, W. Xuan, W. Wang, F.-S. Liang, *ACS Chem. Biol.* **2015**, *10*, 1404; b) J. Poirson, H. Cho, A. Dhillon, S. Haider, A. Z. Imrit, M. H. Y. Lam, N. Alerasool, J. Lacoste, L. Mizan, C. Wong et al., *Nature (London, U. K.)* **2024**.

[54] M. J. Ziegler, K. Yserentant, V. Dunsing, V. Middel, A. J. Gralak, K. Pakari, J. Bargstedt, C. Kern, A. Petrich, S. Chiantia et al., *Nat. Chem. Biol.* **2021**.

[55] C. W. Wright, Z.-F. Guo, F.-S. Liang, *ChemBioChem* **2015**, *16*, 254.

[56] D. E. Brabham, R. H. Biggs, *Photochem. Photobiol.* **1981**, *34*, 33.

[57] a) J. Frackenpohl, G. Bojack, R. Baltz, U. Bickers, M. Busch, J. Dittgen, J. Franke, J. Freigang, E. Grill, S. Gonzalez et al., *Eur. J. Org. Chem.* **2018**, *2018*, 1416; b) J. Frackenpohl, E. Grill, G. Bojack, R. Baltz, M. Busch, J. Dittgen, J. Franke, J. Freigang, S. Gonzalez, I. Heinemann et al., *Eur. J. Org. Chem.* **2018**, *2018*, 1403; c) M. Kepka, C. L. Benson, V. K. Gonugunta, K. M. Nelson, A. Christmann, E. Grill, S. R. Abrams, *J. Plant Physiol.* **2011**, *157*, 2108.

[58] J. M. Nyangulu, K. M. Nelson, P. A. Rose, Y. Gai, M. Loewen, B. Lougheed, J. W. Quail, A. J. Cutler, S. R. Abrams, *Org. Biomol. Chem.* **2006**, *4*, 1400.

[59] M. Okamoto, F. C. Peterson, A. Defries, S.-Y. Park, A. Endo, E. Nambara, B. F. Volkman, S. R. Cutler, *Proc. Natl. Acad. Sci. U. S. A.* **2013**, *110*, 12132.

[60] A. S. Vaidya, F. C. Peterson, D. Yarmolinsky, E. Merilo, I. Verstraeten, S.-Y. Park, D. Elzinga, A. Kaundal, J. Helander, J. Lozano-Juste et al., *ACS Chem. Biol.* **2017**, *12*, 2842.

[61] a) N. Diddi, L. Lai, B. P. Brookbank, S. Hussain, E. Nambara, C. Todd, M. Nourimand, B. Tar'an, D. Song, L. Holbrook et al., *Org. Biomol. Chem.* **2021**, *19*, 2978; b) J. Takeuchi, H. Nagamiya, S. Moroi, T. Ohnishi, Y. Todoroki, *Org. Biomol. Chem.* **2020**, *18*, 4988; c) K. Yoshida, Y. Kondoh, F. Iwahashi, T. Nakano, K. Honda, E. Nagano, H. Osada, *ACS Chem. Biol.* **2019**, *14*, 1964; d) J. Takeuchi, M. Okamoto, T. Akiyama, T. Muto, S. Yajima, M. Sue, M. Seo, Y. Kanno, T. Kamo, A. Endo et al., *Nat. Chem. Biol.* **2014**, *10*, 477; e) J. Takeuchi, T. Ohnishi, M. Okamoto, Y. Todoroki, *Org. Biomol. Chem.* **2015**, *13*, 4278; f) N. Rajagopalan, K. M. Nelson, A. F. Douglas, V. Jheengut, I. Q. Alarcon, S. A. McKenna, M. Surpin, M. C. Loewen, S. R. Abrams, *Biochemistry* **2016**, *55*, 5155; g) C. Che, Y. Zeng, Y. Xu, H. Lu, Y. Xu, X. Zhang, Y. Xiao, J.-Q. Li, Z. Qin, *J. Agric. Food Chem.* **2020**, *68*, 8524.

[62] J. Takeuchi, N. Mimura, M. Okamoto, S. Yajima, M. Sue, T. Akiyama, K. Monda, K. Iba, T. Ohnishi, Y. Todoroki, *ACS Chem. Biol.* **2018**, *13*, 1313.

[63] A. S. Vaidya, F. C. Peterson, J. Eckhardt, Z. Xing, S.-Y. Park, W. Dejonghe, J. Takeuchi, O. Pri-Tal, J. Faria, D. Elzinga et al., *Proc. Natl. Acad. Sci. U. S. A.* **2021**, *118*.

[64] a) J. M. Nyangulu, M. M. Galka, A. Jadhav, Y. Gai, C. M. Graham, K. M. Nelson, A. J. Cutler, D. C. Taylor, G. M. Banowetz, S. R. Abrams, *J. Am. Chem. Soc.* **2005**, *127*, 1662; b) O. A. Kharenko, D. Polichuk, K. M. Nelson, S. R. Abrams, M. C. Loewen, *J. Biochem.* **2013**, *154*, 383; c) N. Kitahata, T. Nakano, K. Kuchitsu, S. Yoshida, T. Asami, *Bioorg. Med. Chem.* **2005**, *13*, 3351; d) T. Anabuki, Y. Ito, K. Ohashi, T. E. Takasuka, H. Matsuura, K. Takahashi, *Bioorg. Med. Chem. Lett.* **2019**, *29*, 126634.

[65] S.-Y. Park, F. C. Peterson, A. Mosquna, J. Yao, B. F. Volkman, S. R. Cutler, *Nature (London, U. K.)* **2015**, *520*, 545.

[66] J. Beltrán, P. J. Steiner, M. Bedewitz, S. Wei, F. C. Peterson, Z. Li, B. E. Hughes, Z. Hartley, N. R. Robertson, A. V. Medina-Cucurella et al., *Nat. Biotechnol.* **2022**.

[67] Z. Li, Y. Shen, J. Beltrán, H. Tian, M. Bedewitz, I. Wheeldon, T. A. Whitehead, S. R. Cutler, W. Zhong, *ACS Sens.* **2023**.

[68] S.-Y. Park, J. Qiu, S. Wei, F. C. Peterson, J. Beltrán, A. V. Medina-Cucurella, A. S. Vaidya, Z. Xing, B. F. Volkman, D. A. Nusinow et al., *Nat. Chem. Biol.* **2023**.

[69] C. Lamberth, A. Jeanguenat, F. Cederbaum, A. de Mesmaeker, M. Zeller, H.-J. Kempf, R. Zeun, *Bioorg. Med. Chem.* **2008**, *16*, 1531.

[70] C. Lamberth, F. Cederbaum, A. Jeanguenat, H.-J. Kempf, M. Zeller, R. Zeun, *Pest Manage. Sci.* **2006**, *62*, 446.

[71] L. Hu, F. Chen, C. Wu, J. Wang, S.-S. Chen, X.-R. Li, J. Wang, L. Wu, J.-P. Ding, J.-C. Wang et al., *iScience* **2021**, *24*, 103177.

[72] L. A. Banaszynski, C. W. Liu, T. J. Wandless, *J. Am. Chem. Soc.* **2005**, *127*, 4715.

[73] a) D. R. Thomsen, R. M. Stenberg, W. F. Goins, M. F. Stinski, *Proc. Natl. Acad. Sci. U. S. A.* **1984**, *81*, 659; b) M. K. Foecking, H. Hofstetter, *Gene* **1986**, *45*, 101.

[74] T. Iwamatsu, *Mech. Dev.* **2004**, *121*, 605.

[75] M. Zeller, C. Lamberth, WO 2003/042168 A1, **2003**.

[76] M. C. Bowden, T. C. Clark, F. D. B. Giordano, B. Jau, H. Schneider, G. Seifert, J. Wiss, M. Zeller, D. Faber, WO 2007/020381 A2, **2007**.

[77] J. B. Grimm, A. J. Sung, W. R. Legant, P. Hulamm, S. M. Matlosz, E. Betzig, L. D. Lavis, *ACS Chem. Biol.* **2013**, *8*, 1303.

[78] J. Wilhelm, S. Kühn, M. Tarnawski, G. Gotthard, J. Tünnermann, T. Tänzer, J. Karpenko, N. Mertes, L. Xue, U. Uhrig et al., *Biochemistry* **2021**, *60*, 2560.

[79] Philipp Pöschko, *Master's thesis*, Heidelberg University, **2021**.

[80] E. Rihtar, T. Lebar, D. Lainšček, K. Kores, S. Lešnik, U. Bren, R. Jerala, *Nat. Chem. Biol.* **2022**.

[81] J. Rowe, M. Grangé-Guermente, M. Exposito-Rodriguez, R. Wimalasekera, M. O. Lenz, K. N. Shetty, S. R. Cutler, A. M. Jones, *Nat. Plants (London, U. K.)* **2023**, *9*, 1103.

[82] M. M. Harmsen, H. J. de Haard, *Appl. Microbiol. Biotechnol.* **2007**, *77*, 13.

[83] G. P. Smith, *Science (Washington, DC, U. S.)* **1985**, *228*, 1315.

[84] a) L. Li, J. O. Fierer, T. A. Rapoport, M. Howarth, *J. Mol. Biol.* **2014**, *426*, 309; b) B. Zakeri, J. O. Fierer, E. Celik, E. C. Chittock, U. Schwarz-Linek, V. T. Moy, M. Howarth, *Proc. Natl. Acad. Sci. U. S. A.* **2012**, *109*, E690-7; c) S. C. Reddington, M. Howarth, *Curr. Opin. Chem. Biol.* **2015**, *29*, 94.

[85] E. R. Ruskowitz, B. G. Munoz-Robles, A. C. Strange, C. H. Butcher, S. Kurniawan, J. R. Filteau, C. A. DeForest, *Nat. Chem.* **2023**.

[86] a) A. Blanc, C. G. Bochet, *J. Org. Chem.* **2002**, *67*, 5567; b) C. G. Bochet, *Angew. Chem., Int. Ed.* **2001**, *40*, 2071; c) P. Klán, T. Šolomek, C. G. Bochet, A. Blanc, R. Givens, M. Rubina, V. Popik, A. Kostikov, J. Wirz, *Chem. Rev. (Washington, DC, U. S.)* **2013**, *113*, 119.

[87] G. R. Fulmer, A. J. M. Miller, N. H. Sherden, H. E. Gottlieb, A. Nudelman, B. M. Stoltz, J. E. Bercaw, K. I. Goldberg, *Organometallics* **2010**, *29*, 2176.

[88] Y. Zhou, E. Bourque, Y. Zhu, E. J. McEachern, C. Harwig, R. T. Skerlj, G. J. Bridger, T.-S. Li, M. Metz, WO 2007/022371 A2, **2006**.

[89] Y. Zhao, D. Mandal, J. Guo, Y. Wu, D. W. Stephan, *Chem. Commun. (Cambridge, U. K.)* **2021**, *57*, 7758.

[90] B. Du, X. Jiang, P. Sun, *J. Org. Chem.* **2013**, *78*, 2786.

[91] V. Ehmke, F. Kilchmann, C. Heindl, K. Cui, J. Huang, T. Schirmeister, F. Diederich, *MedChemComm* **2011**, *2*, 800.

[92] Bureau International des Poids et Mesures (BIPM), *Le Système international d'unités (SI)*. *The International System of Units (SI)*, Sèvres Cedex (France), **2019**.

[93] Committee and Subcommittee on Nomenclature, Properties and Units (SC-C-NPU), *Confirmed minutes for the meeting in Uppsala 2008-10-23 – 25*, **2008**.

7 Appendix

7.1 List of Abbreviation

ABA	abscisic acid
ABI	PYR1/PYL-ABA/OP or PYR1^{Mandi}/PYR1^{Mandi*}-Mandi complex binding protein ABI (amino acids 126-423 of ABI1)[52]
ABI1	PYR1/PYL-ABA/OP or PYR1^{Mandi}/PYR1^{Mandi*}-Mandi complex binding protein ABI1
ABI2	PYR1/PYL-ABA/OP or PYR1^{Mandi}/PYR1^{Mandi*}-Mandi complex binding protein ABI2
ABIaid	PYR1/PYL-ABA/OP or PYR1^{Mandi}/PYR1^{Mandi*}-Mandi complex binding protein ABIaid (amino acids 279-327 of ABI1)[81]
Ac_2O	acetic anhydride
AIBN	azobisisobutyronitrile
AID	auxin-TIR1 binding protein AID
ANT	abscisic acid antagonist ANT
AM	acetoxymethyl (ester)
AP1510	rapalog AP1510
AP1903	rapalog AP1903
AP20187	rapalog AP20187
AP21957	rapalog AP21957
aRap	photocaged rapamycin aRap
brine	saturated, aqueous sodium chloride solution
cal	calorie (1 cal = 4.184 J)
Calcineurin	FKBP12-FK506 complex binding protein calcineurin
CAR	chimeric antigen receptor
cat.	catalytic
ccRICS	cross-correlation raster image spectroscopy
CID	chemical inducer of dimerization
CIP	chemical inducer of proximity
cLuc	C-terminal protein domain of fLuc
CMV	Cytomegalovirus
CPY	carbopyronine
CPY-C6-COOH	6-carboxycarbopyronine
dba	dibenzylideneacetone
DCE	1,2-dichlorethene
DCM	dichloromethane
DIPEA	*N*,*N*-diisopropylethylamine (= Hünig's base)

DMAP	4-(dimethylamino)pyridine
DMF	dimethylformamide
DMSO	dimethyl sulfoxide
dpf	days post fertilization
dRap	photocaged rapamycin dRap
eGFP	enhanced green fluorescent protein eGFP
EDC	1-ethyl-3-(3-dimethylaminopropyl)carbodiimide
ESI	electrospray ionization
EtOAc	ethyl acetate
eq.	equivalent
FCSS	fluorescence cross-correlation spectroscopy
FK506	rapalog FK506
FK1012	rapalog FK1012
FKBP12	FK506/rapamycin binding protein FKBP12
fLuc	firefly luciferase protein fLuc
FQ	fluoroquinoline
FRAP	FKBP-rapamycin complex binding protein FRAP (= mTOR)
FRB	FKBP-rapamycin complex binding protein FRB (amino acids 2020-2113 of FRAP)[12]
FRET	Förster-resonance energy transfer
GA_3	gibberellic acid
GAI	GID1-GA complex binding protein GAI
GFP	green fluorescent protein GFP
GID1	GA_3 binding protein GID1
h	hour
h	Planck constant (*h* = 6.626 070 15 x 10^{-34} J s)[92]
HAB1	PYR1/PYL-ABA/OP or $PYR1^{Mandi}$/$PYR1^{Mandi*}$-Mandi complex receiver protein HAB1
Halo	self-labeling protein HaloTag7
Halo-CPY	Halo ligand: chloroalkane-carbopyronine
HATU	hexafluorophosphate azabenzotriazole tetramethyl uronium
HOBt	hydroxybenzotriazole
HPLC	high performance liquid chromatography
Hz	hertz (1 Hz = 1 s^{-1})[92]
ITC	isothermal titration calorimetry
J	joule
J	coupling constant
l	liter (1 liter = 0.001 m^3)

LC	liquid chromatography
LC-MS	liquid chromatography–mass spectrometry)
Lyn	translocase protein to the outer mitochondrial membrane Lyn
HRMS	high resolution mass spectrometry
ITC	isothermal titration calorimetry
M	molar (mol/l)
Mandi	mandipropamid
mCherry	red fluorescent protein mCherry
ME	methyl ester
MeCN	acetonitrile
MeOH	methanol
min	minute
mol	mole (1 mol = 6.022 140 76 x 10^{-23} elementary entities)[92]
MNI	4-methoxy-7-nitroindolinyl
Ms	mesyl
mTOR	FKBP-rapamycin complex binding protein mTOR (= FRAP)
MS	mass spectrometry
m/z	mass-to-charge ratio
NBS	*N*-bromosuccinimide
neg. ctrl.	negative control
nLuc	N-terminal protein domain of fLuc
NMR	nuclear magnetic resonance
NV	nitroveratryl
OP	opabactin
P	power
P2A	self-cleaving peptide P2A
PANMe	abscisic acid antagonist PANMe (= revABA)
PBS	phosphate-buffered saline
PCR	polymerase chain reaction
PDA	photo diode array
pdb	protein data bank
p.d.u.	procedure defined unit[93]
Ph	phenyl
pMandi	photocaged mandipropamid pMandi
POI	protein of interest
pOP	photocaged opabactin pOP

pos. ctrl.	positive control
PPI	protein-protein interactions
PPG	photolabile protecting group
ppm	parts per million
pRap	photocaged rapamycin pRap
PROTAC	proteolysis targeting chimera
pTsOH	*p*-toluenesulfonic acid
PYL	ABA binding protein PYL (amino acids 33-209 of PYL1)[52]
PYL1	ABA binding protein PYL1
PYR1	ABA binding protein PYR1
$PYR1^{Mandi}$	Mandi binding protein $PYR1^{Mandi}$: sextuple mutant of PYR1 ($PYR1^{Mandi}$ = PYR1 (Y58H, K59R, V81I, F108A, S122G, F159L))
$PYR1^{Mandi*}$	Mandi binding protein $PYR1^{Mandi*}$: quadruple mutant of PYR1 ($PYR1^{Mandi*}$ = PYR1 (K59R, V81I, F108A, F159L)) (crystallizable)
ROI	region of interest
quant.	quantitative
revABA	abscisic acid antagonist revABA (= PANMe)
rLuc	renilla luciferase protein rLuc
rt	room temperature
SiR-Halo	Halo ligand: chloroalkane-silicon rhodamine
TFA	trifluoroacetic acid
THF	tetrahydrofuran
TIR1	auxin binding protein TIR1
TLC	thin layer chromatography
TOMM20	translocase protein to the outer mitochondrial membrane TOMM20
δ	chemical shift
ν	frequency

7.2 Supplementary Figures

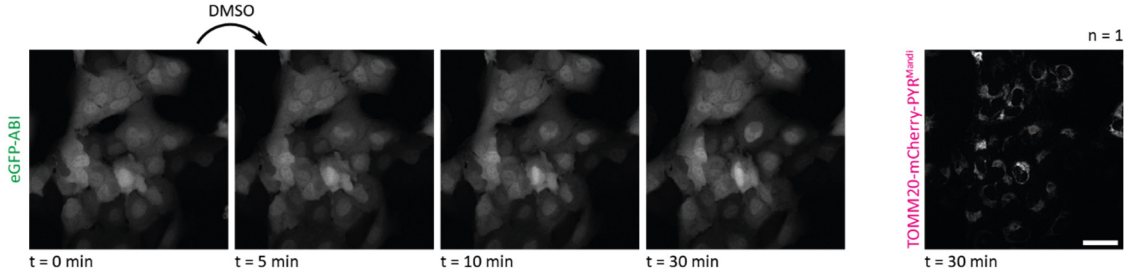

Figure 84: DMSO control PYR^{Mandi} – Addition of DMSO only to live cells expressing TOMM20-mCherry-PYR^{Mandi} and eGFP-ABI has no influence on protein localization. Confocal microscopy images of U2OS FlpIN cells stably expressing TOMM20-mCherry-PYR^{Mandi} and eGFP-ABI before and at different timepoints post addition of different concentrations of DMSO. Indicated number n of replicates. Scale bar at 40 µm.

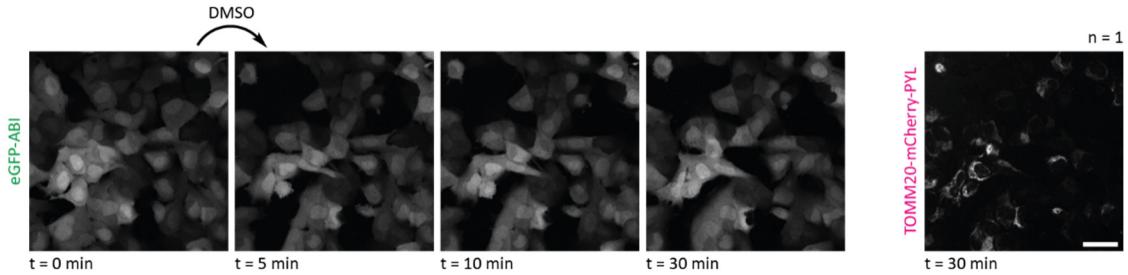

Figure 85: DMSO control PYL – Addition of DMSO only to live cells expressing TOMM20-mCherry-PYL and eGFP-ABI has no influence on protein localization. Confocal microscopy images of U2OS FlpIN cells stably expressing TOMM20-mCherry-PYL and eGFP-ABI before and at different timepoints post addition of different concentrations of DMSO. Indicated number n of replicates. Scale bar at 40 µm.

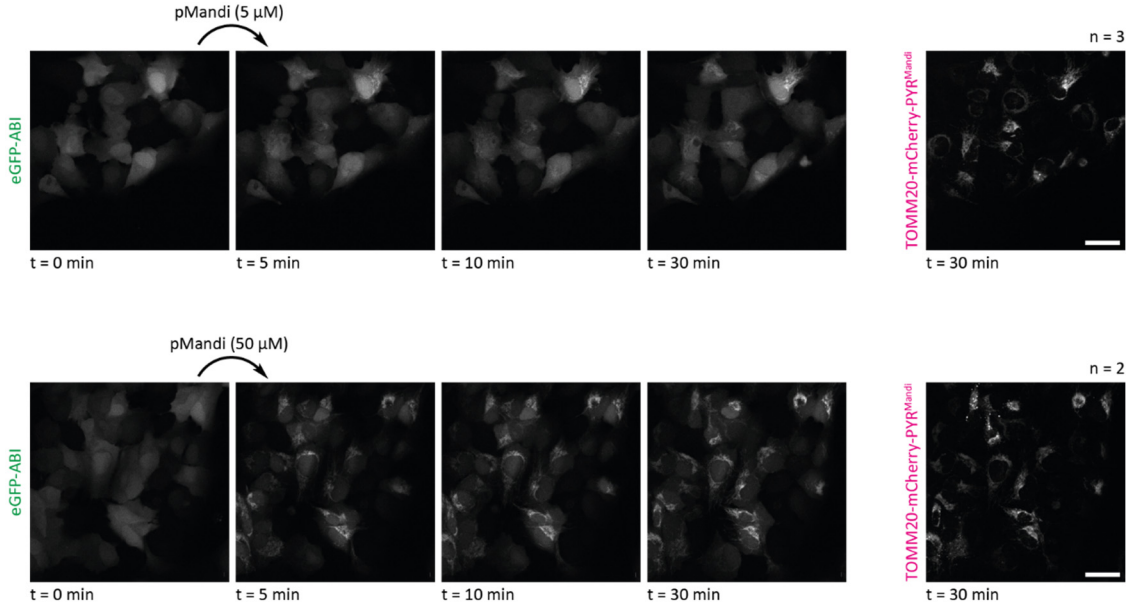

Figure 86: Addition of pMandi induces protein proximity at micromolar concentrations without irradiation in live mammalian cells. Confocal microscopy images of U2OS FlpIN cells stably expressing TOMM20-mCherry-PYR^{Mandi} and eGFP-ABI before and at different timepoints post addition of different concentrations of pMandi. Indicated number n of replicates. Scale bars at 40 µm.

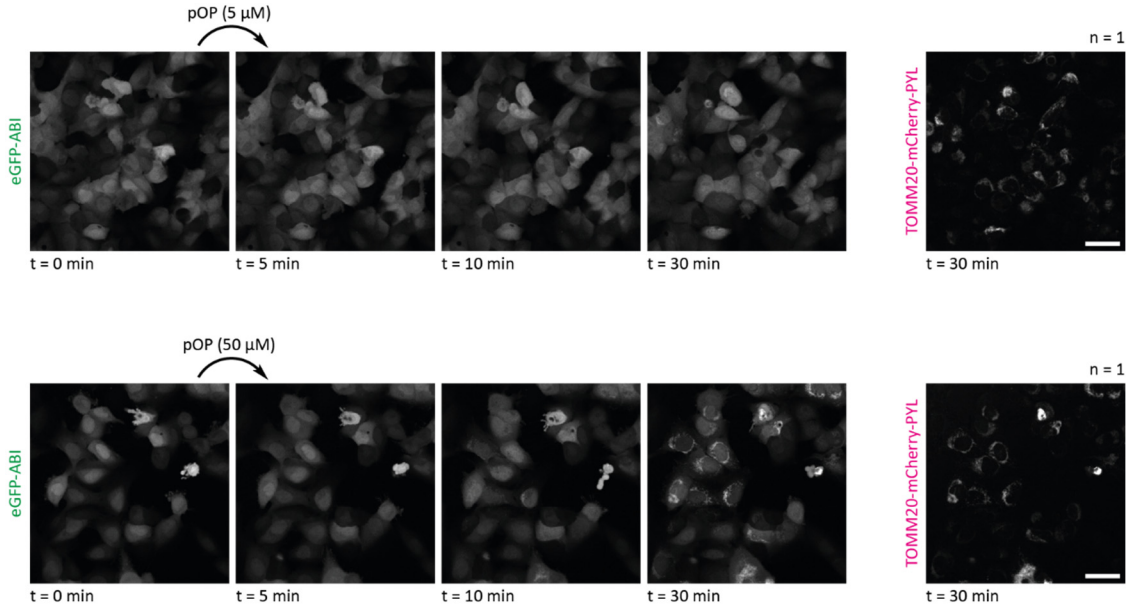

Figure 87: Addition of pOP induces protein proximity at micromolar concentrations without irradiation in live mammalian cells. Confocal microscopy images of U2OS FlpIN cells stably expressing TOMM20-mCherry-PYL and eGFP-ABI before and at different timepoints post addition of different concentrations of pOP. Indicated number n of replicates. Scale bars at 40 µm.

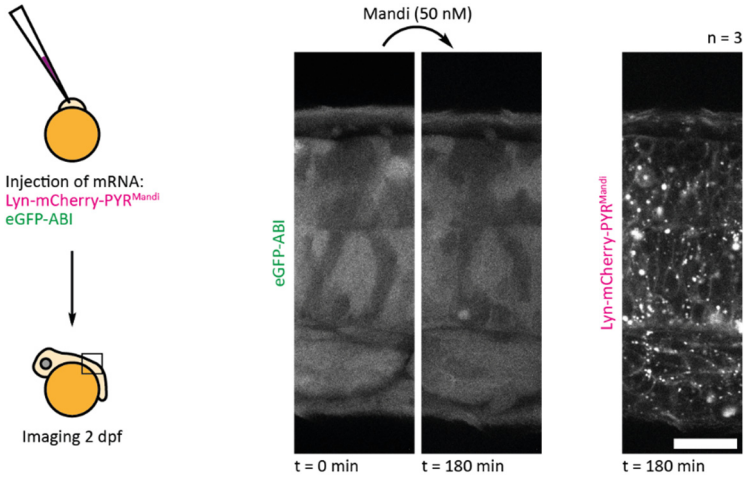

Figure 88: Application of 50 nM Mandi as CIP in live medaka embryos. Medaka embryos were microinjected with mRNA in the one-cell stage and experiments were performed 2 dpf. Addition of Mandi to agarose embedded embryos does not induce protein translocation to the plasma membrane in eGFP-ABI and Lyn-mCherry-PYR^{Mandi} mRNA injected embryos. Confocal microscopy images of the medaka embryo tail before and 180 min post addition of 50 nM Mandi. Indicated number n of replicates. Scale bar at 20 µm. Microinjection was performed by Kaisa Pakari.

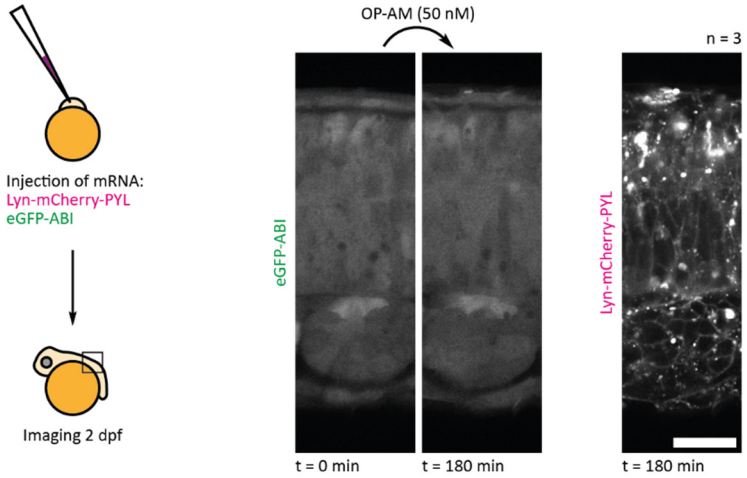

Figure 89: Application of 50 nM OP-AM as CIP in live medaka embryos. Medaka embryos were microinjected with mRNA in the one-cell stage and experiments were performed 2 dpf. Addition of OP-AM to agarose embedded embryos does not induce protein translocation to the plasma membrane in eGFP-ABI and Lyn-mCherry-PYL mRNA injected embryos. Confocal microscopy images of the medaka embryo tail before and 180 min post addition of 50 nM OP-AM. Indicated number n of replicates. Scale bar at 20 µm. Microinjection was performed by Kaisa Pakari.